A new Magneto-Fluid Dynamics model for Low Magnetic Reynolds number regime in the Hybridized Discontinuous Galerkin Framework

Candidate:

Paolo Scuderi

Matricola 263784

Supervisor PoliTo:

Prof. Domenic D'Ambrosio

Supervisors VKI:

Prof. Georg May

Prof. Thierry E. Magin

Thesis submitted in July 2021

The von Karman Institute for Fluid Dynamics

DEPARTMENT OF AERONAUTICS AND AEROSPACE
Short Training Programme & Master's Thesis

A new Magneto-Fluid Dynamics model for Low Magnetic Reynolds number regime in the Hybridized Discontinuous Galerkin Framework

Candidate:
Paolo Scuderi

Advisor:
Giuseppe Matteo Gangemi

Supervisors:
Prof. Georg May
Prof. Thierry E. Magin

Thesis submitted in July 2021

A chi ha saputo starmi vicino...

Abstract

The Magneto-Fluid Dynamics has many aerospace applications when the gas is an ionized mixture. Typically, this happens when the temperature of the mixture is very high. Indeed, we need to consider new degrees of freedom of the molecules, the presence of the chemical reactions, and the possibility to have free electrons that can move from one point to another. This is the typical situation during a normal atmospheric entry problem. In this context, all the physical properties cannot be computed with the classical approximation laws. The Chapman-Enskong method gives us the possibility to perturb the Boltzmann Transport Equation and to understand which are the different contributions (of electrons and heavy particles) to take into account. Hence, the modeling of the transport properties can be conducted. The latter, which are functions of pressure and temperature, can also change their values with the presence of external magnetic and electric fields. The physical models that try to describe all these peculiar characteristics and the macroscopic properties of electrically conducting flows are, from a numerical point of view, highly stiff. In the last years, a simplified version of the full Magneto-Fluid Dynamics system was proposed. Two limiting cases are present based on the dimensionless parameter Magnetic Reynolds number. When it is very small, the externally applied magnetic field is called rigid. Hence, the induced magnetic field can be considered null. Therefore, the classical Navier-Stokes equations with additional external electromagnetic source terms make up the simplified Magneto-Fluid Dynamics system. The source term is composed of the Lorentz force for the momentum equation and the Joule heating for the energy equation. No source terms for the continuity equations must be taken into account under the assumption of frozen flow, which is generally adopted in many hypersonic applications. The system cannot be solved analytically, except where we are considering parallel flow, where the non-linear convective terms drop down, i.e. Hartmann flow. As a consequence, we need to introduce numerical discretization. One of the most innovative methods to solve non-linear PDEs is called Hybridized Discontinuous Galerkin. It can be considered as a mix between FE and FV methods. The hybridization concept introduces the possibility to parallelize efficient the code and to reduce the high computational cost associated with the high-order methods, e.g. Discontinuous Galerkin. In the past years, many Magneto-Fluid Dynamics physical models were developed into FV solvers. From the literature review, only one researcher Group from the Massachusetts Institute of Technology and Imperial College London, in 2019, has developed an MHD model for compressible flow in their HDG solver. The High-Order Unifying Framework, that developed by May et al. in RWTH Aachen and now is currently under improvements at The VKI, was empty of the Magneto-Fluid Dynamics model for a low Magnetic Reynolds number. The implementation from a physical, mathematical, and computer science point of view, is explained in this work. Finally, the model has been tested with simple test cases. Comparison with analytical data has been conducted to validate the model.

Acknowledgement

Il primo di tutti conosciuto al Politecnico di Torino durante il corso di Analisi I è stato *Fiorenzo*. A lui va un grazie per aver superato i primi esami in compagnia, avermi fatto sentire meno spaesato e, soprattutto, per avermi aiutato con i mille problemi informatici; *Vincenzo* per essere stato una scoperta unica e per avermi aiutato in qualsiasi modo quando gli chiesi anche solo un piccolo aiuto. Averne persone così! Il *Gruppo H*: *Edoardo, Gianluca, Cosimo* e *Cristiano* per le nostre uscite, le risate, le pizzate da Pulcinella ai tempi non-Covid19, e soprattutto per aver reso meno stressante il periodo della sessione esami. Siete stati parte fondamentale del mio percorso. *Giulia* per avermi continuamente supportato e sopportato (soprattutto, oserei dire). Per tutti i problemi passati, presenti, e futuri che si sono superati. E' stata una fonte di tutto, lei sa. La sua famiglia per essermi stata vicino e avermi sempre fatto sentire a casa. Il *Gruppo Sardegna*: *Gabriele, Federico, Lorenzo* e *Matteo* per essere stata una scoperta bellissima e una risata continua in giornate complicate. Le serata passate sulla sedia del trenta e lode e gli esami, seppur di corsi differenti, superati insieme. Siamo una famiglia di amici che mi ha dato tanto sotto tutti gli aspetti. *Salvatore* per aver riportato la mia amata Sicilia a Torino. Tutti gli amici che in questi anni di Politecnico mi hanno aiutato e creduto in me quando ho ricoperto ruoli di rappresentanza. Quei pochi amici rimasti dell'infanzia e dalla pallacanestro, loro mi conoscono più degli altri e sanno bene quanto tenessi alla mia Laurea. Tutti i ragazzi dei differenti progetti e team studenteschi di cui ho fatto parte in questi anni: scambiarsi idee e condividere momenti è stato molto gratificante.

Infine, ma non per importanza, la mia famiglia: mia *Mamma*, mio *Papà* e mia *Sorella* per avermi insegnato la più importante delle lezioni! Nonostante qualche alto e basso tipico della nostra convivenza, a voi devo gran parte, se non tutto, questo successo. Conosco bene tutto quello che state immaginando, e spero che questo giorno possa regalarvi una grossa boccata d'aria, tanta gioia e serenità nel sapere che ho concluso uno step importante della mia vita e ora, posso aiutarvi. Sperando di essere stato fonte di vostro orgoglio e gratitudine anche quando le cose non andavano come speravamo, voglio dirvi che vi voglio un bene infinito. Non ci sarebbero parole per descrivere cosa provo anche se spesso non lo dimostro. Per questo vi chiedo scusa, ma sappiate che non è come sembra.

Concludo questo percorso lasciando il Politecnico che è stato per me fonte di ispirazione, miglioramento e soprattutto crescita umana, e ovviamente accademica. Orgoglioso dei massimi risultati raggiunti, spero un giorno di poter fare ritorno da Voi. Siete una seconda Casa, una seconda Famiglia. Nel contempo, non posso far altro che ringraziare ancora una volta tutti coloro che ho citato in questa Tesi, spero possiate essere orgogliosi di me. Ogni singolo vostro insegnamento, tecnico professionale o di lezione di vita, lo porterò con me l'anno prossimo nel Research Master 2021-2022 al The von Karman Institute for Fluid Dynamics. Siete stati tutti parte fondamentale di questo lungo, tortuoso sotto certi aspetti, ma stupendo percorso!
Mi guardo indietro e penso a come sono volati questi anni, quanta strada ho fatto, quanta ne devo ancora fare, come sono cambiato e cresciuto... Ma dopo? Chi lo sa... Cercherò di nuovo, come mi ripeto sempre, di essere l'eroe di me stesso. Ancora un enorme grazie a tutti!

Vostro Paolo

Contents

List of Figures

List of Tables

List of Symbols

Acronyms

VKI	von Karman Institute
PDEs	Partial Different Equations
BTE	Boltzmann Transport Equation
LHS	Left-Hand Side
RHS	Right-Hand Side
FD	Finite Difference
FE	Finite Elements
FV	Finite Volume
AD	Automatic Differentiation or `AutoDiff`
CG	Continuos Galerkin
DG	Discontinuous Galerkin
M++	Mutation ++
OOP	Object Oriented Programming
CFD	Computational Fluid Dynamics
HDG	Hybridized Discontinuous Galerkin
MFD	Magneto-Fluid Dynamics
MHD	Magneto-Hydro Dynamics
MEESST	MHD Enhanced Entry System for Space Transportation

Roman symbols

Kn	Knudsen number	–
Ma	Mach number	–
Re	Reynolds number	–
Pr	Prandtl number	–
Da	Damkohler number	–
Re_m	Magnetic Reynolds number	–
S	Magnetic force number	–
N	Stuart number	–
Ha	Hartmann number	–
Y	mass fraction	–
X	molar fraction	–
N_s	number of species	–
$\underline{\mathbf{I}}$	identity matrix	–
$\mathbf{w}$	state-local vector of conserved variables	various
$\underline{\mathbf{f}}$	flux term	various
$\underline{\mathbf{s}}$	source term	various
$\mathbf{x}$	position vector	m
$\mathbf{u}$	fluid velocity	m/s
$\mathbf{v}$	diffusion velocity	m/s
a	speed of sound	m/s
c	speed of light	m/s
t	time	s
m	mass	kg
$\mathbf{m}$	momentum vector	$kg/\left(m^2\ s\right)$
$\mathbf{f}$	general specific external force	N/kg
$\mathcal{R}$	universal gas constant	$J/\left(kg\ mol\right)$
k_B	Boltzmann's constant	J/K
$\mathcal{M}$	molar mass	kg/mol
p	pressure	Pa
T	temperature	K
n	density number	$1/m^3$
q	charge	C
$\dot{\mathbf{q}}$	conduction heat flux	W/m^2
$\dot{\mathcal{Q}}$	heat production rate	W/m^3
c_p	specific heat capacity at constant pressure	$J/\left(kg\ K\right)$
c_v	specific heat capacity at constant volume	$J/\left(kg\ K\right)$
e	specific energy	J/kg
h	specific enthalpy	J/kg
E	specific total energy	J/kg
H	specific total enthalpy	J/kg
$\mathbf{j}$	density current	A/m^2
$\mathbf{J}$	mass diffusion flux	$kg/\left(m^2\ s\right)$
$\mathbf{E}$	electric field	N/C
$\mathbf{B}$	magnetic field	T

Greek symbols

ε	mass ratio	$-$
γ	heat capacity ratio	$-$
δ	boundary layer thickness	m
ρ	density	kg/m^3
ρ_c	density charge	C/m^3
$\underline{\tau}$	viscous stress tensor	Pa
μ	dynamic viscosity	$kg/(m\ s)$
λ	thermal conductivity	$W/(m\ K)$
σ	electrical conductivity	S/m
ν	kinematic viscosity	m^2/s
κ	thermal diffusivity	m^2/s
ν_m	magnetic diffusivity	m^2/s
μ_0	vacuum permeability	H/m
ε_0	vacuum permittivity	F/m
$\dot{\omega}$	net chemical production rate	$kg/(m^3\ s)$

Sub- and Super-scripts

e	electrons
h	heavy particles
w	wall
i	particle i or i-th spatial direction
j	particle j or j-th spatial direction
F	frozen
E	equilibrium
$ref.$	reference
$appl.$	applied
$ind.$	induced
$amb.$	ambipolar
$conv.$	convection
$cond.$	conduction

Chapter 1

Introduction

Plasmas are ionized gas mixtures. They have a lot of applications in the aerospace field and others. For instance, we need to consider a plasma when we are studying the solar wind [56], or the thermonuclear fusion [23]. In the aerospace field, a large amount of applications are related to the hypersonic regime, the atmospheric entry problem, the plasma propulsion with the Hall trusters, etc... In this work, we will use the High-Order Unifying Framework [59] to develop a computational physical model which can take into account the effects of the application of external electric and magnetic fields on the ionized gas mixture. The presence of free electrons in the gas is a consequence of the high-temperature effects. Indeed, when we are considering the hypersonic regime, the behavior of the fluid is not like in the normal conditions. We are in the hypersonic regime when the Mach number is very high and, in the region post-shock, the temperature increases significantly. For this reason, we cannot consider the gas as perfect. The classical laws drop down, new effects appear, the gas can be chemically reacting, thus it can conduct electricity. This is one of the main problems that, in every space mission, we need to consider. In the re-entry phase (see figure 1.1), as a consequence of strong bow shocks, plasmas appear in the region around the body. In this context, two aspects are crucial: thermal protection system to mitigate the heat fluxes at the wall and preserve the life of astronauts and the telecommunication blackout. The latter is present when the plasma frequency is greater than the radio frequency, thus the signal is reflected. There are different possibilities to mitigate this phenomenon. One of them is regarding the decrease of the plasma frequency. This is possible if we reduce the number of electrons present in a particular region. In order to make it, the application of external electric and magnetic fields can be used. This Master's Thesis project is under the MEESST project of The von Karman Institute for Fluid Dynamics and other Universities and Institutes.

Figure 1.1: Spacecraft during atmospheric entry in the hypersonic regime. Presence of ionized gas mixture (i.e. plasma) in the region behind the strong bow shock. The picture was taken from `https://meesst.eu/technology/`.

1.1   Dimensionless parameter in magnetogasdynamics

Plasma could be considered the four-*th* state of matter. Indeed, it is particular characteristics that are not present in the solid, liquid, and gas states. When the temperature is very high the molecules of the gases start to dissociate. New degrees of freedom are present in the study of the gas mixture. Magneto-Fluid Dynamics studies the behavior of the fluids with the presence of electromagnetic fields. They could be externally applied, or coming from the internal nature of the mixture. In this section, we enumerate the principal dimensionless parameters that are useful in magnetogasdynamics. We have the Reynolds number, the Magnetic Reynolds number, the Hartmann number, the Stuart number, the Mach number, the Prandtl number, the Peclet number, the Alfven number, the Damkohler number, the Knudsen number, the Magnetic force number, the Deybe length, and the plasma frequency which is typical in the study of blackout telecommunication. It reads

$$f_p = \frac{\omega_p}{2\pi} = \frac{1}{2\pi}\sqrt{\frac{n_e e^2}{m_e \varepsilon_0}} \tag{1.1}$$

1.2   Hypersonics and Magneto-Fluid Dynamics

Hypersonic is a regime of fluid motion that appears when the body reaches high velocity with respect to the velocity of sound. In other words, we can call hypersonic the fluid motion for all the Mach numbers greater than 5. However, this is not a clear line between supersonics and hypersonics. Indeed, like in all the physical problems, we cannot distinguish with a clear threshold two different fluid motion regimes. Consequently, Ma = 5 was chosen as a limit over which some physical characteristics become more important than in the other flow regimes. Hypersonics is a very common situation during the atmospheric re-entry, when the spacecraft goes very fast and, for instance for Apollo spacecraft, the Mach number reached also 36. In addition, the hypersonic regime is extremely important in the current days, and during the last years, many studies were conducted to satisfy the request to develop hypersonic transport aircraft to reduce the time of the flights. For these reasons hypersonics is an important part of modern studies in compressible flows.
In hypersonics, as a consequence of the high velocities, shock waves are always near the wall. Hence, the thin shock layer appears. It has many complications in the treatment of hypersonic motion because in a small region close to the wall we will have the boundary layer (subsonic and supersonic) and the shock waves. They could interact, complicating the entire flow field. In addition, again due to the high velocities, behind the shock high-temperature effects are present. This physical aspect does not permit us to treat of the gas as ideal or calorically perfect, because all its thermodynamic properties are now dependent on the pressure and the temperature itself. New degrees of freedom are involved in a fluid motion. Vibrational degrees of freedom are the first to appear. Indeed, the first immediate consequence of the high-temperatures is the change in molecules' behavior. In normal conditions, when the temperature is not high, all the molecules are characterized to have two types of degrees of freedom: the *translational* and the *rotational*. The first one does not depend on the molecules' structure, in other words, the translational degrees are always three as a consequence of the space as a three-dimensional domain. Rotational degrees of freedom, instead, depending on the molecules' structure. These are the typical degrees of freedom during the study of subsonic flows. As mentioned before, when the velocities increase, as a consequence of the high temperatures, in the region post-shock the molecules start to oscillate and behave like a spring. For this reason, the first degrees of freedom that we need to add in the study of hypersonic flows are the *vibrational* ones. Consequently, again with the increasing of the temperature, the molecules become more

exciting. Moreover, chemical reactions appear and atoms could lose some of their electrons. To take into account this effect we need to introduce also the *electronic* degrees of freedom. But this is not the last one, because, when free electrons are present in the gases, obviously they have previously left their atoms. Hence, the latter is now charged positive, in other words also the presence of ions has to be considered. Therefore, also *ionization* degrees of freedom is introduced. When the flow is composed of electrons and heavy particles we can call it partially ionized plasmas. This is the typical situation that appears in the region post-shock of a blunt body when it is immersed in the high-speed flow, such that Ma $\gg$ 1. These are not the only differences between hypersonic and the other flow regime of motion. Indeed, until now, the viscous effects are not mentioned. In the subsonic boundary layer it is well known that the thickness δ of the boundary layer only depends on the local Reynolds number, thus

$$\delta \propto \frac{1}{\sqrt{\text{Re}_x}} \tag{1.2}$$

instead, in hypersonics, also the effects of the pressure become important with respect to the inertial forces. As a consequence, the thickness of the boundary layer is proportional also to the Mach number as follows

$$\delta \propto \frac{\text{Ma}^2}{\sqrt{\text{Re}_x}} \tag{1.3}$$

thus, in hypersonic flows, we are expecting a boundary layer thickness bigger than in the subsonic case. We need also to remember that, as explained before, it is confined in the thin shock layer. Hence, from this discussion, now it is more clear why the hypersonic boundary layer could interact with shock waves with a general complication of the problem.

One of the first scientists who studied the hypersonic regime was Newton. Nowadays, some preliminary analysis are conducted with his theory. The Newtonian Theory gives us a mathematical description of what the percentage inclination of the shock waves is with respect to the inclination of the wall. It is shown that this ratio depends only on the ratio between the specific heat at constant pressure and constant volume. In addition, it expresses also one of the most important concepts of the hypersonics, therefore the Mach number independence. Indeed, all the quantities that we want to compute in the region behind the shock, at one particular value of the Mach number will not change anymore even if the Mach number is increasing continuously. As a consequence, no changes in the engineering quantities of interest are present. Therefore, the forces acting on the body will remain the same. This is one of the most particular aspects of hypersonics. Many examples and well detailed explanations are present in [1]; [2].

Magneto-Fluid Dynamics (MFD) offers several advantages in aerospace applications, e.g. propulsion systems like innovative plasma thruster, external flow control, reduction of wall heat flux, moving of strong bow shock to reduce the high-temperature characteristic behind it, hypersonic vehicle design. All these aspects are typical of the hypersonic regime. During the past years, a lot of papers were developed to study the problem and to build possible numerical strategies to couple together the Navier-Stokes equations, the Maxwell equations, and chemical ones concerning non-thermochemical equilibrium. MacCormack investigate possible numerical strategy [33]; [34]; [32]; [31]. D'Ambrosio and Giordano investigated the bow shock in presence of imposed solenoid magnetic fields under different conditions of the flow field [18]. They use bidimensional simulations over a blunt body in order to evaluate the effects related to having coupled the Navier-Stokes with the Maxwell equations.

In this Master's Thesis work we are going to evaluate the effects of an external applied electric and magnetic field in a flow at high velocity and high-temperature, typical of the supersonic and hypersonic regime of the motion. In this sense, the presence of the magnetic

and electric fields could be derived from other numerical simulations on the same domain. The three-dimensional functional distribution of electromagnetic field can be used as an input file for the code that we are going to develop in this Master's Thesis project.

1.3   High-Order Unifying Computational Framework

The code used in this Master's Thesis work was developed by Woopen, Balan and May [59]. It is a solver based on High-Order discretization. In addition, also hybridization is possible, hence it includes both DG and HDG methods. Several publications are present in literature about the comparison between DG and HDG method to solve the same problem [60]; [58]. The code is linked with other external libraries to allow to include mesh generation, adaptation techniques, and physical aspects related to high-temperature flows. The latter are taken into account with the usage of Mutation++ [52]; [51]. The interface between the code and the external library was developed by Devesse in his Research Master's project at The von Karman Institute for Fluid Dynamics [20]. In this work, the same idea is applied to extend this interface to compute the physical quantities that we want.

The High-Order Unifying Computational Framework is written in C++, it is based on object-oriented programming (OOP) and it is designed to be modular. In this sense, new physical models can be created starting from the already existing and, based on the `DummyModel.h` file. The code uses the Newton-Raphson method to solve the non-linear system that originates from the DG or HDG discretization. Devesse worked on this code and developed several high-enthalpy flow models, both for Euler and Navier-Stokes equations, and a multispecies model [20].

The code requests the Jacobian matrix. To avoid to the developers to coding all the jacobian for each model, the code was structured to use the Automatic Differentiation (AD) algorithm to assemble the Jacobians of the fluxes. As a consequence, a new data type is introduced in the code. It is `AutoDiff` and it stores both the value of the quantities and the derivatives with respect to the chosen variables. This was one of the most difficult issues that Devesse overcame in his project. This is a complete computer science argument. We refer to [20] for other related discussions. Figure 1.2 shows the general scheme for the code used in this project.
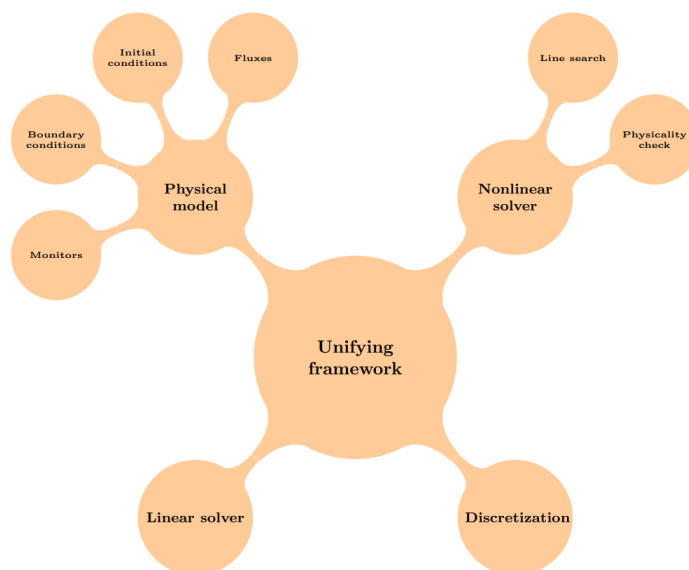
Figure 1.2: High-Order Unifying Framework conceptual scheme. The picture was taken from [59].

1.4 Mutation++

Mutation++ (M++) is a library written in C++ using the OOP. It was developed at The von Karman Institute for Fluid Dynamics [52]; [51]. Its name derives from an acronym: MUlticomponent Thermodynamic And Transport properties for IONized gases in C++. Mutation++ permits us to create the mixture that we want to test through `Mixture object` inside our code. It has been already used in other codes: Atkins and Deiterding used M++ in their FV solver [3] for high Mach number simulations, the same has been done by Gomes, et al [21] in SU2 solver [48], Schrooyen et al. [49] coupled their DG solver with M++ to study material ablation for high-enthalpy flows.

Mutation++ gives the thermodynamic, transport, kinetic, and gas surface interaction terms that are used to close the set of equations that the CFD solver will compute. All these quantities depend on the temperature, pressure, etc... Then, pair the solver and M++ is the major challenge to consider. Figure 2.6 shows the general scheme for Mutation++ library used in this work.
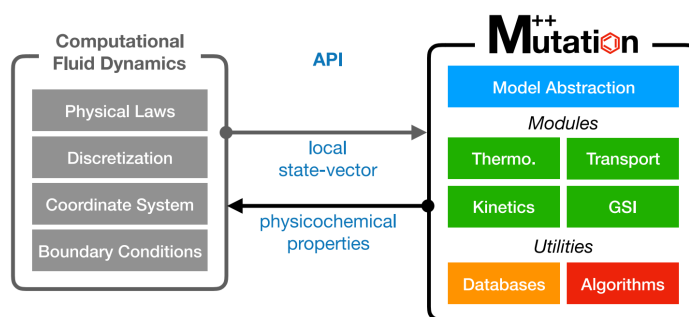
Figure 1.3: Mutation++ conceptual scheme. The picture was taken from [59].

1.5 Aim

The goal of this project is to develop a Magneto-Fluid Dynamics model for low Magnetic Reynolds numbers. In this context, the classical Navier-Stokes system must be coupled with the effects of external forces related to the applied magnetic and electric fields. Hence, the code that we are going to develop in this Master's Thesis project will allow us to make numerical simulation taking into account the effects of high-temperature and also the presence of constant and externally applied electric and magnetic fields that, for instance, can be given in input as the output of other purely electromagnetic simulations.

1.6 Outline

This Master's Thesis work is organized as follows. In Chapter 2, starting from the BTE and with the usage of the Chapman-Enskong method, we will obtain the different contributions, both for the Euler and the Navier-Stokes equations, in the transport properties. Hence, a general description of the effects of high-temperature and the magnetic field will be presented (in the flow chart 1.4 corresponds to "Physical model"). In Chapter 3, the balance laws for MFD will be shown. Different approximation levels are presented, hence, under the assumptions of the continuous regime, frozen flow, and the absence of induced magnetic field, we will write the mathematical equations of our physical model (in the flow chart 1.4 is expressed by "Mathematical model"). In Chapter 4, a general overview of the typical numerical methods to approximately solve PDEs will be present. Hence, at the end,

the high-order discretization based on the HDG methods will be displayed. In Chapter 5, the High-Order Unifying Framework will be analyzed. Finally, the implementation of the model will be explained. In Chapter 6, the validation of the model for the Euler and the Navier-Stokes equations will be demonstrated. To prove them, a comparison with the analytical data provided by the Hartmann flow will be illustrated (all the last steps, in the flow chart 1.4 are inside "Analytical solution"). Then, in Chapter 7, possible future works will be indicated.
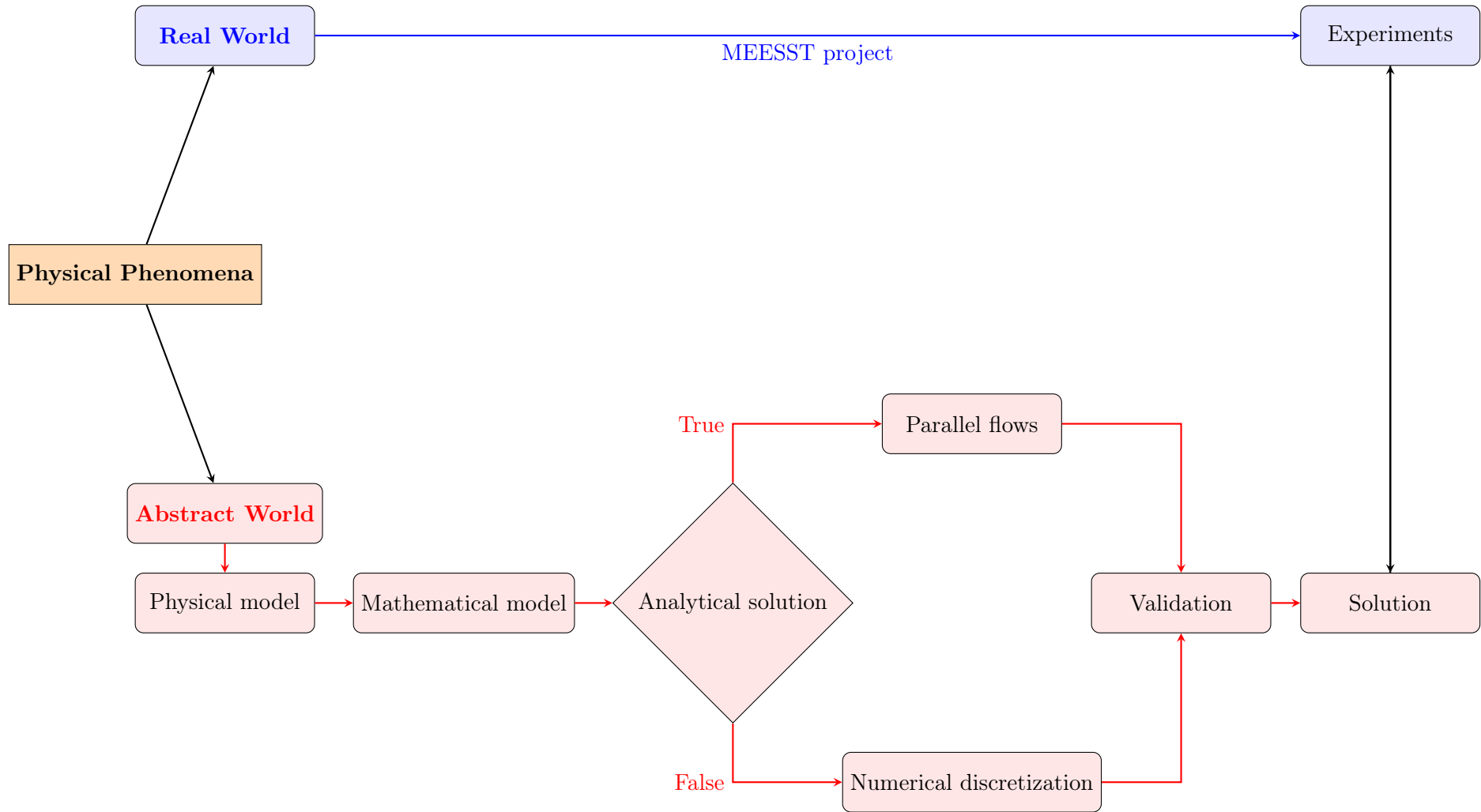
Figure 1.4: Flow chart of the typical engineering approach to study a physical problem. The same will be applied during this Master's Thesis. We are going to consider only the red path.

Chapter 2

From BTE to transport properties

In the most general case, we can consider a gas mixture composed of N_s species, each of them denotes by an index and belonging to the set $\mathcal{S}$, which stores both heavy particles and electrons. From a mathematical point of view, for heavy particles, we write

$$i \in \mathcal{S}_h = \{1, ..., N\} \tag{2.1}$$

and, at the same time, for the electrons, we write

$$\mathcal{S}_e = \{e\} \tag{2.2}$$

bringing all together

$$j \in \mathcal{S} = \mathcal{S}_h \cup \mathcal{S}_e = \{1, ..., N, e\} = \{1, ..., N_s\} \tag{2.3}$$

2.1 Dimensional analysis

In this section, we will show which are the typical spatial and temporal scales in ionized gas mixtures at very high temperatures. To make it possible, the approach of [23] is strictly followed. It is well known that plasma is a reactive ionized gas mixture where we can find the presence of free electrons. As a consequence, it is obvious that, in the most general case, we need to write different equations for each different component. Hence, we will have two sets of equations: one for heavy particles (all the species that are present in our gas mixture) and the other set for free electrons.

Firstly, we need to introduce, like in every dimensional analysis, the reference values. As already said, we are considering two main components, which ratio between their masses is expressed by the following dimensionless parameter

$$\varepsilon = \sqrt{\frac{m_e}{m_h}} \tag{2.4}$$

where m_e is the mass of electrons, while m_h is associated with the mass of heavy particles. This is a very small parameter that drives the thermal non-equilibrium between the electrons and heavy particles. In this description, in the asymptotic fluid limit, the Knudsen number is also thought to be the same order of magnitude as the square root of the previous ratio, i.e. $\text{Kn} \sim \sqrt{\varepsilon}$ [23]. In this context, as a consequence that $\varepsilon \ll 1$, the continuity assumption is verified, thus $\text{Kn} \ll 1$.

By the kinetic theory, in plasmas are present two different velocity scales. The first thermal speed is associated with electrons

$$u_{e,ref.} = \sqrt{k_B \frac{T_{ref.}}{m_{e,ref.}}} \tag{2.5}$$

and the second one to heavy particles

$$u_{h,ref.} = \sqrt{k_B \frac{T_{ref.}}{m_{h,ref.}}} \tag{2.6}$$

The ratio between the two thermal speeds is, again, well expressed by the ε parameter, hence

$$\varepsilon = \sqrt{\frac{m_{e,ref.}}{m_{h,ref.}}} = \frac{u_{h,ref.}}{u_{e,ref.}} \tag{2.7}$$

where $T_{ref.}$ is the dimensional reference temperature. In general, in non-equilibrium we have two different values for the temperature, that is to say, one for heavy particles and one for electrons. It is easy to understand that, if we are considering thermal equilibrium, those two values will be equal. Heavy particles and electrons are continuously subjected to collisions. Their differential cross-sections are of the same order of magnitude. Therefore, the typical mean free molecular path l can be considered identical for all the species in this simplified treatment, hence

$$l_{e,ref.} = l_{h,ref.} = l_{ref.} \tag{2.8}$$

thus, one microscopic reference length is present in this work. On the other hand, the same concept cannot be applied to the time scales. Indeed, having the same order of reference length but, not the same order of thermal speed, we end immediately that electrons and heavy particles do not have the same time scale. In particular, starting from the classical definition of time like the ratio between length and velocity, for electrons the microscopic reference time reads

$$t_{e,ref.} = \frac{l_{e,ref.}}{u_{e,ref.}} = \frac{l_{ref.}}{u_{e,ref.}} \tag{2.9}$$

while for heavy particles

$$t_{h,ref.} = \frac{l_{h,ref.}}{u_h, ref.} = \frac{l_{ref.}}{u_{h,ref.}} \tag{2.10}$$

Hence, two microscopic reference time scales are present, while only one for the length. Consequently, this justifies the presence of two different thermal speeds are present in this analysis.

Now, we would like to analyze the same at the macroscopic level. It is possible to define a dimensional reference macroscopic length, called $L_{ref.}$, form which we can define the Knudsen number like the ratio between the microscopic dimensional reference length and the macroscopic one, namely

$$\text{Kn} = \frac{l_{ref.}}{L_{ref.}} \tag{2.11}$$

In addition, by the definition of macroscopic dimensional reference length, we can define also a macroscopic dimensional reference time. Remembering that it is comparable with the microscopic reference time of heavy particles divided by the square root of the mass's ratio, we have

$$t_{ref.} = \frac{L_{ref.}}{u_{ref.}} = \frac{t_{h,ref.}}{\varepsilon} \tag{2.12}$$

hence, three-dimensional reference time exists in this work. Two are microscopic, the third one is macroscopic. All are related to the mass ratio, therefore we can write

$$\varepsilon = \sqrt{\frac{m_{e,ref.}}{m_{h,ref.}}} = \frac{u_{h,ref.}}{u_{e,ref.}} = \sqrt{\frac{t_{e,ref.}}{t_{ref.}}} = \frac{t_{h,ref.}}{t_{e,ref.}} \tag{2.13}$$

At this point, it is important to introduce a new dimensionless parameter that will be useful in this Chapter: it is the *pseudo-Mach number*. It expresses the ratio between the mean velocity of the fluid and the mean heavy particles velocity. It is supposed to be of order one [23], thus

$$\text{Ma}_h = \frac{u_{ref.}}{u_{h,ref.}} \sim 1 \tag{2.14}$$

therefore, we can assume

$$\|\mathbf{u}\|_2 \sim \|\mathbf{u}_h\|_2 \tag{2.15}$$

The last introduction allows us to find a link between the Knudsen number and the pseudo-Mach number. Indeed, starting from the definition of Knudsen number, substituting the definition of macroscopic dimensional reference time and, finally, remembering that the microscopic dimensional reference length is identical for all the species, the Knudsen number reads

$$\text{Kn} = \frac{l_{ref.}}{L_{ref.}} = \frac{l_{e,ref.}}{t_{ref.}u_{ref.}} = \frac{l_{h,ref.}}{t_{ref.}u_{ref.}} \tag{2.16}$$

then, we need to remind that the macroscopic dimensional reference time can be linked to the microscopic dimensional reference heavy particles time introducing the ε parameter. In this way, we will obtain

$$\text{Kn} = \frac{l_{e,ref.}}{L_{ref.}} = \varepsilon^2 \frac{u_{e,ref.}}{u_{ref.}}$$
$$\text{Kn} = \frac{l_{h,ref.}}{L_{ref.}} = \varepsilon \frac{u_{h,ref.}}{u_{ref.}} \tag{2.17}$$

the first expression needs to be manipulated again. Firstly, we need to express the ratio between the dimensional reference electron thermal speed to the reference dimensional macroscopic velocity as functional of ε. Then, remembering that $t_{e,ref.} = \varepsilon^2 t_{ref.}$, we have

$$\text{Kn} = \frac{l_{e,ref.}}{L_{ref.}} = \varepsilon^2 \frac{u_{e,ref.}}{u_{ref.}} = \varepsilon^2 \frac{u_{e,ref.}}{u_{h,ref.}} \frac{u_{h,ref.}}{u_{ref.}} = \varepsilon \frac{u_{h,ref.}}{u_{ref.}} \tag{2.18}$$

hence, by the definition of pseudo-Mach number, we finally obtain

$$\text{Kn} = \frac{l_{ref.}}{L_{ref.}} = \frac{l_{e,ref.}}{t_{ref.}u_{ref.}} = \frac{l_{h,ref.}}{t_{ref.}u_{ref.}} = \frac{\varepsilon}{\text{Ma}_h} \ll 1 \tag{2.19}$$

where the continuty assumpiton is expressed by $\text{Kn} \ll 1$
.

Secondly, plasmas are characterized by the presence of electric and magnetic fields. In this way, during dimensional analysis, we need to take into account also them. Assuming that the reference electric field satisfies

$$E_{ref.} = \frac{k_B T_{ref.}}{q_{ref.}L_{ref.}} \tag{2.20}$$

such that the intensity of the magnetic field is governed by the Hall parameter, which again has a different expression for electrons and heavy particles, respectively

$$\beta_e = \frac{q_{ref.}B_{ref.}}{m_{e,ref.}} t_{e,ref.} = \varepsilon^{1-b}$$
$$\beta_h = \frac{q_{ref.}B_{ref.}}{m_{h,ref.}} t_{h,ref.} = \varepsilon^{2-b} \tag{2.21}$$

where, we introduced the Larmor frequencies for electrons and heavy particles $q_{ref.}B_{ref.}/m_{ref.}$ multiplied by the respectively kinetic time. In this sense, the magnetic field is assumed

Table 2.1: Possible b values.

b	Ionized mixture
< 0	Unmagnetized
$= 0$	Weakly magnetized
$= 1$	Strongly magnetized

to be proportional to a power of the mass ratio through the integer parameter b, which expresses the magnetization level of plasma. In particular, we can observe that b parameter must not be greater than one for a physical reason. Table 2.1 shows possible extreme values of b and their respectively physical meanings

In addition, we have assumed that the magnetic field is low such that $\beta_e \ll$ Kn. Consequently, from the definitions given we have

$$\varepsilon^{1-b} \ll \frac{\varepsilon}{\text{Ma}_h} \tag{2.22}$$

which reads

$$\varepsilon^b \gg \text{Ma}_h \tag{2.23}$$

thus, since the pseudo-Mach number is assumed to be of the same order of magnitude of one and $b \leq 1$, the mass ratio parameter has to be very small.

Summing up, the small parameter ε that we have introduced in this section gave the possibility to define three-time scales: two microscopic and one macroscopic. On the other hand, only two reference lengths are present: one for the microscopic description and another one for the macroscopic one. Hence, three different velocities have been introduced: two are thermal speed and describe the physical behavior of electrons and heavy particles, the third one describes a macroscopic point of view. Finally, the references for electric and magnetic fields have been introduced thanks to Hall parameter and Larmor frequencies. It is important to show that

$$\varepsilon = \sqrt{\frac{m_{e,ref.}}{m_{h,ref.}}} = \frac{u_{h,ref.}}{u_{e,ref.}} = \sqrt{\frac{t_{e,ref.}}{t_{ref.}}} = \frac{t_{h,ref.}}{t_{ref.}} = \frac{t_{e,ref.}}{t_{h,ref.}} = \frac{\beta_h}{\beta_e} = \text{Kn Ma}_h \ll 1 \tag{2.24}$$

Introducing the Magnetic Reynolds number like the Hall parameter for electrons, we have

$$\text{Re}_m = \beta_e = \varepsilon^{1-b} \ll \text{Kn} = \frac{\varepsilon}{\text{Ma}_h} \ll 1 \tag{2.25}$$

hence, it also satisfies the assumption $\text{Re}_m \ll 1$, namely the magnetic field induced is negligible. In this Master's Thesis work we will show how this assumption drives us through the definition of the classical Navier-Stokes or the Euler equations with the additional of the electromagnetic source term, according to [15]. These equations will be found within the Chapman-Enskog perturbative method starting from Boltzmann equation [23].

From this point, for the rest of only this Chapter, we will refer to dimensionless variables. They are obtained starting from the normalization by the reference values just introduced. To simplify the notation, reference quantities are denoted by the subscript $ref.$, while dimensional quantities by the superscript $*$. In this context, for instance, the dimensionless time and the dimensionless length are, respectively

$$t = \frac{t^*}{t_{ref.}}, \qquad \mathbf{x} = \frac{\mathbf{x}^*}{L_{ref.}} \tag{2.26}$$

2.2 BTE: Boltzmann Transport Equation

The Boltzmann equation (BTE, Boltzmann Transport Equation) describes with a statical approach the behavior of a system in thermal non-equilibrium, in which there are some gradients, hence transport fluxes are present. This equation does not provide us the perfect position in the space of each particle, but it can predict a possible statistical distribution function of all the quantities that we want to study.

The BTE is non-linear where the unknown variable is the probability distribution function in the phase domain, thus in six-dimensional space: three dimensions for the space and the other three for the velocity space.

Generally, it is also used to determine the characteristic properties of the fluid. In addition, with some approximation, from the BTE it is also possible to obtain the Euler and the Navier-Stokes equations. To make it possible, the Chapman-Enskog method has been used [23].

The general BTE reads

$$\frac{\mathrm{D}f}{\mathrm{D}t} = \left(\frac{\partial f}{\partial t} \right)_{coll.} \tag{2.27}$$

where, in the RHS, there is the presence of convection, diffusion, and collision between different particles. In the next pages, we are going to develop all these terms. It is important to remember that, in classical physical space $(t, \mathbf{x})$, the total derivate reads

$$\begin{aligned} \frac{\mathrm{D}f}{\mathrm{D}t} &= \frac{\partial f}{\partial t} + (\nabla_{\mathbf{x}} f) \cdot \frac{\mathrm{d}\mathbf{x}}{\mathrm{d}t} \\ &= \frac{\partial f}{\partial t} + (\nabla_{\mathbf{x}} f) \cdot \mathbf{c} \end{aligned} \tag{2.28}$$

while, when we are considering the phase space domain $(t, \mathbf{x}, \mathbf{c})$, it shall be as follows

$$\begin{aligned} \frac{\mathrm{D}f}{\mathrm{D}t} &= \frac{\partial f}{\partial t} + (\nabla_{\mathbf{x}} f) \cdot \frac{\mathrm{d}\mathbf{x}}{\mathrm{d}t} + (\nabla_{\mathbf{c}} f) \cdot \frac{\mathrm{d}\mathbf{c}}{\mathrm{d}t} \\ &= \frac{\partial f}{\partial t} + (\nabla_{\mathbf{x}} f) \cdot \mathbf{c} + (\nabla_{\mathbf{c}} f) \cdot \frac{\mathbf{F}^{ext}}{m} \end{aligned} \tag{2.29}$$

where there were applied the general definitions of velocity and acceleration. Hence, the velocity is the derivative of the space with respect to time, while the acceleration is the derivative of the velocity with respect to time. Bringing together equation 2.27 and equation 2.29, we have the classical BTE where we can easily find the convection and the diffusion terms

$$\frac{\partial f}{\partial t} + \underbrace{(\nabla_{\mathbf{x}} f) \cdot \mathbf{c}}_{\text{convection}} + \underbrace{(\nabla_{\mathbf{c}} f) \cdot \frac{\mathbf{F}^{ext}}{m}}_{\text{diffusion}} = \left(\frac{\partial f}{\partial t} \right)_{coll.} \tag{2.30}$$

where the external force is goven by $\mathbf{F}^{ext} = q (\mathbf{E} + \mathbf{c} \times \mathbf{B})$. The LHS of equation 2.30 is called *streaming operator* $\mathcal{D}_i (f_i)$, while its RHS is called *scattering collision operator* J_i. Hence, with this substitution, the BTE could be also written, in a more syntetic form, as follow

$$\mathcal{D}_i (f_i) = J_i \tag{2.31}$$

Being exact, the scattering collision operator reads

$$J_i = \sum_{j \in S} J_{ij} (f_i, f_j) \tag{2.32}$$

where

$$J_{ij} (f_i, f_j) = \int \left(f_i' f_j' - f_i f_j \right) (\|\mathbf{c}_i - \mathbf{c}_j\|_2) \, \sigma_{ij} \, \mathrm{d}\omega \, \mathrm{d}\mathbf{c}_j \tag{2.33}$$

where $\sigma_{i,j}$ is the differential cross-section, which mathematical expression is

$$\sigma_{ij} = \sigma_{ij}\left(\mu_{ij}\frac{(\|\mathbf{c}_i - \mathbf{c}_j\|_2)^2}{k_B T_{ref.}}, \boldsymbol{\omega} \cdot \mathbf{e}\right) \tag{2.34}$$

where we have

$$\mu_{ij} = \frac{m_i m_j}{m_i + m_j} \tag{2.35}$$

and

$$\mathbf{e} = \frac{\mathbf{c}_i - \mathbf{c}_j}{\|\mathbf{c}_i - \mathbf{c}_j\|_2} \tag{2.36}$$

where $\boldsymbol{\omega}$ is the relative velocity given by

$$\boldsymbol{\omega} = \frac{\mathbf{c}'_i - \mathbf{c}'_j}{\|\mathbf{c}'_i - \mathbf{c}'_j\|_2} \tag{2.37}$$

i.e. the same quantity denotes by $\mathbf{e}$ but computed after the collision. In other words, $\mathbf{e}$ and $\boldsymbol{\omega}$ represent two relative velocities, the first one before the collision, the second one after the collision.

This section is based on the kinetic theory, which is, for some aspects, different from the classical fluid dynamic description. Indeed, in the fluid dynamic description the gas is modeled as continuos (Kn $\ll$ 1) in terms of macroscopic variables (e.g. $\rho = \rho(t, \mathbf{x})$, or $\mathbf{u} = \mathbf{u}(t, \mathbf{x})$, thus we are referring to the physical space). Instead, in the kinetic description, we assume the mixture composed by a set of species $i \in \mathcal{S} = \mathcal{S}_h \cup \{e\}$ that follow a velocity distribution function f_i in the phase space $(t, \mathbf{x}, \mathbf{c}_i)$, i.e. the possible set of all the positions $\mathbf{x}$ and momenta $\mathbf{c}_i$. In this space, the number of particles that have their position and velocity value in the range of $\mathbf{x}$ and d$\mathbf{x}$, is defined from the probability density function as $dN = f(t, \mathbf{x}, \mathbf{c}_i)\,d^3\mathbf{x}d^3\mathbf{c}_i$. As already said, the mixture is composed of ions, atoms, electrons, and neutral particles, hence all of them contribute to the global property of the fluid. In the following sections, we strictly follow the work [23]. However, a more accurate description is present in [39].

2.3   Macroscopic properties

According to [23], we define the the scalar product as follows

$$\langle\langle \xi, \zeta \rangle\rangle = \sum_{j \in \mathcal{S}} \int \xi_j \odot \overline{\zeta}_j \, d\mathcal{C}_j \tag{2.38}$$

where $\overline{\zeta}_j$ is the conjugate transpose of ζ_j and the symbol $\odot$ represents the fully contracted product in space. Consequently, in this context, in [23] is shown that the macroscopic properties (density, momentum, and total energy) can be expressed as scalar products of the distribution functions and the collisional invariants. Indeed, we have

$$\begin{cases} \rho_i = \langle\langle f, \psi^i \rangle\rangle, & i \in \mathcal{S} = \{1, ..., N_s\} \\ \rho(\mathbf{v}_d - \mathbf{u}_d) = \langle\langle f, \psi^{N_s+d} \rangle\rangle, & d \in \{1, 2, 3\} \\ \rho\left(e + \frac{(\|\mathbf{v} - \mathbf{u}\|_2)^2}{2}\right) = \langle\langle f, \psi^{N_s+4} \rangle\rangle \end{cases} \tag{2.39}$$

where we have introduced the the collisional invariants expressed into axes moving with the gas mixture, that are

$$\begin{cases} \psi^j = (m_i \delta_{ij})_{i \in \mathcal{S}}, & j \in \mathcal{S} \\ \psi^{N_s+d} = (m_i \mathbf{C}_{id})_{i \in \mathcal{S}}, & d \in \{1, 2, 3\} \\ \psi^{N_s+4} = \left(\frac{1}{2} m_i \mathbf{C}_i \cdot \mathbf{C}_i\right)_{i \in \mathcal{S}}, & d \in \{1, 2, 3\} \end{cases} \tag{2.40}$$

2.4 Chapman-Enskog method

Firstly we need to write the Boltzmann equation in dimensionless form for electrons and heavy particles. Respectively, we have

$$\frac{\partial f_e}{\partial t} + (\mathbf{u}_h + \mathbf{C}_e) \cdot \nabla_{\mathbf{x}} f_e + \left(\frac{F_e}{m_e} - \frac{D\mathbf{u}_h}{Dt} \right) \cdot \nabla_{\mathbf{C}_e} f_e - (\nabla_{\mathbf{C}_e} f_e \otimes \mathbf{C}_e) : \nabla \mathbf{u}_h = ...$$

$$... = \sum_{j \in \mathcal{S}} \int \left(f_e' f_j' - f_e f_j \right) \left(\|\mathbf{c}_e - \mathbf{c}_j\|_2 \right) \sigma_{ej} \ d\omega \ d\mathbf{c}_j \tag{2.41}$$

and, for heavy particles ($\forall \ i \in \mathcal{S}_h$) we have

$$\frac{\partial f_i}{\partial t} + (\mathbf{u}_h + \mathbf{C}_i) \cdot \nabla_{\mathbf{x}} f_i + \left(\frac{F_i}{m_i} - \frac{D\mathbf{u}_h}{Dt} \right) \cdot \nabla_{\mathbf{C}_i} f_i - (\nabla_{\mathbf{C}_i} f_i \otimes \mathbf{C}_i) : \nabla \mathbf{u}_h = ...$$

$$... = \sum_{j \in \mathcal{S}} \int \left(f_i' f_j' - f_i f_j \right) \left(\|\mathbf{c}_i - \mathbf{c}_j\|_2 \right) \sigma_{ij} \ d\omega \ d\mathbf{c}_j \tag{2.42}$$

In order to find an approximate solution of the Boltzmann equations for electrons and heavy particles, referring to [23]; [36] we use Enskog expansion.

In the Chapman-Enskog method, the ionized gas mixture is described at successive order of the ε parameter. The number of the order is chosen according to the different time scales that we analyzed before.

Firstly, we need to introduce the species distributions functions for electrons and heavy particles, respectively

$$f_e = f_e^0 \left[1 + (\varepsilon \phi_e) + (\varepsilon \phi_e)^2 + (\varepsilon \phi_e)^3 \right] + \mathcal{O}\left(\varepsilon^4 \right)$$

$$f_i = f_i^0 \left[1 + (\varepsilon \phi_i) + (\varepsilon \phi_i)^2 \right] + \mathcal{O}\left(\varepsilon^3 \right), \qquad \forall i \in S_h \tag{2.43}$$

where f_e^0 and f_i^0 are the zero-*th* order solution which satisfy the Maxwellian distribution functions at different temperatures. To be exact

$$f_e^0 = n_e \left(\frac{m_e}{2\pi k_B T_e} \right)^{\frac{3}{2}} \exp \left(-\frac{m_e C_e}{2 k_B T_e} \right)$$

$$f_i^0 = n_i \left(\frac{m_i}{2\pi k_B T_i} \right)^{\frac{3}{2}} \exp \left(-\frac{m_i C_i}{2 k_B T_i} \right), \qquad \forall i \in \mathcal{S}_h \tag{2.44}$$

In this work, the focus is only based on the Euler and the Navier-Stokes equations. A brief description of the electrons equations for the same level of approximation is present but, for a more accurate discussion, we remind to [23]. For these reasons, we will immediately study the orders ε^0 and ε^1, without considering the lower orders which correspond to the two microscopic time scales. However, always in [23] a long work describes every step.

Table 2.2: Resume and definitions of electrons variables.

Order	Time	Heavy particles, $i \in \mathcal{S}_h$	Electrons, $\{e\}$
ε^0	$t_{ref.}$	Euler	0-th Drift-Diffusion
ε^1	$t_{ref.}/\varepsilon$	Navier-Stokes	1-st Drift-Diffusion

At this point, we substitute the Maxwellian distribution function onto the BTE equation, then we multiplied the BTE by the collisional invariants and we obtain

$$\psi_i^m \mathcal{D}_i\left(f_i\right) = \psi_i^m J_i, \qquad m \in \{1, ...N_s, ..., N_s + d, N_s + d + 1\} \tag{2.45}$$

hence, integration over the velocity yields gives us

$$\int \psi_i^m \mathcal{D}_i\left(f_i\right) \, \mathrm{d}\mathbf{c}_i = \int \psi_i^m J_i\left(f_i\right) \, \mathrm{d}\mathbf{c}_i, \qquad m \in \{1, ...N_s, ..., N_s + d, N_s + d + 1\} \tag{2.46}$$

then, we need to sum up the species. In addition, with the usage of the property of the collisional invariants [23]; [36], we obtain the global conservation equation

$$\langle\langle\psi^m, \mathcal{D}\rangle\rangle = 0, \qquad m \in \{1, ...N_s, ..., N_s + d, N_s + d + 1\} \tag{2.47}$$

All the details of the derivations can be found in [39]; [23]; [36].
The same procedure needs to be repeated at each approximation level.

2.4.1   Order zero-*th*

Finding this solution we will obtain the Euler equations for the heavy particles and the zero-*th* order drift-diffusion equations for electrons.

Heavy particles

We obtain three balance laws: continuity, momentun and energy.

$$\frac{\partial \rho_i}{\partial t} + \nabla \cdot \left(\rho_i \mathbf{u}_h\right) = 0$$

$$\frac{\partial\left(\rho_h \mathbf{u}_h\right)}{\partial t} + \nabla \cdot \left(\rho_h \mathbf{u}_h \otimes \mathbf{u}_h + \frac{1}{\mathrm{Ma}_h^2}p\underline{\mathbf{I}}\right) = \frac{1}{\mathrm{Ma}_h^2}nq\mathbf{E} + \mathbf{j}_0 \times \mathbf{B} \tag{2.48}$$

$$\frac{\partial\left(\rho_h e_h\right)}{\partial t} + \nabla \cdot \left[\left(\rho_h e_h + p_h\right) \mathbf{u}_h\right] = \Delta E_0^{h \to e}$$

where $\Delta E_0^{h \to e}$ is the energy transfered from the heavy particles to the electrons. In addition, summing the first equations all over the heavy species $i \in \mathcal{S}_h$, we have the classical continuity equation

$$\frac{\partial \rho_h}{\partial t} + \nabla \cdot \left(\rho_h \mathbf{u}_h\right) = 0 \tag{2.49}$$

Electrons

We obtain two balance laws: continuity and energy.

$$\frac{\partial \rho_e}{\partial t} + \nabla\left(\rho_e \mathbf{u}_h + \frac{1}{\mathrm{Ma}_h}\rho_e \mathbf{v}_e\right) = 0$$

$$\frac{\partial\left(\rho_e e_e\right)}{\partial t} + \nabla \cdot \left[\left(\rho_e e_e + p_e\right) \mathbf{u}_h\right] = -\frac{1}{\mathrm{Ma}_h}\nabla \cdot \dot{\mathbf{q}}_e + \frac{1}{\mathrm{Ma}_h}\mathbf{J}_e \cdot \mathbf{E}' + \Delta E_0^{e \to h} \tag{2.50}$$

where $\Delta E_0^{e \to h}$ is the zero-*th* order energy transfered from the electrons to the heavy particles.

It is important notice that no equations for the momentum is written. This is one of the most important aspects about the description of the electrons' behaviour. They partecipate to the global mass and global energy, but not in the global momentum. Or rather, their contribution in the global momentum equation is only present in the pressure gradient and, of course, in the Lorentz force. No additional terms.

One particular attention is required for the energy equations of heavy particles and electrons. In the heavy particles we introduced the energy transfered from from heavy particles to electrons like $\Delta E_0^{h\to e}$, while, in the energy electrons equation we have written the energy transfered from electrons to heavy particles like $\Delta E_0^{e\to h}$. Obviously, these two terms are equal in magnitude, but they have opposite sign. Indeed, if a determinate quantity is trasfered from heavy particles to electrons, this means that heavy particles in that situation are losing energy, but, in the same moment, electrons acquire it. In other words, if we consider the plasma with One-Fluid model, we do not need to take into account this contribution, because the sum of these two terms is zero. Moreover, if we are considering a Two-Fluid model, different equation for heavy particles and electrons need to be written, and we need to introduce it. Nevertheless, their global contribution is null. Hence, from a mathematical point of view

$$\Delta E_0^{h\to e} + \Delta E_0^{e\to h} = 0 \qquad (2.51)$$

Summary of the zero-th order

We have just obtained equations two continuity and two energy equations for heavy particles as well as for electrons, but only one momentum equation for heavy particles. All these equations are written in non inertial reference system, thus we have introduced $\mathbf{J}_e$ which is the electrons conduction current in this reference system and $\mathbf{E}' = \mathbf{E} + \text{Ma}_h \mathbf{u}_h \times \mathbf{B}$, i.e. the electric field in heavy particles reference system. Of course, we can write the same equations in an inertial reference system by substituting $\mathbf{J}_e$ with $\mathbf{j}_e$ and $\mathbf{E}'$ with $\mathbf{E}$. These will be arguments of the next Sections.

2.4.2 Order one-*st*

We need to introduce the following defintions for heavy particles

Heavy particles

$$\frac{\partial \rho_i}{\partial t} + \nabla \cdot \left(\rho_i \mathbf{u}_h + \frac{\varepsilon}{\text{Ma}_h} \rho_i \mathbf{v}_i \right) = 0$$

$$\frac{\partial \rho_h \mathbf{u}_h}{\partial t} + \nabla \cdot \left(\rho_h \mathbf{u}_h \otimes \mathbf{u}_h + \frac{1}{\text{Ma}_h^2} p \underline{\mathbf{I}} \right) + \frac{\varepsilon}{\text{Ma}_h^2} \nabla \cdot (\underline{\boldsymbol{\tau}}_h + \underline{\boldsymbol{\tau}}_e) = \frac{1}{\text{Ma}_h^2} nq\mathbf{E} + (\mathbf{j}_0 + \mathbf{j}) \times \mathbf{B}$$

$$\frac{\partial (\rho_h e_h)}{\partial t} + \nabla \cdot (\rho_h e_h \mathbf{u}_h) + (p_h \underline{\mathbf{I}} + \varepsilon \underline{\boldsymbol{\tau}}_h) : \nabla \mathbf{u}_h = -\frac{\varepsilon}{\text{Ma}_h} \nabla \cdot \dot{\mathbf{q}}_h + \frac{\varepsilon}{\text{Ma}_h} \mathbf{J}_h \cdot \mathbf{E}' + ...$$

$$... + \Delta E_0^{h\to e} + \varepsilon \Delta E_1^{h\to e}$$

$$(2.52)$$

where $\Delta E_1^{h\to e}$ is the first order energy transfered from the heavy particles to the electrons. In addition, summing the first equations all over the heavy species $i \in \mathcal{S}_h$, we have again

$$\frac{\partial \rho_h}{\partial t} + \nabla \cdot (\rho_h \mathbf{u}_h) = 0 \qquad (2.53)$$

In other words, the contributon of the mass diffusion is null if we take into account all the species.

Electrons

$$\frac{\partial \rho_e}{\partial t} + \nabla \left(\rho_e \mathbf{u}_h + \frac{1}{\text{Ma}_h} \rho_e \mathbf{v}_e + \frac{\varepsilon}{\text{Ma}_h} \mathbf{v}_e^2 \right) = 0$$

$$\frac{\partial \left(\rho_e e_e \right)}{\partial t} + \nabla \cdot \left(\rho_e e_e \mathbf{u}_h \right) + p_e \nabla \cdot \mathbf{u}_h = -\frac{1}{\text{Ma}_h} \nabla \cdot \left(\dot{\mathbf{q}}_e + \varepsilon \dot{\mathbf{q}}_e^2 \right) + \frac{1}{\text{Ma}_h} \left(\mathbf{J}_e + \varepsilon \mathbf{J}_e^2 \right) \cdot \mathbf{E}' + ...$$

$$... + \varepsilon \text{Ma}_h \mathbf{J}_e \cdot \mathbf{u}_h \times \mathbf{B} + \Delta E_0^{e \rightarrow h} + \varepsilon \Delta E_1^{e \rightarrow h}$$

$$\tag{2.54}$$

where $\Delta E_1^{e \rightarrow h}$ is the first order energy transfered from the electrons to the heavy particles.

Summary of the first order

From the definition of Knudsen number (see equation 2.19) and, with the initial assumption $\text{Ma}_h \sim 1$, we can write the last equations in a more compact form. In this way, we emphasize the scale on which the transport takes place. It is well known that we are considering the continuous model, thus $\text{Kn} \ll 1$. In this context, the last equations put in evidence which are the principal terms involved in the physical description. These equations will be manipulated in the next pages to obtain something more useful for our project.

Note that these equations are always written in a non-inertial reference system which is moving with the mean flow velocity $\mathbf{u}$.

2.5   Transport fluxes

Solving the conservative equations, we need to introduce some closure equations in order to compute the viscous stress tensor, the heat flux, and the density current. These three terms are related to the thermodynamic and transport properties of the flow. In this section, we will analyze how they can be computed.

All the following expressions are obtained in the most generalized case for weakly or unmagnetized plasmas in thermochemical non-equilibrium, thus two temperatures are present. Instead, in the case of thermochemical equilibrium is easy to get the equations from the ones just mentioned, with the only constrain $T_e = T_h = T$.

2.5.1   Notation

In the most general case the transport fluxes are anisotropic, that is their mathematical translation is a tensor. It is important to remember that this is valid only in the presence of a strong magnetic field applied. In the case of weakly and unmagnetized plasmas, the transport coefficients are well expressed by the isotropic functions, i.e. scalar quantity. In order to generalize the treatment, we need to introduce the unit vector of the magnetic field as

$$\mathcal{B} = \frac{\mathbf{B}}{\|\mathbf{B}\|_2} \tag{2.55}$$

then the following matrices

$$\underline{\mathbf{M}}^{\|} = \mathcal{B} \otimes \mathcal{B}$$

$$\underline{\mathbf{M}}^{\perp} = \underline{\mathbf{I}} - \mathcal{B} \otimes \mathcal{B}$$

$$\underline{\mathbf{M}}^{\odot} = \begin{pmatrix} 0 & -\mathcal{B}_3 & \mathcal{B}_2 \\ \mathcal{B}_3 & 0 & -\mathcal{B}_1 \\ -\mathcal{B}_2 & \mathcal{B}_1 & 0 \end{pmatrix} \tag{2.56}$$
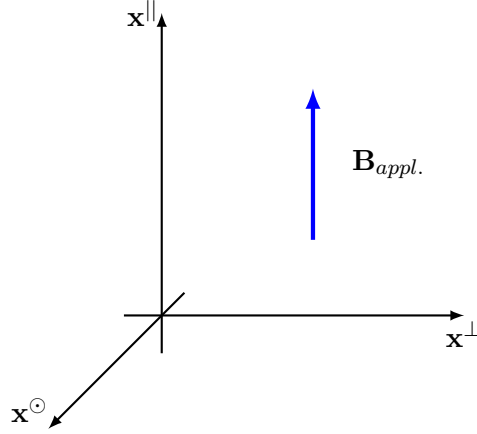
Figure 2.1: Notation for anisotropic transport coefficients.

hence, the vector $\mathbf{x}$ can be spitted into

$$\mathbf{x}^{||} = \underline{\mathbf{M}}^{||}\mathbf{x}$$
$$\mathbf{x}^{\perp} = \underline{\mathbf{M}}^{\perp}\mathbf{x} \tag{2.57}$$
$$\mathbf{x}^{\odot} = \underline{\mathbf{M}}^{\odot}\mathbf{x}$$

where, in the $(\mathbf{x}, \mathcal{B})$ plane, $\mathbf{x}^{||}$ is the component of $\mathbf{x}$ parallel to $\mathbf{B}$, $\mathbf{x}^{\perp}$ is the perpendicular direction with respect the magnetic field, while $\mathbf{x}^{\odot}$ in in the transverse direction. In additon, it is simple to verified that $\mathbf{x} = \mathbf{x}^{||} + \mathbf{x}^{\perp}$. Figure 2.1 shows what just explained. In the most general case, when strongly magnetic fields are externally applied, the transport coefficients are anisotropic, given by

$$\underline{\boldsymbol{\mu}} = \underline{\mathbf{M}}^{||}\mu^{||} + \underline{\mathbf{M}}^{\perp}\mu^{\perp} + \underline{\mathbf{M}}^{\odot}\mu^{\odot} \tag{2.58}$$

where μ is the general transport coefficients that we want to analyze. It is important to note that this is the most complicated situation. Indeed, when we are considering not strongly magnetized plasmas, for instance, the weakly magnetized ($b = 0$) or the unmagnetized case ($b < 0$), the anisotropic structure of transport coefficients drops down. In these last situations, the transverse component of the transport coefficient is the first to vanish $\mu^{\odot} = 0$, while the perpendicular transport coefficient tends to the parallel one, i.e. $\mu^{\perp} \to \mu^{||}$. From a physical point of view, this means that transport is efficient in the same plane where the magnetic field is present, while no transport is present in the transverse direction.

2.5.2 Diffusion driving forces

In this section, we introduce the diffusion driving force for electrons and heavy particles.

Electrons

The first-order electrons diffusion driving force reads, according to [23], as follows

$$\mathbf{d}_e = \frac{1}{p_e}\left(\nabla p_e - n_e q_e \mathbf{E}'\right) \tag{2.59}$$

while, the second-order electrons diffusion driving force is given by

$$\mathbf{d}_e^2 = -\frac{n_e q_e}{p_e}\mathrm{Ma}_h^2 \mathbf{u}_h \times \mathbf{B} \tag{2.60}$$

These are the mathematical expressions for strongly magnetized plasmas. We remember that the intensity of the magnetic field is taken into account by the b parameter. For strongly magnetized plasmas its value is one. When we are considering weakly magnetized or unmagnetized plasmas ($b = 0$ and $b < 0$, respectively), some modifications appear. Obviously, in these cases, the effect of the magnetic field is lower than in the previous, i.e. strongly magnetized plasma. In this sense, remembering that $\mathbf{E'} = \mathbf{E} + \mathbf{u}_h \times \mathbf{B}$ (with the approximation of the pseudo-Mach number), the second term in the RHS can be neglected. Hence, we will have for the first-order electrons diffusion driving force

$$\mathbf{d}_e = \frac{1}{p_e} \left(\nabla p_e - n_e q_e \mathbf{E} \right) \tag{2.61}$$

while no change is present in the second-order electrons diffusion driving force.

Heavy particles

The heavy particles diffusion driving force reads, according to [23], as follows

$$\mathbf{d}_i = \frac{1}{p_h} \left(\nabla p_i - n_i q_i \mathbf{E'} - n_i \mathbf{F}_{ie} \right), \qquad i \in \mathcal{S}_h \tag{2.62}$$

where $\mathbf{F}_{ie}$ is the average electron forces acting on the i-th heavy particles. This terms gives us the possibility to link the behaviour of heavy particles with the electrons one. The most general mathematical expression for the average electron force acting on the heavy particles i is the following

$$\mathbf{F}_{ie} = -\frac{p_e}{n_i \mathrm{Ma}_h} \left[\underline{\boldsymbol{\alpha}}_{ei} \mathbf{d}_e - \underline{\boldsymbol{\chi}}_i^e \nabla \left(\ln T_e \right) \right], \qquad i \in \mathcal{S}_h \tag{2.63}$$

where, with the initial assumption $\mathrm{Ma}_h \sim 1$, it reads

$$\mathbf{F}_{ie} = -\frac{p_e}{n_i} \left[\underline{\boldsymbol{\alpha}}_{ei} \mathbf{d}_e - \underline{\boldsymbol{\chi}}_i^e \nabla \left(\ln T_e \right) \right], \qquad i \in \mathcal{S}_h \tag{2.64}$$

Both the last equations show the link between hevay particles and electrons, The average electrons force that acts of heavy particle is proportional to the electron diffusion driving force and the electron temperature gradient through the electrons pressure and the mixture number density of the i-th heavy particle. In addition, we specify that $\underline{\boldsymbol{\alpha}}_{ei}$ and $\underline{\boldsymbol{\chi}}_i^e$ are the anisotropic transport coefficients. For weakly and unmagnetized plasmas, where the transverse coefficients drop down to zero and the perpendicular ones are identical to their parallel component, the simplified version of the average electron force acting on heavy particle i is presented as follows

$$\mathbf{F}_{ie} = -\frac{p_e}{n_i} \left[\alpha_{ei} \mathbf{d}_e - \chi_i^e \nabla \left(\ln T_e \right) \right], \qquad i \in \mathcal{S}_h \tag{2.65}$$

where α_{ei} and χ_i^e are the isotropic transport coefficients.
Equation 2.62 can be written again as function of only the temperature of hevay particles, thus thanks to the ideal gas law $p = \rho \mathcal{R} T / \mathcal{M} = n k_B T$, we have

$$\mathbf{d}_i = \frac{1}{n k_B T_h} \left(\nabla p_i - n_i q_i \mathbf{E'} - n_i \mathbf{F}_{ie} \right), \qquad i \in \mathcal{S}_h \tag{2.66}$$

then, substituiting equation 2.65 in last expression obtained, we will have

$$\mathbf{d}_i = \frac{1}{n k_B T_h} \left[\nabla p_i - n_i q_i \mathbf{E'} + p_e \alpha_{ei} \mathbf{d}_e - p_e \chi_i^e \nabla \left(\ln T_e \right) \right], \qquad i \in \mathcal{S}_h \tag{2.67}$$

2.5.3 Diffusion velocities

In this section we introduce the diffusion driving force for electrons and heavy particles.

Electrons

Kolesnikov [29] found how the thermal diffusion influences the heavy particles diffusion velocity
The first-order electrons diffusion velocity reads, according to [23], as follows

$$\mathbf{v}_e = -D_e \left[\mathbf{d}_e - \chi_e \nabla \left(\ln T_e \right) \right] \tag{2.68}$$

while, the second-order electrons diffusion velocity is given by

$$\mathbf{v}_e^2 = \sum_{j \in \mathcal{S}_h} \alpha_{ej} \mathbf{v}_j \tag{2.69}$$

Heavy particles

The heavy particles diffusion velocity of species $i \in \mathcal{S}_h$ reads, according to [23], as follows

$$\mathbf{v}_i = -\sum_{j \in \mathcal{S}_h} D_{ij} \left[\mathbf{d}_i + \chi_{h,j} \nabla \left(\ln T_h \right) - \frac{n_i}{p_h} \mathbf{F}_{ie} \right], \qquad i \in \mathcal{S}_h \tag{2.70}$$

where Kolesnikov included, also, the cross contribution electron temperature gradient multiplied by the thermal diffusion of electrons [29], i.e. the term $\chi_{e,j} \nabla \left(\ln T_e \right)$.
Equation 2.70 satisfies the mass conservation constrain

$$\sum_{j \in \mathcal{S}_h} \rho_j \mathbf{v}_j = 0 \tag{2.71}$$

2.5.4 Stress tensor

In this section, we introduce the stress tensor for electrons and heavy particles. In classical fluid dynamics, it is associated with the pressure contribution perpendicular to the surface and the viscous stress, governed by Newton's law. Here, the same concepts are present, but the introduction of electrons has to be taken into account. Obviously, the total stress tensor will be

$$\underline{\boldsymbol{\tau}} = \underline{\boldsymbol{\tau}}_e + \underline{\boldsymbol{\tau}}_h \tag{2.72}$$

Electrons

Electrons do not contribute to shear stress due to their mass disparity compared to heavy particles. Indeed, the dimensionless parameter ε is very small. Hence, we have

$$\underline{\boldsymbol{\tau}}_e = \underline{\mathbf{0}} \tag{2.73}$$

Heavy particles

The heavy particles viscous tensor reads, according to [23], as follows

$$\underline{\boldsymbol{\tau}}_h = -\mu_h \underline{\mathbf{S}} \tag{2.74}$$

where the tensor $\underline{\mathbf{S}}$ is defined, for Newtonian fluid with the application of Stokes' hypothesis, as follows

$$\underline{\mathbf{S}} = \nabla \mathbf{u}_h + \left(\nabla \mathbf{u}_h \right)^T - \frac{2}{3} \left(\nabla \cdot \mathbf{u}_h \right) \underline{\mathbf{I}} \tag{2.75}$$

Finally, we can obtain the general form of the stress tensor. No contribution of electrons must be considered. For this reason, we can omit the subscript h in the transport property. Hence, we have

$$\underline{\boldsymbol{\tau}} = -\mu \left[\nabla \mathbf{u}_h + (\nabla \mathbf{u}_h)^T - \frac{2}{3} (\nabla \cdot \mathbf{u}_h) \, \underline{\mathbf{I}} \right] \tag{2.76}$$

(a) μ.   (b) E_{amb}.
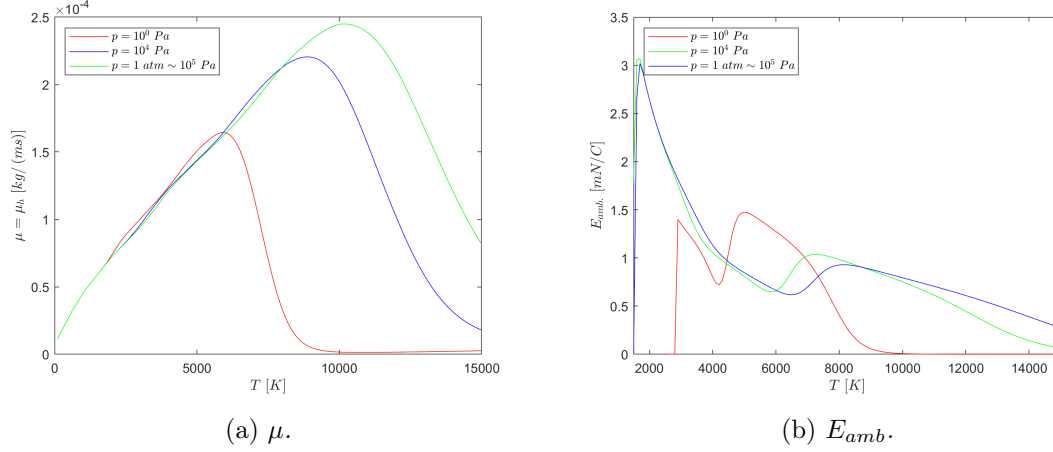
Figure 2.2: Effect of the pressure on the dynamic viscosity and the ambipolar electric field for air 11 species.

2.5.5   Heat flux

In the simplified situation, we can express the heat flux thanks to Fourier's laws, hence the heat flux is supposed to be proportional to the temperature local gradient through a coefficient, that we call thermal conductivity. It is important to remember that the negative sign, which is present in this Law, means that the heat transport is against the temperature gradient, that is the heat flux is from a hotter body to a colder one. However, Fourier's law is a strong simplification. In this section, we will show the main contribution of electrons and heavy particles in the total heat flux. Obviously, the total heat flux will be

$$\dot{\mathbf{q}} = \dot{\mathbf{q}}_e + \dot{\mathbf{q}}_h + \dot{\mathbf{q}}_e^2 \tag{2.77}$$

hence, according to [50], we have

$$\dot{\mathbf{q}} = - \left(\lambda_h + \lambda_e + \lambda_{Soret} + \lambda_R \right) \nabla T \tag{2.78}$$

where λ_R is the reactive thermal conductivity, and it can be expressed by the classical contribution and by the Brutler-Brokaw reactive thermal conductivity, as figure 2.3 shows.

(a) $\lambda_{reac.}$.

(b) λ_{bb}.

(c) *Variations.*

(d) *Error analysis.*
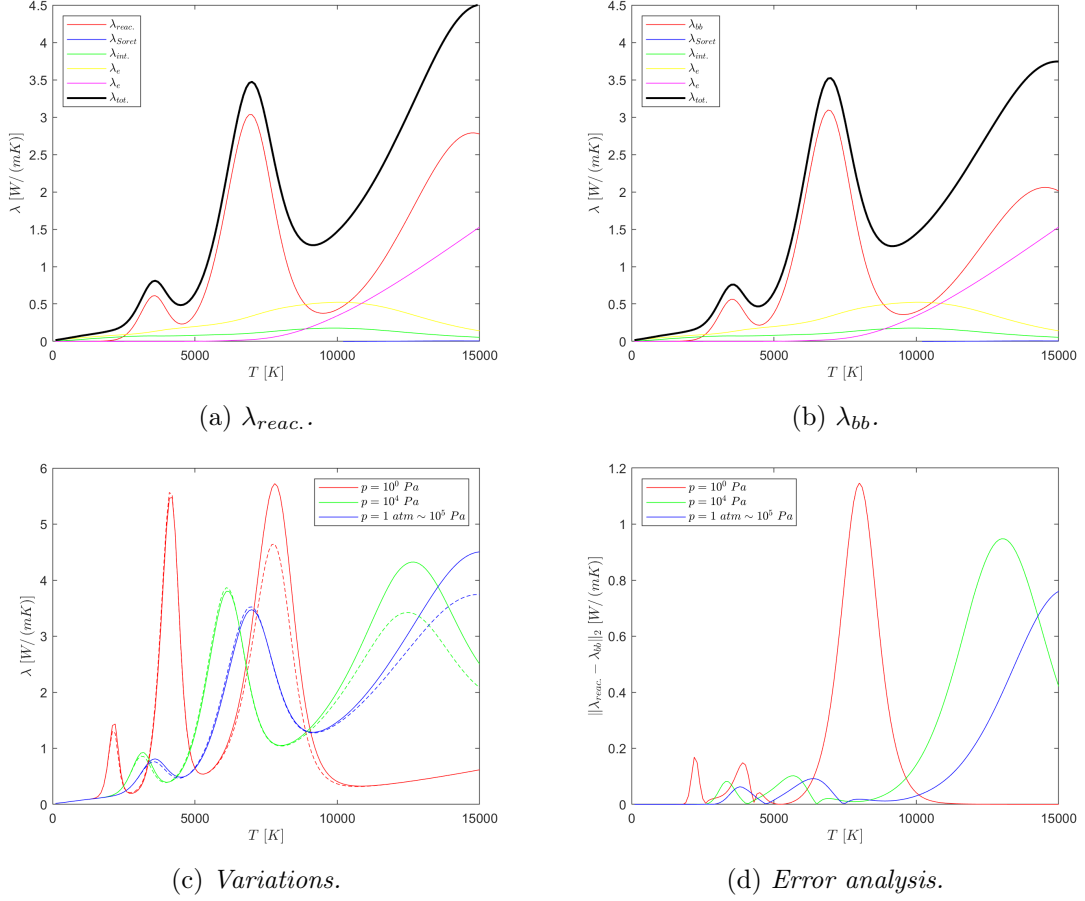
Figure 2.3: Contributions in thermal conductivity λ for air 11 species, $p = 1\ atm$. Reactive thermal conductivity and Brutler-Brokaw reactive thermal conductivity. Effect of the pressure on the different approximations.

Electrons

The first-order electrons heat flux reads, according to [23], as follows

$$\dot{\mathbf{q}}_e = -\lambda_e \nabla T_e + p_e \chi_e \mathbf{v}_e + \rho_e h_e \mathbf{v}_e \tag{2.79}$$

while, the second-order electrons heat flux is given by

$$\dot{\mathbf{q}}_e^2 = p_e \sum_{j \in \mathcal{S}_h} \chi_{e,j} \mathbf{v}_j + \rho_e h_e \mathbf{v}_e^2 \tag{2.80}$$

where the translational thermal conductivity λ_e and the thermal diffusion ratio $\chi_{e,Tj}$ of electrons are expressed with the second order Laguerre-Sonine approximation [36]; [35]. The effects on the thermal electron conductivity of the pressure and the magnetic field is shown in figure 2.4.

(a) $B = 0\ T$.

(b) $B = 2\ T$.

(c) $B = 0\ T$.

(d) $B = 2\ T$.

(e) $B = 0\ T$.

(f) $B = 2\ T$.
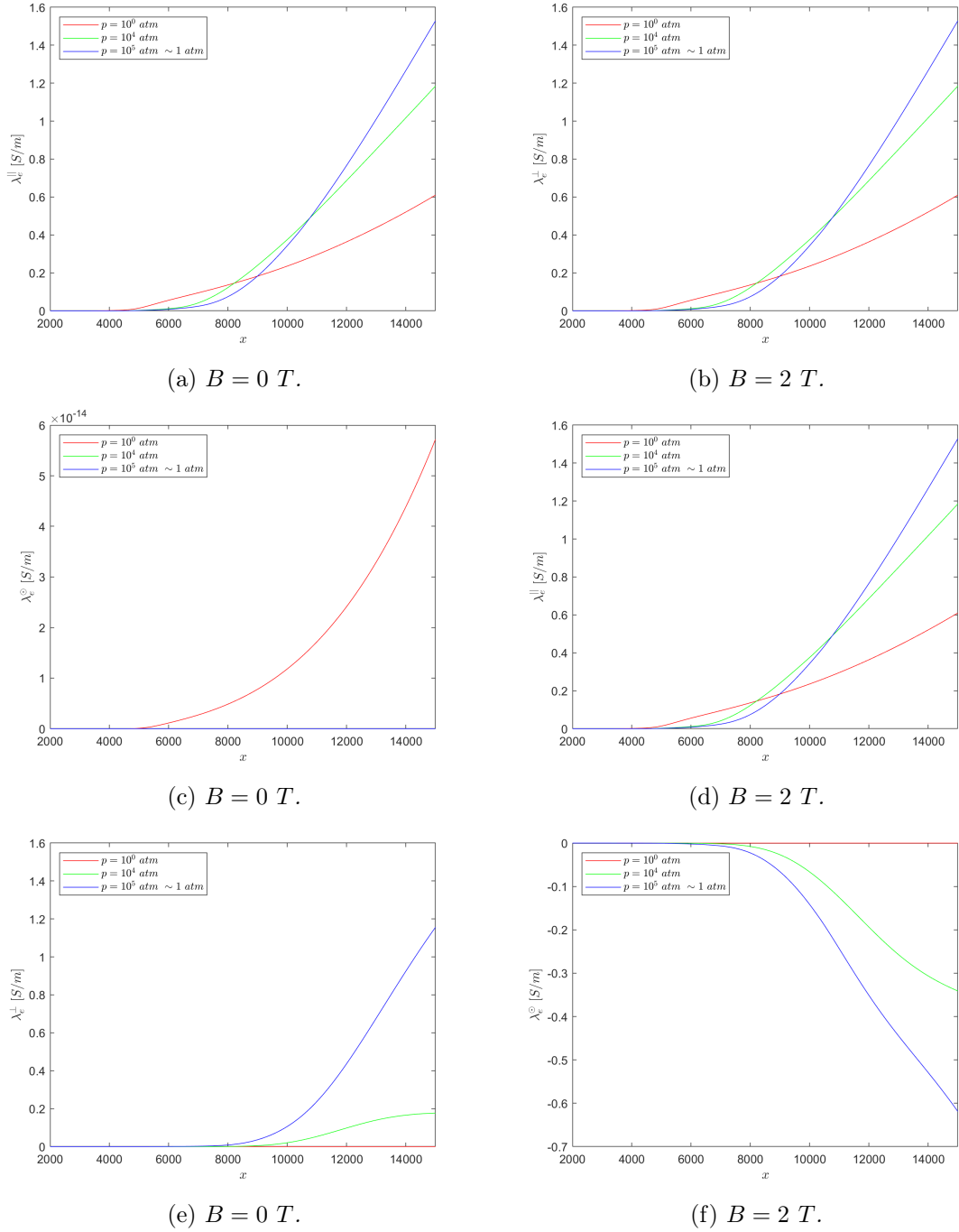
Figure 2.4: Anisotropic electron thermal conductivity. Effects of the pressure and the magnetic fields.

Heavy particles

The heavy particles heat flux reads, according to [23], as follows

$$\dot{\mathbf{q}}_h = -\lambda_h \nabla T_h + p_h \sum_{j \in \mathcal{S}} \chi_{h,j} \mathbf{v}_j + \sum_{j \in \mathcal{S}} \rho_j h_j \mathbf{v}_j \qquad (2.81)$$

where the translational thermal conductivity (λ_h) and the thermal diffusion ratio $(\chi_{h,Tj})$ of the *i-th* heavy particle are expressed with the second order Laguerre-Sonine approximation

[36]; [35]. In addition, h_i is the specific enthalpy. The latter is made up as follows

$$h_i = h_{T,i} + h_{F,i}, \qquad i \in \mathcal{S}_h \tag{2.82}$$

where $h_{T,i}$ is the specific translational enthalpy evaluated at the translational temperature T_h of the i-th heavy particle, while $h_{F,i}$ is the specific formation enthalpy.
Equation 2.81 can be also written as function of only the temperature of heavy particles, thus thanks to the ideal gas law $p = \rho \mathcal{R} T / \mathcal{M} = n k_B T$, we have

$$\dot{\mathbf{q}}_h = -\lambda_h \nabla T_h + n k_B T_h \sum_{j \in \mathcal{S}} \chi_{h,j} \mathbf{v}_j + \sum_{j \in \mathcal{S}} \rho_j h_j \mathbf{v}_j \tag{2.83}$$

Finally, from equation 2.83, the electrical conductivity is the sum of two contributions: the classical Fourier and the correction called Eucken. The first term is the dominant at low temperatures, where the behaviour of the thermal conductivity is similar to the dynamic viscosity. Indeed, we seek its approximation thanks to the Prandtl number defintion. Instead, the second term takes into account the rotational, vibrational and electronic thermal conductivity. Hence, its contribution is bigger at high temperature.

2.5.6 Density current

This is a crucial point for our work. Indeed, this Master's Thesis aims to introduce the electromagnetic source term to evaluate its effect on the classical solution of the Euler or the Navier-Stokes equations. In this context, the electrical conductivity of the mixture must not be equal to zero, because, if this should not be true, obviously the conduction current will be null, and, consequently, no source terms will be in our system. In this section, we introduce the contribution of electrons and heavy particles to the total electrical conductivity. The total heat flux will be

$$\mathbf{j} = \mathbf{j}_e + \mathbf{j}_h + \mathbf{j}_e^2 + n q \mathbf{u}_h \tag{2.84}$$

that stores both the conduction and convection contribution. In addition, the electrical conductivity reads

$$\sigma_e = \sum_{i,j \in \mathcal{S}} n_i q_i D_{ij} k_{ij} \tag{2.85}$$

which is present in the generalized Ohm's law for magnetized ionized gas mixtures (note the substitution of the mean heavy particles velocity with the mean velocity and the assumption of isotropic electrical conductivity, i.e. we are considering weakly or unmagnetized mixtures)

$$\mathbf{j} = n q \mathbf{u} + \sigma_e \left(\mathbf{E} + \mathbf{u} \times \mathbf{B} \right) - \sum_{i,j \in \mathcal{S}} \left[\frac{1}{n k_B T_h} \nabla p_j - \frac{y_j p}{n k_B T_h} \nabla \left(\ln p \right) \right] - \dots$$
$$\dots - \sum_{i,j \in \mathcal{S}} \left[\chi_{h,j} \nabla \left(\ln T_h \right) \chi_{e,j} \nabla \left(\ln T_e \right) \right] \tag{2.86}$$

which shows how the current flows. Three different mechanisms are presented: the first one is associated with the convection term (this is the term that, with the *MDH approximation*, is assumed to be null), the second one is related to the conduction term, while the last one is due to the presence of spatial temperature and pressure gradients. Generally, the order of magnitude of electron diffusion velocity with respect to that of heavy particles depends on the driving forces. In general, there are two common cases:

- **No spatial gradients**: in this situation, the density current is given only by the interactions between the electromagnetic field and the velocity field. No driving forces associated with pressure and thermal gradients are present. Hence, it can be shown that the heavy particles diffuse slower than the electrons, hence

$$\|\mathbf{v}_i\|_2 \ll \|\mathbf{v}_e\|_2, \qquad i \in \mathcal{S}_h = \mathcal{S} \backslash \mathcal{S}_e \tag{2.87}$$

thus, the total density current is dominated by the electrons' contribution, therefore

$$\mathbf{j} \simeq \mathbf{j}_e = n_e q_e \mathbf{v}_e \tag{2.88}$$

In this case, the electrical conductivity is given by

$$\sigma_e = n_e q_e D_{ee} k_e \tag{2.89}$$

where the electrical conductivity given in equation 2.89 is expressed by the first and the second order Laguerre-Sonine approximations [36] and [35].

- **Ambipolar assumption**: in this case, the electrons diffusion velocity is the same order of magnitude as that of ions, hence

$$\|\mathbf{v}_i\|_2 \sim \|\mathbf{v}_e\|_2, \qquad i \in \mathcal{S}_h \backslash \mathcal{S}_n \tag{2.90}$$

where $\mathcal{S}_n$ represents the set of neutral heavy particles. The ambipolar assumption written with its mathematical translation is

$$\sum_{j \in \mathcal{S}} x_j q_j \mathbf{v}_j = 0 \tag{2.91}$$

which meaning is that the conduction current is assumed to be zero, therefore

$$\mathbf{j} \sim 0 \tag{2.92}$$

Under the ambipolar assumption there is the possibility to have an electric field. This is shown as a function of the temperature in figure 2.2. The effects of the pressure and the magnetic field on the electrical conductivity are shown in figure 2.5.
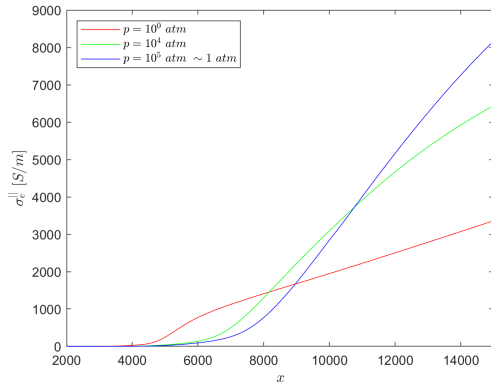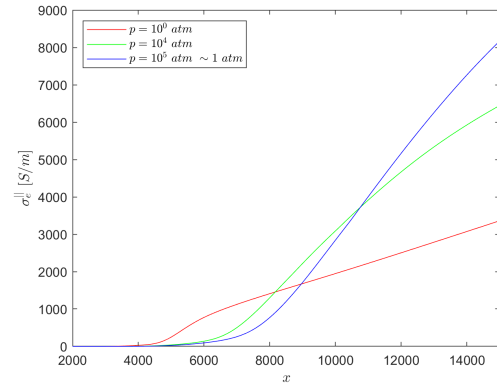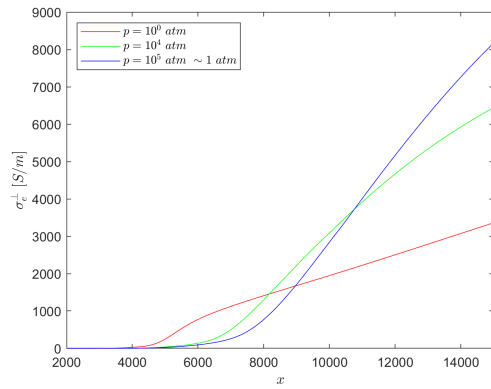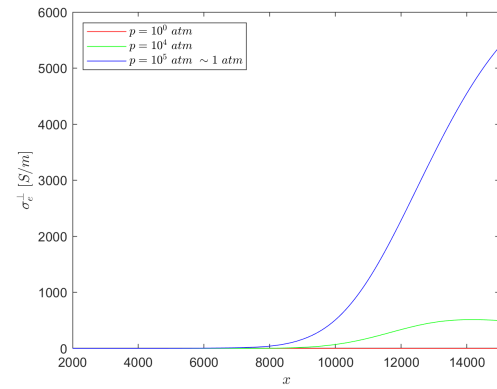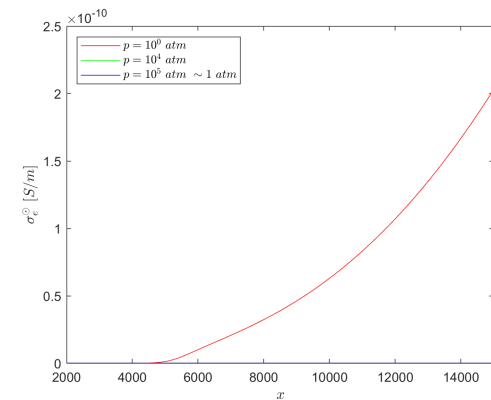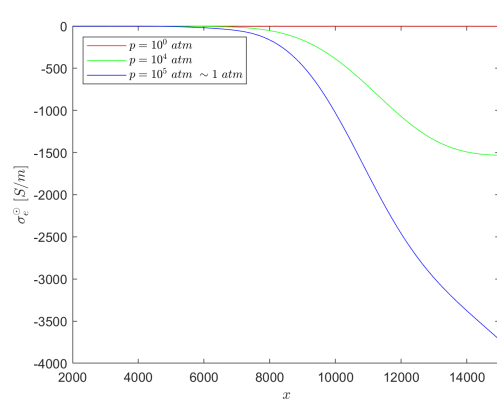
Figure 2.5: Anisotropic electrical conductivity. Effects of the pressure and the magnetic fields.

2.6   Overview of transport fluxes

In the previous sections, the description of all the different fluxes for electrons and heavy particles has been shown. Summing up, there are three main transport fluxes: diffusion velocity, stress tensor, and heat flux. General expressions for each one of them have been written in the previous sections. In these definitions, transport coefficients appear. They are what we need to compute to obtain the numerical solution. In general, we can say that they are strongly dependent on the temperature and the pressure of the mixture. These coefficients are well computed by the Mutation $++$ library [52]; [51]. Then, in the most general case, the transport matrices for electrons and heavy particles can be assembled and, finally, the fluxes will be computed. Here it is shown a general resume.

Table 2.3: Resume and definitions of heavy particles variables, general case.

Heavy particles, $i \in \mathcal{S}_h$	Simbol	Definition
Pressure	p_h	$n_h T_h$
Charge	$n_h q_h$	$\displaystyle\sum_{i \in \mathcal{C}} n_i q_i$
Diffusion velocity	$\mathbf{v}_i$	$\displaystyle\frac{1}{n_i} \int \mathbf{C}_i f_i \phi_i \ \mathrm{d}\mathbf{C}_i$
Mean species velocity	$\mathbf{u}_i$	$\mathbf{u}_h + \dfrac{\varepsilon}{Ma_h}\mathbf{v}_i$
Viscous tensor	$\underline{\boldsymbol{\tau}}_h$	$\displaystyle\sum_{i \in \mathcal{S}_h} \int m_i \mathbf{C}_i \otimes \mathbf{C}_i f_i \phi_i \ \mathrm{d}\mathbf{C}_i$
Conduction current density	$\mathbf{j}_h$	$\displaystyle\sum_{i \in \mathcal{S}_h} n_i q_i \mathbf{u}_i$
Heat flux	$\dot{\mathbf{q}}_h$	$\displaystyle\sum_{i \in \mathcal{S}_h} \int \frac{1}{2} m_i \mathbf{C}_i \cdot \mathbf{C}_i \mathbf{C}_i f_i \phi_i \ \mathrm{d}\mathbf{C}_i$

Table 2.4: Resume and definitions of heavy particles variables.

	Def.	$b \leq 1$
$\mathbf{d}_i$	Diffusion driving force	$\dfrac{1}{p_h}\left(\nabla p_i - n_i q_i \mathbf{E}' - n_i \mathbf{F}_{ie}\right)$
$\mathbf{v}_i$	$\dfrac{1}{n_i}\displaystyle\int \mathbf{C}_i f_i \phi_i \ \mathrm{d}\mathbf{C}_i$	$-\displaystyle\sum_{j\in\mathcal{S}_h} D_{ij}\mathbf{d}_j - \theta_i^h \nabla\left(\ln T_h\right)$
$\underline{\boldsymbol{\tau}}_h$	$\displaystyle\sum_{i\in\mathcal{S}_h}\int m_i \mathbf{C}_i \otimes \mathbf{C}_i f_i \phi_i \ \mathrm{d}\mathbf{C}_i$	$-\mu_h\left[\nabla\mathbf{u}_h + (\nabla\mathbf{u}_h)^T - \dfrac{2}{3}\left(\nabla\cdot\mathbf{u}_h\right)\underline{\mathbf{I}}\right]$
$\dot{\mathbf{q}}_h$	$\displaystyle\sum_{i\in\mathcal{S}_h}\int \dfrac{1}{2} m_i \mathbf{C}_i \cdot \mathbf{C}_i \mathbf{C}_i f_i \phi_i \ \mathrm{d}\mathbf{C}_i$	$\displaystyle\sum_{j\in\mathcal{S}}\rho_j h_j \mathbf{v}_j - \lambda_h \nabla T_h + nk_B T_h \sum_{j\in\mathcal{S}} k_{h,Tj}\mathbf{v}_j$

Table 2.5: Resume and definitions of electrons variables, general case.

Electrons, $\{e\}$	Simbol	Definition
Pressure	p_e	$n_e T_e$
Charge	$n_e q_e$	-
Diffusion velocity 1st order	$\mathbf{v}_e$	$\dfrac{1}{n_e}\displaystyle\int \mathbf{C}_e f_e \phi_e \ \mathrm{d}\mathbf{C}_e$
Diffusion velocity 2nd order	$\mathbf{v}_e^2$	$\dfrac{1}{n_e}\displaystyle\int \mathbf{C}_e f_e \phi_e^2 \ \mathrm{d}\mathbf{C}_e$
Mean electrons velocity 1st order	$\mathbf{u}_e$	$\mathbf{u}_h + \dfrac{1}{Ma_h}\mathbf{v}_e$
Mean electrons velocity 2st order	$\mathbf{u}_e^2$	$\mathbf{u}_e + \dfrac{\varepsilon}{Ma_h}\mathbf{v}_e^2$
Viscous tensor	$\underline{\boldsymbol{\tau}}_e$	$\displaystyle\int \mathbf{C}_e \otimes \mathbf{C}_e f_e \phi_e \ \mathrm{d}\mathbf{C}_e$
Conduction current density 1st order	$\mathbf{j}_e$	$n_e q_e \mathbf{u}_e$
Conduction current density 2nt order	$\mathbf{j}_e^2$	$n_e q_e \mathbf{u}_e^2$
Heat flux 1st order	$\dot{\mathbf{q}}_e$	$\displaystyle\int \dfrac{1}{2}\mathbf{C}_e \cdot \mathbf{C}_e \mathbf{C}_e f_e \phi_e \ \mathrm{d}\mathbf{C}_e$
Heat flux 2nd order	$\dot{\mathbf{q}}_e^2$	$\displaystyle\int \dfrac{1}{2}\mathbf{C}_e \cdot \mathbf{C}_e \mathbf{C}_e f_e \phi_e^2 \ \mathrm{d}\mathbf{C}_e$

Table 2.6: Resume and definitions of electrons variables, first order.

	Def.	$b \leq 0$
$\mathbf{d}_e$	Diffusion driving force	$\dfrac{1}{p_e}\left(\nabla p_e - n_e q_e \mathbf{E}'\right)$
$\mathbf{v}_e$	$\dfrac{1}{n_e}\displaystyle\int \mathbf{C}_e f_e \phi_e \, \mathrm{d}\mathbf{C}_e$	$-D_e \mathbf{d}_e - \theta_e \nabla\left(\ln T_e\right)$
$\underline{\boldsymbol{\tau}}_e$	$\displaystyle\int \mathbf{C}_e \otimes \mathbf{C}_e f_e \phi_e \, \mathrm{d}\mathbf{C}_e$	$\underline{\mathbf{0}}$
$\dot{\mathbf{q}}_e$	$\displaystyle\int \dfrac{1}{2}\mathbf{C}_e \cdot \mathbf{C}_e \mathbf{C}_e f_e \phi_e \, \mathrm{d}\mathbf{C}_e$	$-D_e \mathbf{d}_e - \theta_e \nabla\left(\ln T_e\right)$

Table 2.7: Resume and definitions of electrons variables, second order.

	Def.	$b \leq 0$
$\mathbf{d}_e^2$	Diffusion driving force	$-\dfrac{n_e q_e}{p_e}\mathrm{Ma}_h^2 \mathbf{u}_h \times \mathbf{B}$
$\mathbf{v}_e^2$	$\dfrac{1}{n_e}\displaystyle\int \mathbf{C}_e f_e \phi_e^2 \, \mathrm{d}\mathbf{C}_e$	$-\delta_{b0} D_e \mathbf{d}_e^2 - \displaystyle\sum_{j \in \mathcal{S}_h} \alpha_{ej} \mathbf{d}_j^2$
$\dot{\mathbf{q}}_e^2$	$\displaystyle\int \dfrac{1}{2}\mathbf{C}_e \cdot \mathbf{C}_e \mathbf{C}_e f_e \phi_e^2 \, \mathrm{d}\mathbf{C}_e$	$-\delta_{b0} p_e \theta_e \mathbf{d}_e^2 - p_e \displaystyle\sum_{j \in \mathcal{S}_h} \chi_j^e \mathbf{d}_j^2 + \rho_e h_e \mathbf{v}_e^2$

2.7 Conservation equations

In this section, we briefly summarize the equations obtained by using the Chapman-Enskng method. We will show how, starting from these sets, we will obtain the classical form of the Euler and the Navier-Stokes equations, keeping in mind the initial assumption $\mathrm{Ma}_h \sim 1$. Consequently, it is important to understand the physical contribution of the ε parameter. It is very small for the hypothesis introduced in [23]. Hence, in the next step, we can assume to neglecting these terms according to the previous works [36];[35]; [50]. Anyway, all the equations obtained read

$$\frac{\partial \rho_e}{\partial t} + \nabla \cdot (\rho_e \mathbf{u}_h) + \nabla \cdot (\rho_e \mathbf{v}_e) = \dot{\omega}_e$$

$$\frac{\partial \rho_i}{\partial t} + \nabla \cdot (\rho_i \mathbf{u}_h) + \nabla \cdot (\rho_i \mathbf{v}_i) = \dot{\omega}_i, \qquad\qquad i \in \mathcal{S}_h$$

$$\frac{\partial (\rho_h \mathbf{u}_h)}{\partial t} + \nabla \cdot (\rho_h \mathbf{u}_h \otimes \mathbf{u}_h + p\underline{\mathbf{I}}) - \nabla \cdot (-\underline{\boldsymbol{\tau}}_h) = nq\mathbf{E} + \mathbf{j}_h \times \mathbf{B}, \qquad\qquad i \in \mathcal{S}_h$$

$$\frac{\partial (\rho_e e_e)}{\partial t} + \nabla \cdot [(\rho_e e_e + p_e)\,\mathbf{u}_h] - \nabla \cdot (-\dot{\mathbf{q}}_e) = \mathbf{j}_e \cdot \mathbf{E} + \Delta E_0^{e\to h} + \Delta E_1^{e\to h}$$

$$\frac{\partial (\rho_h e_h)}{\partial t} + \nabla \cdot [(\rho_h e_h + p_h)\,\mathbf{u}_h] - \nabla \cdot \left(\underline{-\boldsymbol{\tau}}_h \mathbf{u}_h - \dot{\mathbf{q}}_h\right) = \mathbf{j}_h \cdot \mathbf{E} + \Delta E_0^{h\to e} + \Delta E_1^{h\to e}, \qquad i \in \mathcal{S}_h$$

$$(2.93)$$

now, remembering that the total pressure is defined as $p = p_e + p_h$, the totale mixture number density is $n = n_e + n_h$, the total mixture charged is defined as $\rho_c = nq = n_e q_e + \sum_{j \in \mathcal{S}_h} n_j q_j$, the total heat flux is $\dot{\mathbf{q}} = \dot{\mathbf{q}}_e + \dot{\mathbf{q}}_h + \dot{\mathbf{q}}_e^2$, the total stress tensor is only composed by the heavy particles contribution, the total density current is $\mathbf{j} = \mathbf{j}_e + \mathbf{j}_h + \mathbf{j}_e^2 + nq\mathbf{u}_h$, the total momentum is associated only with the heavy particles contribution, i.e. $\rho\mathbf{u} = \rho_h\mathbf{u}_h$, the mixture internal energy is $\rho e = \rho_e e_e + \rho_h e_h$, the total stress tensor is given only by the heavy particles contribution, i.e. $\underline{\boldsymbol{\tau}} = -\underline{\boldsymbol{\tau}}_h = \mu\underline{\mathbf{S}}$, while the total energy is $\rho E = \rho e + \rho_h \left(\|\mathbf{u}_h\|_2\right)^2/2$ (where the kinetic energy reads as reported in [23]), the heavy particles mean velocity corrisponds to the general velocity vector $\mathbf{u} = (u_1, ..., u_d)^T$ where d is the dimension of the problem, we have

$$\frac{\partial \rho_i}{\partial t} + \nabla \cdot (\rho_i \mathbf{u}) - \nabla \cdot (-\mathbf{J}_i) = \dot{\omega}_i, \qquad\qquad i \in \mathcal{S}_h$$

$$\frac{\partial (\rho\mathbf{u})}{\partial t} + \nabla \cdot (\rho\mathbf{u} \otimes \mathbf{u} + p\underline{\mathbf{I}}) - \nabla \cdot \underline{\boldsymbol{\tau}} = \rho_c\mathbf{E} + \mathbf{j} \times \mathbf{B} \qquad\qquad (2.94)$$

$$\frac{\partial (\rho E)}{\partial t} + \nabla \cdot [(\rho E + p)\,\mathbf{u}] - \nabla \cdot (\underline{\boldsymbol{\tau}}\mathbf{u} - \dot{\mathbf{q}}) = \mathbf{j} \cdot \mathbf{E}$$

that is the classical set of Navier-Stokes equations for chemically reacting and conducting flows. In this Master's Thesis work we are going to consider chemical equilibrium. In this context, no diffusive terms for the mass equations need, in addition, the mass equations must be substitute with the global continuity law. Hence, we have

$$\frac{\partial \rho}{\partial t} + \nabla \cdot (\rho\mathbf{u}) = 0$$

$$\frac{\partial (\rho\mathbf{u})}{\partial t} + \nabla \cdot (\rho\mathbf{u} \otimes \mathbf{u} + p\underline{\mathbf{I}}) - \nabla \cdot \underline{\boldsymbol{\tau}} = \rho_c\mathbf{E} + \mathbf{j} \times \mathbf{B} \qquad\qquad (2.95)$$

$$\frac{\partial (\rho E)}{\partial t} + \nabla \cdot [(\rho E + p)\,\mathbf{u}] - \nabla \cdot (\underline{\boldsymbol{\tau}}\mathbf{u} - \dot{\mathbf{q}}) = \mathbf{j} \cdot \mathbf{E}$$

which are the equations that describe the physical model of Magneto-Fluid Dynamics under the assumption of frozen flow ($\mathrm{Da} \to 0$) and no induced magnetic field ($\mathrm{Re}_m \ll 1$). For our application, the electric and magnetic fields are externally applied.

2.8   Summary

This chapter showed which are the sets of equations that we introduced in the High-Order Unifying Framework [59] and how the high temperature can change the physical properties of the gases. These characteristics are evaluated with the library Mutation++, developed at The von Karman Institute for Fluid Dynamics (VKI). The interface between the two codes (High-Order Unifying Framework and Mutation++) has already been developed by Devesse [20] and it was used to create the physical model of this Master's Thesis. Figure 2.6 shows the general scheme for the library Mutation++.
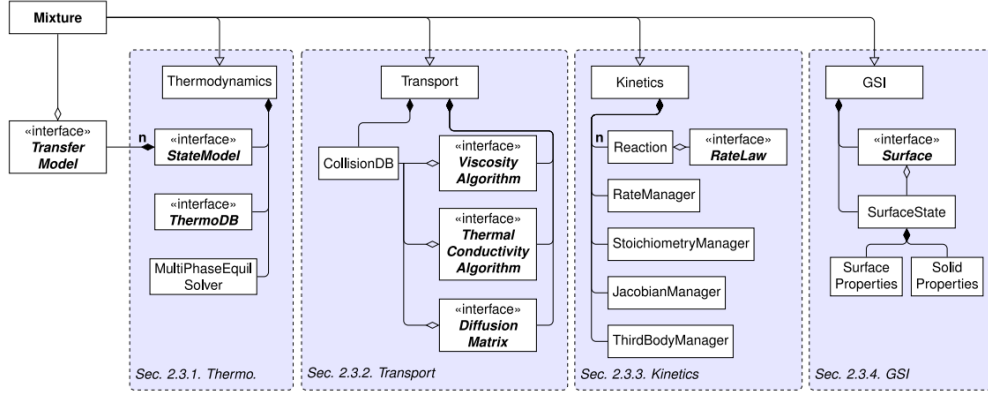
Figure 2.6: Mutation++ structure and different module. How the micture properties are computed. The picture taken from [51].

The next pictures are related to the air with 11 species, i.e. e^-, N^+, O^+, N_2^+, O_2^+, N, O, NO, N_2 and O_2 but only three elements, i.e. oxygen, nitrogen and electrons. The reactions are ruled by the Park's mechanism [45]. Figure 2.7 describes the mass fraction $Y_i = m_i/m$. We will use only this mixture to create and validate the new model of this Master's Thesis. It will very simply be to adapt it to more mixtures, or to change only the mixture, for instance, dioxide of carbon with eight species, argon with three species, etc...
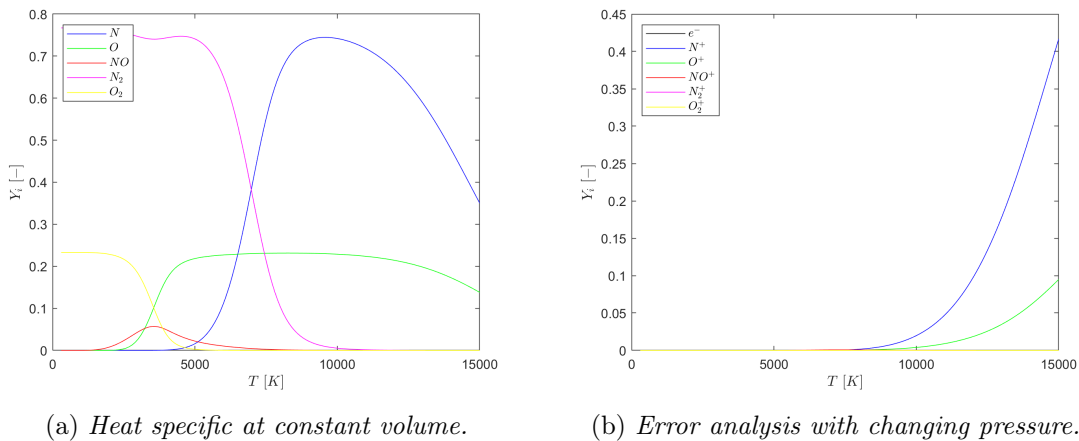
(a) *Heat specific at constant volume.*   (b) *Error analysis with changing pressure.*

Figure 2.7: Mass fractions for air 11 species.

Chapter 3

Physical models and governing equations

By now it is well known that the High-Order Unifying Framework developed by May et al. [59] works with the conservative form of the equations. This chapter will show the governing equations and the physical model of our interest.

3.1 The physical significance of balance equations

The typical balance equation is the mathematical translation of the basic physical principles. It reads, in the differential form, as follows

$$\frac{\partial \phi}{\partial t} + \nabla \cdot \boldsymbol{\Phi} = \dot{\phi} \tag{3.1}$$

where ϕ is the variable of our interest, $\boldsymbol{\Phi}$ represents its flux, and $\dot{\phi}$ its production with respect to the time. All these variables are referred to the volume. The flux can be split into convective and diffusive parts. The first one is associated with the macroscopic behavior of the flow field, while the second one with the microscopic mechanisms which are present everywhere else. In this sense, by applying the convection-diffusion splitting, the total flux is expressed as follows

$$\boldsymbol{\Phi} = \rho \phi \mathbf{u} + \mathbf{J} \tag{3.2}$$

hence, bringing together equation 3.1 with equation 3.2, we have

$$\frac{\partial \phi}{\partial t} + \nabla \cdot (\rho \phi \mathbf{u}) + \nabla \cdot \mathbf{J} = \dot{\phi} \tag{3.3}$$

that corresponds to the typical balance law written in the conservative and differential form. The same can be also written in the integral form. In this sense, we are not considering an infinitesimal volume of fluid, but an integral volume. It is important to notice that the volume Ω is arbitrary. Hence, it is possible to integrate equation 3.3 and, with the application of Gauss' Theorem, we can write it as follows

$$\frac{\mathrm{d}}{\mathrm{d}t} \int_{\Omega} \phi \, \mathrm{d}\Omega + \int_{\partial\Omega} \rho \phi \mathbf{u} \cdot \mathbf{n} \, \mathrm{d}\partial\Omega + \int_{\partial\Omega} \mathbf{J} \cdot \mathbf{n} \, \mathrm{d}\partial\Omega = \int_{\Omega} \dot{\phi} \, \mathrm{d}\Omega \tag{3.4}$$

that is the classical integral form of the balance equation.

Equations 3.3 and 3.4 are the general balance laws that describe the fluid motion. These forms still persists also when electromagnetic fields are applied to the fluid. In the next steps, we are going to write equation 3.3 by specializing for mass, momentum, and matter energy.

3.2   Navier-Stokes equations for electrically conducting flows

In the most general case, the fluid can be considered as a mixture that contains different species, each one with a given density. Its variation during the time can be caused by the convection phenomena, the production through chemical reactions, and the diffusion expressed by Fick's law. Hence, we can write equation 3.3 for each specie density as follows

$$\frac{\partial \rho_i}{\partial t} + \nabla \cdot (\rho_i \mathbf{u}) - \nabla \cdot (-\mathbf{J}_i) = \dot{\omega}_i \tag{3.5}$$

where the diffusive flux is expressed by

$$\mathbf{J}_i = \rho_i \mathbf{v}_i \tag{3.6}$$

where $\mathbf{v}_i$ is the diffusion velocity (in S.I. $[m/s]$). It is important to notice that the sum over all the species of the different diffusive fluxes is null. In other words, if we consider the fluid from a global point of view, we do not see its contribution. Therefore, the total mass cannot diffuse. It is also important to notice that the global density of the mixture is given by the sum of each density $\rho = \sum_{i=1}^{N_s} \rho_i$. Hence, if we sum together all the equations 3.5, we will obtain the global continuity equation, which reads

$$\frac{\partial \rho}{\partial t} + \nabla \cdot (\rho \mathbf{u}) = 0 \tag{3.7}$$

The same passages need to be applied to obtain the momentum and the energy equations. Hence, we have

$$\frac{\partial (\rho \mathbf{u})}{\partial t} + \nabla \cdot (\rho \mathbf{u} \otimes \mathbf{u} + p\underline{\mathbf{I}}) - \nabla \cdot \underline{\boldsymbol{\tau}} = \rho_c \mathbf{E}_{appl.} + \mathbf{j} \times \mathbf{B}_{appl.}$$
$$\frac{\partial (\rho E)}{\partial t} + \nabla \cdot [(\rho E + p) \mathbf{u}] - \nabla \cdot (\underline{\boldsymbol{\tau}} \mathbf{u} - \mathbf{J}_u) = \mathbf{j} \cdot \mathbf{E}_{appl.} \tag{3.8}$$

where $\mathbf{J}_u$ is part of the energy diffusive flux and it stores both the heat contribution (given by Fourier's Law) and the electromagnetic effects.

3.3   Maxwell equations

In S.I. Maxwell equations describe the behavior of the electromagnetic field. Their most generalized expression, that is used when there is also the presence of electromagnetic source (which are mathematically described by the density charge ρ_c and the conduction current $\mathbf{j}$), they read

$$\nabla \cdot \mathbf{E} = \frac{\rho_c}{\varepsilon_0}$$
$$\nabla \cdot \mathbf{B} = 0$$
$$\nabla \times \mathbf{E} = -\frac{\partial \mathbf{B}}{\partial t} \tag{3.9}$$
$$\nabla \times \mathbf{B} = \mu_0 \mathbf{j} + \mu_0 \varepsilon_0 \frac{\partial \mathbf{E}}{\partial t}$$

where the speed of light is defined, through the vacuum permeability μ_0 (in S.I. $[H/m]$) and the vacuum permittivity ε_0 (in S.I. $[F/m]$), as follows

$$c = \frac{1}{\sqrt{\mu_0 \varepsilon_0}} = 299792458 \frac{m}{s} \tag{3.10}$$

In general, the Maxwell equations are the mathematical translation of different physical principles: the last two, where there is the presence of the curl of the electric and magnetic

fields, and they have connected with the other field thanks to the partial derivative with respect to the time, are called Faraday's Law and Ampére-Maxwell's Law, respectively. These two equations established the link between the electric and the magnetic field. The variation in the time of one field originates the other one, thus the electric and magnetic field can be thought of as an electromagnetic wave that propagates with the speed of light, which is a physical value constant that nobody can reach. Instead, the first two equations are called Gauss' Laws for the electric and magnetic fields. The second one tells us the solenoidal property of the magnetic field. The same is satisfied by the electric field only when there are not source terms to be taken into account, i.e. where the density charge is null.

In the numerical discretization, these are the possibilities to have some discontinuities at the interface between two nearby mesh elements. When we are computing the numerical solution over time, these discontinuities propagate with the speed of light and they will transport signals that affect the solution after a determinate time.

3.4   Magneto-Fluid Dynamics

If the flow can conduct electricity, there will be a mutual interaction between the fluid flow and the electromagnetic field. These interactions are only possible if in the mixture there is the presence of charged particles, thus electrons, but not only, also positive ions, e.g. cation. As a consequence, for low temperature, when the system does not include these charged particles, the physical model, that we are going to describe in this section, is not possible to apply. Or rather, it is possible to apply it, but no changing should be present in its solution compared to the solution computed with the classical Navier-Stokes or Euler equations.

The presence of charged particles in a fluid under the application of externally electric and magnetic fields introduces a new external force: the Lorentz force. In addition, we should also take into account that the electric field is the sum of the induced electric field and the electrostatic part. On the other hand, also the magnetic field can be split in this way. Generally, we can define the electric and the magnetic field as functions of a scalar potential ϕ and a vectorial potential $\mathbf{A}$, i.e.

$$\mathbf{E} = -\nabla\phi - \frac{\partial \mathbf{A}}{\partial t}$$
$$\mathbf{B} = \nabla \times \mathbf{A}$$

(3.11)

Electric and magnetic fields create the electromagnetic field. During its numerical simulations, discontinuities appear at the interfaces. As a consequence, when we compute the solution over time, different waves propagate with the speed of light. These waves are the consequence of numerical discontinuities. On the other hand, the same happens for the normal fluid dynamic problem. The biggest issue is related to the magnitude of the propagation velocity of the discontinuities. In classical fluid dynamics, the discontinuities propagate with the speed of sound, which is a thermodynamic property of the mixture that we are considering, due to the fact it is proportional to the square root of the temperature. In the electromagnetic simulation, the discontinuities propagate with the speed of light. In this context, the two speeds have different orders of magnitude. Hence, when we are going to select the correct time step to compute the solution along the time, we must consider the most restrictive case, i.e. the speed of light. Therefore, the stability condition introduces the correct time step for the electromagnetic part of the simulation, while a too short temporal stencil for the fluid dynamic problem. Hence, the electromagnetic field will be well computed, while the fluid dynamic field not. This is the biggest disadvantage of Magneto-Fluid Dynamics numerical simulations. In order to overcome this problem,

different numerical methods were proposed in the previous years, like [17]; [18]; [33]; [34]; [32]; [31]; [6]; [16]; [19]; [7]. From a mathematical point of view, we can affirm that the system mades up of Navier-Stokes and Maxwell equations is stiff. Hence, the stiffness of the system is associated to stability conditions. However, the scope of this Master's Thesis is not based on the development of a numerical method to evolve over the time the full Magneto-Fluid Dynamics system. We will base this work on the steady-state solution of a physical model valid when the Magnetic Reynolds number is very small.

In this section, a method to develop the physical model is shown starting from the classical conservation laws. After, the *MHD approximation* is introduced, then we will focus our discussion on the set of equations of interest of us.

3.5   Derivation of Full MFD system

At this point, we have already written the Navier-Stokes equations for electrically conducting flows. In addition, also Maxwell equations have been presented. For a three dimensional problem ($d = 3$), we will have $d + 2$ scalar equations which arise from the Navier-Stokes equations, $2d + 2$ scalar equations from Maxwell's ones, one scalar equation for the continuity of the charge, and N_s continuity equations, one for each species.

All these equations make up the full Magneto-Fluid Dynamics system. In the next section, we will introduce some physical approximations to reduce the complexity of the system. In these terms, we will introduce the simplified Magneto-Fluid Dynamics system.

3.5.1   Simplified MFD system

In engineering applications, especially for aerospace ones, the full system is not solved. Several numerical methods were developed in the previous years, but the huge computational cost still to be very high. In order to make it considerable for our application, we introduce the *MHD approximation*. It is a list of hypothesis which give us the possibility to simplify the full Magneto-Fluid Dynamics system of equations under particular conditions. Here, there is the presentation of the different hypothesis:

- **Displacement current density**: the displacement current density, that is the term $\varepsilon_0 \partial_t \mathbf{E}$, is the lowest of the terms present in the Ampére's law. In fact, in typical engineering applications, the electric field does not change during time with very high frequencies. If this happens, this hypothesis is not possible to apply. In the other cases, we can neglect it. Hence, Ampére's laws, under this condition will be

$$\nabla \times \mathbf{B} = \mu_0 \mathbf{j} \tag{3.12}$$

  thus, if we apply the divergence operator, remembering that the divergence of the curl is always null, we will have

$$\nabla \cdot \mathbf{j} = 0 \tag{3.13}$$

  therefore, from the continuity equation for the charge, this means that there will not be variations over the time of the total charge density. In other words, the latter remains constant in time, thus it is a function only of the space, i.e.

$$\rho_c = \rho_c\left(t, \mathbf{x}\right) \longrightarrow \rho_c = \rho_c\left(\mathbf{x}\right) = \rho_c\left(x_1, x_2, x_3\right) \tag{3.14}$$

- **Convection current density**: this second hypothesis can be thought of as derived from the previous one. Indeed, if we consider the total current density we have

$$\mathbf{j} = \mathbf{j}_{conv.} + \mathbf{j}_{cond.} \tag{3.15}$$

thus, we have split the current density into two terms: the first one related to the convection part and the second one which describes the conduction phenomena. These two terms have not the same order of magnitude, more preciously we have

$$\|\mathbf{j}_{conv.}\|_2 \ll \|\mathbf{j}_{cond.}\|_2 \tag{3.16}$$

hence, this hypothesis is based on the denial of the first term. As a consequence, it is simple to understand that there is not the possibility to have the velocity field null because this should mean that we are considering a static case and convection is not possible if everything remains in its positions. Then, we need to impose that the density charge is null. This second hypothesis is not always applied. For instance, if we are considering D'Ambrosio's approach [15] we need to introduce it, while if we would like t to follow Giordano's approach [22] we do not take into account this second hypothesis.

Finally, from the first two hypotheses, we have assumed that the density charged is a function only of the space and it could be considered null.

- **Generalized Ohm'law**: at this stage, the current density is made up only of the conduction term. In this sense, we need to introduce a physical model to write the physical phenomena into a mathematical form. The generalized Ohm's law gives us this possibility. It models the conduction term as follows

$$\mathbf{j}_{cond.} = \sigma_e \left(\mathbf{E} + \mathbf{u} \times \mathbf{B} \right) \tag{3.17}$$

Summing up, the *MHD aproximation* return us two main ideas: the density charge does not vary during the time and it could be assumed null; the current density is modeled with conduction term that is described by the generalized Ohm's law.

From this point, it is very simple to understand why we obtain a simplified Magneto-Fluid Dynamics system. Indeed, from Ampére's law, with the results of the approximation just adopted by D'Ambrosio, we have

$$\begin{aligned} \nabla \times \mathbf{B} &= \mu_0 \mathbf{j} \\ &= \mu_0 \sigma_e \left(\mathbf{E} + \mathbf{u} \times \mathbf{B} \right) \end{aligned} \tag{3.18}$$

where the only unknown variable is the electric field, hence

$$\mathbf{E} = \frac{1}{\mu_0 \sigma_e} \nabla \times \mathbf{B} - \mathbf{u} \times \mathbf{B} \tag{3.19}$$

that can be substituted in the Ampére-Maxwell's law, thus

$$\nabla \times \left(\frac{1}{\mu_0 \sigma_e} \nabla \times \mathbf{B} - \mathbf{u} \times \mathbf{B} \right) = -\partial_t \mathbf{B} \tag{3.20}$$

that, after some manipulations, give us the *magnetic induction equation*

$$\frac{\partial \mathbf{B}}{\partial t} + \nabla \cdot \left(\mathbf{u} \otimes \mathbf{B} - \mathbf{B} \otimes \mathbf{u} \right) + \frac{1}{\mu_0 \sigma_e} \nabla \times \left(\nabla \times \mathbf{B} \right) = 0 \tag{3.21}$$

The mathematical passages that we have just made to obtain the magnetic induction equation are written in [15] where there is shown that this introduces the coupling between the Navier-Stokes equations and the Maxwell equations. Indeed, modifications in the momentum and energy equations appear as a consequence of the introduction of the Maxwell stress tensor. It stores the contribution of the magnetic pressure and also one term

links with a fictitious magnetic stress $(\mathbf{B} \otimes \mathbf{B})/\mu_0$. Finally, we can write the simplified Magneto-Fluid Dynamics system for *non-thermochemical equilibrium* as follows

$$
\frac{\partial}{\partial t}
\begin{pmatrix} \rho_i \\ \rho \\ \rho\mathbf{u} \\ \rho E_B \\ \mathbf{B} \end{pmatrix}
+ \nabla \cdot
\begin{pmatrix}
\rho_i \mathbf{u} \\
\rho\mathbf{u} \\
\rho\mathbf{u} \otimes \mathbf{u} + \left(p + \dfrac{(\|\mathbf{B}\|_2)^2}{2\mu_0}\right)\underline{\mathbf{I}} - \dfrac{\mathbf{B} \otimes \mathbf{B}}{\mu_0} \\
\left(p + \rho E_B + \dfrac{(\|\mathbf{B}\|_2)^2}{2\mu_0}\right)\mathbf{u} - \dfrac{\mathbf{u} \cdot \mathbf{B}}{\mu_0}\mathbf{B} \\
\mathbf{u} \otimes \mathbf{B} - \mathbf{B} \otimes \mathbf{u}
\end{pmatrix}
- \nabla \cdot
\begin{pmatrix} -\mathbf{J}_i \\ 0 \\ \underline{\boldsymbol{\tau}} \\ \underline{\boldsymbol{\tau}}\mathbf{u} - \dot{\mathbf{q}} \\ 0 \end{pmatrix}
= \ldots
$$

$$
= \ldots \frac{1}{\mu_0 \sigma_e}
\begin{pmatrix}
\dot{\omega}_i \\
0 \\
0 \\
\dfrac{1}{\mu_0}\left[(\nabla \times \mathbf{B})^2 + \mathbf{B} \cdot (\nabla^2 \mathbf{B})\right] \\
\nabla^2 \mathbf{B}
\end{pmatrix}
\tag{3.22}
$$

where an additional continuity equations are present, one for each species in which the mass flux $\mathbf{J}_i$ is expressed by equation 3.6. In addition, a modified value of the total energy per unit of mass is expressed by the following formula, where there is also the introduction of the magnetic field

$$
\begin{aligned}
\rho E_B &= \rho E + \frac{(\|\mathbf{B}\|_2)^2}{2\mu_0} \\
&= \rho\left(e + \frac{(\|\mathbf{u}\|_2)^2}{2}\right) + \frac{(\|\mathbf{B}\|_2)^2}{2\mu_0}
\end{aligned}
\tag{3.23}
$$

If the non-equilibrium thermochemical kinetics is neglected, no diffusive and source terms there will be in the continuity equations, hence the simplified Magneto-Fluid Dynamics system written in the conservative form will be

$$
\frac{\partial}{\partial t}
\begin{pmatrix} \rho \\ \rho\mathbf{u} \\ \rho E_B \\ \mathbf{B} \end{pmatrix}
+ \nabla \cdot
\begin{pmatrix}
\rho\mathbf{u} \\
\rho\mathbf{u} \otimes \mathbf{u} + \left(p + \dfrac{(\|\mathbf{B}\|_2)^2}{2\mu_0}\right)\underline{\mathbf{I}} - \dfrac{\mathbf{B} \otimes \mathbf{B}}{\mu_0} \\
\left(p + \rho E_B + \dfrac{(\|\mathbf{B}\|_2)^2}{2\mu_0}\right)\mathbf{u} - \dfrac{\mathbf{u} \cdot \mathbf{B}}{\mu_0}\mathbf{B} \\
\mathbf{u} \otimes \mathbf{B} - \mathbf{B} \otimes \mathbf{u}
\end{pmatrix}
- \nabla \cdot
\begin{pmatrix} 0 \\ \underline{\boldsymbol{\tau}} \\ \underline{\boldsymbol{\tau}}\mathbf{u} - \dot{\mathbf{q}} \\ 0 \end{pmatrix}
= \ldots
$$

$$
= \ldots \frac{1}{\mu_0 \sigma_e}
\begin{pmatrix}
0 \\
0 \\
\dfrac{1}{\mu_0}\left[(\nabla \times \mathbf{B})^2 + \mathbf{B} \cdot (\nabla^2 \mathbf{B})\right] \\
\nabla^2 \mathbf{B}
\end{pmatrix}
\tag{3.24}
$$

hence, in general, the simplified Magneto-Fluid Dynamics system for *thermochemical equilibrium* is made up of two vectorial equations and two scalar equations, instead of the classical one vectorial equation and two scalar equations of the Navier-Stokes system.

Now, two limiting cases based on the Magnetic Reynolds number parameter are presented

- **Small Magnetic Reynolds number**: in this case, the complexity of the system is reduced. It is the classical set of Navier-Stokes equations with the additional electromagnetic source term, composed by the Lorentz force and the Joule heating, respectively for the momentum and energy equation. It is the system of the research studies in this Master's Thesis work. In this situation, the magnetic field is called *rigid*. Indeed, the magnetic field can be thought of as the sum of the applied and the induced magnetic field, i.e.

$$\mathbf{B} = \mathbf{B}_{appl.} + \mathbf{B}_{ind.} \tag{3.25}$$

hence, the last equation of system 3.24 can be modified. In order to make it we need to remember the mathematical vectorial identity

$$\nabla \cdot (\mathbf{u} \otimes \mathbf{B} - \mathbf{B} \otimes \mathbf{u}) = \mathbf{u} \cdot \nabla \mathbf{B} - \mathbf{B} \cdot \nabla \mathbf{u} + \mathbf{B} \left(\nabla \cdot \mathbf{u} \right) + \mathbf{u} \left(\nabla \cdot \mathbf{B} \right) \tag{3.26}$$

and, from Gauss's equation for the magnetic field 3.9, we can simplify the last term as a consequence of the solenoid property of the magnetic field $\nabla \cdot \mathbf{B} = 0$. Hence, equation 3.26 reads

$$\nabla \cdot (\mathbf{u} \otimes \mathbf{B} - \mathbf{B} \otimes \mathbf{u}) = \mathbf{u} \cdot \nabla \mathbf{B} - \mathbf{B} \cdot \nabla \mathbf{u} + \mathbf{B} \left(\nabla \cdot \mathbf{u} \right) \tag{3.27}$$

then, with the substitution of the equation 3.25 and the application of the property 3.26, the last equation of the 3.24 system reads

$$\begin{aligned} \partial_t \mathbf{B}_{appl.} + \partial_t \mathbf{B}_{ind.} + \mathbf{u} \cdot \nabla \mathbf{B}_{appl.} + \mathbf{u} \cdot \nabla \mathbf{B}_{ind.} - \mathbf{B}_{appl.} \cdot \nabla \mathbf{u} - ... \\ ... - \mathbf{B}_{ind.} \cdot \nabla \mathbf{u} + \mathbf{B}_{appl.} \left(\nabla \cdot \mathbf{u} \right) + \mathbf{B}_{ind.} \left(\nabla \cdot \mathbf{u} \right) = \nu_m \nabla^2 \mathbf{B}_{appl.} + \nu_m \nabla^2 \mathbf{B}_{ind.} \end{aligned} \tag{3.28}$$

where the magnetic viscosity has been defined as $\nu_m = (\mu_0 \sigma_e)^{-1}$ (in S.I. $\left[m^2/s \right]$. In addition, we recall that the applied magnetic field does not change over time and space, thus the last equation is now written as follows

$$\begin{aligned} \partial_t \mathbf{B}_{ind.} + \mathbf{u} \cdot \nabla \mathbf{B}_{ind.} - \mathbf{B}_{ind.} \cdot \nabla \mathbf{u} + \mathbf{B}_{ind.} \left(\nabla \cdot \mathbf{u} \right) = ... \\ ... = \mathbf{B}_{appl.} \cdot \nabla \mathbf{u} - \mathbf{B}_{appl.} \left(\nabla \cdot \mathbf{u} \right) + \nu_m \nabla^2 \mathbf{B}_{ind.} \end{aligned} \tag{3.29}$$

now, we can estimate the order of magnitude of each term. Before, we need to remember that we can define two reference times. We define both them starting from a reference length l, the magnetic viscosity ν_m and the fluid velocity $\|\mathbf{u}\|_2$. Thus, we have:

- Time for the adaptation of the magnetic field at the fluid motion, i.e the typical physical time of the induction mechanism, which reads

$$t_b = \frac{L_{ref}^2}{\nu_m} \tag{3.30}$$

- Time to evolve of the magnetic field, i.e. the typical time of the diffusion mechanism of the magnetic field, which reads

$$t_f = \frac{L_{ref}}{\|\mathbf{u}\|_2} \tag{3.31}$$

where, their ratio is expressed by the Magnetic Reynolds number, i.e. $\mathrm{Re}_m = t_b/t_f$. Hence according to $\mathrm{Re}_m \ll 1$, we have

$$t_b \ll t_f \tag{3.32}$$

Now, we can analyze the order of magnitude of equation 3.29. We notice that the LHS has order $\mathcal{O}\left(t_f^{-1}\right)$, while the RHS has order $\mathcal{O}\left(t_c^{-1}\right)$. Therefore, the LHS is negligible with respect to the RHS. As a consequence, the first two terms of the RHS need to be balanced by the last one, i.e.

$$\frac{\mathbf{B}_{appl.}}{t_f} \sim \frac{\mathbf{B}_{ind.}}{t_b} \tag{3.33}$$

which means

$$\mathbf{B}_{ind.} \sim \frac{t_b}{t_f}\mathbf{B}_{appl.} = \mathrm{Re}_m\ \mathbf{B}_{appl.} \tag{3.34}$$

therefore, if the Magnetic Reynolds number is very small, we have

$$\mathbf{B}_{ind.} \ll \mathbf{B}_{appl.} \tag{3.35}$$

thus, the magnetic field can be considered constant. No induction effects are present under the low Magnetic Reynolds number regime, i.e.

$$\mathbf{B} \sim \mathbf{B}_{appl.} \tag{3.36}$$

that justifies why the magnetic field is called rigid.

- **Large Magnetic Reynolds number**: the code is currently empty of this model. This could be a possible idea for further developments. In this situation, the system is equivalent to system 3.24 but, the magnetic induction equation stores only the convective term. No diffusion effects of the magnetic field are taken into account. In addition, no source terms related to the magnetic field are present, but an additional vectorial equation for the induced magnetic field needs to be considered. In this situation, the magnetic field is called *frozen*.

3.6   Closure equations

Both the previous systems are not closed from a mathematical point of view. In other words, the number of unknown variables is greater than the number of scalar equations. This forces us to introduce the closure equations, which are relations that describe, from a physical point of view, the mechanisms of the transport fluxes (mass, momentum, and energy) to solve the system. In mathematical languages, we will introduce scalar equations to increase the number of available equations to reach the same number of the total unknown variables. In this context, physical laws that describes all the diffusive fluxes need to be taken into account. In classical fluid dynamics, they are represented by the Fick's law, Newton's law, and Fourier's law, respectively for mass, momentum, and heat fluxes. In the current section, we will introduce them and we will explain the typical effects related to high temperature. The situation has been more precisely explained in the previous Chapter where, thanks to the perturbation of BTE equation we have shown how to obtain the Euler and the Navier-Stokes equations and how the transport coefficients can be evaluated also when the external magnetic field is applied, like in our problem.

3.6.1   Thermodynamics

In this Master's Thesis work all the thermodynamic and transport properties will be computed by Mutation++ library [52]; [51]. In particular, for each mixture we have different

species, which are denoted by the index $i = \{1, ..., N_s\}$ where N_s represents the number of species in the mixture. By the classical definition of specific heat we have

$$
\begin{aligned}
c_v &= \frac{\mathrm{d}e}{\mathrm{d}T} \\
c_p &= \frac{\mathrm{d}h}{\mathrm{d}T}
\end{aligned}
\tag{3.37}
$$

According to [20] each species in the mixture is considered to have the same behavior of a thermally perfect gas. This hypothesis is often made in hypersonic applications. As a consequence, we can define the specific energy and the specific enthalpy (i.e. in S.I. $[J/kg]$) like a function of the temperature and, remembering that we are working with mixtures that contain N_s species, we need to consider all the thermodynamic properties for each species. For this reason, in the following formulas, the subscript i is added in each definition. Starting from the specific energy and the specific enthalpy for each species $(\forall i \in \{1, ..., N_s\})$, we have

$$
\begin{aligned}
e_i - e_{0,i} &= \int_{T_0}^{T} c_{v,i} \; \mathrm{d}T \\
h_i - h_{0,i} &= \int_{T_0}^{T} c_{p,i} \; \mathrm{d}T
\end{aligned}
\tag{3.38}
$$

Hence, for a general mixture where there is the presence of several species, we need to add all the contributions weighted by their mass fraction $Y_i = m_i/m$. In other words, all the species contribute to the specific energy and specific enthalpy, but with a different weight that is taken into account by the mass fraction. As a consequence $(\forall i \in \{1, ..., N_s\})$, we have we have

$$
\begin{aligned}
e &= \sum_{i=1}^{N_s} e_i Y_i \\
h &= \sum_{i=1}^{N_s} h_i Y_i
\end{aligned}
\tag{3.39}
$$

where $h = e + p/\rho$. In addition, in the low-enthalpy model, the pressure is computed with the classical ideal law $p = \rho \mathcal{R} T / \mathcal{M} = n k_B T$, i.e.

$$
p = \rho (\gamma - 1) \left(E - \frac{(\|\mathbf{u}\|_2)^2}{2} \right)
\tag{3.40}
$$

hence, without any consideration regarding the real gas effects, which are typically taken into account van der Waals' Law. However, when different species are present in the mixture, the use of Dalton's Law to compute the total pressure is more accurate than equation 5.5, i.e.

$$
p = \sum_{i=1}^{N_s} p_i = \sum_{i=1}^{N_s} \rho_i \frac{\mathcal{R}}{\mathcal{M}_i} T, \qquad i \in \{1, ..., N_s\}
\tag{3.41}
$$

3.6.2 Transport and high-temperature effects

In the flow, there could be regions where the temperature is very high. This typically happened in the post-shock region where, as a consequence of the strong shock, the total temperature is constant because the process is adiabatic, but the static temperature increase. Consequently, the Mach number in the region post-shock will be, of course, lower than free stream conditions. Hence, the kinetic energy associated with the high speed is moved increases the internal energy of the molecules. The high temperature excites the

vibrational energy, thus it causes dissociation and, if the temperature is very high, also ionization. As a result, the heat flux at the wall is dominant.

When the temperature is very high the theory developed for calorically perfect gases drops down. Indeed when high temperature is reached the gases start to dissociate and ionize and the specific heat is a function of both pressure and temperature. Under these conditions, the gas becomes chemically reacting. Also, the transport properties are taken from the same Mutation++ library. In this section, we need to introduce the transport properties that allow us to introduce the electromagnetic source term in our equations.

Viscous stress tensor

The mixture is considered to be Newtonian. In this sense, with Stokes's hypothesis, we have, thanks to Newton's law

$$\underline{\boldsymbol{\tau}} = \mu \left[\nabla \mathbf{u} + (\nabla \mathbf{u})^T - \frac{2}{3} \left(\nabla \cdot \mathbf{u} \right) \underline{\mathbf{I}} \right] \tag{3.42}$$

where μ is the dynamic viscosity. It is the transport property. Of course, it is null in the Euler physical model, indeed in that situation, all the diffusive fluxes vanish. Some mathematical laws (see figure 3.1) were developed to analyze its variations with the temperature:

- **Power Law**

$$\mu = \mu_{ref} \left(\frac{T}{T_{ref}} \right)^{\omega} \tag{3.43}$$

  where T_{ref} is a reference temperature, μ_{ref} is the dynamic viscosity at the reference temperature and ω is an empirical value (for air $\omega = 0.75$).

- **Sutherland's Law**

$$\mu = S \frac{\sqrt[3]{T^2}}{T + \chi} \tag{3.44}$$

  where $S = 1.458 \times 10^{-6} \ kg/\left(ms\sqrt{K} \right)$ and $\chi = 110.4 \ K$.

Heat flux

In general, the heat flux is defined by the Fourier's law, thus

$$\dot{\mathbf{q}} = -\lambda \nabla T \tag{3.45}$$

where λ is the thermal conductivity and κ the thermal diffusivity. The behavior of the thermal conductivity at low temperature is quite similar to the dynamic viscosity one (see figure 3.2). In this sense, it can be computed starting from the definition of the Prandtl number, i.e.

$$\lambda = \frac{\mu c_p}{\text{Pr}} \tag{3.46}$$

Typical value of Prandtl number for air is $0.71 - 0.72$. In general, in the liquid the Prandtl number is higher than in the gases. For instance, for water at $T = 20°C$ it reaches 7. On the other hand, liquid metals (e.g. Hg, Na) have Prandtl number very low.

(a) *Dynamic viscosity μ approximations.*

(b) *Error analysis in μ.*

(c) *Effect of the pressure on μ.*

(d) *Effect of the pressure in the approximations of μ.*
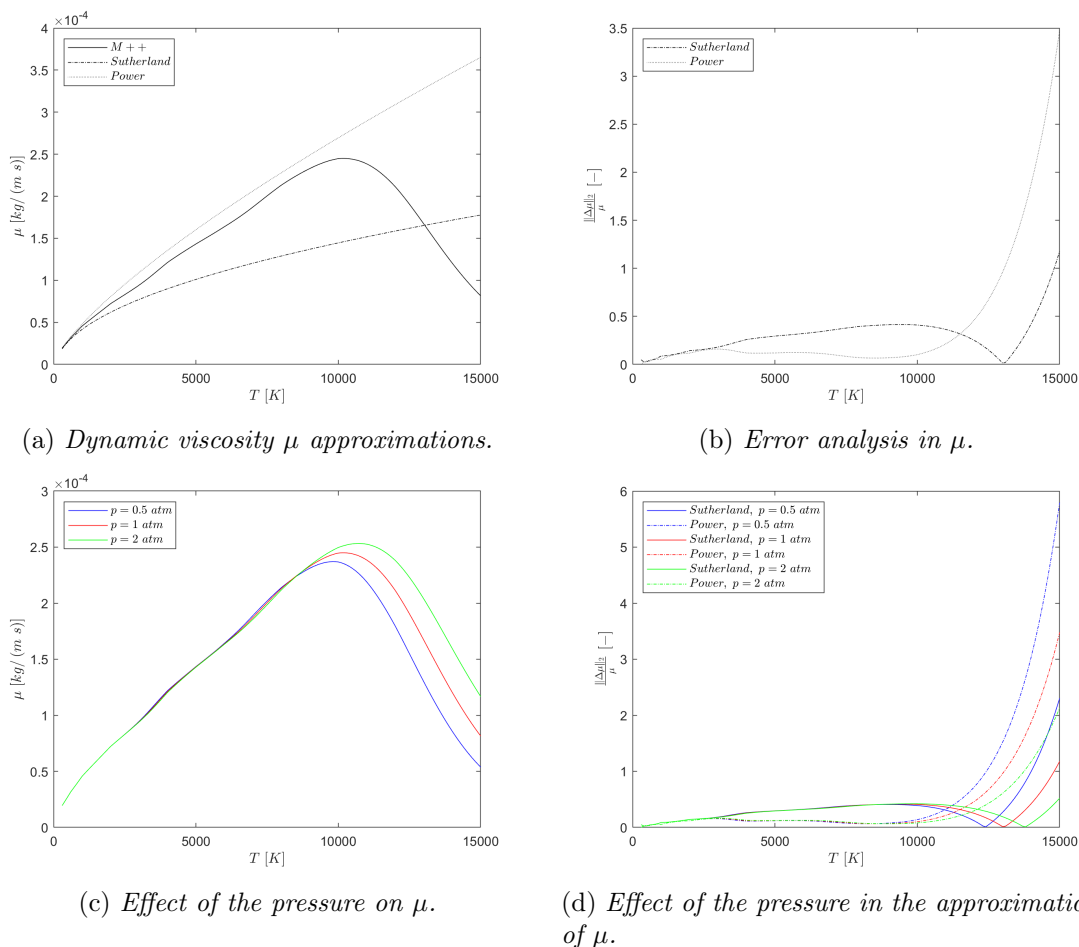
Figure 3.1: Dynamic viscosity computed with the Power law and the Sutherland's law models. Comparison with the M++ solution which takes into account the high-temperature effects. Effects of the pressure on the dynamic viscosity and its approximations.

Electrical conductivity

Briefly, we remind that the most general source term for the Navier-Stokes electrically conducting flow model has the following aspect

$$\underline{\mathbf{s}}\left(\mathbf{w}, \nabla \mathbf{w}\right) = \begin{pmatrix} 0 \\ \rho_c \mathbf{E}_{appl.} + \mathbf{j} \times \mathbf{B}_{appl.} \\ \mathbf{j} \cdot \mathbf{E}_{appl.} \end{pmatrix} \qquad (3.47)$$

thus, it contains the Lorentz force and the Joule heating in the momentum and energy equations, respectively. Of course, no source terms are needed for the continuity equations if we are not going to consider chemical reactions, namely no production of species is allowed in that physical model.

The electric and magnetic fields are externally imposed by the user, thus no transport properties are needed to compute them, however, there will be the possibility, under the ambipolar assumption, to neglecting the density current and to introduce the ambipolar electric field, which will be given by the same external library. In order to evaluate the density current vector and the total density charge, we need to couple again the High-Order Unifying framework [20]. It should be noted that, in a mixture composed of different species including ions and electrons, the total density charge is not made up only of the density

(a) *Thermal conductivity approximations.*

(b) *Error analysis in* λ.

(c) *Heat specific at constant volume.*

(d) *Error analysis with changing pressure.*
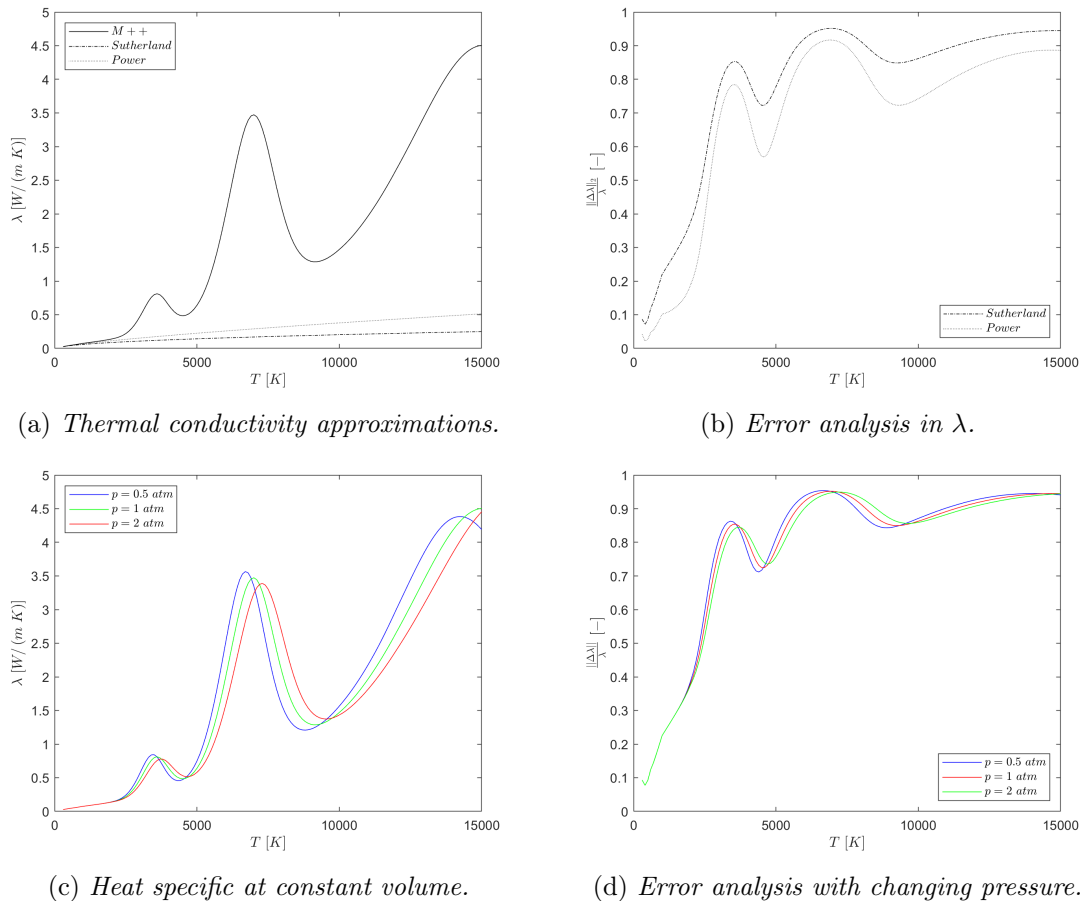
Figure 3.2: Thermal conductivity computed with the Prandtl apprximation. Comparison with the M++ solution which takes into account the high-temperature effects. Effects of the pressure on the thermal conductivity and its approximations.

charge of the electrons, but again with a weighted sum of all the density charge, hence

$$\rho_c = \sum_{i=1}^{N_s} \rho_{c,i} Y_i \tag{3.48}$$

where $Y_i = m_i/m$ is the mass fraction. Obviously, the non charged species do not contribute to ρ_c.

On the other hand, the latter term that has not been yet specified is the density current **j**. It expresses the interaction between the electromagnetic field externally applied and the fluid motion. Its general expression is

$$\mathbf{j} = \mathbf{u} \sum_{i=1}^{N_s} \rho_{c,i} Y_i + \sigma_e \left(\mathbf{E}_{appl} + \mathbf{u} \times \mathbf{B}_{appl} \right) \tag{3.49}$$

where it has been split into two contributions: the first one is associated to the convection phenomena and the second term to the conduction current. In general, the electrical conductivity is anisotropic in the case of a strong magnetic field applied. Otherwise, its behavior can be easily assumed isotropic.

3.6.3 Chemical reactions effects

In normal hypersonic applications, when chemical reactions are present at high temperatures, different assumptions of the behavior of the fluid give different solutions. As a

consequence of the high temperature, the molecules of the mixture increase their degree of freedom, namely also the vibrational, electronic and ionization degree of freedom will be computed. The mixture that is chemically reacting can be studied based on the dimensionless parameter Damkohler number

$$\text{Da} = \frac{t_f}{t_c} \tag{3.50}$$

that expresses the ratio between the typical flow time and the chemical time. In normal aerospace hypersonic applications we have Da ~ 1. As a consequence, the most accurate physical models introduce N_s continuity equations, one for each species present in the mixture. Studying the flow from a numerical point of view we consider two extreme cases:

- **Frozen flow**: this is the case when the Damkohler number is very low, i.e.

$$\text{Da} \to 0 \tag{3.51}$$

  By the definition of the Damkohler like the ratio between the typical flow time and the chemical time, the consideration of frozen flow involves that the chemical reaction time is a different order of magnitude greater than the flow time. Hence, chemical reactions have a small effect on the behavior of the fluid. Therefore this effect can be neglected, thus no adding equations for modeling the different mixture species is needed. The system is made up of the classical set of the well known Navier-Stokes equations with only one single continuity equation. The latter is obtained by summing all the continuity equations for each species. In this situation, the heat specific at pressure constant introduced in equation 3.37 is expressed as follows

$$c_p^F = \sum_{i=1}^{N_s} Y_i c_{p,i}$$
$$c_v^F = \sum_{i=1}^{N_s} Y_i c_{v,i} \tag{3.52}$$

  where $Y_i = m_i/m$ is the mass fraction. In this physical model, the equations will be the classical Navier-Stokes set

$$\frac{\partial \rho}{\partial t} + \nabla \cdot (\rho \mathbf{u}) = 0$$
$$\frac{\partial (\rho \mathbf{u})}{\partial t} + \nabla \cdot (\rho \mathbf{u} \otimes \mathbf{u} + p\underline{\mathbf{I}}) - \nabla \cdot \underline{\boldsymbol{\tau}} = \rho \mathbf{f} \tag{3.53}$$
$$\frac{\partial (\rho E)}{\partial t} + \nabla \cdot [(\rho E + p) \mathbf{u}] - \nabla \cdot (\underline{\boldsymbol{\tau}} \mathbf{u} - \dot{\mathbf{q}}) = \rho \mathbf{f} \cdot \mathbf{u} + \dot{\mathcal{Q}}$$

- **Local thermodynamic equilibrium**: in this case we have

$$\text{Da} \to \infty \tag{3.54}$$

  In this case, the local thermodynamic composition at one point in the flow is the same in the equilibrium conditions of temperature and pressure. When the flow is considered in local thermo-chemical equilibrium we need to modify the normal Navier-Stokes equations. We must add one equation for each element. Not one equation for each species, that is if we are working with a mixture made up of 11 species (for instance air11) we do not need to introduce 11 continuity equations, but

only one for each element. In this situation, the specific heat capacity at constant pressure and volume introduced in equation 3.37 are expressed as follows

$$c_p^E = c_p^F + \sum_{i=1}^{N_s} h_i \left(\frac{\mathrm{d}Y_i}{\mathrm{d}T}\right)_{p,Y_e}$$
$$c_v^E = c_v^F + \sum_{i=1}^{N_s} e_i \left(\frac{\mathrm{d}Y_i}{\mathrm{d}T}\right)_{p,Y_e}$$

(3.55)

that shows as, when the gas starts to dissociate and ionize due to the high temperature c_p^F and c_p^E have a completely different behavior that depend on

$$\mathrm{err}_{c_p} = \sum_{i=1}^{N_s} h_i \left(\frac{\mathrm{d}Y_i}{\mathrm{d}T}\right)_{p,Y_e}$$
$$\mathrm{err}_{c_v} = \sum_{i=1}^{N_s} e_i \left(\frac{\mathrm{d}Y_i}{\mathrm{d}T}\right)_{p,Y_e}$$

(3.56)

In this physical model, the equations will be the classical Navier-Stokes equations with an additional equation for each element

$$\frac{\partial \rho}{\partial t} + \nabla \cdot (\rho \mathbf{u}) = 0$$
$$\frac{\partial (\rho \mathbf{u})}{\partial t} + \nabla \cdot (\rho \mathbf{u} \otimes \mathbf{u} + p\underline{\mathbf{I}}) - \nabla \cdot \underline{\boldsymbol{\tau}} = \rho \mathbf{f}$$
$$\frac{\partial (\rho E)}{\partial t} + \nabla \cdot [(\rho E + p)\mathbf{u}] - \nabla \cdot (\underline{\boldsymbol{\tau}} \mathbf{u} - \dot{\mathbf{q}}) = \rho \mathbf{f} \cdot \mathbf{u} + \dot{\mathcal{Q}}$$
$$\frac{\partial (\rho \mathbf{Y}_e)}{\partial t} + \nabla \cdot (\rho \mathbf{Y}_e \mathbf{u}) - \nabla \cdot (-\mathbf{J}_e) = 0$$

(3.57)

Figure 3.3 shows he differences between the frozen and LTE condition for the ratio of heat specific and the speed of sound $a = \sqrt{\gamma p/\rho}$. It is shown that the biggest variations are present when the temperature is very high, which is a classical situation in the hypersonic applications in the regions post-shocks.

Figure 3.4 shows the heat specific at constant pressure for frozen and LTE conditions. In the right part of the figure, the difference between them is taken into account. The latter plot shows that for very high temperatures the difference will be important, even if it oscillates and it does not have a precious trend with the increment of the temperature.

Figure 3.5 repeat the same concept also for the heat specific evaluated at constant volume. In both the figures also the effects of variation in the pressure are considered. the behavior is quite the same, no huge variations are present if we consider small variations in the pressure.

(a) $\gamma = \frac{c_p}{c_v}$

(b) *Speed of sound.*
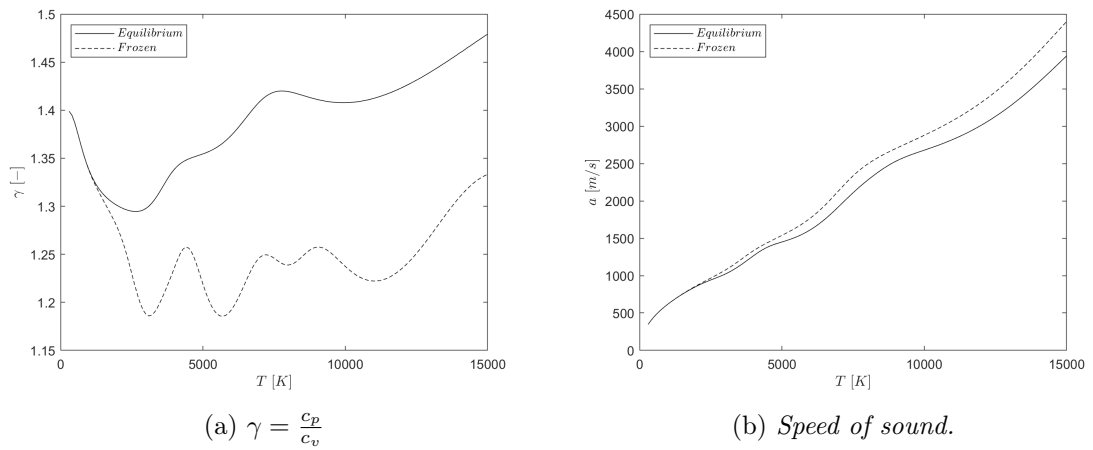
Figure 3.3: Frozen flow and LTE model: effects on γ and a for air 11 at $p = 1\ atm$.

(a) *Heat specific at constant pressure.*

(b) *Error analysis in c_p with changing pressure.*
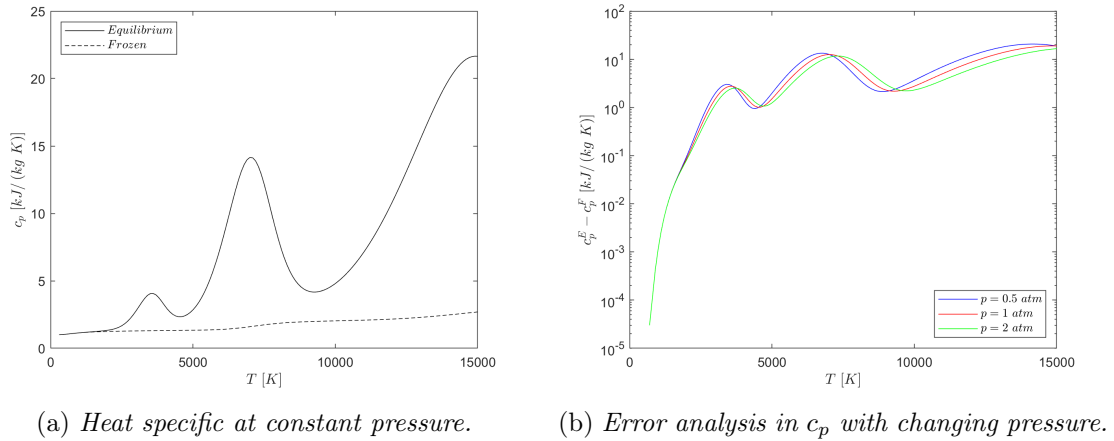
Figure 3.4: Frozen flow and LTE model: effects on c_p for air 11.

(a) *Heat specific at constant volume.*

(b) *Error analysis in c_v with changing pressure.*
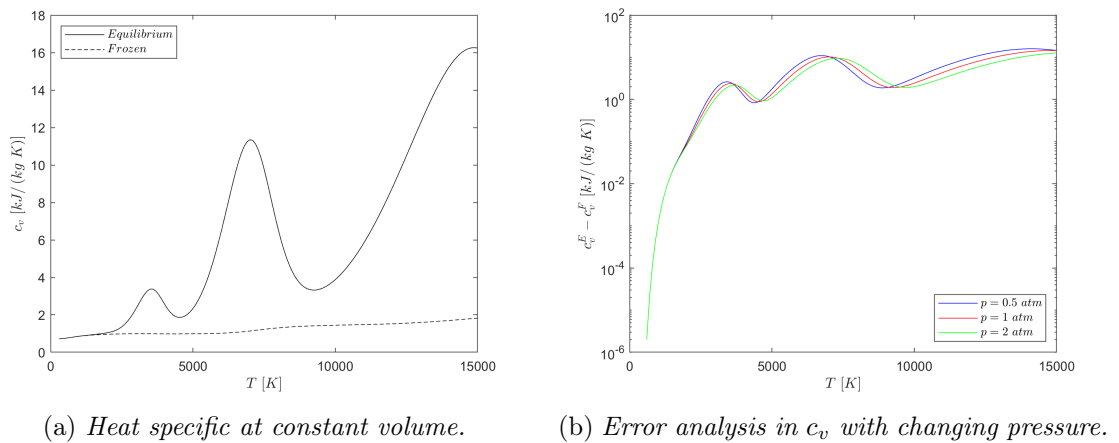
Figure 3.5: Frozen flow and LTE model: effects on c_v for air 11.

3.7 Summary

In this Chapter we have shown the typical governing equations for electrically conducting flow. Starting from the full MFD system, thanks to the *MHD approximation*, we have obtained the simplified version of the MFD system. Then, assuming no chemical production rate and the frozen flow condition, we have conducted a dimensional analysis based on the Magnetic Reynolds number. Two small limiting cases were presented. In our case, we will consider the option under the continuity hypothesis, i.e. $\mathrm{Kn} \ll 1$; the frozen flow assumption, i.e. $\mathrm{Da} \to 0$,; and the absence of induced magnetic field, i.e. the magnetic field is called rigid $\mathrm{Re}_m \ll 1$. In this situation, the physical model is translated into mathematical language as follows

$$\frac{\partial \rho}{\partial t} + \nabla \cdot (\rho \mathbf{u}) = 0$$

$$\frac{\partial (\rho \mathbf{u})}{\partial t} + \nabla \cdot (\rho \mathbf{u} \otimes \mathbf{u} + p \underline{\mathbf{I}}) - \nabla \cdot \underline{\boldsymbol{\tau}} = \rho_c \mathbf{E}_{appl.} + \mathbf{j} \times \mathbf{B}_{appl.} \qquad (3.58)$$

$$\frac{\partial (\rho E)}{\partial t} + \nabla \cdot [(\rho E + p) \mathbf{u}] - \nabla \cdot (\underline{\boldsymbol{\tau}} \mathbf{u} - \dot{\mathbf{q}}) = \mathbf{j} \cdot \mathbf{E}_{appl.}$$

where the density current is given by the generalized Ohm's law as follows

$$\mathbf{j} = \rho_c \mathbf{u} + \sigma_e \left(\mathbf{E}_{appl.} + \mathbf{u} \times \mathbf{B}_{appl.} \right) \qquad (3.59)$$

and the density charge reads

$$\rho_c = \sum_{i=1}^{N_s} \rho_{c,i} Y_i \qquad (3.60)$$

Chapter 4

Numerical Methods

The physical behavior of all the systems is described by using ODEs or PDEs. Several examples are present in [38]. In general, we can split PDEs into three different groups based on their mathematical properties. Elliptic equations, like the stationary heat equation (e.g. Poisson equation), have their A matrix definite, parabolic equations have their A matrix singular, while the hyperbolic equations have all eigenvalues real.

At this point, it is important to remember that we are going to solve the Navier-Stokes equations which are non-linear partial differential equations (PDEs). Even if the normal set of Navier-Stokes equations is empty of the electromagnetic source term, his mathematical structure does not change. In other words, the non-linearity is associated with the convective terms, namely, it is always present, both in the Euler and in the Navier-Stokes equations, hence also in ideal fluids which have null viscosity.

The main problem related to the non-linearity does not permit us to find analytical solutions for the fluid problems, unless we are going to consider very simple tests case where, as a consequence of the approximations, the convective terms disappear and we will be able to solve the full system analytically. Typical examples in fluid dynamics are parallel flows, thus when the velocity field does not vary in one direction, for instance $\mathbf{u} = (u_1 (x_2, x_3), u_2 (x_2, x_3), u_3 (x_2, x_3))^T$. Naturally, these peculiar cases have not engineering applications.

To find a solution for our problem, having understood that we can not use the analytical approach, we have other two possibilities: experimental results and numerical analysis.

The first one is very useful, but it requires many costs and a lot of time to change some details in the experiments. For this reason, it is important to verify the numerical data for simplified geometry with experimental data, especially for hypersonics. In addition, a limited number of facilities for high speed and plasma flows are present all over the World. In this way, during the previous years, many numerical methods were developed. This was also possible with the improvement in the field of computer science (the future field of studies would be also quantum computing).

The aim of this Master's Thesis, due to the high energy required for the experiments, is associated with the numerical analysis.

Numerical methods use maths rules to discretize the equations and to find the solutions in specific points. After that, with a strategy that depends on the numerical method that we are using, the numerical schemes rebuild an approximate solution for all the other points. Namely, it is very simple to understand that, even if we select the perfect numerical method (which does not exist), we will always obtain a numerical solution that is quite different from the analytical (when it is possible to find) or from the real solutions (that come out from the experimental results). Good numerical methods can reduce these errors to find the best approximative solution. During the past years, a lot of numerical methods were introduced for different types of equations. For instance, elliptic equations are well solved

by finite elements methods (FE methods), parabolic equations by finite difference methods
(FD methods), and hyperbolic equations by finite volume methods (FV methods).

Here, it is presented a brief discussion of the most important numerical methods. We
anticipate that the code which was used in this Master's Thesis is based on the Hybridized
Discontinuous Galerkin method (HDG), which is a sort of mix between FE method and
FV method.

4.1   Motivation: Fluid Dynamics equations

In classical fluid dynamics, the behavior of the fluid motion can be described from an
inviscid point of view, e.g. ideal fluid, by the Euler equations and, for real fluid, by Navier-
Stokes equations.

Navier-Stokes equations are a set of scalar and vectorial PDEs which describe the motion
of the viscous fluid. In addition, the Euler equations are always PDEs and they can be
derived by the Navier-Stokes equations neglecting the viscous terms. In other words, the
Navier-Stokes equations are more general than the Euler equations.

During the XIX sec. the French C.L. Navier and the Anglo-Irish G.G. Stokes developed
separately the Navier-Stokes equations. Currently, they are one of the unsolved problems
of modern Mathematics together with Riemann's Hypothesis, NP and P problems, etc...
The irresolvability of the Navier-Stokes equations is strictly connected with the non-linear
terms which describe the convective contribution of the fluxes.

The Navier-Stokes equations, like the Euler ones, are a set of laws regarding the mass,
momentum, and energy contained in an infinitesimal, or finite, volume. They describe the
fluid motion in two different ways. The first approach is called the Lagrangian approach
and its equations are classified as non-conservative. Instead, the second one is called the
Eulerian approach and it gives conservative equations.

However, the system is not well determined. More spefically, in the most general case
without any source term (e.g. classical three dimensional Navier-Stokes simulation, thus
$d = 3$) we have $m = d + 2$ scalar equations and $4d + 2$ unknown variables (d for the
velocity vector $\mathbf{u} = (u_1, ..., u_d)^T$, other d for the heat flux vector $\dot{\mathbf{q}} = (\dot{q}_1, ..., \dot{q}_d)^T$, 2 for the
density ρ and the specific internal energy e, and $2d$ for the symmetric stress tensor). As a
consequence, the system has order

$$\infty^{(4d+2)-m} = \infty^{3d} \tag{4.1}$$

For these reasons, in the previous Chapters, closure equations have been developed.

4.2   Overview of classical numerical methods

In this section, a list of the most important numerical methods present in the literature is
explained. The main pros and cons are presented. This is not an exhaustive section about
all the numerical methods present in the literature. For specific discussion, we address to
[38].

4.2.1   Finite Difference method (FD)

These methods are used with the differential form of the equations and, initially, were
developed for parabolic PDEs. The simpler method to discretize PDE is based on the
mathematical definitions of derivatives. In the FD method, we need to divide both the
spatial and temporal domain into specific points, called nodes, where the solution will be
computed. The connections between these nodes are based on the mathematical definition
of derivatives. Hence, in general, for the first derivatives, we will have three different

possibilities: backward, central, or forward, with different orders of approximation. In particular, the second one is the second-order approximation, while the first and the third ones are the first-order approximation. It is important, for this method, to remember the Taylor expansion to reconstruct the solution between two, or more, nearby nodes.

4.2.2   Finite Volume method (FV)

These methods are used with the integral form of the equations and they work fine for hyperbolic PDEs. With the FV method, we are spitting the domain in cells and we will compute the solution for each cell. There are two different possibilities: we can decide to compute the solution in the center of the cells (called vertex-centered) or in the vertex of the cells (called cell-centered). To be specific, for each cell we will have one solution and the solution over the cell is computed with its mean value. The fluxes connect two nearby cells. The choice of the sloper introduces the possibility to have numerical instabilities. In general, the sloper of the approximate solutions in each cell is chosen according to the stability problem and the choice of different schemes (e.g. ENO, WENO, etc...). The sloper is limited, in this sense we cannot reach High-Order accuracy, thus we cannot increase at the very high value the degree of the polynomial function that approximates the solution in each cell. For this reason, during the last years, to overcome this problem, High-Order methods have been developed.

In addition, discontinuities appear in each interface between two nearby cells. When the approximate solution evolves in time, as a consequence of the discontinuities at the interface, different signals propagate and affect the solution. In order to understand which will be the solution after a selected future time, we need to solve a Riemann problem for each interface. This increases the computational cost. To reduce it, there is also the possibility to solve an approximate Riemann problem. In addition, in 1959, Gudunov's schemes were though. They are methods that solve exact (or approximate) the Riemann problem in each interface. They are based on three different steps: in the first step, the solution is reconstructed starting from the cell averages. In the second step, the reconstructed data are evolved over the time (this is the only physical step of the whole procedure). Finally, in the third step, the solution is averaged over each cell to obtain the cell averages. Hence, the steps are Reconstruction, Evolve, and Average. For this reason, the method is also called REA algorithm.

4.2.3   Finite Element method (FE)

Initially, these methods were thought for elliptic PDEs. Their main idea is to approximate the solution with shape functions in each element. In other words, the solution is well computed in precise points in the domain (called nodes) and approximate otherwise. The main idea is quite similar to FD method, but FE method differs from FD method by the way it finds the approximate solution in all the points that are not nodes. While in FD method two different nodes are connected with the usage of the concept of derivatives, in FE method, the link is established with these particular shape functions (for instance, Lagrange or Hermite functions). It is obvious that the order of accuracy increases if we are considering shape functions of higher polynomial degrees.

4.3   High-Order numerical methods

In Computational Fluid Dynamics (CFD), when we want to simulate flows at very high velocity, thus hypersonic regimes, FV methods are generally used. This choice is related to the high stability of these methods based on the upwind calculation of the fluxes between two nearby cells. The FV methods have the advantage to be very stable but, on the other hand, they are low order accurate and, in presence of high gradients, as in the regions pre- and post-shock, they introduce a large amount of artificial viscosity. As a consequence, even if we are computing the solution without diffusive fluxes, therefore with the Euler equations, variations in the entropy appear because they are caused by the artificial dissipation [8].

In this context, during the last years, numerical researchers interested in fluid dynamics have developed many numerical methods based on Discontinuous Galerkin (DG) discretization. This type of discretization becomes from the Continuous Galerkin (CG) one. In CG, at the interface of two nearby elements is imposed the no jump condition. Instead, in DG discretization jumps between two nearby elements are possible. Hence, again as in FV methods, with the DG discretization, at the interface discontinuities are present. Subsequently, when the numerical solution is proceeding over time, a Riemann problem has to be solved for each interface: exactly the same of FV method. Hence, the idea to simulate compressible flows with DG discretization is not new [14]; [47]; [53]. Nguyen et al. [40] developed a RANS and URANS models based on one equation Spalart-Allmaras model and they applied them to flat plate, NACA 0012 airfoil ($Re = 1.85 \times 10^6$) and bidimensional cylinder ($Re_D = 3 \times 10^6$), all subsonic or transonic test cases. Schrooyen et al. [49] used DG solver to simulate gas surface interaction and ablation in high-enthalpy environment; Lv and Ihme developed a DG solver to simulate chemical reacting flow for combustion [30]; Ching and Ihme simulated compressible multiphase flows [11]. They made subsonic and supersonic numerical tests, reaching also Mach 12. Again, Ching, Lv and Ihme used DG solver in hypersonic re-entry applications [9]; [10]; [12] to study heat transfer and particle tracking. They simulated at Mach 17, but assuming ideal gas law and without considering the effects of chemical production, high temperature, and the possibility of external electromagnetic field applied. Hartmann and Houston [24] simulated with DG discretization external subsonic flow over NACA 0012 airfoil and the internal transonic flow inside a converging-diverging nozzle. Both the previous cases studied by Hartmann and Houston were conducted with Euler equations.

All the just mentioned works are based on DG methods, which main disadvantage is the high computational cost. Within this trend, a new formulation in the DG method was introduced.

Hybridizable Discontinuous Galerkin (HDG) methods are variation of the classical DG discretization. The requirement to switch from DG to HDG is to reduce the computational cost. In HDG methods, indeed, an additional degree of freedom is added. This, which at the first stage could be thought as an increment of the global computational cost, permits us to decouple the problem and to make the hybridization. In this sense, firstly the problem related to the additional degree of freedom between nearby elements is solved, then the solution is approximate in each element. The elements were previously connected with fluxes, as in FV methods, by the resolution of the first problem. In this way, the overall computational cost is reduced. Nguyen, Peraire et al. [43] were the first to introduce HDG methods in fluid dynamics. Woopen, Balan, May and Schutz made comparisons between DG and HDG discretization in the same solver that is used for this Master's Thesis project [60]. Firstly, the usage of HDG methods for scalar model convective diffusion equation (which is a standard basic scalar model for Navier-Stokes equations) was proposed by Nguyen et al. [41]; [42] and then applied to incompressible and compressible Navier-Stokes equations [44]; [46]. They reached also Mach 20, but they simulate only a single species

flow with ideal gas law. In addition, supersonic flows were simulated with HDG solver by Vila-Prez et al. [55] with the addition of HLL Riemann solver to solve the evolution of the discontinuities at the interface between two nearby elements. The implementation of the Magneto-Fluid Dynamics model with HDG methods is at the beginning stages. In the literature Ciuca, Nguyen et al. [13] developed a model that solved classical Navier-Stokes with an additional equation that describes the induction of the magnetic field. This is typically used in magnetohydrodynamics (MHD) analysis.

In this project, we are interested in the application of low Magnetic Reynolds number in hypersonic flows, thus when the presence of externally applied electromagnetic fields is taken into account in the source term, without any additional vectorial equation. In other words, no induction magnetic field is considered.

4.3.1 General concept Galerkin methods

Only in the last years, when the computers were improvemented, and the researcher would have wanted to find the numerical solutions with the fewer errors possible, that the interest for High-Order methods appeared.

The HDG method is a High-Order numerical method based on the FE and FV methods. It is derived from the DG discretization, but, in order to reduce the computational cost due to the high numerical resolution, an hybridization is applied. The hybridization consists of the introduction of an additional unknown variable.

The HDG methods were initially developed for elliptic problems. For this reason, to show you the main ideas, we start from a simple 1D elliptic model problem with non-homogeneous Dirichlet boundary conditions, strictly following the May's approach [37], we have

$$
\begin{aligned}
-\partial_{xx}u &= f, \quad x \in \Omega = (-1,1) \\
u(-1) &= a \\
u(1) &= b
\end{aligned}
\tag{4.2}
$$

which analytical solution can be found with classical integration, and it reads

$$\Omega$$

$$(-1,0) \qquad\qquad (0,1)$$
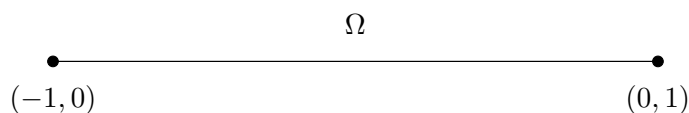
Figure 4.1: Domain of the Problem 4.2.

$$
u(x) = -\frac{f}{2}x^2 + c_1 x + c_2
\tag{4.3}
$$

where, with the restriction imposed by the Dirichlet boundary conditions, we have to fix the values of constants that appear as a consequence of the integration

$$
\begin{aligned}
c_1 &= \frac{b-a}{2} \\
c_2 &= \frac{a+b+f}{2}
\end{aligned}
\tag{4.4}
$$

bringing together equations 4.3 and 4.4 we have the general solution of 4.2

$$
u(x) = \frac{f}{2}\left(1 - x^2\right) + \frac{a}{2}\left(1 - x\right) + \frac{b}{2}\left(1 + x\right)
\tag{4.5}
$$

Now, we could imagine to split the general problem into more problems (for instance two) on the same domain and to establish a connection between them with the adding of a new degree of freedom. In figure 4.1 there is a sketch of the 1D domain in which we are solving the Poisson model problem.

This domain is split into two other domains, which are represented in figure 4.2. The choice of the color will be more clear in the next pages but is associated with the post-processing of the solutions. Thus, in this simple model, we have decided to split the problem 4.2 into two different elliptic problems on two different domain Ω_1 and Ω_2 such that $\Omega = \Omega_1 \cup \Omega_2$. In this sense, we can re-write the initial Problem 4.2 as follows

$$
\begin{aligned}
-\partial_{xx} u_1 = f, \qquad & x \in \Omega_1 = (-1, 0) \\
u_1(-1) = a & \\
u_1(0) = \lambda &
\end{aligned}
\tag{4.6}
$$

and

$$
\begin{aligned}
-\partial_{xx} u_2 = f, \qquad & x \in \Omega_2 = (0, 1) \\
u_2(0) = \lambda & \\
u_2(1) = b &
\end{aligned}
\tag{4.7}
$$

which is, instead, based on figure 4.2.
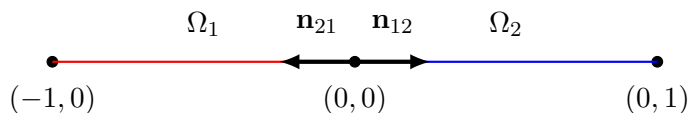
Figure 4.2: Domain of the Problem 4.6 (red, left) and Problem 4.7 (blue, right).

With this operation, we have split the initial Problem 4.2 into two different problems, each one with a specific solution. Finally, we need to establish the connection in $x = 0$ between u_1 and u_2 through λ, which ensures the continuity, but not the differentiability of the general solution in $x = 0$.

Obviously, the left Problem 4.6 and the right Problem 4.7 have two different solutions. In particular, for the left Problem 4.6, appling its boundary conditions we are able to obtain the values of its constants as

$$
\begin{aligned}
c_{1,1} &= \lambda - a - \frac{f}{2} \\
c_{1,2} &= \lambda
\end{aligned}
\tag{4.8}
$$

instead, for the right Problem 4.7, we have

$$
\begin{aligned}
c_{2,1} &= -\left(\lambda - b - \frac{f}{2}\right) \\
c_{2,2} &= \lambda
\end{aligned}
\tag{4.9}
$$

which means that the respective solutions are

$$
\begin{aligned}
u_1(x) &= -\frac{f}{2}x^2 - \left(a + \frac{f}{2}\right)x + \lambda(x + 1) \\
u_2(x) &= -\frac{f}{2}x^2 + \left(b + \frac{f}{2}\right)x - \lambda(x - 1)
\end{aligned}
\tag{4.10}
$$

Equations 4.10 show that the solutions depend on the λ parameter. Of course, only one value of λ can guarantee the continuity and the differentiability of the global solution in $x = 0$.

Figures 4.3, 4.4 and 4.5 show what we have just said. For two different sets of non-homogeneous Dirichlet boundary conditions according to the table 4.1. The results are present in figures 4.3, 4.4 and 4.5. In addition, for each set of boundary conditions, we have chosen two different values of λ parameter. The dashed lines are always related to the global solution, obtained without any splitting in more domains. However, always the external force of the Poisson problem is taken equal to one.

Table 4.1: Boundary conditions for the conceptual examples for the HDG discretization.

	Case A	Case B
$u(-1) = a$	1	0
$u(1) = b$	0	0.3
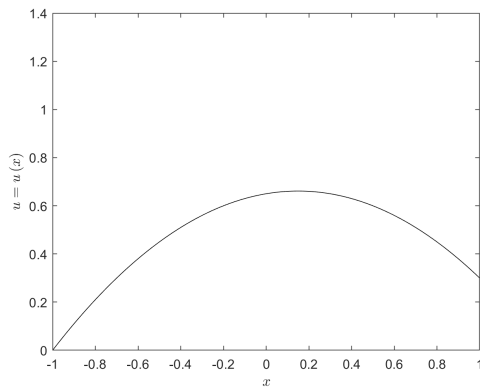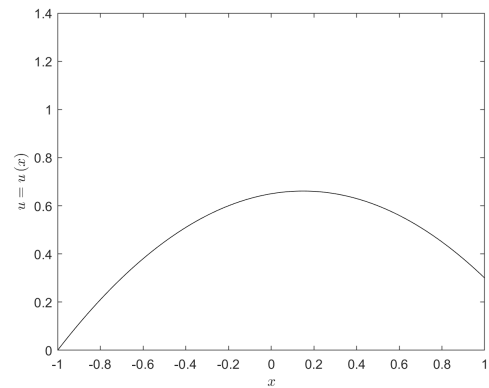
(a) *Case A.*   (b) *Case B.*

Figure 4.3: Analytical solution of Problem 4.2 for $f = 1$. Two different set of Dirichlet boundary conditions: on the left Case A, on the right Case B.
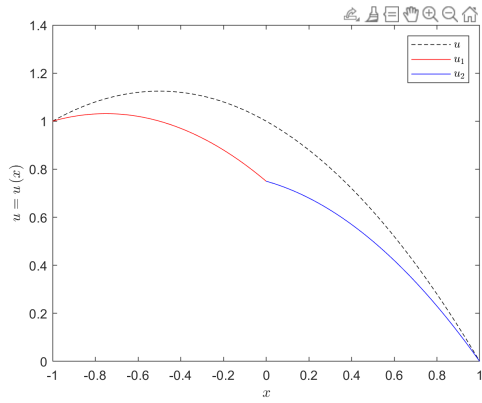
(a) *Case A.*
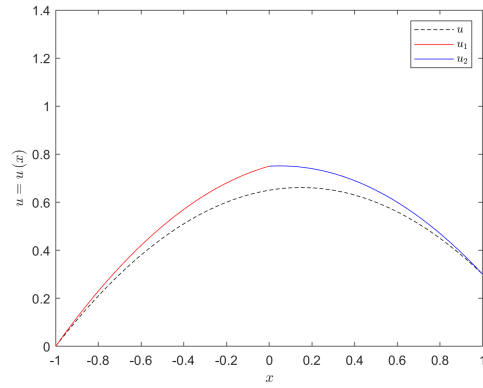
(b) *Case B.*

Figure 4.4: Solution of Problem 4.6 and 4.7 for $\lambda = 0.75$.
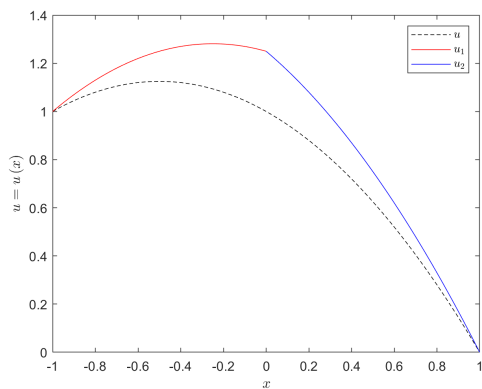
(a) *Case A.*
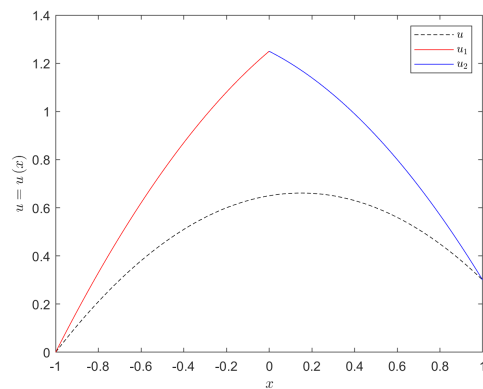
(b) *Case B.*

Figure 4.5: Solution of Problems 4.6 and 4.7 for $\lambda = 1.25$.

For this reason, the next step is to seek a constrain that forces the λ parameter such that the solution of Problems 4.6 and 4.7 will be equal to the solution of model problem 4.2.

Firstly, for any test function $v \in H_0^1(\Omega)$ we can integrate the two problems

$$-\int_{\Omega_1} \nabla^2 u_1 v \, \mathrm{d}x = \int_{\Omega_1} fv \, \mathrm{d}x$$
$$-\int_{\Omega_2} \nabla^2 u_2 v \, \mathrm{d}x = \int_{\Omega_2} fv \, \mathrm{d}x \tag{4.11}$$

summing together, only one equation is obtained

$$-\int_{\Omega_1} \nabla^2 u_1 v \, \mathrm{d}x - \int_{\Omega_2} \nabla^2 u_2 v \, \mathrm{d}x = \int_{\Omega_1} fv \, \mathrm{d}x + \int_{\Omega_2} fv \, \mathrm{d}x \tag{4.12}$$

integrating by parts, remembering that $\int_{\Omega_1} fv \, \mathrm{d}x + \int_{\Omega_2} fv \, \mathrm{d}x = \int_{\Omega} fv \, \mathrm{d}x$

$$-\int_{\Gamma} \nabla u_1 \cdot \mathbf{n}_{12} v \, \mathrm{d}s + \int_{\Omega_1} \nabla u_1 \cdot \nabla v \, \mathrm{d}x - \int_{\Gamma} \nabla u_2 \cdot \mathbf{n}_{21} v \, \mathrm{d}s + \int_{\Omega_2} \nabla u_2 \cdot \nabla v \, \mathrm{d}x = \int_{\Omega} fv \, \mathrm{d}x \tag{4.13}$$

which we can write again, incorporating the Γ integrals, as follows

$$\int_{\Omega_1} \nabla u_1 \cdot \nabla v \, \mathrm{d}x + \int_{\Omega_2} \nabla u_2 \cdot \nabla v \, \mathrm{d}x - \int_{\Gamma} (\nabla u_1 - \nabla u_2) \cdot \mathbf{n}_{12} v \, \mathrm{d}s = \int_{\Omega} fv \, \mathrm{d}x \tag{4.14}$$

and defining $\overline{u} := \Omega \to \mathbb{R}$ as

$$\overline{u} := \begin{cases} u_1, & \mathbf{x} \in \Omega_1 \\ u_2, & \mathbf{x} \in \Omega_2 \end{cases} \tag{4.15}$$

equation reads

$$\int_{\Omega} \nabla \overline{u} \cdot \nabla v \, \mathrm{d}x = \int_{\Omega} fv \, \mathrm{d}x + \int_{\Gamma} (\nabla u_1 - \nabla u_2) \cdot \mathbf{n}_{12} v \, \mathrm{d}s \tag{4.16}$$

All these passages have shown how we have re-written our initial problem in a different form. Equation 4.16 seems the classical variational formulation. It should have been if there was not the additional source term caused by the integration by parts and the previous choice to have split the main problem into more different problems. As a consequence, to find the general variational formulation, we have to impose that the latter integral is null, namely that its integral function respects the following condition

$$(\nabla u_1 - \nabla u_2) \cdot \mathbf{n}_{12} = 0 \tag{4.17}$$

where it is important to notice that the condition is not imposed on the test function caused it will not be, obviously, null.

In this sense, the initial Problem 4.2, now is re-formulated as follows

$$\begin{aligned} -\nabla \cdot \boldsymbol{\sigma}|_K &= f|_K, & \mathbf{x} \in K \\ \boldsymbol{\sigma}|_K &= \nabla u|_K, & \mathbf{x} \in K \\ u|_K &= \lambda|_{e_K}, & \mathbf{x} \in e_K \\ u|_K &= 0, & \mathbf{x} \in \partial K \cap \partial \Omega \\ [\![\boldsymbol{\sigma}]\!] &= 0, & \mathbf{x} \in \Gamma \end{aligned} \tag{4.18}$$

which is the problem that we need to solve for each element of the mesh.

The previous procedure can easily be extended in more dimensions with the same ideas, and it is the base to develop DG methods. This generalized idea was strictly derived by [37]. Here many prophetical examples are also present.

4.3.2   Continuos and Discontinuos Galerkin method (CG and DG)

The main difference between the continuous and discontinuous formulation is based on the possibility to have discontinuities at the interface of two nearby elements. In the CG method, the shape functions are piece-wise continuous. Hence, the approximate global function is continuous at the interface, but the continuity condition does not ensure the differentiability of the same function. In other words, the solution gradients could have not physical significance at the interface, therefore the global solution loses its physical significance. Consequently, the possibility to have jumps in the interfaces has been introduced with the DG approach. Figure 4.6 shows this principal aspect of the two different methodologies. However, the solution in each element with the CG method is computed with the classical FE idea based on shape functions, as well as for the DG method.
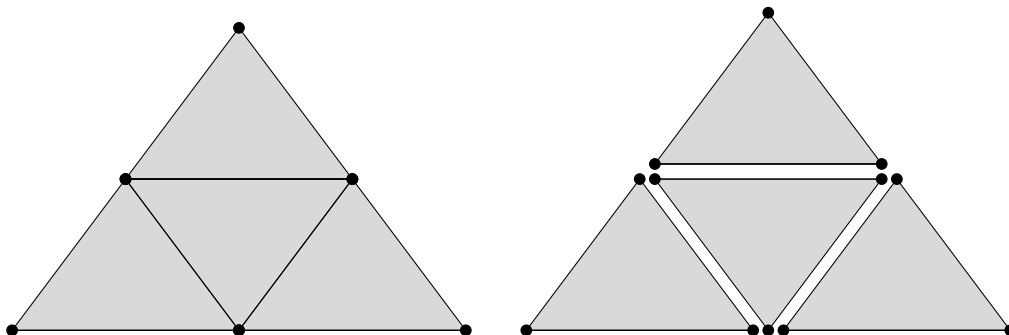
Figure 4.6: CG (left) and DG (right), bidimensional approach.

The DG method gives us the possibility to solve locally the problem for each element. Indeed, no continuity conditions need to be imposed for the test functions at the interfaces. Hence, the shape functions could be chosen null outside the element where we want to solve locally the problem. In this context, it is easy to understand that the method is well structured for mesh refinement (both p, h or hp-refinement).

4.3.3   Hybridized Discontinuos Galerkin method (HDG)

The HDG method improves the DG method with the introduction of an additional degree of freedom between two nearby elements. This degree of freedom has, from a mathematical point of view, $d-1$ dimension, where d is the number of spatial dimensions of the problem. Therefore, if we are working on a one-dimensional problem ($d = 1$), the trace will be a point, while, if we are working in a bidimensional domain ($d = 2$), the trace will be an edge and finally, if we are computing a three-dimensional simulation ($d = 3$), the trace will be a surface. However, the mesh will be made up of both the contributions, thus elements and traces.

At this point, the discretized problem is solved in two different steps:

- **Trace variables**: in this first step, the problem is not solved for each element. This first round aims to establish a connection between the traces using the elements of the mesh. This is possible because we are solving conservative laws. In this sense, the numerical scheme must respect the conservative property. This first computation in the global HDG method gives us in the output the solution for the trace λ_h. This is saved and will be used as the boundary condition for the element-by-element problem.

- **Element-by-Element**: the second step to complete the HDG process resolution, is to solve, for an individual element, its local problem. We need to impose the properly boundary conditions. The latter are given from the previous step. At the same time,

the previous step is solved in the Γ_h set. Now, when we want to compute the solution for each element, we need to split the solution obtained in the previous step on Γ_h set into the left and the right possible value for each trace. This splitting procedure justifies the previous definition of the $\partial \mathcal{T}_h$ set. This is the crucial point of the HDG method. With this splitting, we can obtain the proper Dirichlet boundary conditions for each interior element. For the mesh element which has one, or more, edge/s of the boundary, we imposed on that edge/s the boundary conditions thanks to the Γ_h^b set. Hence, the polynomial solution with p grade can be computed for each element solving several local DG problems.
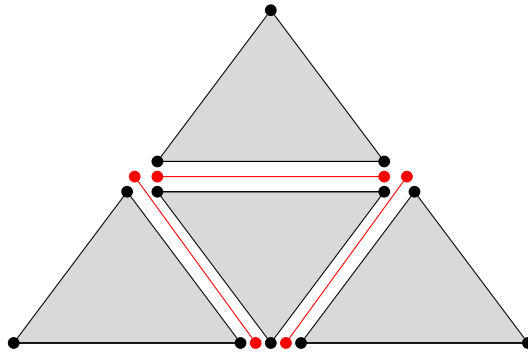
Figure 4.7: HDG, bidimensional approach.
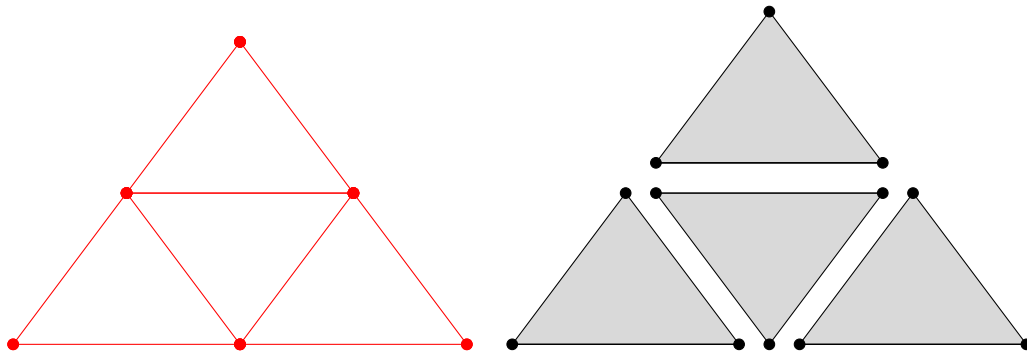
Figure 4.8: HDG bidimensional approach: resolution steps. The first only for the trace variables (left), the second (right) is a DG problem for each element, when the Dirichlet boundary conditions are given from the first step.

Suming up, figure 4.9 and 4.10 show the HDG conceptual approach for one dimensional and bidimensional cases.

Figure 4.9: HDG one dimensional approach. Elements (black) and trace (red).

The method can be also efficiently parallelized in order to reduce more the overall computational cost. However, it is:

- **Hybrid**: because it is a mixed formulation on FV and FE methods where, to make it possible, an additional degree of freedom called trace is added. It gives us the possibility to establish a connection between the elements without solving the problem for
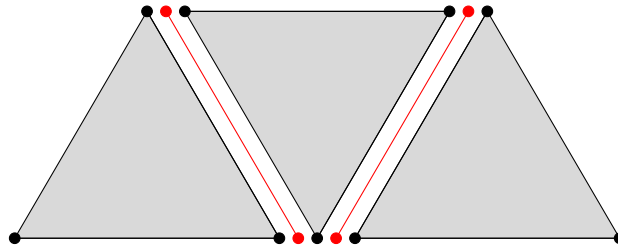
Figure 4.10: HDG bidimensional approach. Elements (grey) and trace (red).

all the elements. Indeed, the concept of hybridization stands on splitting the problem into two problems: the first one for trace variables, the last one for each element. In addition, it is also shown that the hybridization concept has many advantages on the mathematical implications in the splitting of the matrices.

- **Mixed**: because we are searching an approximation both the potentianl w_h and the flux $\boldsymbol{\sigma}_h$

4.4 Navier-Stokes discretization

We can write the classical system of Navier-Stokes equations in the conservative differential form. It is important to introduce the possibility to have source terms to consider the external electromagnetic source term.

The compressible Navier-Stokes equations can be written as follows

$$\partial_t \mathbf{w} + \nabla \cdot \underline{\mathbf{f}}_c(\mathbf{w}) - \nabla \cdot \underline{\mathbf{f}}_v(\mathbf{w}, \nabla \mathbf{w}) = \underline{\mathbf{s}}(\mathbf{w}, \nabla \mathbf{w}) \tag{4.19}$$

where, if we introduce the generalized function $\underline{\mathbf{f}}(\mathbf{w}, \nabla \mathbf{w})$ which stores both the convective and diffusive fluxes, and we assume steady state conditions, we will write again equation 4.19 as follows

$$\nabla \cdot \underline{\mathbf{f}}(\mathbf{w}, \nabla \mathbf{w}) = \underline{\mathbf{s}}(\mathbf{w}, \nabla \mathbf{w}) \tag{4.20}$$

that is the generalized system that describes the physical behavior of the fluid in different cases under the steady-state approach. It contains three different equations: two scalar equations that express the conservation of mass (the continuity equation) and the conservation of the energy (i.e. the first principle of thermodynamics) and one vectorial equation (called momentum equation) that corresponds to Newton's Law. The latter equation can be rewritten as d scalar equations, where d represents the number of the dimension of the problem that we want to analyze. On the same idea, we can define m as the number of scalar equations that form the full system. Of course, if we do not take into consideration any chemical reactions and thermodynamic non-equilibrium, we will have $m = d + 2$. Instead, if we consider the possibility to introduce chemical reactions, the number of scalar equations will increase because we have N_s continuity equations, one for each species. Hence, in this situation, we will have $m = d + 1 + N_s$. On the other hand, it is easy to understand that if we are studying a multi-temperature model, the number of scalar equations will be $m = d + 1 + N_t$. In addition, in the most general case, we will have $m = d + N_s + N_t$ scalar equations. Obviously, all these possibilities are valid when we do not introduce any other vectorial equations in the full system. In the code the m parameter is often called `COMP`.

At this point, it is important to remember that our problem needs appropriate boundary conditions on the edge of the domain Ω. In this sense, the problem is written as

$$\nabla \cdot \underline{\mathbf{f}}(\mathbf{w}, \nabla \mathbf{w}) = \underline{\mathbf{s}}(\mathbf{w}, \nabla \mathbf{w}), \qquad \mathbf{x} \in \Omega \subset \mathbb{R}^d$$
$$\underline{\mathbf{B}}(\mathbf{w}) = (\mathbf{u}, \ \mathbf{q} \cdot \mathbf{n}), \qquad \mathbf{x} \in \partial\Omega \tag{4.21}$$

where $\mathbf{w}$ is the state-local vector of the conserved variables, which general definition is

$$\mathbf{w}: \ \mathbb{R}^m \times (0, \infty) \to \mathcal{D} \subset \mathbb{R}^{m=d+2} \tag{4.22}$$

and $\mathcal{D}$ is the space of the possible value that the state-local vector could be assumed during the simulation. To give a definition of this space is important to remember that the state-local vector of the conserved variables looks like

$$\mathbf{w} = \begin{pmatrix} \rho \\ \mathbf{m} \\ \rho E \end{pmatrix} \equiv \begin{pmatrix} \rho \\ \rho\mathbf{u} \\ \rho E \end{pmatrix} \equiv \rho \begin{pmatrix} 1 \\ \mathbf{u} \\ E \end{pmatrix} \tag{4.23}$$

where ρ is the density of the mixture (in S.I. $\left[kg/m^3\right]$), $\mathbf{u} = (u_1, ..., u_d)^T$ is the fluid velocity vector (in S.I. $[m/s]$) and E the specific total energy (in S.I. $[J/kg]$). As a consequence, we can define the variations of the state-local vector in each direction of the problem. In this sense, we shall obtain

$$\nabla \mathbf{w}: \ \mathbb{R}^m \times (0, \infty) \to \mathcal{D} \subset \mathbb{R}^{m \times d} \equiv \mathbb{R}^{(d+2) \times d} \tag{4.24}$$

After these definitions, it is very simple to understand the mathematical form of the convective, diffusive, and source terms. In particular, we will have, for the convective fluxes

$$\underline{\mathbf{f}}_c\left(\mathbf{w}\right):\ \mathcal{D}\to\mathbb{R}^{m\times d}\equiv\mathbb{R}^{(d+2)\times d} \tag{4.25}$$

while, for the diffusive flux

$$\underline{\mathbf{f}}_v\left(\mathbf{w},\nabla\mathbf{w}\right):\ \mathcal{D}\times\mathbb{R}^{m\times d}\to\mathbb{R}^{m\times d}\equiv\mathbb{R}^{(d+2)\times d} \tag{4.26}$$

and, for the source term

$$\underline{\mathbf{s}}\left(\mathbf{w},\nabla\mathbf{w}\right):\ \mathcal{D}\times\mathbb{R}^{m\times d}\to\mathbb{R}^{m\times d}\equiv\mathbb{R}^{(d+2)\times d} \tag{4.27}$$

Until now, in all the mathematical definitions given, there was the presence of the space $\mathcal{D}$, but it has not yet been defined. Previously, we anticipated that it contains all the possible physical solutions to the problem. It is well known that we cannot expect a negative density, a negative energy, or a velocity vector that has lower, or higher, scalar components than the dimension of the problem. For these reasons, it is important to define this space as follows

$$\mathcal{D}:=\left\{\mathbf{w}=(\rho,\mathbf{m},\rho E)^T\ |\ \rho>0,\mathbf{m}\in\mathbb{R}^d,E-\frac{1}{2}\left(\frac{\|\mathbf{m}\|_2}{\rho}\right)^2\right\} \tag{4.28}$$

which encloses all the observations that we made before.

4.5   Spatial discretization

Assuming that we are working with a mesh made up of triangular elements denotes by K. In general, the element near the K-triangular element is called K', and the edge that they have in common is named, in the most general case, e. More specifically, if we consider two nearby elements, we denote K^- the left one and K^+ the right one, like figure 4.14 shows. In addition, each element has a boundary denoted by ∂K.
The set of each K-triangular element is called triangulation. More precisely, we call $\mathcal{T}_h$ the collection of disjoint, non-overlapping elements which tessellated the domain Ω, like figure 4.11 shows. Its mathematical translation is the following

$$\mathcal{T}_h=\{K\} \tag{4.29}$$

such that

$$\Omega:=\bigcup_{K\in\mathcal{T}_h}K \tag{4.30}$$

Each triangular element has three edges that can be on the boundary of the domain (what we called $\partial\Omega$) or inside it. We need to divide these two cases:

- **Interior boundary**: for each of them, we call $\partial\mathcal{T}_h$ the set of all the element boundary of each element. Thus, if we are considering two nearby elements, their common edges, in $\partial\mathcal{T}_h$, appears twice, i.e.

$$\partial\mathcal{T}_h:=\{\partial K\backslash\partial\Omega\ |\ K\in\mathcal{T}_h\} \tag{4.31}$$

In the same way, we can define a different set where the common edges are store just one. It is called Γ_h, see figure 4.12

$$\Gamma_h:=\left\{e\ :\ e=\partial K^-\cap\partial K^+\text{ for }K^-,K^+\in\mathcal{T}_h;\ \text{meas}_{d-1}e\neq0\right\} \tag{4.32}$$
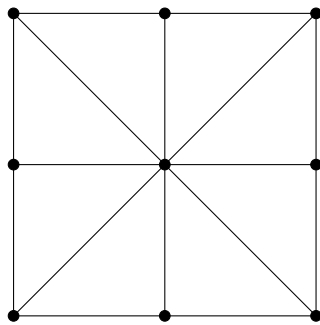
Figure 4.11: Scheme of domain Ω split into a collection of non-overlapping triangular elements K.

(a) $\partial\mathcal{T}_h$ (b) Γ_h
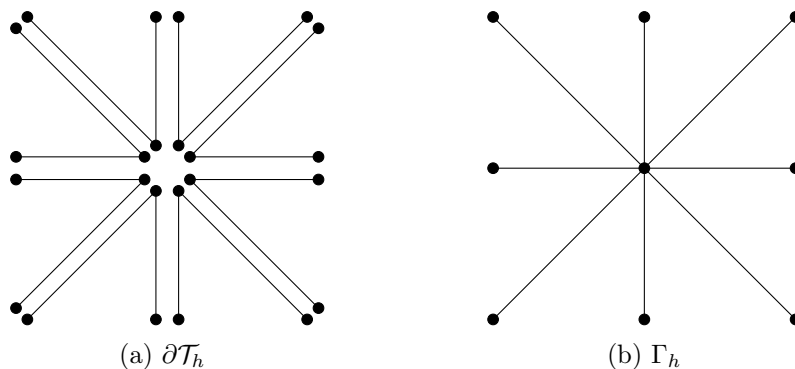
Figure 4.12: Internal egdes.

- **External boundary**: we call it Γ_h^b. It stores all the edges of all the triangular elements that are on the boundary of the domain (see figure 4.12). Hence, its mathematical translation is

$$\Gamma_h^b := \bigcup_{K\in\mathcal{T}_h} \partial K \cap \partial\Omega \tag{4.33}$$
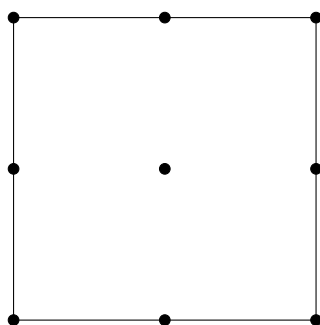
Figure 4.13: Scheme of Γ_h^b.

Now, let us consider two nearby triangular elements of the triangulation $\mathcal{T}_h$. As already mentioned, we call K^- the left element and K^+ the right one. Their common edge is e where we can notice the presence of two outward pointing normals: $\mathbf{n}^-$ and $\mathbf{n}^+$ for the left and the right element, respectively. Each element has its boundary, hence we have ∂K^- for the left triangular element and ∂K^+ for the right one. Figure 4.14 shows all these definitions.
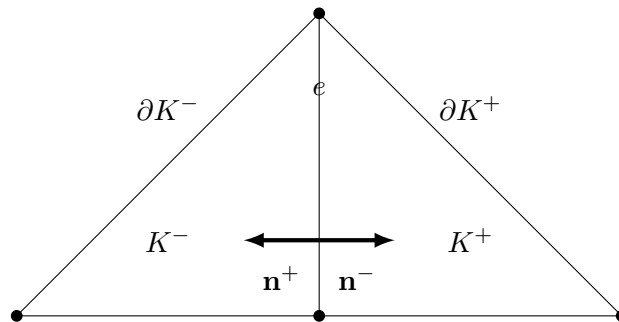
Figure 4.14: Two nearby triangular elements of the mesh. Notations and definitions.

Discontinuities are allowed at the edges. As a consequence, we need to identify the jump between the two nearby elements and, in addition, the mean value. There are two cases to take into account which depend on the edge that we are considering. In other words, if the edge is internal, we will have some definitions, if it is external we will have others rules. However, the definitions of the jump operator ($[\![...]\!]$), according to [37], is split into scalar and vector-valued function. Respectively, for the interior edges (thus Γ_h), we have

$$\begin{aligned}
[\![u]\!] &= u^- \mathbf{n}^- + u^+ \mathbf{n}^+ \\
[\![\mathbf{q}]\!] &= \mathbf{q}^- \cdot \mathbf{n}^- + \mathbf{q}^+ \cdot \mathbf{n}^+
\end{aligned} \tag{4.34}$$

where it is important to notice that the jump for a scalar function is a vector, while the jump operator applied on a vector-value function returns a scalar. Furthermore, the jump is null for a continuous function.

In the same way, we can define the operator of the mean value ($\{...\}$) for scalar and vector-value function in the interior edges. Respectively, we have

$$\begin{aligned}
\{u\} &= \frac{u^- + u^+}{2} \\
\{\mathbf{q}\} &= \frac{\mathbf{q}^- + \mathbf{q}^+}{2}
\end{aligned} \tag{4.35}$$

These definitions change when we are considering edges on the boundary of the domain (thus Γ_h^b, that is $\partial\Omega$). In fact, in this situation, there is not the presence of the two outward unit normals, but we have only one outward unit normal. Hence, the jump operator is defined as follows

$$\begin{aligned}
[\![u]\!] &= u\mathbf{n} \\
[\![\mathbf{q}]\!] &= \mathbf{q} \cdot \mathbf{n}
\end{aligned} \tag{4.36}$$

while the mean values look like

$$\begin{aligned}
\{u\} &= u \\
\{\mathbf{q}\} &= \mathbf{q}
\end{aligned} \tag{4.37}$$

In each triangular element, we are going to approximate the solution with a function of order p. Usually, the polynomial degree of two nearby elements does not vary. However, if it happens, we have two different polynomial degrees: p_{K^-} for the left triangular element and p_{K^+} for the right one. The polynomial degree of the shared interface is chosen as the higher of them, i.e.

$$p_e = \max\{p_{K^-}; p_{K^+}\} \tag{4.38}$$

4.5.1 Approximation spaces

We denote $\Pi^p\left(\mathcal{D}\right)$ the set of polynomials of maximum degree p on the some domain $\mathcal{D}$. We introduce discontinuos functions space

$$
\begin{aligned}
\mathbf{V}_h &= \left\{v \in L^2\left(\Omega\right) \ : \ v|_K \in \Pi^{p_K} \in \left(K\right), \ K \in \mathcal{T}_h\right\}^{m \times d} \\
W_h &= \left\{w \in L^2\left(\Omega\right) \ : \ w|_K \in \Pi^{p_K} \in \left(K\right), \ K \in \mathcal{T}_h\right\}^{m}
\end{aligned}
\tag{4.39}
$$

and the mesh skeleton

$$
M_h = \left\{\mu \in L^2\left(\Gamma_h\right) \ : \ w|_K \in \Pi^{p_e} \in \left(K\right), \ e \in \Gamma_h\right\}^{m}
\tag{4.40}
$$

where $L^2\left(\Omega\right)$ is the space of square integrable functions on the domain $\mathcal{D}$. Hence, $\mathbf{v} \in \mathbf{V}_h$, $w \in W_h$ and $\mu \in \mathbf{M}_h$ are piecewise polynomials of degree p which can be discontinuos across edges (for $\mathbf{v}$ and for w) or vertices (for μ).

4.6 Notation

We denote these inner products as follows

$$
\begin{aligned}
(v, w)_{\mathcal{T}_h} &:= \sum_{K \in \mathcal{T}_h} \int_K vw \ \mathrm{d}x \\
(\mathbf{v}, \mathbf{w})_{\mathcal{T}_h} &:= \sum_{K \in \mathcal{T}_h} \int_K \mathbf{v} \cdot \mathbf{w} \ \mathrm{d}x \\
\langle v, w\rangle_{\partial\mathcal{T}_h} &:= \sum_{K \in \mathcal{T}_h} \int_{\partial K} vw \ \mathrm{d}\sigma \\
\langle v, w\rangle_{\Gamma_h} &:= \sum_{e \in \Gamma_h} \int_e vw \ \mathrm{d}\sigma
\end{aligned}
\tag{4.41}
$$

In addition, we can define the number of elements

$$
n_e := |\mathcal{T}_h|
\tag{4.42}
$$

and the number of internal faces (trace variables)

$$
n_f := |\Gamma_h|
\tag{4.43}
$$

The projection of w onto the skeleton of the mesh is λ, namely

$$
\lambda := w|_{\Gamma_h}
\tag{4.44}
$$

4.7 Different formulations of the problem

The first step to discretize with the HDG method our equations is to write again them, which in the most general case are a system of partial differential equations of the second order, like a system of the first order. In order to make it, we need to reformulate the problem by introducing the quantity

$$
\underline{\boldsymbol{\sigma}} = \nabla\mathbf{w}
\tag{4.45}
$$

namely, our starting problem now is posed as follows

$$
\begin{aligned}
\underline{\boldsymbol{\sigma}} - \nabla\mathbf{w} &= 0, & \mathbf{x} \in \Omega \subset \mathbb{R}^d \\
\nabla \cdot \left[\underline{\mathbf{f}_c}\left(\mathbf{w}\right) - \underline{\mathbf{f}_d}\left(\mathbf{w}, \underline{\boldsymbol{\sigma}}\right)\right] &= \underline{\mathbf{s}}\left(\mathbf{w}, \underline{\boldsymbol{\sigma}}\right), & \mathbf{x} \in \Omega \subset \mathbb{R}^d \\
\underline{\mathbf{B}}\left(\mathbf{w}\right) &= \left(\mathbf{u}, \dot{\mathbf{q}} \cdot \mathbf{n}\right), & \mathbf{x} \in \partial\Omega
\end{aligned}
\tag{4.46}
$$

which is the strong formulation.

Hence, we can introduce the DG discretization of the problem.
In equations 4.46 we have written the strong and mixed form of our problem.
Now we are interested in the mixed and variational formulation of the problem. To find
them, we must introduce test functions as follows

$$(\boldsymbol{\tau}_h, \phi_h) \in \mathbf{V}_h \times W_h \tag{4.47}$$

and by multiplying problem 4.46 against test functions 4.47. Then, integrating by part
the last equation, finally, we will have the standard DG discretization written in the mixed
formulation of the problem, namely the DG discretization of the problem will be

Finding $\mathsf{x}_h^{DG} := (\boldsymbol{\sigma}_h, w_h) \in \mathbb{X}_h^{DG} := \mathbf{V}_h \times W_h$ s.t. $\forall\, \mathsf{y}_h^{DG} := (\boldsymbol{\tau}_h, \phi_h) \in \mathbb{X}_h^{DG}$ such that

$$
\begin{aligned}
0 &= \mathcal{N}_h^{DG}\left(\mathsf{x}_h^{DG}, \mathsf{y}_h^{DG}\right) \\
&= \mathcal{N}_h^{DG}\left(\boldsymbol{\sigma}, w_h; \boldsymbol{\tau}_h, \phi_h\right) \\
&:= (\boldsymbol{\tau}_h, \boldsymbol{\sigma})_{\mathcal{T}_h} + (\nabla \cdot \boldsymbol{\tau}_h, w_h)_{\mathcal{T}_h} - \langle \boldsymbol{\tau}_h \cdot \mathbf{n}, \hat{w} \rangle_{\partial \mathcal{T}_h} - \\
&\quad - (\nabla \phi_h, \mathbf{f}_c\left(w_h\right) - \mathbf{f}_v\left(w_h, \boldsymbol{\sigma}_h\right))_{\mathcal{T}_h} - (\phi_h, s\left(w_h, \boldsymbol{\sigma}_h\right))_{\mathcal{T}_h} + \langle \phi_h, \hat{f}_c - \hat{f}_v \rangle_{\partial \mathcal{T}_h} + \\
&\quad + \mathcal{N}_{h,sc}^{DG}\left(\boldsymbol{\sigma}_h, w_h; \phi_h\right) + \mathcal{N}_{h,\partial\Omega}^{DG}\left(\boldsymbol{\sigma}_h, w_h; \boldsymbol{\tau}_h, \phi_h\right)
\end{aligned}
\tag{4.48}
$$

At this point, we can switch from the DG formulation of the problem to the HDG one.
In order to make it possible we need to introduce the additional degree of freedom related
to the trace variables of the mesh. This is taken into account by λ_h. Consequently, our
final problem will be:

Finding $\mathsf{x}_h := (\boldsymbol{\sigma}_h, w_h, \lambda_h) \in \mathbb{X}_h := (\mathbf{V}_h, W_h, M_h)$ such that $\forall\, \mathsf{y}_h := (\boldsymbol{\tau}_h, \phi_h, \mu_h) \in \mathbb{X}_h$
is verified that

$$
\begin{aligned}
0 &= \mathcal{N}_h\left(\mathsf{x}_h, \mathsf{y}_h\right) \\
&= \mathcal{N}_h\left(\boldsymbol{\sigma}_h, w_h, \lambda_h; \boldsymbol{\tau}_h, \phi_h, \mu_h\right) \\
&:= (\boldsymbol{\tau}_h, \boldsymbol{\sigma}_h)_{\mathcal{T}_h} + (\nabla \cdot \boldsymbol{\tau}_h, w_h)_{\mathcal{T}_h} - \langle \boldsymbol{\tau}_h \cdot \mathbf{n}, \lambda_h \rangle_{\partial \mathcal{T}_h} - \\
&\quad - (\nabla \phi_h, \mathbf{f}_c\left(w_h\right) - \mathbf{f}_v\left(w_h, \boldsymbol{\sigma}_h\right))_{\mathcal{T}_h} - (\phi_h, s\left(w_h, \boldsymbol{\sigma}_h\right))_{\mathcal{T}_h} + \langle \phi_h, \hat{f}_c - \hat{f}_v \rangle_{\partial \mathcal{T}_h} + \\
&\quad + \mathcal{N}_{h,sc}\left(\boldsymbol{\sigma}_h, w_h; \phi_h\right) + \mathcal{N}_{h,\partial\Omega}\left(\boldsymbol{\sigma}_h, w_h; \boldsymbol{\tau}_h, \phi_h\right) + \\
&\quad + \langle \mu_h, [\![\hat{f}_c - \hat{f}_d]\!] \rangle_{\Gamma_h}
\end{aligned}
\tag{4.49}
$$

where in the formulations 4.48 and 4.49 we have introduced also the shock-capturing and
the boundary operator both for the DG and HDG formulation, respectively $\mathcal{N}_{h,sc}$ and
$\mathcal{N}_{h,\partial\Omega}$. More precisely, the last one reads

$$
\begin{aligned}
\mathcal{N}_{h,\partial\Omega}\left(\boldsymbol{\sigma}_h, w_h; \phi_h\right) &:= \langle \boldsymbol{\tau}_h \cdot \mathbf{n}, w_{\partial\Omega}\left(w_h\right) \rangle_{\Gamma_h}^b + \\
&\quad + \langle \phi_h, \left(\mathbf{f}_c\left(w_{\partial\Omega}\left(w_h\right)\right) - \mathbf{f}_v\left(w_{\partial\Omega}\left(w_h\right), \boldsymbol{\sigma}_{\partial\Omega}\left(w_h, \mathbf{q}_h\right)\right)\right) \cdot \mathbf{n} \rangle_{\Gamma_h}^b
\end{aligned}
\tag{4.50}
$$

where the fluxes are computed in two different ways [59]: Roe-like approach for the con-
vective flux, and BB2-like method for the diffusive flux.

4.8   Summary

In this Chapter we have shown the most common numerical methods used to solve PDEs.
An overview of FD, FE, and FV methods has been presented. The most important advan-
tages and disadvantages for each one of these methods have been tabled. Then, introducing

the Fluid Dynamic equations for hypersonic flows, problems related to the low order of FV methods were compared to the high-order methods. In this sense, it has been shown how in the last years the attention has been focused on the DG methods. On the other hand, the high computational cost of these methods has necessarily introduced the hybridization concept. Hence, in the second part of this Chapter, the HDG discretization of the Navier Stokes system for electrically conducting flow has been presented.

Chapter 5

The code: High-Order Unifying Framework

The High-Order Unifying Framework works with the conservative form of the equations. Currently, no implementation for time-dependent solutions is implemented. Furthermore, it is continuously under development. It is a modular code, well extensible at the implementation of new physical models. It assembles automatically the Jacobian matrices. In order to make it, it uses the `AutoDiff` data type, which stores both the value of the variables and their derivatives.

5.1 Automatic Differentiation (AD)

In computer science, Automatic Differentiation is a typical way to compute the derivatives of functions. The High-Order Unifying Framework works with AD [59]. The AD is based on the classical derivatives rules for sum, difference, product, and division. Furthermore, its algorithm is made up of the chain rule.

In general, we can say that there are two different procedures to use the chain rule to obtain derivatives. Their concepts and ideas are the same, but they are applied in two different strategies

- Forward accumulation

$$\frac{\partial w_i}{\partial x} = \frac{\partial w_i}{\partial w_{i-1}} \frac{\partial w_{i-1}}{\partial x} \tag{5.1}$$

- Reverse accumulation

$$\frac{\partial x}{\partial w_i} = \frac{\partial x}{\partial w_{i+1}} \frac{\partial w_{i+1}}{\partial w_i} \tag{5.2}$$

AutoDiff type

AutoDiff is the computer science type used to store both the value and its derivatives. In this sense also the current code works with it. On the other hand, the library Mutation++ [51]; [52] does not use AD. In order to correctly compute all the physical quantities that we need in our code, a thermodynamic interface was developed by Devesse [20] to introduce the effects of high temperature and chemical reactions, typical situations in hypersonic flight.

In this Master's Thesis, the idea developed by Devesse [20] has been applied to evaluate the electrical conductivity. In this way, if for further developments there will be the necessity to implement boundary conditions for the electromagnetic term, the AD step will be already completed.
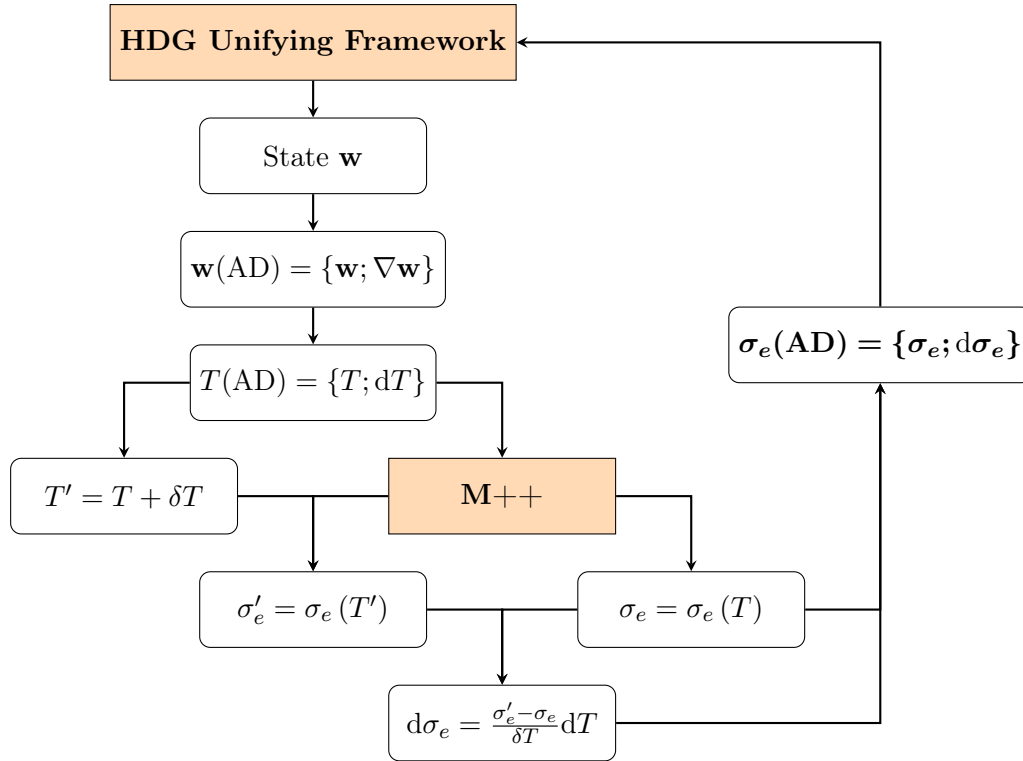
Figure 5.1: Flow chart to interface the High-Order Unifying Framework to the Mutation++ library. This explains how to overcome the problem of AutoDiff data type which stores, at the same time, the value of the variables and their derivatives. The general idea was strictly taken by Devesse [20].

5.2   Dummy model structure

All the models are built on the `dummymodel.h` structure. Inside there are all the functions that are required to the construction of each physical model based on the conservative differential form of the equations. The most important parameters are the `bool` type `Convection`, `Diffusion` and `Source`. They can be set as `true` or `false` based on the conservative form of the equations. In addition, we have `NumDerVar` that is an `int` type variable and it stores the number of derivated variables that the `EvalDerVar` function computes. Finally, `NumBdryCoeff` parameter, like the previous one, is `int` type variable and it contains the number of the coefficients that we want to receive in output in the `coefficiens-NE-p-extra.txt` file.

There are parameters related to the physical aspects of the model that can be changed by the user as s/he wants. Then, the most important variables to take into account are the following: `state` which stores `sparam`, `dervar`, `bcstate`, `bcnr` which contains the integer value that corrisponds to the boundary conditions type (take a look at `bdrystate.h` file and remember that, inside `Netgen` geometry creation the `bc` value is `bcnr + 1`).

5.3   General output

During the simulation, the code computes all the quantities for each cell. Hence, the routine is called for each triangular, or quadrilateral, element. Then, it gives us different output files:

- **Solution file**: it stores the numerical solution for the Paraview post-processing and the binary file to start again the simulation from the previous just computed solution. The first one is the file.dat, while the second one the file.out. The structure of the name file is always the same `solution-NE-p-extra.txt`.

- **Log file**: it contains some information about the adaptation process. In general, there is a number of rows equal to the number of the iterations during the adaptation procedure (from one to the final value inserted in the `run.py` script). The meaning of its columns is the following: number of elements of the mesh, the ndof value (number of global point inside all the elements), the time to compute the solution at that iteration and, finally, the difference between the current time and the starting time. The name of this file is `log-p-extra.txt`.

- **Error file**: it stores the following columns: number of elements, the ndof value (number of global point inside all the elements), then other thirteen columns in bidimensional simulations which represent the following paramter: $\text{ndof}^{-1/d}$, where d is the dimension of the problem. These last columns are concerning with the error estimation. The name of the file is `errordata.csv`.

- **Coefficients file**: it is organized in this way: the first column stores the `bcnr` parameter (thus, the type of boundary conditions), then there are d columns that store the `sparam.pos` parameters, thus the coordinates of each cell. Of course, in bidimensional simulations, there are only x and y values, while in tridimensional there is also the presence of z column. The third block of columns stores the value of the computed coefficients. For instance, in inviscid simulation, we are interested in the coefficient of pressure (hence, only one column is present and it contains the c_p value), while in the viscous simulation we introduce also the coefficient of friction (hence, two columns are present, one for c_p value and the last one for c_f value). The name of this file is `coefficiens-NE-p-extra.txt`.

- **Mesh file**: it is a file to open in Paraview for the post-processing and viewing of the mesh generated by the solver. The denomination of this file is `mesh-NE-p-extra.dat`.

`NE` represents the number of elements in the mesh, `p` the polynomial degree for the approximate function in each cell and `extra` what we want, for instance, the Mach number, the angle of attack, the Reynolds number or all the fluid dynamic parameters that describe the simulation. The code is open to everyone, in this sense everyone can change and adapt it to his needs.

5.4 Physical models

The code [59] is continuously under developments and it is used for research activities. In the code, there are already developed several physical models. In this section, we will go to describe them.

5.4.1 Compressible Euler

The Euler equations are made up of inviscid continuity, momentum, and energy equations. Hence, in the conservative differential form, we can write

$$\nabla \cdot \underline{\mathbf{f}}_c (\mathbf{w}) = 0 \tag{5.3}$$

where the state-local vector and the convective fluxes are defined as follows

$$\mathbf{w} = \begin{pmatrix} \rho \\ \mathbf{m} \\ \rho E \end{pmatrix} \qquad \underline{\mathbf{f}}_c (\mathbf{w}) = \begin{pmatrix} \rho \mathbf{u} \\ \rho \mathbf{u} \otimes \mathbf{u} + p\underline{\mathbf{I}} \\ (\rho E + p) \mathbf{u} \end{pmatrix} \tag{5.4}$$

where the pressure is related to the other conservative variables thanks to the equation of state

$$p = \rho (\gamma - 1) \left(E - \frac{(\|\mathbf{u}\|_2)^2}{2} \right) \tag{5.5}$$

and the temperature is defined through the ideal gas law by

$$T = \frac{1}{(\gamma - 1) c_v} \frac{p}{\rho} = \frac{1}{c_v} \left(E - \frac{(\|\mathbf{u}\|_2)^2}{2} \right) \tag{5.6}$$

The full model is well explained in [4].

5.4.2   Compressible Navier-Stokes

The Navier-Stokes equations in the conservative differential form are given by

$$\nabla \cdot \underline{\mathbf{f}}_c (\mathbf{w}) - \nabla \cdot \underline{\mathbf{f}}_v (\mathbf{w}, \nabla \mathbf{w}) = 0 \tag{5.7}$$

where the vector of conserved variables and the convective fluxes coincide with the Euler equations. Also, the pressure and temperature are the same. Instead, the diffusive fluxes, are given by

$$\underline{\mathbf{f}}_v (\mathbf{w}, \nabla \mathbf{w}) = \begin{pmatrix} 0 \\ \boldsymbol{\tau} \\ \boldsymbol{\tau}\mathbf{u} - \dot{\mathbf{q}} \end{pmatrix} \tag{5.8}$$

where the stress tensor $\boldsymbol{\tau}$ depends on the nature of the fluid. For Newtonian fluid, it is defined, after the application of Stokes' hypothesis, as follows

$$\boldsymbol{\tau} = \mu \left[\nabla \mathbf{u} + (\nabla \mathbf{u})^T - \frac{2}{3} (\nabla \cdot \mathbf{u}) \underline{\mathbf{I}} \right] \tag{5.9}$$

where μ is the dynamic viscosity defined by Sutherland's law as

$$\mu = \nu \rho = S \frac{\sqrt[3]{T^2}}{T + \chi} \tag{5.10}$$

with $S = 1.458 \times 10^{-6} \ kg/\left(m \ s \ \sqrt{K} \right)$, $\chi = 110.4 K$ and ν is the kinematic viscosity (in S.I. $\left[m^2/s \right]$). In addition, the heat flux is defind by the Fourier's law, thus

$$\dot{\mathbf{q}} = -\lambda \nabla T \tag{5.11}$$

where λ is the thermal conductivity (in S.I. $[W/(m \ K)]$), while $\kappa = \lambda/(\rho c_p)$ is the thermal diffusivity (in S.I. $\left[m^2/s \right]$). The ratio between the extension of kinematic and thermal boundary layers is expressed by the Prandtl number, thus

$$\Pr = \frac{\mu c_p}{\lambda} = \frac{\nu}{\kappa} \propto \left(\frac{\delta}{\delta_T} \right)^2 \tag{5.12}$$

Typical value of Prandtl number for air is $0.71 - 0.72$. In general, in the liquid, the Prandtl number is higher than in the gases. For instance, water (at $T = 20°C$) it reaches 7. On the other hand, liquid metals (Hg, Na) have Prandtl number very low. The full model is well explained in [4].

5.4.3 Compressible Euler high-enthalpy

The mathematical structure of these equations coincides with the classical Euler equations. No diffusive fluxes are present, hence

$$\nabla \cdot \underline{\mathbf{f}}_c(\mathbf{w}) = 0 \tag{5.13}$$

the differences are based on the closure equations. Indeed, as a consequence of the high-temperature, all the physical quantities are not more constant. In this models, developed by [20], the external terms are computed by Mutation++ library [52]; [51]. For instance, when we are considering a mixture composed of different species, we cannot compute the pressure through equation 5.5, but with the combination of Dalton's law and perfect gas law [27], we have

$$p = \sum_{i=1}^{N_s} \rho_i \frac{\mathcal{R}}{\mathcal{M}_i} T \tag{5.14}$$

where $\mathcal{R}$ is the universal gas constant (in S.I. 8.3145 $J/(\text{mol } K)$), while $\mathcal{M}_i$ is molar mass.

5.4.4 Compressible Navier-Stokes high-enthalpy

The set of equations is equal to Compressible Navier-Stokes, thus

$$\nabla \cdot \underline{\mathbf{f}}_c(\mathbf{w}) - \nabla \cdot \underline{\mathbf{f}}_v(\mathbf{w}, \nabla \mathbf{w}) = 0 \tag{5.15}$$

the only differences, like in the Euler high-enthalpy version, are based on the closure equations. Indeed, as a consequence of the high temperature, all the physical quantities are not more constant. In this models, developed by [20], the external terms are computed by Mutation++ library [52]; [51].

5.4.5 Turbulence modelling

In turbulence modeling, the set of equations contains both convective and diffusive fluxes. The number of scalar equations depends on the number of closure

$$\nabla \cdot \underline{\mathbf{f}}_c(\mathbf{w}) - \nabla \cdot \underline{\mathbf{f}}_v(\mathbf{w}, \nabla \mathbf{w}) = \underline{\mathbf{s}}(\mathbf{w}, \nabla \mathbf{w}) \tag{5.16}$$

Spalart-Alarms RANS turbulence modelling

This is a turbulence model where there is an additional equation to solve in order to describe the Reynolds stress tensor. Hence, for Spalart-Alarms, we will have $m = d + 3$ scalar equations

$k - \omega$ RANS turbulence modelling

In the $k - \omega$ turbulence model we are going to introduce two different scalar equations that describe the behavior of the specific turbulent kinetic energy k and the specific turbulent dissipation rate ω. In this sense, we have $m = d + 4$ scalar equations. The complete model is well explained in [61].

5.4.6 Multispecies

This model is completely explained in [20]. It is used to simulate chemical non-equilibrium where, as a consequence of non-equilibrium, source terms for mass equations are added. In addition, the continuity equation is not unique like in the previous cases, but we will have

a number of continuity equations equal to the number of species that are involved in the physical-chemical processes. Hence, we have

$$\nabla \cdot \underline{\mathbf{f}}_c \left(\mathbf{w} \right) - \nabla \cdot \underline{\mathbf{f}}_v \left(\mathbf{w}, \nabla \mathbf{w} \right) = \underline{\mathbf{s}} \left(\mathbf{w}, \nabla \mathbf{w} \right) \tag{5.17}$$

where

$$\mathbf{w} = \begin{pmatrix} \rho_i \\ \mathbf{m} \\ \rho E \end{pmatrix} \qquad \underline{\mathbf{f}}_c \left(\mathbf{w} \right) = \begin{pmatrix} \rho_i \mathbf{u} \\ \rho \mathbf{u} \otimes \mathbf{u} + p \underline{\mathbf{I}} \\ \left(\rho E + p \right) \mathbf{u} \end{pmatrix} \qquad \underline{\mathbf{f}}_v \left(\mathbf{w}, \nabla \mathbf{w} \right) = \begin{pmatrix} -\mathbf{J}_i \\ \underline{\tau} \\ \underline{\tau} \mathbf{u} - \dot{\mathbf{q}} \end{pmatrix} \tag{5.18}$$

while the source term is

$$\underline{\mathbf{s}} \left(\mathbf{w}, \nabla \mathbf{w} \right) = \begin{pmatrix} \dot{\omega}_i \\ \mathbf{0} \\ 0 \end{pmatrix} \tag{5.19}$$

where $\dot{\omega}_i$ is the chemical mass production per unit of volume in the unit of time.

5.5   Relaxation

To solve the non-linear system of the HDG method (4.49) the code [59] uses the Newton-Raphson method. Following, for instance [58], we have

$$\mathcal{N}'_h \left[\mathsf{x}^n_h \right] \left(\delta \mathsf{x}^n_h; \mathsf{y}_h \right) = -\mathcal{N}_h \left(\mathsf{x}^n_h; \mathsf{y}_h \right), \qquad \forall \mathsf{y}_h \in \mathsf{X}_h \tag{5.20}$$

where $\mathcal{N}'_h \left[\mathsf{x}^n_h \right] \left(\delta \mathsf{x}^n_h; \mathsf{y}_h \right)$ denotes the Fréchet derivative of $\mathcal{N}_h \left(\delta \mathsf{x}^n_h; \mathsf{y}_h \right)$ with respect to x^n_h, while $\mathcal{N}_h \left(\mathsf{x}^n_h; \mathsf{y}_h \right)$ is the residual. It continues the loop until the residual will be lower than a threshold, thus

$$\mathcal{N}_h \left(\mathsf{x}^n_h; \mathsf{y}_h \right) \leq \text{threshold} \tag{5.21}$$

then, it updates the solution as

$$\mathsf{x}^{n+1}_h = \mathsf{x}^n_h + \delta \mathsf{x}^n_h \tag{5.22}$$

This method is stable if the initial guess is chosen near the solution. It is also obvious that nobody can know a priori this aspect. In order to avoid stability problem of the numerical methods, that could give solutions without physical significance, in the code a modified Newton-Raphson method has been implemented [60]

$$\left(\phi_h, \frac{1}{\Delta t^n} \delta w^n_h \right)_{\mathcal{T}_h} + \mathcal{N}'_h \left[\mathsf{x}^n_h \right] \left(\delta \mathsf{x}^n_h; \mathsf{y}_h \right) = -\mathcal{N}_h \left(\mathsf{x}^n_h; \mathsf{y}_h \right) \tag{5.23}$$

where

$$\Delta t^n_k := \text{CFL}^n \frac{|K|}{\lambda_c + 4\lambda_d} \tag{5.24}$$

which CFL in chosen as

$$\text{CFL}^n := \begin{cases} c_0 \left[3 \left(\dfrac{n}{n_0} \right)^2 - 2 \left(\dfrac{n}{n_0} \right)^3 \right], & n \leq n_0 \\[4mm] \text{CFL}^{n-1} \left\{ 1 + c_1 \max \left[0, \log \left(\dfrac{||\mathcal{N}^{n-1}_h||_2}{||\mathcal{N}^n_h||_2} \right) \right] \right\}, & n > n_0 \end{cases} \tag{5.25}$$

where, c_0, c_1 and n_0, depends on the problem of interest. In addition, it notices that for $n > n_0$ it is easy to notice that if the numerical solution is not converging we have $||\mathcal{N}^n_h||_2 \geq ||\mathcal{N}^{n-1}_h||_2$, thus CFL^n remains constant (for $n > n_0$), instead, when we have $||\mathcal{N}^n_h||_2 < ||\mathcal{N}^{n-1}_h||_2$, namely when the solution is converging, the CFL^n increases.
It is very simple notice that for $\Delta t^n \to \infty$ the modified Newton-Raphson method drops down and the classical Newton-Raphson method is applied. This is the case when, according to the previous observation, the solution is converging, hence the $\text{CFL}^n \to \infty$, thus $\mathsf{x}^n_h \to \mathsf{x}_h$.

5.6 Hybridiation

Equations 5.23 obtained by the application of the Newton-Raphson method are a system of linear equations in the unknown quantity δx_h^n. Remind that x_h is a vector, which defintion is $x_h := (q_h, w_h, \lambda_h)$ In this sense, equations 5.26 are linear system in the unknown quantites $(\delta Q, \delta W, \delta \Lambda)^T$ which contains the expansion coefficients of δx_h. Hence, following [60], we have

$$\begin{pmatrix} A & B & R \\ C & D & S \\ L & M & N \end{pmatrix} \begin{pmatrix} \delta Q \\ \delta W \\ \delta \Lambda \end{pmatrix} = \begin{pmatrix} F \\ G \\ H \end{pmatrix} \tag{5.26}$$

In order to reduce the complexity of the problem, a good strategy is to implement a method that can solve the global system without assembly it. In other words, until this moment the process to find the discretization of our equations with DG or HDG methods is the same. Now, we are interested in optimizing the solution. To make it possible, we remind that in the HDG method we have previously introduced a new degree of freedom, which connects two nearby elements. This is $\delta \Lambda$, the third component of the vector δx_h. Hence, our hybridization is based on splitting the system 5.26 into two other systems. More specifically we will have

$$\begin{cases} \begin{pmatrix} A & B \\ C & D \end{pmatrix} \begin{pmatrix} \delta Q \\ \delta W \end{pmatrix} + \begin{pmatrix} R \\ S \end{pmatrix} \delta \Lambda = \begin{pmatrix} F \\ G \end{pmatrix} \\ \begin{pmatrix} L & M \end{pmatrix} \begin{pmatrix} \delta Q \\ \delta W \end{pmatrix} + N \delta \Lambda = H \end{cases} \tag{5.27}$$

In this way, we have re-formulated the problem. Firstly, it was on the unknown variables δQ δW and $\delta \Lambda$, now we have a set of two different equations on two unknown quantities $(\delta Q, \delta W)$ and $\delta \Lambda$. In other words, we have increased the number of unknown quantities splitting the initial unknown vector δx_h into two parts. This mathematical passage, which could be found not useful, permits us to re-write the system for the only unknown variable $\delta \Lambda$. Indeed, we can obtain

$$\begin{pmatrix} \delta Q \\ \delta W \end{pmatrix} = \begin{pmatrix} A & B \\ C & D \end{pmatrix}^{-1} \left[\begin{pmatrix} F \\ G \end{pmatrix} - \begin{pmatrix} R \\ S \end{pmatrix} \delta \Lambda \right] \tag{5.28}$$

substituting, we have

$$\begin{pmatrix} L & M \end{pmatrix} \begin{pmatrix} A & B \\ C & D \end{pmatrix}^{-1} \left[\begin{pmatrix} F \\ G \end{pmatrix} - \begin{pmatrix} R \\ S \end{pmatrix} \delta \Lambda \right] + N \delta \Lambda = H \tag{5.29}$$

that is

$$\begin{pmatrix} L & M \end{pmatrix} \begin{pmatrix} A & B \\ C & D \end{pmatrix}^{-1} \begin{pmatrix} F \\ G \end{pmatrix} - \begin{pmatrix} L & M \end{pmatrix} \begin{pmatrix} A & B \\ C & D \end{pmatrix}^{-1} \begin{pmatrix} R \\ S \end{pmatrix} \delta \Lambda + N \delta \Lambda = H \tag{5.30}$$

namely, the only unknown variable is $\delta \Lambda$

$$\left[N - \begin{pmatrix} L & M \end{pmatrix} \begin{pmatrix} A & B \\ C & D \end{pmatrix}^{-1} \begin{pmatrix} R \\ S \end{pmatrix} \right] \delta \Lambda = H - \begin{pmatrix} L & M \end{pmatrix} \begin{pmatrix} A & B \\ C & D \end{pmatrix}^{-1} \begin{pmatrix} F \\ G \end{pmatrix} \tag{5.31}$$

This the final solution. Solving equation 5.31 we have the possibility to know, firstly, $\delta \Lambda$ and after, using equation 5.28, to compute $(\delta Q, \delta W)$.
The matrix on the LHS of equation 5.31 is sparse $n_f \times n_f$ block matrix, where we remind that n_f is the number of the internal faces. The same is verified for DG discretization,

the only difference is based on the number of non-zero elements in the matrix on the LHS. Indeed, for the HDG method, the number of non-zero elements is lower than for the DG discretization. More specifically, table 5.1 represents the order of the non-zero elements present in that matrix for the two methods. It is important remember that d is the spatial dimension of the problem, m the number of scalar equations that describes the physical solution of the problem (e.g. for the classical Euler of Navier-stokes equations $m = d + 2$, instead, when we are working with non chemical equilibrium, new continuity equations are added, thus $= d + 1 + N_s$, while if we are considering also multitemperature models we need to add energy equations, and in these terms we will have $m = d + N_s + N_t$), p is the polynomial degree, $n_e := |\mathcal{T}_h|$ and $n_f := |\Gamma_h|$

Table 5.1: DG vs HDG. Number of non-zero elements.

Method	Non-zero elements
DG	$\mathcal{O}\left((d+2)\, n_e m^2 p^{2d}\right)$
HDG	$\mathcal{O}\left((2d+1)\, n_f m^2 p^{2d-2}\right)$

In the code [59] the system is solved with ILU(n) (Incomplete LU decomposition) pre-conditioned GMRES (Generalized Minimal RESidual method) available on PETSc library [5].

Note that the main difference between DG and HDG method is that in the DG discretization the numerical trace of the solution is defined explicitly in terms of w_h, while, in the HDG discretization, it is an unknown variable called λ_h.

5.7 Shock-capturing

The High-Order Unified Framework [59] adopts the shock-capturing approach developed by Hartmann and Houston [24]. Shocks are present in a compressible flow, thus when the relative variations of the fluid density are not negligible. Usually, this situation appears when Ma $\geq 0.3 - 0.4$, namely when the effects of pressure force is twice (approximately) the magnitude of inertial force. As a consequence of the compressible behavior of the fluid, from a mathematical point of view we have $\nabla \cdot \mathbf{u} \neq 0$. Compressible flows can be divided into subsonic or supersonic. The first case is associated when the Mach number is lower than 1 (or rather, lower than $0.7 - 0.8$ because of the transitional regime). The second case is related otherwise. When the flow is supersonic, the discontinuities appear in the physical and numerical simulations. Shocks are one of them and they are the most difficult to study from a numerical point of view. Indeed, large gradients of the quantities are present in a very small region. Numerical schemes do not much stable in the presence of high variations. Consequently, in the equations, a stabilization term has to be introduced. The methods implemented in the code (see [60]) use the following stabilization term

$$\nabla \cdot \left[\varepsilon\left(\mathbf{w}, \nabla \mathbf{w}\right), \nabla \mathbf{w}\right] \tag{5.32}$$

where, the artificial viscosity ε is computed with the norm of the residual of convective fluxes for each K element, namely we will have a different value of the artificial viscosity for each element that is computed starting from ε_0, a user-defined parameter. Formalism gives us

$$\varepsilon_K = \frac{\varepsilon_0 \tilde{h}_K^{2-\beta}}{|K|} \int_K \| \left[\nabla \cdot \underline{\mathbf{f_c}}\left(\mathbf{w}\right)\right]_i \|_1 = \frac{\varepsilon_0 \tilde{h}_k^{2-\beta}}{|K|} \int_K \sum_{i=1}^{m=d+2} \| \left[\nabla \cdot \underline{\mathbf{f_c}}\left(\mathbf{w}\right)\right]_i \|_2 \tag{5.33}$$

where there is also the introduction of mesh size parameter $\tilde{h}_K$ of the K element, defined as $\tilde{h}_K = h_k/p_k$. It has been introduced in order to accelerate the convergence of the artificial viscosity ε to zero, thus reducing the artificial perturbation introduced as a consequence of fluid dynamic shocks.

The shock-capturing function has also to be discretized. In its discretization the surface integral contribution is negligible, thus, only the volume contribution is taken into account, namely, with mathematical definitions, we have

$$\mathcal{N}_{h,sc}\left(\boldsymbol{\sigma}_h, w_h, \phi_h\right) := \left(\nabla\phi_h, \varepsilon\left(w_h, \boldsymbol{\sigma}_h\right)\boldsymbol{\sigma}_h\right)_{\mathcal{T}_h} \tag{5.34}$$

In conclusion, it is important to notice that this term is involved only in local discretization.

5.8 Mesh refinement

The code includes both isotropic and anisotropic mesh refinement. It is defined:

- **Isotropic mesh refinement**: this method is also called "shape regular" because it refines the mesh using only elements with a bounded aspect ratio, thus stretched elements are avoided.

- **Anisotropic mesh reniment**: with the application of this method also the use of stretched elements is possible in the regions of rapid variations of the numerical solution. The anisotropic mesh refinement routine of the code computes principal directions and stretching ratio.

During the mesh refinement, the code starts with anisotropic mesh refinement computing principal directions and stretching ratio. Subsequently, the isotropic desirable element is found with the adjoint-based error estimation. Finally, the new mesh is generated and new iterations for the computation start. The new mesh is always generated with BAMG (Bidimensional Anisotropic Mesh Generator) [25], free available with Free-FEM [26].

5.9 Adaptation

In general, we have to chose between h, p or hp adaptation. Ideally, we can improve the numerical solution, i.e. reducing the error, with the incrementation of the polynomial degree that reconstructs the solution for each element, or splitting the initial element into more ones. The first one is called p-adaptation, while the second one is the h-adaptation. Obviously, hp-adaptation includes both strategies.

In the code is implemented a strategy that is based on a sensor defined for each element. This sensor was initially thought by Persson and Peraire [47]. In [60] there is well explained all the adaptation procedure. However, summing up, in the code [59], the smoothness sensor is defined for each K element as follows

$$S_K := \frac{\displaystyle\sum_{K\in\mathcal{T}_h}\int_K (w-w^*)(w-w^*)\ \mathrm{d}\mathbf{x}}{\displaystyle\sum_{K\in\mathcal{T}_h}\int_K ww\ \mathrm{d}\mathbf{x}} = \frac{(w-w^*, w-w^*)_K}{(w, w)_K} \tag{5.35}$$

and for each element the choice between h or p refinement id based on a threshold ε_S according to

$$S_K : \begin{cases} < \varepsilon_S, & p\text{-refinement} \\ \geq \varepsilon_S, & h\text{-refinement} \end{cases} \tag{5.36}$$

For each element, it possible to build the patch $P(K)$ which contains whole the element and some piece of its neighbors. Hence, β dimensionless parameter is defined as the ratio between two derivatives: at the numerator, the maximum derivative, and, at the denominator the derivative evaluated in the perpendicular direction to the numerator one. Thus, its mathematical formulation is

$$\beta = \left(\frac{w^{p+1}}{w_\perp^{p+1}} \right)^{\frac{1}{1+p}} \tag{5.37}$$

where w^{p+1} is the maximum $p+1$ derivative of w. After that, having computing the anisotropy dimensionless parameter β, it is possible to evaluate the new element size from the its defition, i.e.

$$\beta = \frac{h_1}{h_2} \tag{5.38}$$

hence, also the element orientation θ. Then, the element sizes and the orientation are used to compute the metric. Subsequently, the new mesh is created with BAMG. All the process continues until the threshold (defined by the user) is reached.

5.10   Adjoint-based error estimation

Adaptation procedure is important to reduce the error and obtain more meticulous numerical results, i.e. good simulations can well estimate the engineering and physical quantities of interest, hence solve, or understand, the initial problem. In order to evaluate the error we need to introduce a target function J_h. Remembering that x_h is the approximation of x, we can introduce an error quantity that reads

$$e_h := J_h(\mathrm{x}) - J_h(\mathrm{x}_h) \tag{5.39}$$

that is the difference between the specific target function of the problem evaluate with and without the numerical approximation x_h.

Having understood what is the target function, we need to use Taylor expansion for deriving the adjoint-based error estimation strategy. Hence, expanding $J_h(\mathrm{x})$ with Peano form of the remainder, we have

$$J_h(\mathrm{x}) = J_h(\mathrm{x}_h) + J_h'(\mathrm{x}_h)(\mathrm{x} - \mathrm{x}_h) + \mathcal{O}\left((\|\mathrm{x} - \mathrm{x}_h\|_2)^2 \right) \tag{5.40}$$

thus, defining $\delta \mathrm{x}_h = \mathrm{x} - \mathrm{x}_h$, we have

$$J_h(\mathrm{x}) = J_h(\mathrm{x}_h) + J_h'(\mathrm{x}_h)\,\delta \mathrm{x}_h + \mathcal{O}\left((\|\delta \mathrm{x}_h\|_2)^2 \right) \tag{5.41}$$

Now, the same idea is applied to the Newton-Raphson formulation. Hence, we have

$$\mathcal{N}_h(\mathrm{x}; \mathrm{y}_h) = \mathcal{N}_h(\mathrm{x}_h; \mathrm{y}_h) + \mathcal{N}_h'(\mathrm{x}_h; \mathrm{y}_h)(\mathrm{x} - \mathrm{x}_h; \mathrm{y}_h) + \mathcal{O}\left((\|\mathrm{x} - \mathrm{x}_h\|_2)^2 \right) \tag{5.42}$$

and, again, recalling the previous definition of $\delta \mathrm{x}_h$, we have

$$\mathcal{N}_h(\mathrm{x}; \mathrm{y}_h) = \mathcal{N}_h(\mathrm{x}_h; \mathrm{y}_h) + \mathcal{N}_h'(\mathrm{x}_h; \mathrm{y}_h)(\delta \mathrm{x}_h; \mathrm{y}_h) + \mathcal{O}\left((\|\delta \mathrm{x}_h\|_2)^2 \right) \tag{5.43}$$

where, as a consequence of the consistentcy of the discretization, the LHS is null, thus $\mathcal{N}_h(\mathrm{x}; \mathrm{y}_h) = 0$. Hence, equation 5.43 reads

$$-\mathcal{N}_h(\mathrm{x}_h; \mathrm{y}_h) = \mathcal{N}_h'(\mathrm{x}_h; \mathrm{y}_h)(\delta \mathrm{x}_h; \mathrm{y}_h) + \mathcal{O}\left((\|\delta \mathrm{x}_h\|_2)^2 \right) \tag{5.44}$$

Substituting equation 5.44 into 5.41, and neglecting the term of order greaten than one, we have

$$e_h := J_h\left(\mathrm{x}\right) - J_h\left(\mathrm{x}_h\right) \approx \eta := -\mathcal{N}_h\left(\mathrm{x}_h; \mathrm{z}_h\right) \tag{5.45}$$

In equation 5.45 a new parameter appears. This is the adjoint solution $\mathrm{z}_h := \left(\tilde{q}_h, \tilde{w}_h, \tilde{\lambda}_h\right) \in$ $\tilde{\mathbb{X}}_h$. The adjoint solution is the connection between the target functional of our interest, that everyone could change in the code, and the residuals. It is important notice that the evaluation of the error could be computed also with local approch, thus in a single K element. In this case we have η_K. For more details, see [60], from this section was inspired by.

The previous choice of target functional The code [59] is continuously under development and it is used for research activities. Several publications are reported in the Bibliography. Here, in this small paragraph, a list of the previous target function is presented with reference to papers. In the code, one of the possible geometry to test the numerical algorithm is NACA 0012 airfoil. The simulation with this geometry can be done with an inviscid or viscous model, hence with the Euler or the Navier-Stokes equations, respectively. Consequently, two target functions are present by Woopen, May and Schutz in [62]. For the Euler model they used

$$J\left(w\right) = \int_{\partial\Omega_w} p\left(w\right)\boldsymbol{\beta}\cdot\mathbf{n}\ \mathrm{d}\sigma \tag{5.46}$$

while for Navier-Stokes model they used

$$J\left(w, \boldsymbol{\sigma}\right) = \int_{\partial\Omega_w} \left[p\left(w\right) - \boldsymbol{\tau}\left(w, \boldsymbol{\sigma}\right)\right]\boldsymbol{\beta}\cdot\mathbf{n}\ \mathrm{d}\sigma \tag{5.47}$$

where $\boldsymbol{\beta}$ is different for evaluation of drag or lift. For drag we have $\beta_D = \left(\cos\alpha, \sin\alpha\right)^T/c_\infty$, while for lift we have $\beta_L = \left(-\sin\alpha, \cos\alpha\right)^T/c_\infty$, where $c_\infty = \gamma p_\infty \mathrm{Ma}_\infty^2 l/2$.

In the same work [62] they also tested a bump smooth in which the target function was defined as a dimensionless parameter that represents the production of entropy. In this sense

$$J\left(w\right) = \sqrt{\frac{1}{|\Omega|}\int_\Omega \left[\frac{p}{p_\infty}\left(\frac{\rho}{\rho_\infty}\right)^{-\gamma} - 1\right]^2\ \mathrm{d}x} \tag{5.48}$$

Again in [62] the same researcher group studied the bidimensional convection-diffusion scalar defining the target function as

$$J\left(\boldsymbol{\sigma}, w\right) = \int_{\partial\Omega} \boldsymbol{\psi}\left(w - \varepsilon\mathbf{n}\cdot\boldsymbol{\sigma}\right)\ \mathrm{d}\sigma \tag{5.49}$$

where they choose $\boldsymbol{\psi}\left(x, y\right) = \cos\left(2\pi x\right)\sin\left(2\pi y\right)$.

For more accurate detail we remind to [37]; [60].

5.11   Boundary conditions

The High-Order Unifying framework has already implemented a lot of boundary conditions. Hence, in this section, we shall enumerate them.

5.11.1   Slip wall

This is the classical boundary conditions for the Euler model, where, due to the assumption that the gas can be considered ideal, that is its viscosity is null, namely the Reynolds number of the flow is infinity, no boundary layers are present in the region near the wall. For this reason, the velocity vector is perpendicular to the normal wall. From a mathematical point of view, we have

$$\mathbf{u} \cdot \mathbf{n} = 0 \tag{5.50}$$

that is, in terms of the state-local vector of conserved variables

$$\mathbf{w}_{\partial\Omega}\left(\rho, \mathbf{m}, \rho E\right) := \left(\rho, \mathbf{m}, \rho E\right) \tag{5.51}$$

5.11.2   No-slip wall

$$\mathbf{u} = 0 \tag{5.52}$$

that is, in terms of the state-local vector of conserved variables

$$\mathbf{w}_{\partial\Omega}\left(\rho, \mathbf{m}, \rho E\right) := \left(\rho, \mathbf{0}, \rho E\right) \tag{5.53}$$

- Adiabatic no-slipp wall

$$\nabla T \cdot \mathbf{n} = 0 \tag{5.54}$$

- Isothermal no-slip wall

$$T_w = \text{const.} \tag{5.55}$$

5.11.3   Symmetry plane

In terms of the state-local vector of conserved variables, we have

$$\mathbf{w}_{\partial\Omega}\left(\rho, \mathbf{m}, \rho E\right) := \left(\rho, \left(\underline{\mathbf{I}} - \mathbf{n} \otimes \mathbf{n}\right)\mathbf{m}, \rho E\right) \tag{5.56}$$

5.11.4   Far field

The far field conditions are computed base on the characteristic upwinding. Starting from the convective fluxes we can obtain the Jacobian matrix. Reminding that we are working with a bidimensional problem, that is $d = 2$, we shall have two different Jacobian matrices. However, in bidimensional case the convective flux is expressed as follows

$$\underline{\mathbf{f}}_c = \begin{pmatrix} \mathbf{f}_{c,1} & \mathbf{f}_{c,2} \end{pmatrix} = \begin{pmatrix} \rho u & \rho v \\ \rho u^2 + p & \rho v u \\ \rho u v & \rho v^2 + p \\ \rho u H & \rho v H \end{pmatrix} \tag{5.57}$$

where

$$\mathbf{f}_{c,1} = \begin{pmatrix} \rho u \\ \rho u^2 + p \\ \rho u v \\ \rho u H \end{pmatrix} = \begin{pmatrix} w_2 \\ \dfrac{w_2^2}{w_1} + (\gamma - 1)\left(w_4 - \dfrac{w_2^2 + w_3^2}{2w_1}\right) \\ w_2\dfrac{w_3}{w_1} \\ \gamma w_2\dfrac{w_4}{w_1} - \left(\dfrac{\gamma - 1}{2}\right)\left[\dfrac{w_2^2 + w_3^2}{w_1^2}\right]w_2 \end{pmatrix} \tag{5.58}$$

and

$$
\mathbf{f}_{c,2} = \begin{pmatrix} \rho v \\ \rho v u \\ \rho v^2 + p \\ \rho v H \end{pmatrix} = \begin{pmatrix} w_3 \\ w_3 \dfrac{w_2}{w_1} \\ \dfrac{w_3^2}{w_1} + (\gamma - 1)\left(w_4 - \dfrac{w_2^2 + w_3^2}{2w_1}\right) \\ \gamma w_3 \dfrac{w_4}{w_1} - \left(\dfrac{\gamma - 1}{2}\right)\left[\dfrac{w_2^2 + w_3^2}{w_1^2}\right] w_3 \end{pmatrix} \tag{5.59}
$$

Note that $H = h + (\|\mathbf{u}\|_2)^2 / 2 = E + p/\rho$. After some manipulations we will obtain different Jacobian matricies, one for each direction

$$
\nabla \cdot \underline{\mathbf{f}}_c(\mathbf{w}) = \frac{\partial \underline{\mathbf{f}}_c(\mathbf{w})}{\partial \mathbf{x}} = \frac{\partial \underline{\mathbf{f}}_c(\mathbf{w})}{\partial \mathbf{w}} \frac{\partial \mathbf{w}}{\partial \mathbf{x}} \tag{5.60}
$$

thus

$$
\frac{\partial \mathbf{f}_{c,1}}{\partial \mathbf{w}} = \begin{pmatrix} 0 & 1 & 0 & 0 \\ \left(\dfrac{\gamma-3}{2}\right)\dfrac{w_2^2}{w_1^2} + \left(\dfrac{\gamma-1}{2}\right)\dfrac{w_3^2}{w_1^2} & (3-\gamma)\dfrac{w_2}{w_1} & (1-\gamma)\dfrac{w_3}{w_1} & \gamma-1 \\ -w_3\dfrac{w_2}{w_1^2} & \dfrac{w_3}{w_1} & \dfrac{w_2}{w_1} & 0 \\ \left[-\gamma\dfrac{w_4}{w_1^2} + (\gamma-1)\dfrac{w_2^2+w_3^2}{w_1^3}\right]w_2 & \gamma\dfrac{w_4}{w_1} + (1-\gamma)\dfrac{w_2^2}{w_1^2} - \left(\dfrac{\gamma-1}{2}\right)\dfrac{w_2^2+w_3^2}{w_1^2} & (1-\gamma)w_3\dfrac{w_2}{w_1^2} & \gamma\dfrac{w_2}{w_1} \end{pmatrix} \tag{5.61}
$$

and

$$
\frac{\partial \mathbf{f}_{c,2}}{\partial \mathbf{w}} = \begin{pmatrix} 0 & 0 & 1 & 0 \\ -w_3\dfrac{w_2}{w_1^2} & \dfrac{w_3}{w_1} & \dfrac{w_2}{w_1} & 0 \\ \left(\dfrac{\gamma-3}{2}\right)\dfrac{w_3^2}{w_1^2} + \left(\dfrac{\gamma-1}{2}\right)\dfrac{w_2^2}{w_1^2} & (1-\gamma)\dfrac{w_2}{w_1} & (3-\gamma)\dfrac{w_3}{w_1} & \gamma-1 \\ \left[-\gamma\dfrac{w_4}{w_1^2} + (\gamma-1)\dfrac{w_2^2+w_3^2}{w_1^3}\right]w_3 & (1-\gamma)w_3\dfrac{w_2}{w_1^2} & \gamma\dfrac{w_4}{w_1} + (1-\gamma)\dfrac{w_3^2}{w_1^2} - \left(\dfrac{\gamma-1}{2}\right)\dfrac{w_2^2+w_3^2}{w_1^2} & \gamma\dfrac{w_3}{w_1} \end{pmatrix} \tag{5.62}
$$

Another way to obtain a generalized form for the Jacobian matrices, according to [28], is the following

$$
\underline{\mathbf{f}}_c = \mathbf{w}u_n + p\mathbf{a}_2
$$

where

$$
\mathbf{a}_2 = \begin{pmatrix} 0 & \mathbf{n} & u_n \end{pmatrix}^T \tag{5.63}
$$

where $u_n = \sum_{i=1}^{d} u_i n_i$. Hence, we have

$$
\begin{aligned}
u_n &= n_1 u + n_2 v + n_3 w \\
&= n_1 \frac{w_2}{w_1} + n_2 \frac{w_3}{w_1} + n_3 \frac{w_4}{w_1}
\end{aligned} \tag{5.64}
$$

thus, we have

$$
\begin{aligned}
\frac{\partial u_n}{\partial \mathbf{w}} &= \frac{1}{w_1}\begin{pmatrix} -\dfrac{w_2 n_1 + w_3 n_2 + w_4 n_3}{w_1} & n_1 & n_2 & n_3 & 0 \end{pmatrix} \\
&= \frac{1}{\rho}\begin{pmatrix} -u_n & n_1 & n_2 & n_3 & 0 \end{pmatrix}
\end{aligned} \tag{5.65}
$$

Finally, the Jacobian matrix is

$$\frac{\partial \underline{\mathbf{f_c}}}{\partial \mathbf{w}} = \frac{\partial \mathbf{w}}{\partial \mathbf{w}} u_n + \frac{\partial u_n}{\partial \mathbf{w}} \mathbf{w} + \mathbf{a_2} \frac{\partial p}{\partial \mathbf{w}} + p \frac{\partial \mathbf{a_2}}{\partial \mathbf{w}}$$

$$= u_n \underline{\mathbf{I}} + \frac{\partial u_n}{\partial \mathbf{w}} \mathbf{w} + \mathbf{a_2} \frac{\partial p}{\partial \mathbf{w}}$$

In any case, in the end, for a bidimensional problem we will have the following eigenvalues

$$u_n, \qquad u_n, \qquad u_n + c, \qquad u_n - c \tag{5.66}$$

with their corresponding eigenvectors (see [28]).

5.11.5   Inflow and Outflow

In addition, also the inflow and outflow boundary conditions are implemented in the code. Generally speaking, these types of boundary conditions, can be computed with the usage of Riemann invariants. The number of prescribed boundary conditions depends on the type of in- and out- flow. In general, if we are considering a subsonic outflow test case, we need to prescribe the outlet pressure while, if the out region is supersonic, we do not need to prescribe any variables. In the inflow region, if it is supersonic we need to prescribe three different quantities while, if it is subsonic, only two are satisfactory. For these reasons, the subsonic outflow boundary condition will influence the solution computed in our Navier-Stokes test case, as shown in the next Chapter.

5.12   Normalization

All the CFD solvers work with the dimensionless form of the equations. This is a crucial step in the coding phase of the algorithm. Indeed, in normal fluid motions, we will have different quantities like the pressure, the velocity, the density, etc... that have different order of magnitude. For instance, the pressure in a normal condition like $1\ atm$ is, in the S.I., $\sim 10^5\ Pa$. On the other hand, the density in the same conditions will be $\sim 10^0\ kg/m^3$. These differences could introduce numerical error in the solutions of the flow field. This is due to the catastrophic cancellation. To overcome this issue we need to introduce the dimensionless form of the equations. In this way, all the quantities that describe the fluid field will have the same order of magnitude and the solver will be able to compute correctly their value. In the end, in the post-processing phase, the engineer could analyze the output with non-dimensional values or, if s/he prefers, with the dimensional form.

There are many methods to find the dimensionless form, for instance, we can select the reference pressure as the total pressure. In these terms, all the values of the pressure will be between zero and one. The same could be though for the temperature. In order to define a normalization scheme, four independent value of the following variables need to be chosen: L, $\|\mathbf{u}\|_2$, ρ, p, T and e.

In the code [59] the choice was based on

$$p_{re.f}, \qquad \rho_{ref.}, \qquad T_{ref.}, \qquad L_{ref.} \tag{5.67}$$

hence, the other values will be

$$\|\mathbf{u}_{ref.}\|_2 = \sqrt{\frac{p_{ref.}}{\rho_{ref.}}} \tag{5.68}$$

the reference energy by

$$e_{ref.} = (\|\mathbf{u}_{ref.}\|_2)^2 = \frac{p_{ref.}}{\rho_{ref.}} \tag{5.69}$$

obviousy, the latter is applied also for the enthalpy $h_{ref.} = e_{ref.}$. The reference time by

$$t_{ref.} = \frac{L_{ref.}}{\|\mathbf{u}_{ref.}\|_2} = L_{ref.}\sqrt{\frac{p_{ref.}}{\rho_{ref.}}} \tag{5.70}$$

Consequently, we can define all the normalized operator, i.e.

$$\tilde{\nabla} = \frac{\nabla}{L_{ref.}}$$
$$\tilde{\partial}_t = \frac{\partial_t}{t_{ref.}} \tag{5.71}$$

and the dimensionless chosen quantities as follows

$$\tilde{p} = \frac{p}{p_{ref.}}, \quad \tilde{\rho} = \frac{\rho}{\rho_{ref.}}, \quad \tilde{T} = \frac{T}{T_{ref.}}, \quad \tilde{L} = \frac{L}{L_{ref.}} \tag{5.72}$$

while the dimensionless derived quantities as follows

$$\|\tilde{\mathbf{u}}\|_2 = \frac{\|\mathbf{u}\|_2}{\|\mathbf{u}_{ref.}\|_2}, \quad \tilde{e} = \frac{e}{e_{ref.}}, \quad \tilde{h} = \frac{h}{h_{ref.}}, \quad \tilde{t} = \frac{t}{t_{ref.}} \tag{5.73}$$

With the application of these definitions, we can find the dimensionless version of the set of equations to implement in the High-Order Unifying Framework. The general form for the conservative laws is

$$\partial_t \mathbf{w} + \nabla \cdot \underline{\mathbf{f}}_c(\mathbf{w}) - \nabla \cdot \underline{\mathbf{f}}_v(\mathbf{w}, \nabla \mathbf{w}) = \underline{\mathbf{s}}(\mathbf{w}, \nabla \mathbf{w}) \tag{5.74}$$

that, for steady solutions, we have

$$\nabla \cdot \underline{\mathbf{f}}_c(\mathbf{w}) - \nabla \cdot \underline{\mathbf{f}}_v(\mathbf{w}, \nabla \mathbf{w}) = \underline{\mathbf{s}}(\mathbf{w}, \nabla \mathbf{w}) \tag{5.75}$$

that is the full system for Navier-Stokes equations, i.e.

$$\frac{\partial \rho}{\partial t} + \nabla \cdot (\rho \mathbf{u}) = 0$$
$$\frac{\partial (\rho \mathbf{u})}{\partial t} + \nabla \cdot (\rho \mathbf{u} \otimes \mathbf{u} + p\underline{\mathbf{I}}) - \nabla \cdot \underline{\boldsymbol{\tau}} = \rho \mathbf{f} \tag{5.76}$$
$$\frac{\partial (\rho E)}{\partial t} + \nabla \cdot [(\rho E + p)\mathbf{u}] - \nabla \cdot (\underline{\boldsymbol{\tau}}\mathbf{u} - \dot{\mathbf{q}}) = \rho \mathbf{f} \cdot \mathbf{u} + \dot{\mathcal{Q}}$$

in typical aerospace applications, the effects of the external forces, often related to the gravitational force, are negligible. On the other hand, as we mentioned before, in this particular case, we cannot neglect the effects due to the electromagnetic field. In other words, the external forces will be only associated with the last one. In this way, the full system will be

$$\frac{\partial \rho}{\partial t} + \nabla \cdot (\rho \mathbf{u}) = 0$$
$$\frac{\partial (\rho \mathbf{u})}{\partial t} + \nabla \cdot (\rho \mathbf{u} \otimes \mathbf{u} + p\underline{\mathbf{I}}) - \nabla \cdot \underline{\boldsymbol{\tau}} = \rho_c \mathbf{E}_{appl.} + \mathbf{j} \times \mathbf{B}_{appl.} \tag{5.77}$$
$$\frac{\partial (\rho E)}{\partial t} + \nabla \cdot [(\rho E + p)\mathbf{u}] - \nabla \cdot (\underline{\boldsymbol{\tau}}\mathbf{u} - \dot{\mathbf{q}}) = \mathbf{j} \cdot \mathbf{E}_{appl.}$$

that for the steady-states, it looks like

$$\nabla \cdot (\rho \mathbf{u}) = 0$$
$$\nabla \cdot (\rho \mathbf{u} \otimes \mathbf{u} + p\underline{\mathbf{I}}) - \nabla \cdot \underline{\boldsymbol{\tau}} = \rho_c \mathbf{E}_{appl.} + \mathbf{j} \times \mathbf{B}_{appl.} \tag{5.78}$$
$$\nabla \cdot (\rho H \mathbf{u}) - \nabla \cdot (\underline{\boldsymbol{\tau}}\mathbf{u} - \dot{\mathbf{q}}) = \mathbf{j} \cdot \mathbf{E}_{appl.}$$

where ρ is the density, $\rho_c = n_c q$ the density charge, $\mathbf{u}$ the velocity vector, p the pressure, $\underline{\boldsymbol{\tau}}$ the viscous stress tensor, E the total energy per unit of mass, $H = E + p/\rho$ the specific total enthalpy, $\dot{\mathbf{q}}$ the heat flux, $\mathbf{B}_{appl.}$ the externally imposed magnetic field, $\mathbf{E}_{appl.}$ the externally imposed elecric field and $\mathbf{j}$ the density current vector.

To satisfy the conservative form of the system, we can split it into conservative, diffusive, and source terms. For the first two, we have

$$\underline{\mathbf{f}}_c\left(\mathbf{w}\right) = \begin{pmatrix} \rho\mathbf{u} \\ \rho\mathbf{u}\otimes\mathbf{u} + p\underline{\mathbf{I}} \\ \rho H\mathbf{u} \end{pmatrix} \qquad \underline{\mathbf{f}}_v\left(\mathbf{w}, \nabla\mathbf{w}\right) = \begin{pmatrix} 0 \\ \underline{\boldsymbol{\tau}} \\ \underline{\boldsymbol{\tau}}\mathbf{u} - \dot{\mathbf{q}} \end{pmatrix} \qquad (5.79)$$

while, for the source term, we have

$$\underline{\mathbf{s}}\left(\mathbf{w}, \nabla\mathbf{w}\right) = \begin{pmatrix} 0 \\ \rho_c\mathbf{E}_{appl.} + \mathbf{j}\times\mathbf{B}_{appl.} \\ \mathbf{j}\cdot\mathbf{E}_{appl.} \end{pmatrix} \qquad (5.80)$$

Now, we can start the normalization procedure following [15] and what just explained before, we have

$$\nabla\cdot\tilde{\underline{\mathbf{f}}}_c\left(\mathbf{w}\right) - \nabla\cdot\left[\underline{\boldsymbol{\theta_1}}\ \tilde{\underline{\mathbf{f}}}_v\left(\mathbf{w}, \nabla\mathbf{w}\right)\right] = \underline{\boldsymbol{\theta_2}}\ \tilde{\underline{\mathbf{s}}}\left(\mathbf{w}, \nabla\mathbf{w}\right) \qquad (5.81)$$

where, if we consider a three-dimensional problem $(d = 3)$ and we remind that the number of scalar equations for this set of equations is $m = d + 2$, we have

$$\underline{\boldsymbol{\theta_1}} = \frac{\sqrt{\gamma}\ \mathrm{Ma}}{\mathrm{Re}}\ \mathrm{diag}\left(0, \mathbf{1}, 1\right) \qquad\qquad \underline{\boldsymbol{\theta_2}} = \sqrt{\gamma}\ \mathrm{Ma}\ \mathrm{S}\ \mathrm{Re}_m\ \mathrm{diag}\left(0, \mathbf{1}, 1\right)$$

$$= \frac{\sqrt{\gamma}\ \mathrm{Ma}}{\mathrm{Re}}\begin{pmatrix} 0 & & & & \\ & 1 & & & \\ & & 1 & & \\ & & & 1 & \\ & & & & 1 \end{pmatrix} \qquad = \sqrt{\gamma}\ \mathrm{Ma}\ \mathrm{S}\ \mathrm{Re}_m\begin{pmatrix} 0 & & & & \\ & 1 & & & \\ & & 1 & & \\ & & & 1 & \\ & & & & 1 \end{pmatrix} \qquad (5.82)$$

finally, the steady-state dimensionless physical model that describes the situation of Magneto-Fluid Dynamics under low Magnetic Reynolds number assumption, reads

$$\tilde{\nabla}\cdot\left(\tilde{\rho}\tilde{\mathbf{u}}\right) = 0$$

$$\tilde{\nabla}\cdot\left(\tilde{\rho}\tilde{\mathbf{u}}\otimes\tilde{\mathbf{u}}\right) - \frac{\sqrt{\gamma}\ \mathrm{Ma}}{\mathrm{Re}}\tilde{\nabla}\cdot\tilde{\underline{\boldsymbol{\tau}}} = \sqrt{\gamma}\ \mathrm{Ma}\ \mathrm{S}\ \mathrm{Re}_m\ \left(\tilde{\rho}_c\tilde{\mathbf{E}}_{appl.} + \tilde{\mathbf{j}}\times\tilde{\mathbf{B}}_{appl.}\right)$$

$$\tilde{\nabla}\cdot\left(\tilde{\rho}\tilde{H}\tilde{\mathbf{u}}\right) - \frac{\sqrt{\gamma}\ \mathrm{Ma}}{\mathrm{Re}}\tilde{\nabla}\cdot\left(\tilde{\underline{\boldsymbol{\tau}}}\tilde{\mathbf{u}} - \frac{\gamma}{(\gamma-1)\,\mathrm{Pr}}\tilde{\dot{\mathbf{q}}}\right) = \sqrt{\gamma}\ \mathrm{Ma}\ \mathrm{S}\ \mathrm{Re}_m\ \left(\tilde{\mathbf{j}}\cdot\tilde{\mathbf{E}}_{appl.}\right)$$

$$(5.83)$$

where the electric and magnetic reference values have been chosen equal to one. In this sense, the user can easily insert the typical value that s/he wants, without changing anything. We remember that this model is valid for Magneto-Fluid Dynamics simulation under the condition of low Magnetic Reynolds number, i.e. the magnetic field induced is negligible, hence it can be considered applied constant in space and time. In addition, the model is valid under the frozen fluid physical condition, thus when the time of the fluid is a different order of magnitude lower than the time of the typical chemical reactions, i.e., from a mathematical point of view, when the Damkohler number is very low.

5.13   Model implementation with electromagnetic source term

Now, we impose the electric field and the magnetic field and we are going to compute the electromagnetic source term. We remember that in the physical model of our interest the

source term is made up of Lorentz force for the momentum equation and Joule heating in the energy equation, which general form is

$$\underline{\mathbf{s}}\left(\mathbf{w}, \nabla\mathbf{w}\right) = \begin{pmatrix} 0 \\ \rho_c\mathbf{E}_{appl.} + \mathbf{j} \times \mathbf{B}_{appl.} \\ \mathbf{j} \cdot \mathbf{E}_{appl.} \end{pmatrix} \tag{5.84}$$

where to evaluate all these scalar components, the cross products will be analyzed separately. Hence, we have

$$\mathbf{u} \times \mathbf{B}_{appl.} = \begin{vmatrix} \mathbf{e}_1 & \mathbf{e}_2 & \mathbf{e}_3 \\ u & v & w \\ B_x & B_y & B_z \end{vmatrix}$$

$$= \mathbf{e}_1 \begin{vmatrix} v & w \\ B_y & B_z \end{vmatrix} - \mathbf{e}_2 \begin{vmatrix} u & w \\ B_x & B_z \end{vmatrix} + \mathbf{e}_3 \begin{vmatrix} u & v \\ B_x & B_y \end{vmatrix} \tag{5.85}$$

$$= \begin{pmatrix} vB_z - wB_y \\ wB_x - uB_z \\ uB_y - vB_x \end{pmatrix}$$

We remember that σ_e is the electrical conductivity (in S.I. $[S/m]$). It is important to consider that, under particular physical conditions (like strong magnetic field applied, etc...) the electrical conductivity does not be considered as a scalar because the transport mechanism is not the same in each direction. To overcome this problem we need to switch to a formulation where the electrical conductivity is a tensor. For the sake of simplicity, now we will consider the case where σ_e is scalar, which is typical for unmagnetized or weakly magnetized ionized gas mixtures. Hence, it is possible to compute the density current as follows

$$\mathbf{j} = \rho_c\mathbf{E}_{appl.} + \sigma_e\left(\mathbf{E}_{appl.} + \mathbf{u} \times \mathbf{B}_{appl.}\right) = \begin{pmatrix} \rho_cE_x + \sigma_e\left(E_x + vB_z - wB_y\right) \\ \rho_cE_y + \sigma_e\left(E_y + wB_x - uB_z\right) \\ \rho_cE_z + \sigma_e\left(E_z + uB_y - vB_x\right) \end{pmatrix} = \begin{pmatrix} j_x \\ j_y \\ j_z \end{pmatrix} \tag{5.86}$$

then, the Lorentz force will be

$$\mathbf{j} \times \mathbf{B}_{appl.} = \begin{vmatrix} \mathbf{e}_1 & \mathbf{e}_2 & \mathbf{e}_3 \\ j_x & j_y & j_z \\ B_x & B_y & B_z \end{vmatrix}$$

$$= \mathbf{e}_1 \begin{vmatrix} j_y & j_z \\ B_y & B_z \end{vmatrix} - \mathbf{e}_2 \begin{vmatrix} j_x & j_z \\ B_x & B_z \end{vmatrix} + \mathbf{e}_3 \begin{vmatrix} j_x & j_y \\ B_x & B_y \end{vmatrix}$$

$$= \begin{pmatrix} j_yB_z - j_zB_y \\ j_zB_x - j_xB_z \\ j_xB_y - j_yB_x \end{pmatrix}$$

$$= \begin{pmatrix} \left[\rho_cE_y + \sigma_e\left(E_y + wB_x - uB_z\right)\right]B_z - \left[\rho_cE_z + \sigma_e\left(E_z + uB_y - vB_x\right)\right]B_y \\ \left[\rho_cE_z + \sigma_e\left(E_z + uB_y - vB_x\right)\right]B_x - \left[\rho_cE_x + \sigma_e\left(E_x + vB_z - wB_y\right)\right]B_z \\ \left[\rho_cE_x + \sigma_e\left(E_x + vB_z - wB_y\right)\right]B_y - \left[\rho_cE_y + \sigma_e\left(E_y + wB_x - uB_z\right)\right]B_x \end{pmatrix}$$

$$= \begin{pmatrix} \left(\rho_c + \sigma_e\right)\left(E_yB_z - E_zB_y\right) + \sigma_eB_x\left(wB_z + vB_y\right) - \sigma_eu\left(B_z^2 + B_y^2\right) \\ \left(\rho_c + \sigma_e\right)\left(E_zB_x - E_xB_z\right) + \sigma_eB_y\left(uB_x + wB_z\right) - \sigma_ev\left(B_x^2 + B_z^2\right) \\ \left(\rho_c + \sigma_e\right)\left(E_xB_y - E_yB_x\right) + \sigma_eB_z\left(vB_y + uB_x\right) - \sigma_ew\left(B_y^2 + B_z^2\right) \end{pmatrix}$$

$$\tag{5.87}$$

while the Joule heating

$$
\begin{aligned}
\mathbf{j} \cdot \mathbf{E}_{appl.} &= j_x E_x + j_y E_y + j_z E_z \\
&= (\rho_c + \sigma_e)\left(E_x^2 + E_y^2 + E_z^2\right) + \sigma_e\left[E_x\left(vB_z - wB_y\right) + E_y\left(wB_x - uB_z\right) + E_z\left(uB_y - vB_x\right)\right] \\
&= \rho_c\left(E_x^2 + E_y^2 + E_z^2\right) + \sigma_e\left(E_x^2 + E_y^2 + E_z^2 - \begin{pmatrix} 1 \\ 1 \\ 1 \end{pmatrix} \cdot \left(\begin{pmatrix} u & 0 & 0 \\ 0 & v & 0 \\ 0 & 0 & w \end{pmatrix}\begin{pmatrix} E_y B_z - E_z B_y \\ E_z B_x - E_x B_z \\ E_x B_y - E_y B_x \end{pmatrix}\right)\right)
\end{aligned}
$$
(5.88)

5.13.1   Effect of cross-product in bidimensional simulation

Equation 5.87 and 5.88 give the mathematical structure of the source term in three-dimensional simulation. Looking at it, and remembering that the definitions of cross-product returns a vector outside the plane where the multiplied vector are contained, it is easy to understand that for bidimensional cases it will be null. Therefore, no efforts should have been in coding. However, the problem is based on the fact that also in the bidimensional simulation we need to introduce Lorentz force and Joule heating. On the other hand, the code [59] works with a definite mathematical and informatics structure based on the initial conditions of the problem. In other words, if we are working on a bidimensional simulation, we cannot introduce a three-dimensional source term. It is not possible for compatibility and physical reasons. By the way, it is necessary to build a routine that can avoid this problem and compute the correct electromagnetic source structure. The calculation of the source terms will be conduct in the most general case (i.e. $d = 3$), then the routine will check the effective dimension of the problem, and it will fix only the components of Lorentz force to be taken into account. In this context, also the possibility to introduce electric and magnetic fields outside the plane of the bidimensional simulation needs to be considered. The main idea is to think of a bidimensional simulation as figure 5.2 shows.
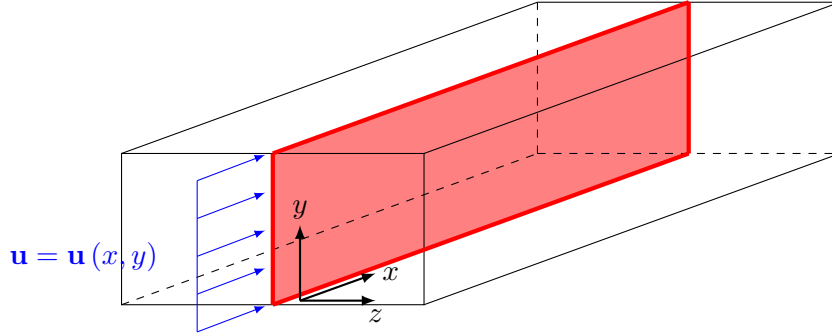
Figure 5.2: The scheme of the geometry to overcome the problem of losing contribution during the computation of the Lorentz force in the momentum equation.
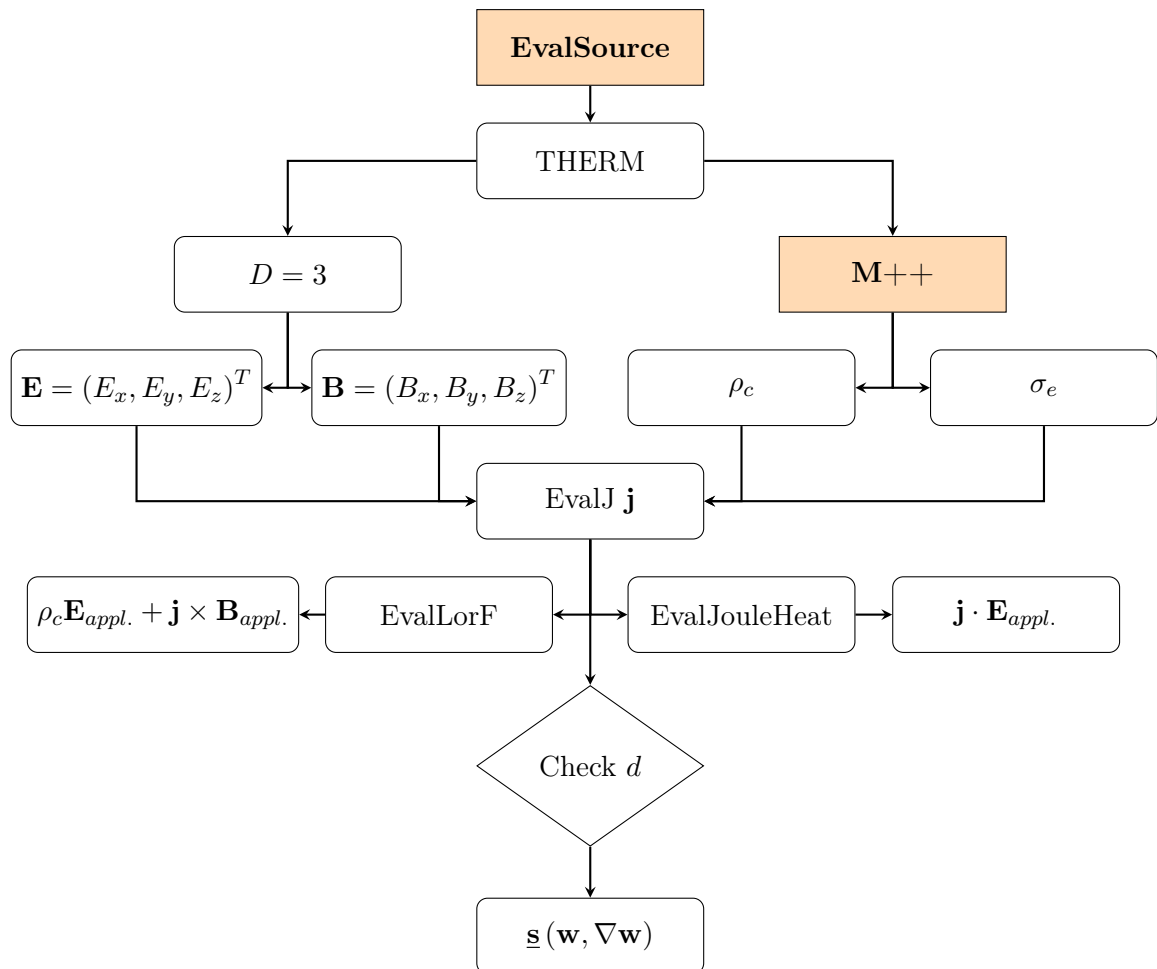
Figure 5.3: Flow chart to evaluate the source term of the model developed in the High-Order Unifying Framework. The interface with the library Mutation++ is briefly explained in the figure 5.1. In this way, we overcome the problem related to the loss of the contribution of Lorentz force in the momentum equation. The transport properties are evaluated with the scheme 5.1. All the code is present in the two Appendices.

5.14 Summary

This Chapter gave a general overview of the High-Order Unifying Framework [59]. The typical structure base on the `AutoDiff` data type has been shown. Then, the typical output and the physical models already existing were tabled. Hence, the general concepst of the code were described: the modified Newton-Raphson method, the relaxation technique, how the shock-capturing works, the concept of refinement, the adjoint-based error estimation, and, finally, the typical boundary conditions. Then, at the end of the Chapter, the normalization procedure of the equations of our interest has been shown. Hence, the normalized system for electrically conducting flows under the assumption of frozen flow was tabled. In the end, the scheme for the implementation of the source term has been presented.

Chapter 6

Validation

In this Chapter, we are going to test the models implemented in the High-Order Unifying Framework that we have already explained in the previous Chapters. We will start with the Euler model, neglecting the viscous fluxes and all the physical properties associated with it. Then, their introduction is essential to develop a real physical model. Hence, in the second step, we will test the Navier-Stokes model. The results are analyzed with kinematic physical considerations and compared to the analytical solution provided by Hartman [39]. Hartmann flow is also compared with the analytical solution of Poiseuille flow. Then, the numerical results are presented and theoretical considerations are exposed.

6.1 Euler model

In this section, we are considering this set of equations

$$\frac{\partial \rho}{\partial t} + \nabla \cdot (\rho \mathbf{u}) = 0$$

$$\frac{\partial (\rho \mathbf{u})}{\partial t} + \nabla \cdot (\rho \mathbf{u} \otimes \mathbf{u} + p \underline{\mathbf{I}}) = \rho_c \mathbf{E}_{appl.} + \mathbf{j} \times \mathbf{B}_{appl.} \qquad (6.1)$$

$$\frac{\partial (\rho E)}{\partial t} + \nabla \cdot [(\rho E + p) \mathbf{u}] = \mathbf{j} \cdot \mathbf{E}_{appl.}$$

6.1.1 Channel test case

It is a good practice to start from the Euler model in order to test the implementation and how the electromagnetic source terms works. In the Euler model, we are not considering all the viscous fluxes that are normally present in a real situation. In other words, this is a theoretical abstraction to make sure that the source term is working correctly. Indeed, in the source term, there is the presence of the Lorentz force and Joule heating. All of these quantities are related to the density current, which is made up of two terms: convective and conduction. In the normal application, the first one is neglected as a consequence that the total charge density can be considered zero. In this sense, only the conduction term is present. Hence, electrical conductivity appears. Testing the implementation of the Euler model with the addition of electromagnetic source term, we can use typical kinematic considerations based on the second Newton's law

$$\sum \mathbf{F} = m \mathbf{a} \qquad (6.2)$$

that is the typical expression of the momentum equations in the Navier-Stokes model. In this section, we are going to test if the implementation of the electromagnetic source term is correct. To make it possible we are considering a channel and we will apply an electric and magnetic field such that the Lorentz force is along the positive direction or, in the

negative direction. Hence, in the first case, the particles of fluid are accelerating, while in the second case they will decelerate. Of course, to make us sure about the good coding implementation, also a further simulation with electric and magnetic field imposed null has been conducted. In this latter case, no variations will be present. The simulations have been conducted with Mach number Ma = 2, angle of attack $\alpha = 0°$, reference length $L = 1$, $\gamma = 1.4$, Magnetic Reynolds number $\text{Re}_m = 0.001$, while the Magnetic force number S = 100. The temperature of the gas mixture has been set to $T = 2500\ K$, and we imposed an external fictitious scalar electrical conductivity $\sigma_e = 0.1$, while $\rho_c = 0$. The computation for each iteration has been automatically stopped when the residuals will reach the threshold equal to 10^{-8}. It is important to notice that, for increments in the value of the density current, the variations of the entropy will increase, obviously. Hence, also the computational time will increase. The latter also increases when we are going to consider higher order of the function that approximates the solution for each element. The last two concepts are presented in figure 6.4. In figures 6.2 and 6.3 the comparison between the high-enthalpy version and the model implemented in this work with null electric and magnetic fields is provided. As we expected, there are no changes in the two post-processing. Hence, we can affirm that the source term is correctly implemented. The structured triangular mesh used for these simulations is shown in figure 6.1. In table 6.2 the number of elements is tabled for the p-adaptation procedure, while in the table 6.1 there are the different cases that have been tested. The Paraview post-processing of the latter is shown in figure 6.5. In figure 6.6 the values for typical fluid dynamic variables are provided for a line placed at $y = 0.25$. Obviously, in the meantime, the pressure decreases. The behavior of the temperature is different. It increases its value along the channel, and its increment is higher for the bigger magnitude of the electric fields. Hence, the behaviour of the Mach number is not unique and we cannot consider it to evaluate if the flow is accelerating or decelerating.
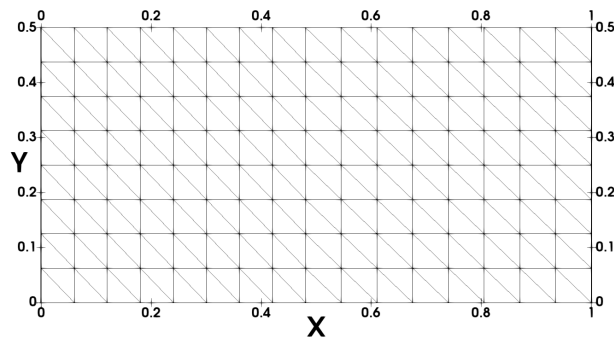
Figure 6.1: Channel Euler test case: triangular mesh with $n_e = 256$, $p = 4$, $n_p = 3848$, for $p = 4$. (see table 6.2).

Table 6.1: Channel Euler test cases.

	Case A	Case B	Case C	Case D	Case E
E_z	-15	-10	-5	0	5
j_z	> 0	> 0	~ 0	< 0	< 0
$\mathbf{j} \times \mathbf{B}_{appl.}\vert_x$	> 0	> 0	~ 0	< 0	< 0

(a) *Euler high-enthalpy.*

(b) *Euler electromagnetic.*
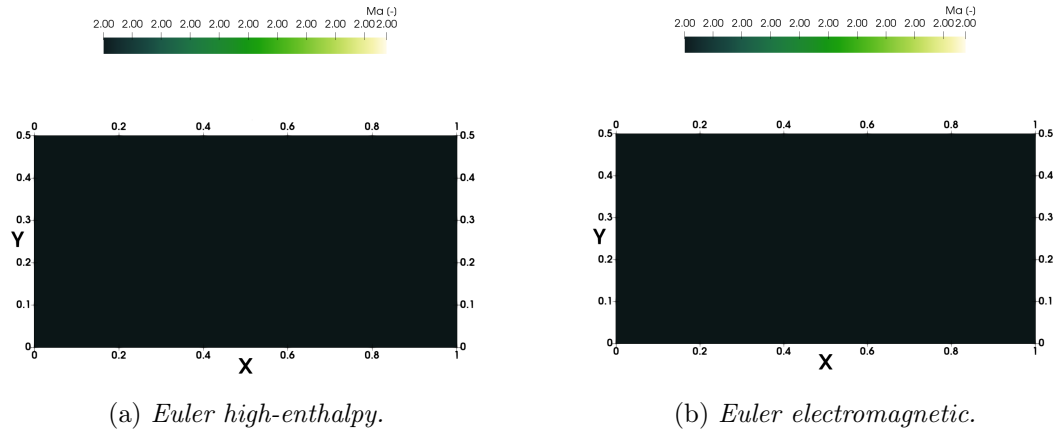
Figure 6.2: Channel Euler test case: post-processing.

(a) *Mach number.*

(b) *Dimensionless pressure.*
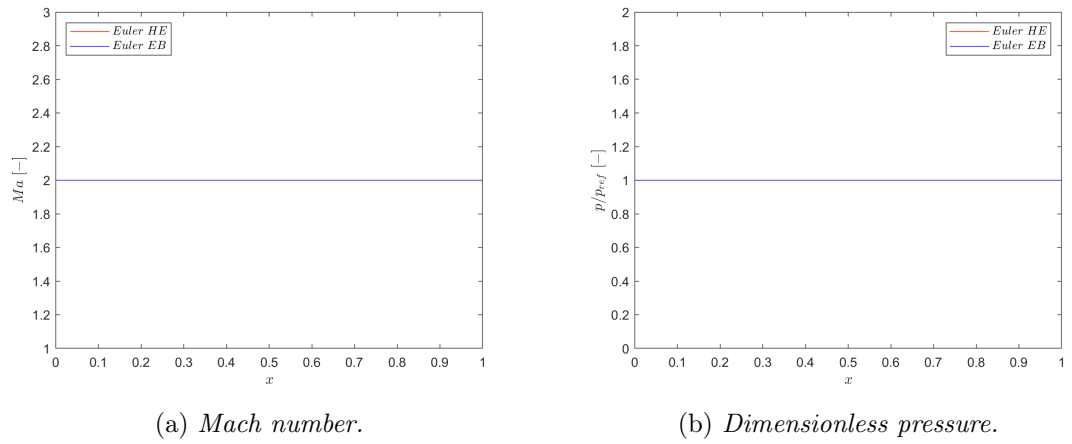
Figure 6.3: Channel Euler test case: post-processing of the fluid dynamic variables.

(a) *Time of each iteration.*

(b) *Total time.*
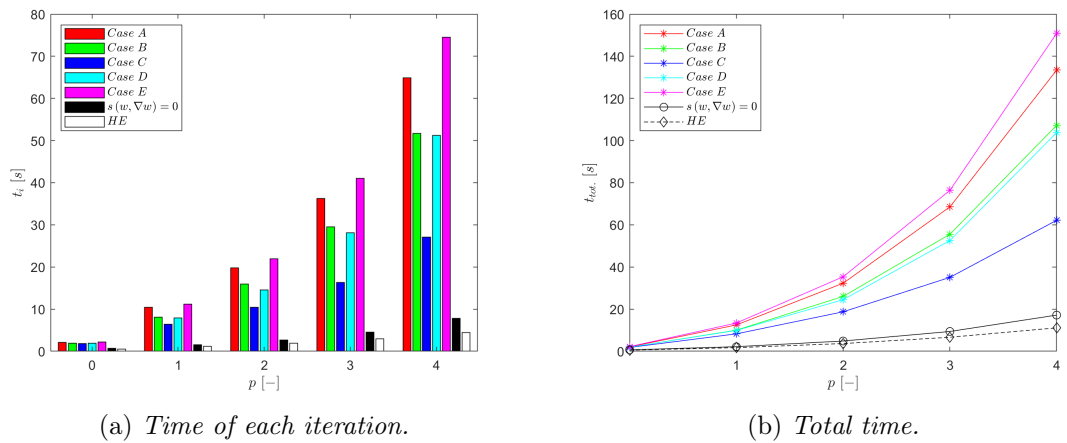
Figure 6.4: Channel Euler test case: time of the simulations.

Table 6.2: Relation n_e and n_p for p-adaptation in Channel test case.

	$p=0$	$p=1$	$p=2$	$p=3$	$p=4$
n_e	256	256	256	256	256
n_p	256	768	1536	2560	3848

(a) *Case A.*

(b) *Case B.*

(c) *Case C.*

(d) *Case D.*
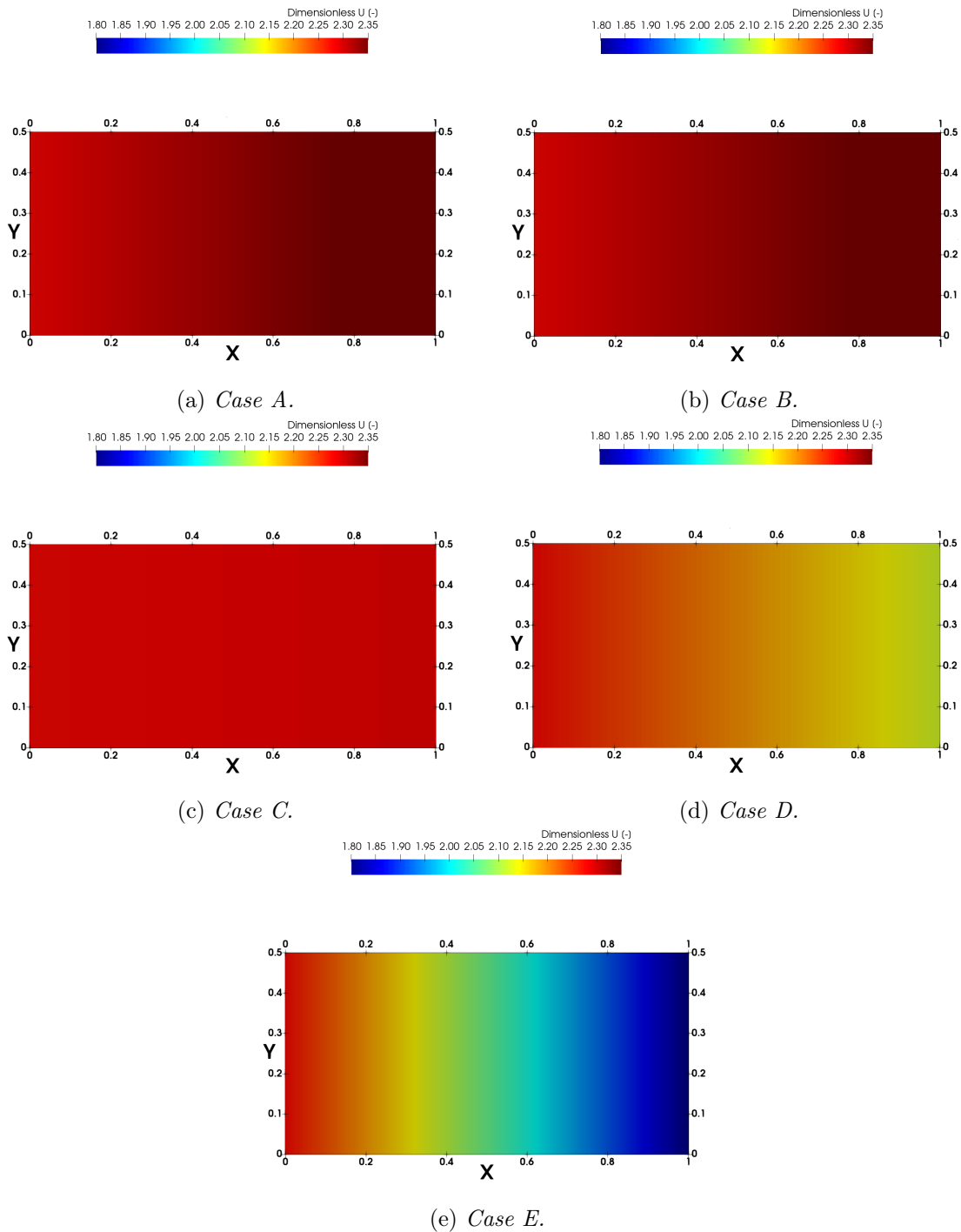
(e) *Case E.*

Figure 6.5: Channel Euler test case: effect of the Lorentz force on the dimensionless velocity.

(a) *Mach number.*

(b) *Entropy.*

(c) *Temperature.*

(d) *Pressure.*

(e) *Velocity.*
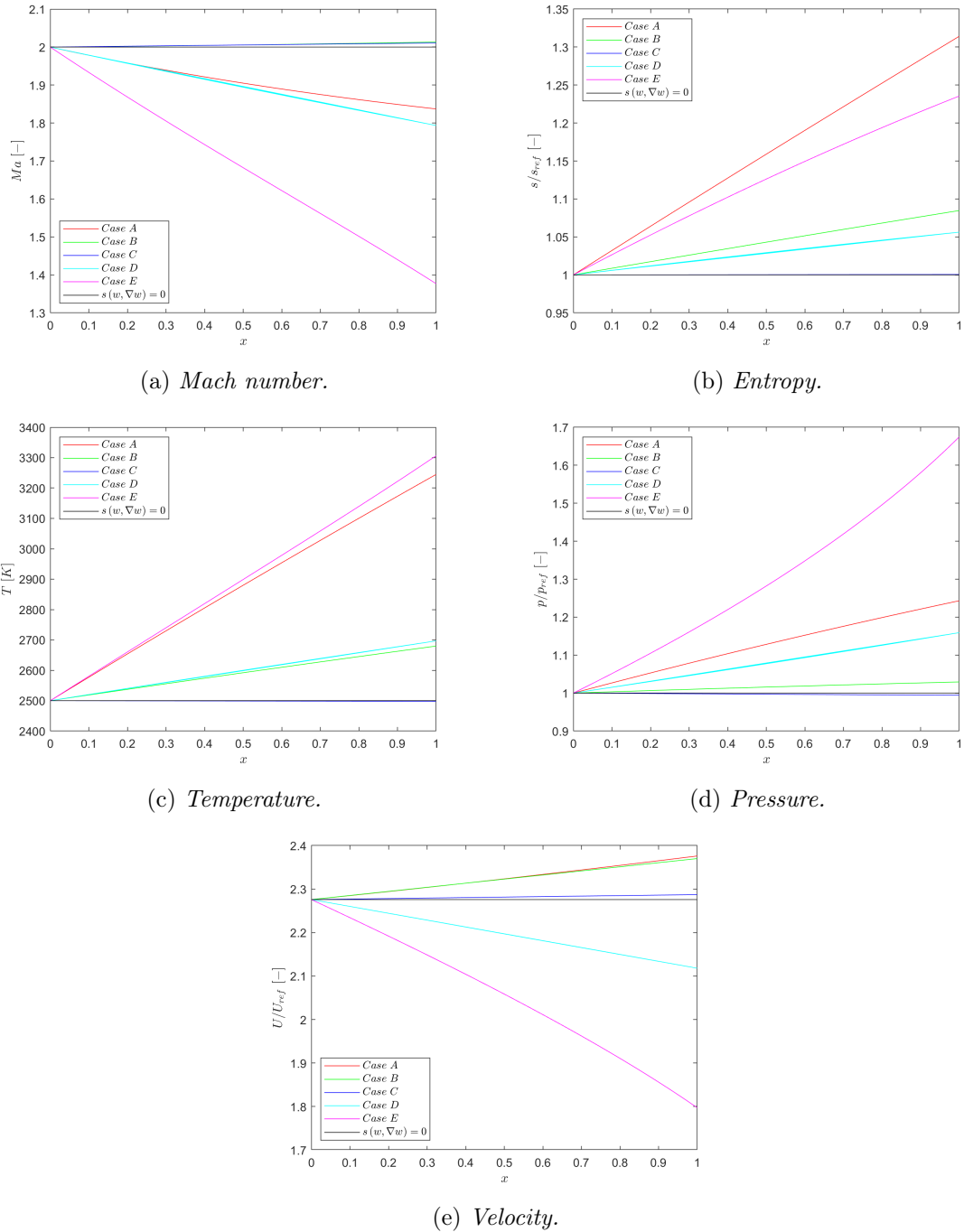
Figure 6.6: Channel Euler test case: effect of the Lorentz force on the fluid dynamic variables.

6.1.2   Shock test case

The numerical domain is composed of far-field inflow, the inclined wall of an angle $\theta \sim 4°$ such that the flow will expand, i.e. from $(0;0)$ to $(0.5;+0.035)$. Then, far-field boundary conditions are prescribed elsewhere. The simulations have been conducted with the following initial parameters: Ma = 2.5, angle of attack $\alpha = 0°$, reference length $L = 1$, $\gamma = 1.4$, Magnetic Reynolds number $Re_m = 0.001$, and the Magnetic force number S = 100. The gas mixture is air with eleven species, i.e e^-, N^+, O^+, NO^+, N_2^+, O_2^+, N, O, NO, N_2 and O_2 with the thermodynamic database of Mutation++ library based on the Rotor Rigid Harmonic Oscillator (RRHO) [52]; [51]. The temperature has been fixed at $T = 2500 \ K$. The artificial viscosity parameter has been chosen equal to $\varepsilon_{art.visc.} = 0.08$. The initial mesh has a number of initial elements equal to 128. The computation for each iteration has been automatically stopped when the residuals reached the threshold ofequal to 10^{-8}. The adaptation procedure has been conducted with 15 number of iterations. For each iteration, the step has been chosen equal to 1.2. In this sense, the adaptation procedure is based on the following rule

$$
\begin{aligned}
n_e^{old} &= n_e \times s^q, & \forall q = \{0, ..., F\} \\
n_e^{new} &= n_e \times s^{q+1}, & \forall q = \{0, ..., F\}
\end{aligned}
\tag{6.3}
$$

where s is the step, F the final number of the iterations (i.e. 15 in our case) and n_e is the initial mesh size (i.e. 128). We selected the parabolic functions to approximate the solution in each elements. In this sense, we have $p = 2$. In addition, we need to remember that this is only a test case to understand if the model that we have implemented works well. Indeed, we are testing the Euler version. Therefore, no diffusive fluxes are present. Hence, from a physical point of view, no presence of electrical conductivity should be considered. However, if we do not take it into account, there are not changes with respect to the classical Euler model. To evaluate them, we need to impose a dummy, un-physical, value of the electrical conductivity. As a consequence, we chose $\sigma_e = 0.1$, which is not so far from the temperature of the mixture. In addition, the same concept needs to be applied to the total density charge. In this situation, to avoid the presence of round-off machine, which could introduce numerical errors, it has been fixed null, i.e. $\rho_c = 0$.

In order to verify the correct numerical solution of the code also in presence of shocks, two types of simulations have been initially analyzed, then the effects of different electromagnetic applied source terms have been taken into account. Firstly, we imposed null electric and magnetic fields. We compared this numerical result with the classical Euler high-enthalpy solution, which does not consider the presence of electromagnetic source. Figures 6.7, 6.8 and 6.9 show the adapted mesh, the Paraview post-processing and the Mach and normalized pressure for a line placed at $y = 0.1$, respectively. Between the two solutions there is a perfect deal. The oscillations present in figure 6.9 for a line placed at $y = 0.1$ are concerned with the numerical stabilization. To reduce them, we can think to introduce a bigger artificial viscosity, but at the same time we need to take into account that the solution will be more affected by the numerical error, even if they are small. In addition, we can notice that these oscillations are present because of the small computational resources.

Secondly, the effects of various external electromagnetic source are tested. We chose a fixed magnetic field in the positive direction of y axis, hence $\mathbf{B} = (0, B_y, 0)^T$, with $B_y = 2$. In addition, to simplify the numerical solution and to reduce the overall computational cost, we imposed an electric field on the z direction, thus we have $\mathbf{E} = (0, 0, E_z)^T$. The values of the z component of the electric fields are present in table 6.3. In figure 6.11 the adaptation of the meshes is shown, in figure 6.12 the post-processing of the dimensionless magnitude of the velocity is presented, while figure 6.13 shows the most important fluid

(a) *Euler high-enthalpy.*

(b) *Euler electromagnetic.*
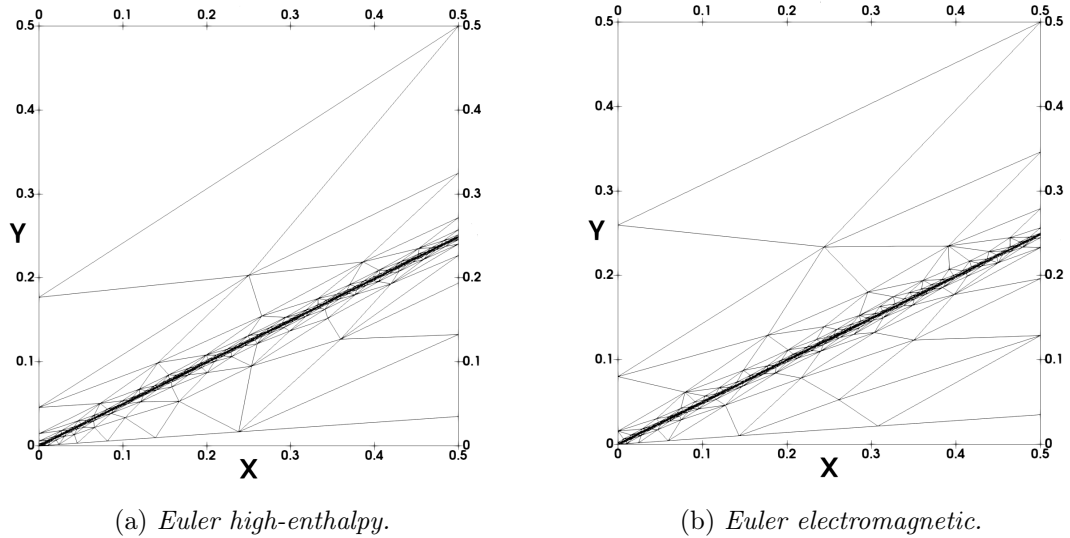
Figure 6.7: Shock test case: adapted meshes. $n_e = 1499$ for Euler high-enthalpy, $n_e = 1491$ for Euler electromagnetic with null source terms. Both with $p = 2$.

(a) *Euler high-enthalpy.*

(b) *Euler electromagnetic.*
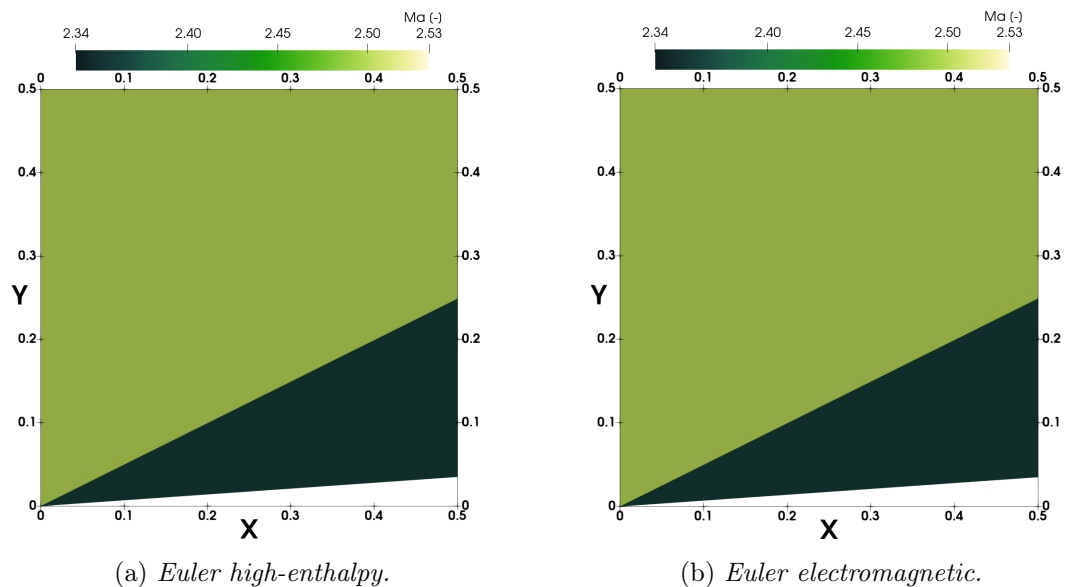
Figure 6.8: Shock test case: post-processing.

dynamic variables for a line placed at $y = 0.1$. The global time for different simulations, like the time for each iteration, is shown in figure 6.10. The simulations conducted with the Euler electromagnetic model have the time including between two extreme values: the time of the Euler high-enthalpy version and the time for the Euler electromagnetic version with null electric and magnetic fields. The different cases are shown in table 6.3. In the post-processing we can see the same concepts already explained in the channel test case. All the physical quantities follow the same behaviour of the channel test case. The oscillation is bigger when the flow is accelerating, i.e. cases A and B certainly. Figure 6.11 shows how the slope of the shock is changing: when the Lorentz force is in the negative direction of the x axis, the slope is bigger, while, when it is in the positive direction of the x axis, the slope is lower.

(a) *Mach number.*

(b) *Dimensionless pressure.*
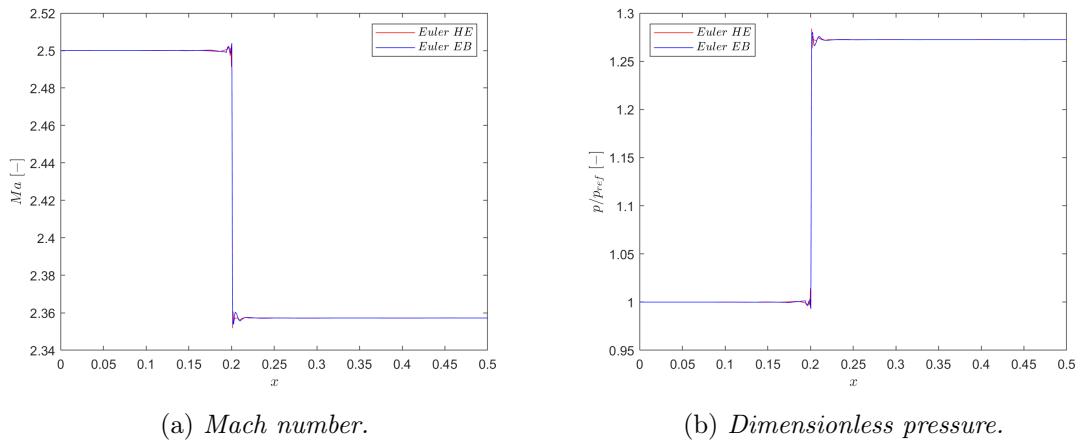
Figure 6.9: Shock test case: post-processing of the fluid dynamic variables.

Table 6.3: Shock test cases.

	Case A	Case B	Case C	Case D	Case E
E_z	-15	-10	-5	0	5
j_z	> 0	> 0	~ 0	< 0	< 0
$\mathbf{j} \times \mathbf{B}_{appl.}\vert_x$	> 0	> 0	~ 0	< 0	< 0
n_e	1573	1533	1492	1511	1496
n_p	9438	9198	8952	9066	8976

(a) *Time of each iteration.*

(b) *Total time.*
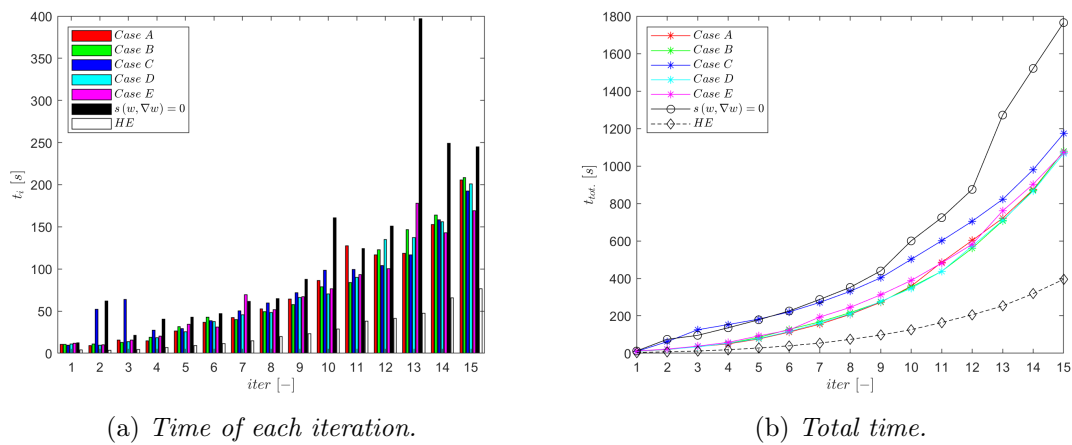
Figure 6.10: Shock Euler test case: time of the simulations.

(a) *Case A.*

(b) *Case B.*

(c) *Case C.*

(d) *Case D.*
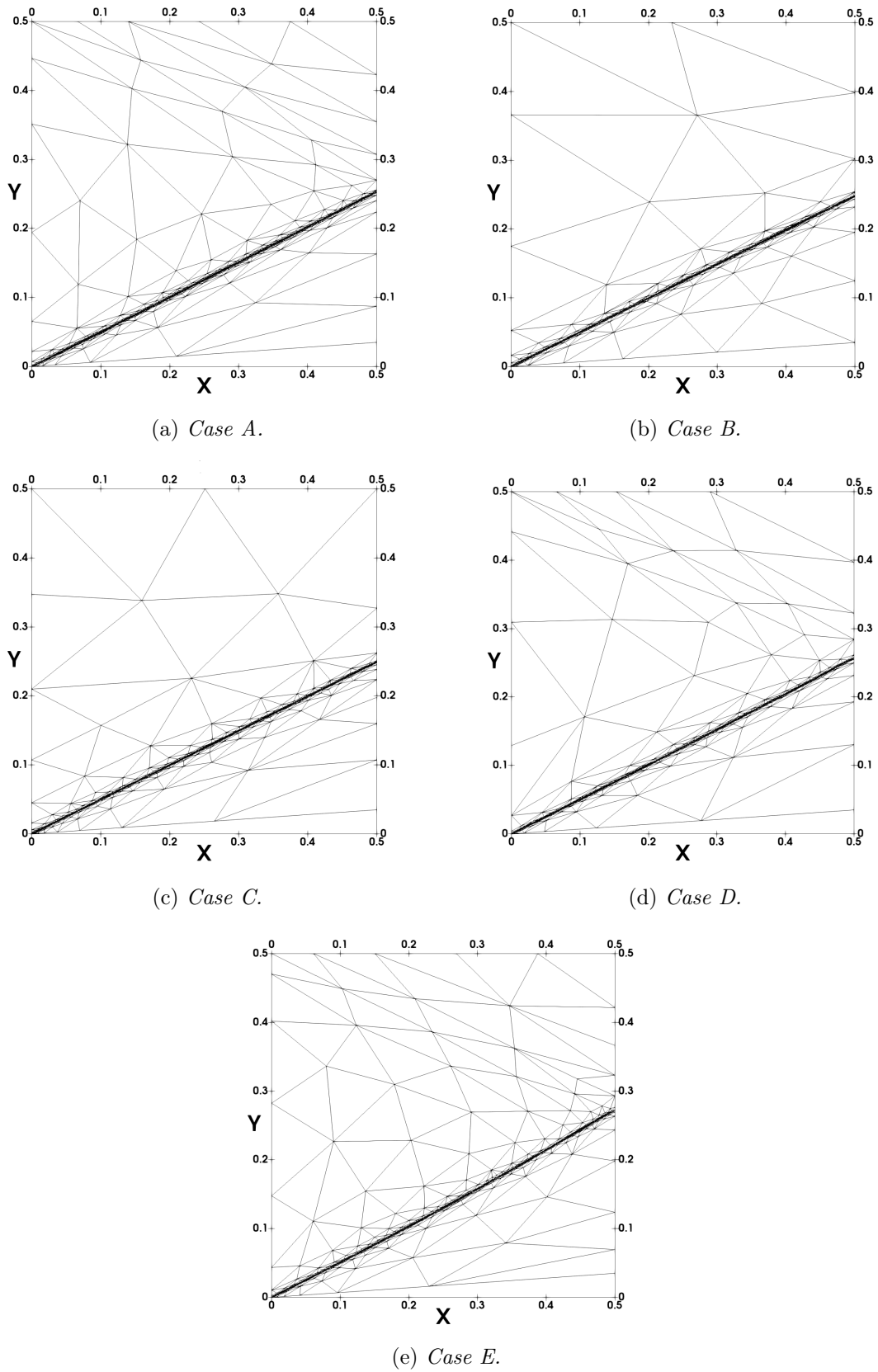
(e) *Case E.*

Figure 6.11: Shock test case: adaptation of the meshes.

(a) *Case A.*

(b) *Case B.*

(c) *Case C.*

(d) *Case D.*
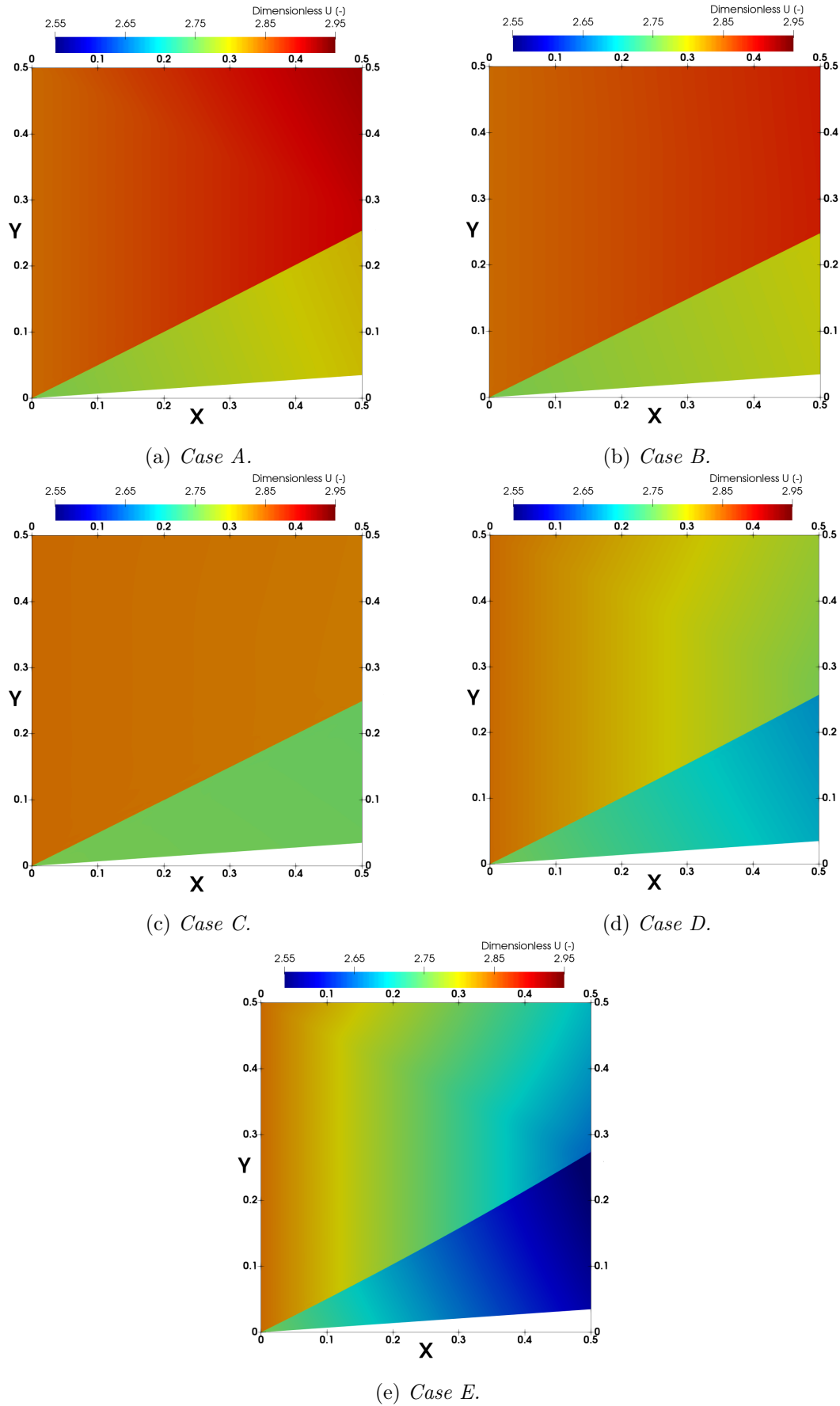
(e) *Case E.*

Figure 6.12: Shock test case: effect of the Lorentz force on the dimensionless velocity.
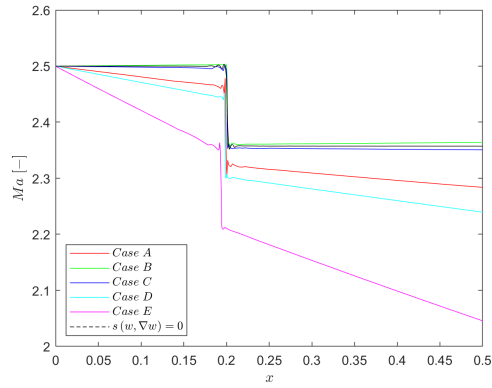
(a) *Mach number.*
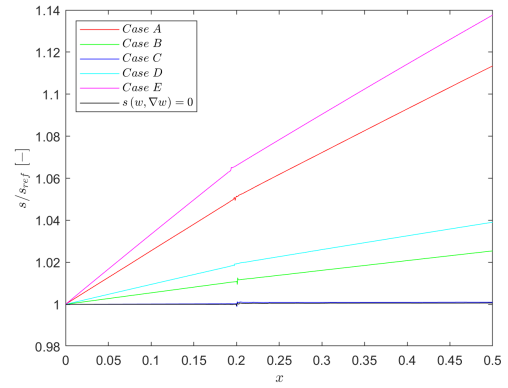
(b) *Entropy.*
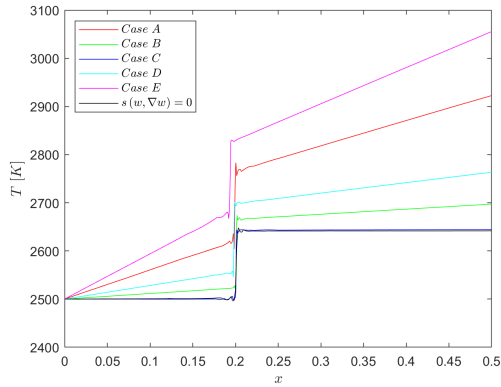
(c) *Temperature.*
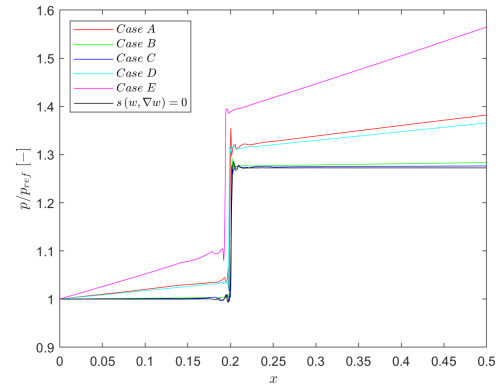
(d) *Pressure.*
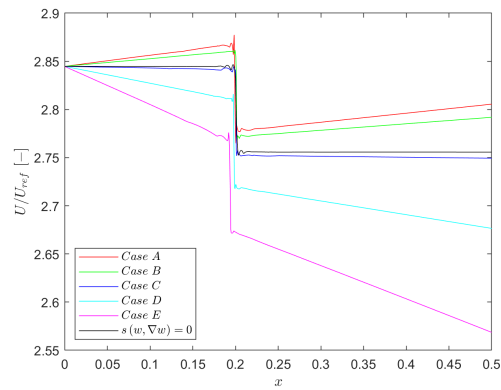
(e) *Velocity.*

Figure 6.13: Shock test case: effect of the Lorentz force on the fluid dynamic variables.

6.1.3   Expansion test case

In this section we are going to test the supersonic expansion test case. The numerical domain is composed of far-field inflow, the inclined wall of an angle $\theta \sim -4°$ such that the flow will expand, i.e. from $(0; 0)$ to $(0.5; -0.035)$. Then, far-field boundary conditions are prescribed elsewhere. The simulations have been conducted with infinity Mach number $\text{Ma} = 2.5$, and angle of attack null. The reference length for the normalization has been set $L = 1$, while the ratio of the specific heat has been set $\gamma = 1.4$. In other words, exactly the same physical and mathematical parameters of the shock test case have been chosen. Consequently, the same gas mixture is considered: air with 11 species at $T = 2500\ K$. Again, we set the value of the electrical conductivity equal to $\sigma_e = 0.1$, while $\rho_c = 0$. The Magneto-Fluid Dynamic parameters have been chosen as follows: Magnetic Reynolds number $\text{Re}_m = 0.001$, while the Magnetic force number $\text{S} = 100$. The initial mesh size is $n_e = 128$, and 15 loops have been chosen for the adaptation, always with step $s = 1.2$. The mesh adaptation procedure follows exactly the same rules of the previous shock test case. Figure 6.14 shows the two adapted meshes for the classical Euler high-enthalpy solution and the same solution computed with the simplified Magneto-Fluid Dynamic model implemented in this work. For the latter, we imposed null the electric and the magnetic fields, in order to understand if the implementation of our new model works correctly. Figure 6.15 shows the post-processing of these solutions. No variations are present, as expected. Indeed, if no external electromagnetic field is applied, the solution of our model is equal to the classical Euler high-enthalpy solution. However, many computational resources are required for this model. This is an immediatly consequence of the computation of the source term, even if it is null. Consequently, numerical errors, which depend on the type machine using for the simulations, will appear. Nevertheless, we will have the same final post-processing. This is also well shown in figure 6.16.

(a) *Euler high-enthalpy.*   (b) *Euler electromagnetic.*
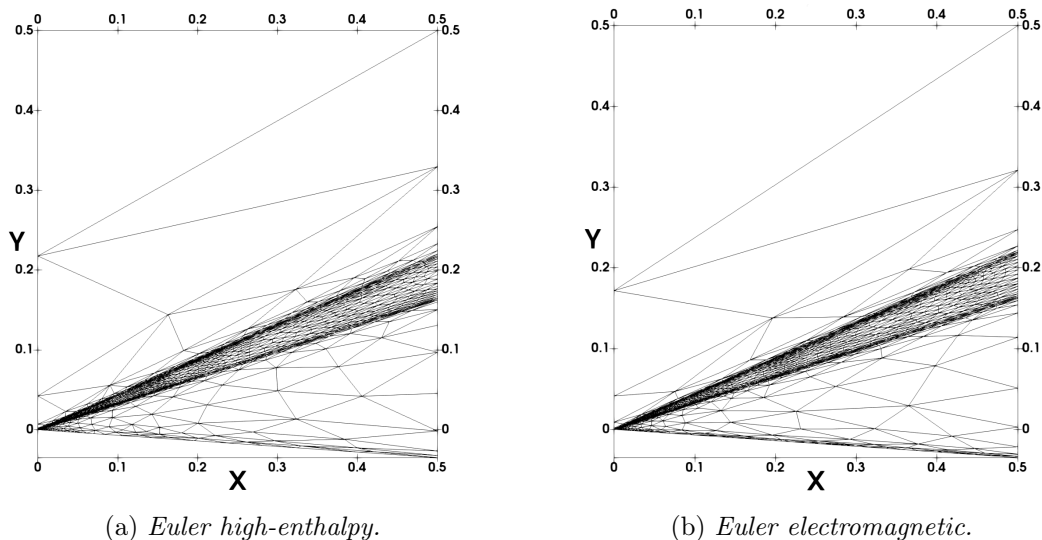
Figure 6.14: Expansion test case: adapted meshes. $n_e = 1742$ for Euler high-enthalpy, $n_e = 1799$ for Euler electromagnetic with null source terms.

In this second step, we run different simulations with various external sources. We imposed the same magnetic field $\mathbf{B} = (0, B_y, 0)^T$ and several electric fields $\mathbf{E} = (0, 0, E_z)^T$. These values are fictitious, and they are only useful to understand the behaviour of the model implemented in [59]. We chose $B_y = 2$, while the different values of the z-component of the electric fields are written in table 6.4. Then, the figures 6.18, 6.19 and 6.20 show the adapted meshes, the Paraview post-processing and the behaviour of the physical quantities

(a) *Euler high-enthalpy.*   (b) *Euler electromagnetic.*
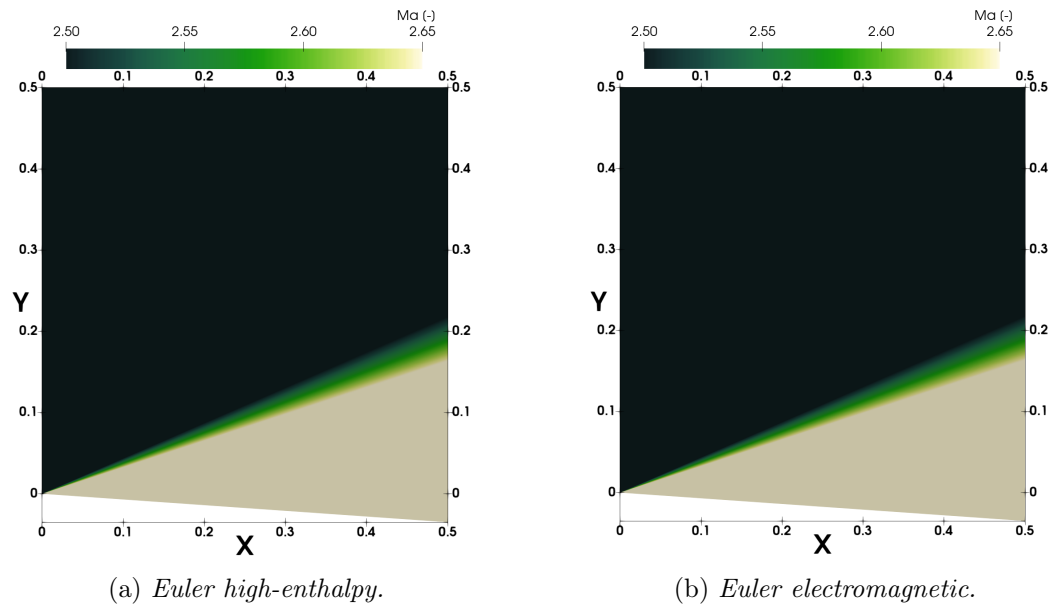
Figure 6.15: Expansion test case: post-processing.

(a) *Mach number.*   (b) *Dimensionless pressure.*
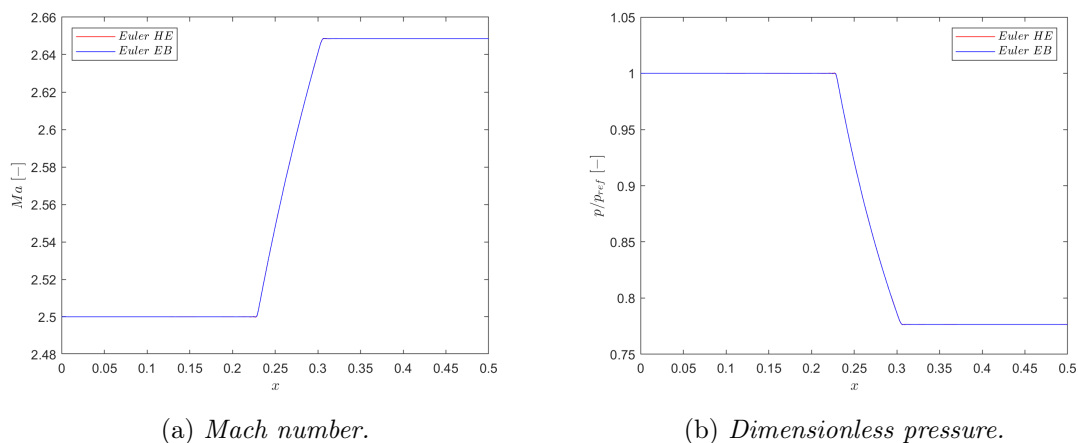
Figure 6.16: Expansion test case: post-processing of fluid dynamic variables.

of our interest. It is important to notice that, when the density current is very small, even
with the presence of externally applied electric and magnetic fields, the contribution of the
Lorentz force, like that of Joule heating, is null. In this context, either there are no changes
in entropy or they are present in small entities (see figure 6.20). The higher computational
time is associated with the presence of null electric and magnetic fields, while the lowest
computational time, for the Euler electromagnetic cases, is given by the situation where
the density current is null. Approximately the same happened for the channel and the
shock test cases. The only difference is that the case C for the shock test case is the
higher time when electric and magnetic fields are applied, while for the expansion it is
the lowest. However, all the cases tested are included between the two extreme conditions:
Euler high-enthalpy and Euler electromagnetic with null electric and magnetic fields, which
are the lowest and the highest case from a computational time point of view, respectively.
Hence, this is the behaviour of the code in the supersonic regime (see figures 6.10 and 6.17).
However, figures 6.18, 6.19 and 6.20 show the adapted meshes, the Paraview and Matlab
post-processings for a line placed at $y = 0.1$. Again, as in the shock test cases, we can
notice the different slope of the expasion fans in figure 6.19. Obviously, the same happens

for the meshes, figure 6.18. In the post-processing there is not the presence of oscilations because these are related with the presence of strong gradients in small regions, i.e. shocks. Instead, here we are considering the expansions, which is an iso-entropy phenomena. In this context, the variations of entropy shown in figure 6.20 are given by the application of the external forces, i.e. Lorentz forces. Indeed, we can notice that these variations are bigger when the density current is greater.

Table 6.4: Expansion test cases.

	Case A	Case B	Case C	Case D	Case E
E_z	-15	-10	-5	0	5
j_z	> 0	> 0	~ 0	< 0	< 0
$\mathbf{j} \times \mathbf{B}_{appl.}\vert_x$	> 0	> 0	~ 0	< 0	< 0
n_e	1716	1733	1780	1753	1649
n_p	10296	10398	10680	10518	9894
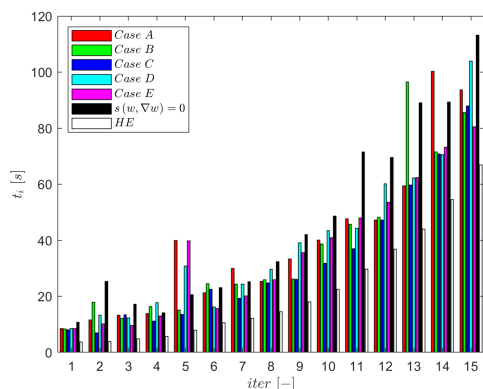
(a) *Time of each iteration.*
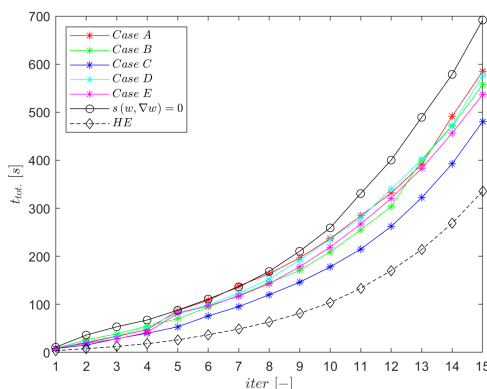
(b) *Total time.*

Figure 6.17: Expansion Euler test case: time of the simulations.
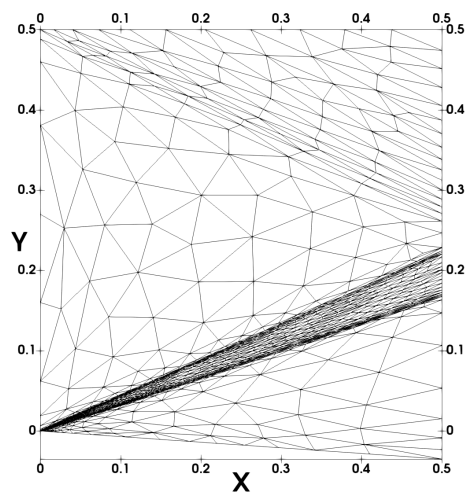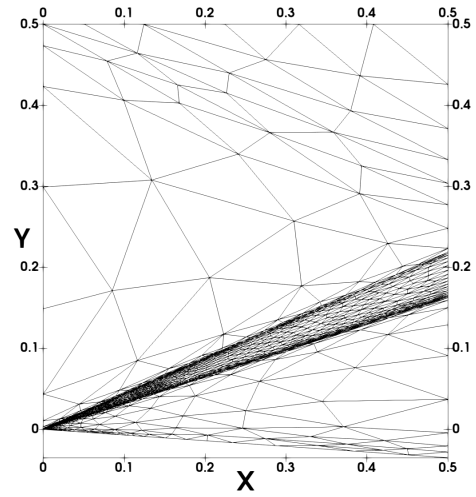
(a) *Case A.*

(b) *Case B.*
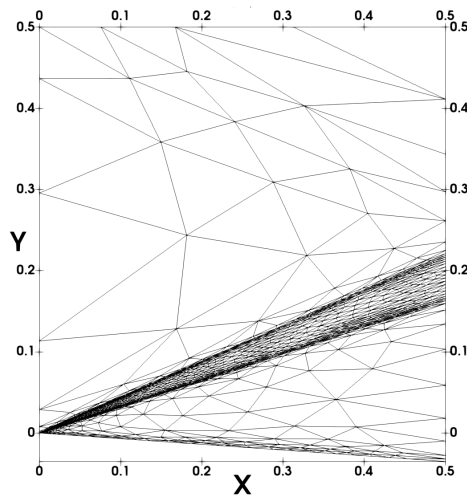
(c) *Case C.*
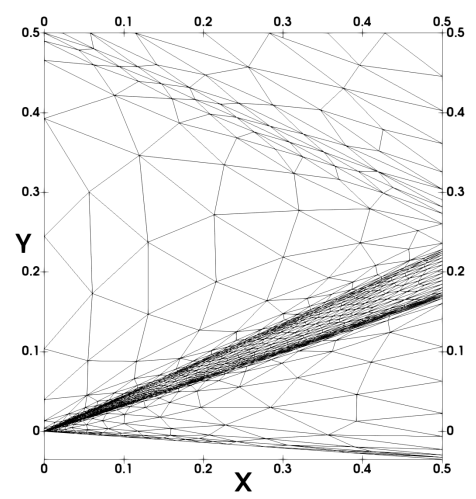
(d) *Case D.*
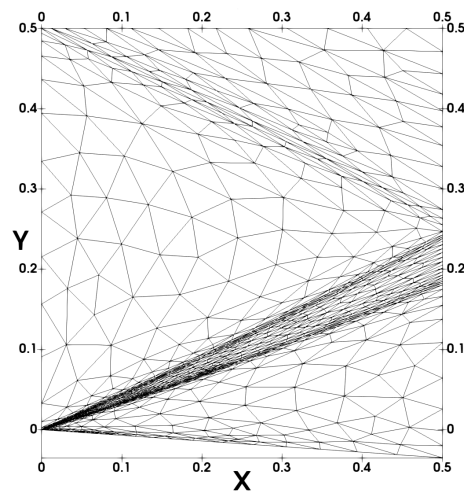
(e) *Case E.*

Figure 6.18: Expansion test case: adaptation of the meshes.

(a) *Case A.*

(b) *Case B.*

(c) *Case C.*

(d) *Case D.*
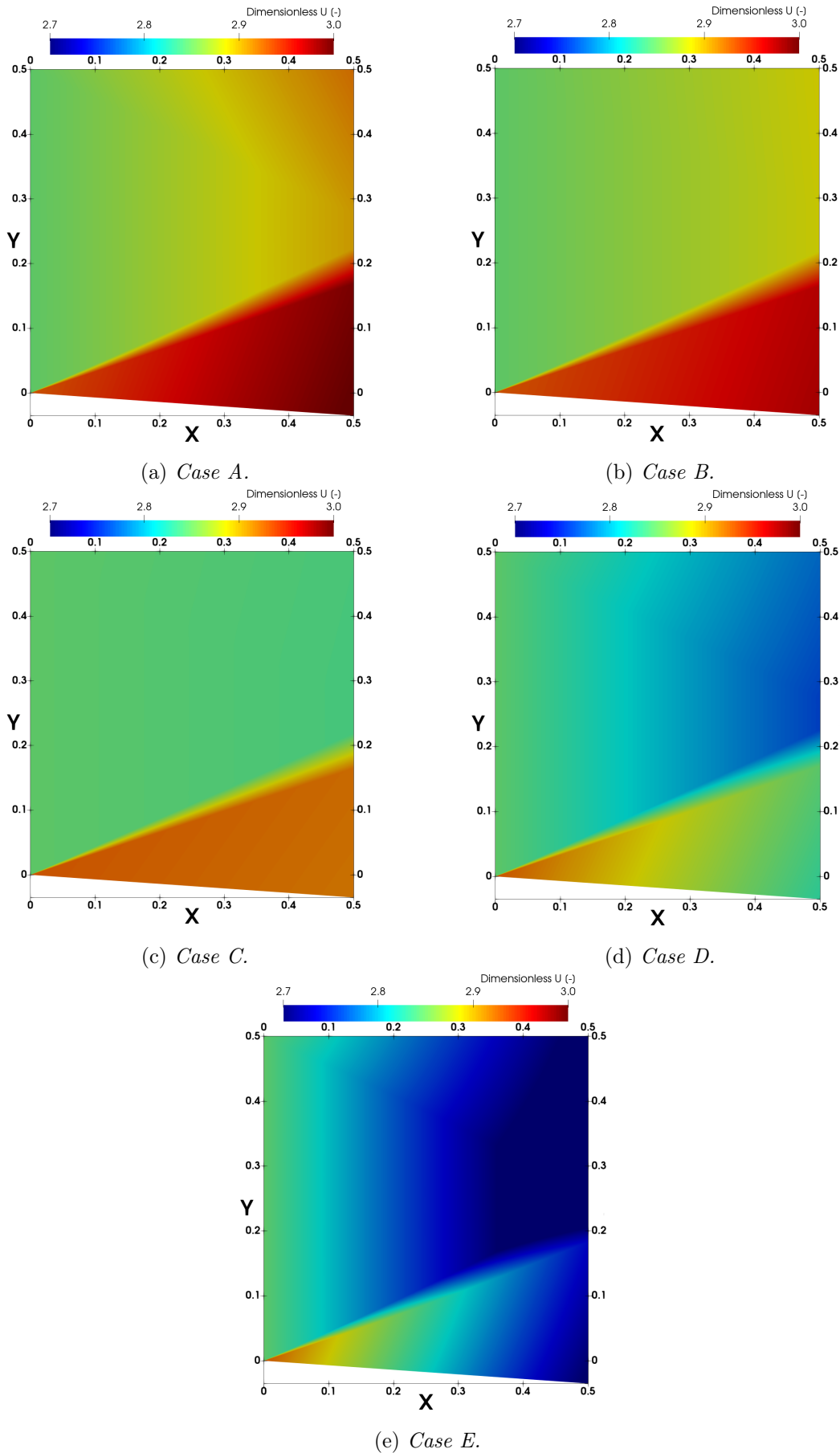
(e) *Case E.*

Figure 6.19: Expansion test case: effect of the Lorentz force on the dimensionless velocity.
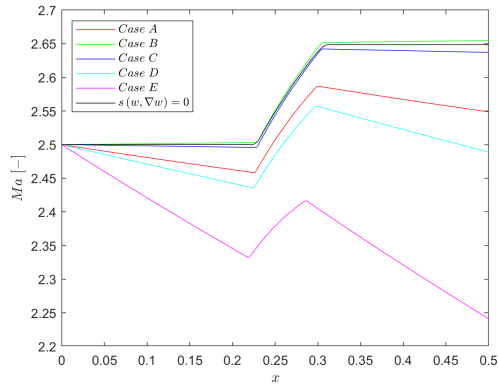
(a) *Mach number.*
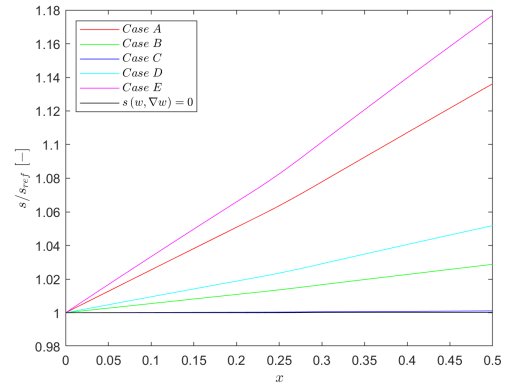
(b) *Entropy.*
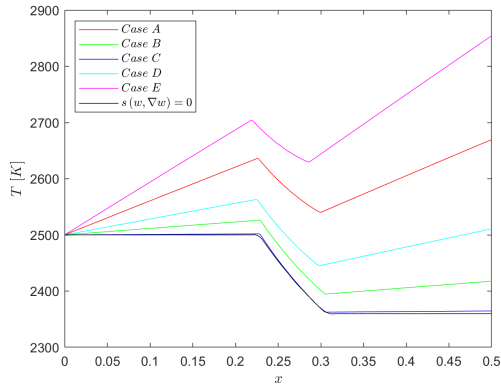
(c) *Temperature.*
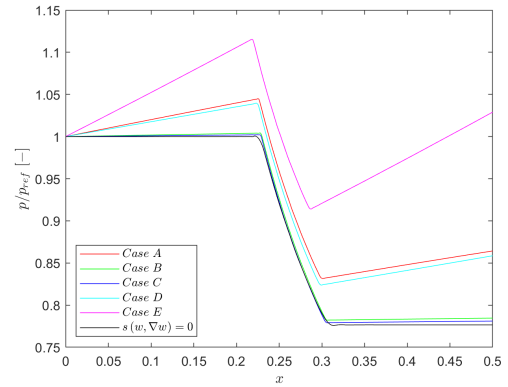
(d) *Pressure.*
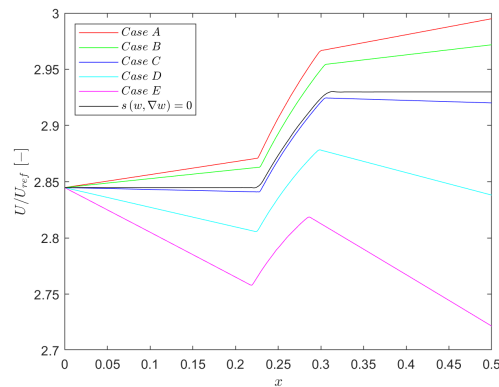
(e) *Velocity.*

Figure 6.20: Expansion test case: effect of the Lorentz force on the fluid dynamic variables.

6.2   Navier-Stokes model

In this section, we are considering this set of equations

$$\frac{\partial \rho}{\partial t} + \nabla \cdot (\rho \mathbf{u}) = 0$$

$$\frac{\partial (\rho \mathbf{u})}{\partial t} + \nabla \cdot (\rho \mathbf{u} \otimes \mathbf{u} + p\underline{\mathbf{I}}) - \nabla \cdot \underline{\tau} = \rho_c \mathbf{E}_{appl.} + \mathbf{j} \times \mathbf{B}_{appl.} \tag{6.4}$$

$$\frac{\partial (\rho E)}{\partial t} + \nabla \cdot [(\rho E + p)\,\mathbf{u}] - \nabla \cdot (\underline{\tau}\mathbf{u} - \dot{\mathbf{q}}) = \mathbf{j} \cdot \mathbf{E}_{appl.}$$

6.2.1   Hartmann flow

In these steps, we will use the index notation for the sake of simplicity. Writing the Navier-Stokes equation for incompressible, chemically non-reacting flows, and remembering that the energy equation is decoupled as a consequence of the possibility to calculate the temperature field from the knowledge of the density and pressure field through the perfect gas law or, if we would like to take into consideration the effects of real gases, through the Wan der Walls equations, the continuity equation reads

$$\frac{\partial \rho}{\partial t} + \rho \frac{\partial u_j}{\partial x_j} = 0 \tag{6.5}$$

while the general form of the momentum equation reads

$$\rho \frac{\partial u_i}{\partial t} + \rho u_j \frac{\partial u_i}{\partial x_j} + \frac{\partial p}{\partial x_i} - \frac{\partial}{\partial x_j}\left(\mu \frac{\partial u_i}{\partial x_j}\right) = f_i \tag{6.6}$$

hence, if we consider constant dynamic viscosity, the latter equation will be

$$\rho \frac{\partial u_i}{\partial t} + \rho u_j \frac{\partial u_i}{\partial x_j} + \frac{\partial p}{\partial x_i} - \mu \frac{\partial^2 u_i}{\partial x_j^2} = f_i \tag{6.7}$$

namely, considering a bidimensional problem, the momentum equation for each component will be

$$\rho \frac{\partial u}{\partial t} + \rho \left(u \frac{\partial u}{\partial x} + v \frac{\partial u}{\partial y} + w \frac{\partial u}{\partial z}\right) + \frac{\partial p}{\partial x} - \mu \left(\frac{\partial^2 u}{\partial x^2} + \frac{\partial^2 u}{\partial y^2} + \frac{\partial^2 u}{\partial z^2}\right) = f_x \tag{6.8}$$

$$\rho \frac{\partial v}{\partial t} + \rho \left(u \frac{\partial v}{\partial x} + v \frac{\partial v}{\partial y} + w \frac{\partial v}{\partial z}\right) + \frac{\partial p}{\partial y} - \mu \left(\frac{\partial^2 v}{\partial x^2} + \frac{\partial^2 v}{\partial y^2} + \frac{\partial^2 v}{\partial z^2}\right) = f_y \tag{6.9}$$

Now, we introduce the steady-state and parallel flow assumptions. In this sense, for the steady-state assumption, all the derivatives with respect to the time will be neglected. The scheme of the domain is illustrated in figure 6.21. Finally, the usage of parallel flow gives us the possibility to obtain an analytical solution. Indeed, from the definition of a parallel flow, we have for a three-dimensional case

$$\mathbf{u} = (u,\ v,\ w)^T \equiv (u\,(y),\ 0,\ 0)^T \tag{6.10}$$

consequently, equation 6.8 will be

$$\frac{\partial p}{\partial x} - \mu \frac{\partial^2 u}{\partial y^2} = f_x \tag{6.11}$$

and equation 6.9 reads

$$\frac{\partial p}{\partial y} = 0 \implies p|_y = \text{cost.} \tag{6.12}$$

This is the set of partial differential equations that describes the flow field for our particular problem. These equations are not non-linear, indeed no convective terms are present. Consequently, they can be solved analytically. It is convenient to write again the equation 6.11 in this way

$$\mu \frac{\partial^2 u}{\partial y^2} = \frac{\partial p}{\partial x} - f_x \tag{6.13}$$

At this stage, it is important to understand which is the contribution of the external force f_x. Indeed, if it is a function of the velocity we cannot consider it constant during the integration, leading to modifications in results. To make a more clear discussion in the next passages we will obtain the analytical solution for both cases.

It is also important to notice that, for parallel, we immediately have the solution for the vorticity. Indeed, the problem is bidimensional, hence the only vorticity component is along the third direction. From a mathematical point of view, we have

$$\boldsymbol{\omega} = \nabla \times \mathbf{u} = \begin{vmatrix} \mathbf{e}_1 & \mathbf{e}_2 & \mathbf{e}_3 \\ \partial_{e_1} & \partial_{e_2} & \partial_{e_3} \\ u_1 & u_2 & u_3 \end{vmatrix} = \left(\frac{\partial u_1}{\partial x_2} - \frac{\partial u_2}{\partial x_1} \right) \mathbf{e}_3 \tag{6.14}$$

that is, for this parallel flow

$$\boldsymbol{\omega} = \omega_z = \frac{\partial u}{\partial y} \tag{6.15}$$

Now, we split the discussion in two separate sections: the first one when we can consider constant the external force, the second one in the opposite case. Subsequently, a brief discussion of the results is present and a comparison with our numerical code is presented to validate the Navier-Stokes model with the presence of electromagnetic source term.
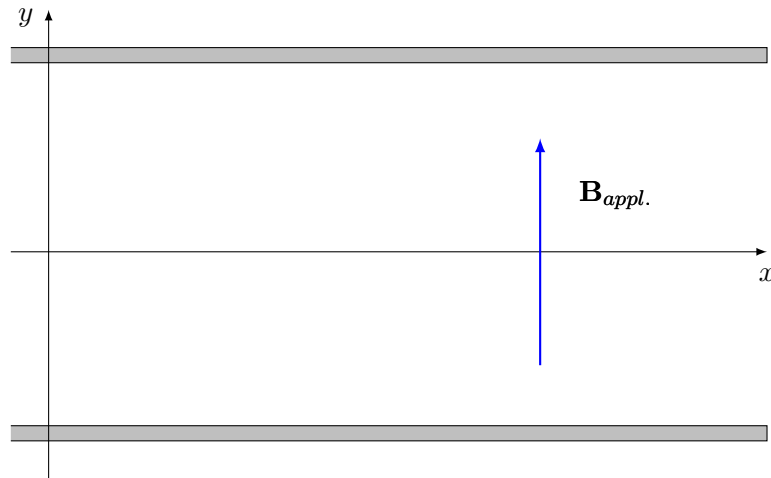
Figure 6.21: The scheme for the parallel Hartmann flow.

6.2.2 $f_x \neq f_x(u(y))$

This is the most simplest case. Equation 6.13 is well integrable

$$\mu \int_{-h}^{+h} \frac{\partial^2 u}{\partial y^2} \, \mathrm{d}y = \int_{-h}^{+h} \left(\frac{\partial p}{\partial x} - f_x \right) \, \mathrm{d}y \tag{6.16}$$

and we obtain

$$\mu \frac{\partial u}{\partial y} = \left(\frac{\partial p}{\partial x} - f_x \right) y + c_1 \tag{6.17}$$

then, the second integration is needed, hence

$$\mu \int_{-h}^{+h} \frac{\partial u}{\partial y} \, \mathrm{d}y = \int_{-h}^{+h} \left[\left(\frac{\partial p}{\partial x} - f_x \right) y + c_1 \right] \, \mathrm{d}y \tag{6.18}$$

and we have

$$\mu u \left(y \right) = \left(\frac{\partial p}{\partial x} - f_x \right) \frac{y^2}{2} + c_1 y + c_2 \tag{6.19}$$

that can be written again like (note that $a = c_1/\mu$ and $b = c_2/\mu$)

$$u \left(y \right) = \left(\frac{\partial p}{\partial x} - f_x \right) \frac{y^2}{2\mu} + ay + b \tag{6.20}$$

where the a and b constant are found wih the imposition of boundary conditions, that are

$$u \left(y = -h \right) = u \left(y = +h \right) = 0 \tag{6.21}$$

thus, we have

$$\begin{cases} a = 0 \\ b = - \left(\frac{\partial p}{\partial x} - f_x \right) \frac{h^2}{2\mu} \end{cases} \tag{6.22}$$

namely, the final analytical solution is

$$u \left(y \right) = - \left(\frac{\partial p}{\partial x} - f_x \right) \frac{h^2}{2\mu} \left[1 - \left(\frac{y}{h} \right)^2 \right], \qquad -1 \leq \frac{y}{h} \leq 1 \tag{6.23}$$

hence, the vorticity reads

$$\omega_z \left(y \right) = \left(\frac{\partial p}{\partial x} - f_x \right) \frac{1}{\mu} y, \qquad -1 \leq \frac{y}{h} \leq 1 \tag{6.24}$$

This is the typical parabolic velocity profile of the Poiseuille flow with the addition of a contribution related to the external force along the x direction. If we do not consider it we obtain the classical Poiseuille velocity profile. Of course, the maximum of the velocity is present in its middle, thus for $y/h = 0$, namely

$$u_{max} = - \left(\frac{\partial p}{\partial x} - f_x \right) \frac{h^2}{2\mu} \tag{6.25}$$

while the maximum and the minimum of the vorticty are at the top and at the bottom of the wall, respectively, i.e.

$$\omega_{z,max/min} = \pm \left(\frac{\partial p}{\partial x} - f_x \right) \frac{1}{\mu} h \tag{6.26}$$

consequently, the dimensionless velocity profile is the same of the Poiseuille flow

$$\frac{u \left(y \right)}{u_{max}} = 1 - \left(\frac{y}{h} \right)^2 \tag{6.27}$$

and the same happens for the vorticity

$$\frac{\omega_z \left(y \right)}{\omega_{z,max}} = \frac{y}{h} \tag{6.28}$$

Figure 6.22 shows the velocity and vorticity for the Hartmann flow.

(a) *Velocity.*
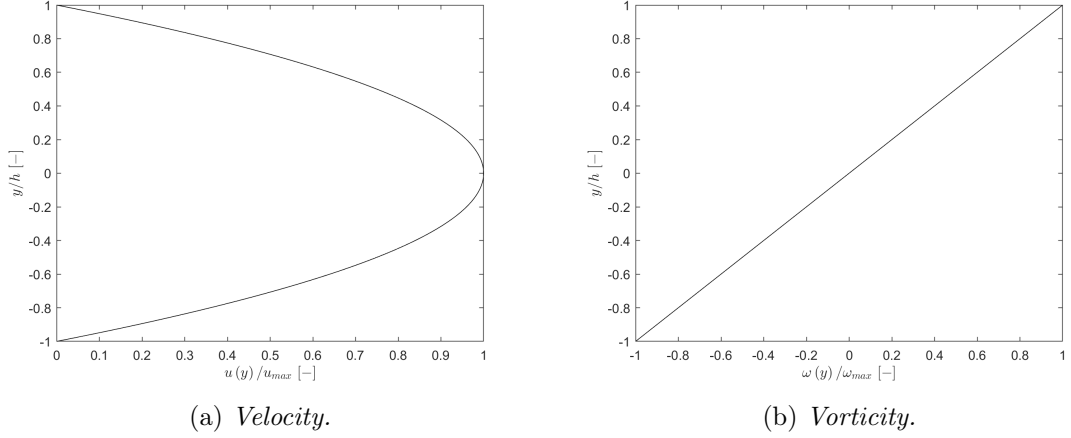
(b) *Vorticity.*

Figure 6.22: Poiseuille flow: normalization of the velocity and vorticity profiles.

6.2.3 $f_x = f_x\left(u\left(y\right)\right)$

In this case, the discussion is more complicated. For instance, in our case, the external force is only along x axis and it represents the Lorentz force. As already well discussed in the previous Chapters, now it is well known that the Lorentz force, which acts on an elementary fluid volume, reads

$$\mathbf{j} \times \mathbf{B}_{appl.} = \left[\rho_c \mathbf{u} + \sigma_e \left(\mathbf{E}_{appl.} + \mathbf{u} \times \mathbf{B}_{appl.}\right)\right] \times \mathbf{B}_{appl.} \tag{6.29}$$

and, for the sake of simplicity, in this discussion, we can consider the total density charge null. In addition, to make the effects more evaluable, according to [39] we can suppose the electric field applied proportional to the applied magnetic field through the electrical conductivity. In this sense, the order of Lorentz force will be

$$\mathbf{j} \times \mathbf{B}_{appl.} \sim \sigma_e u B^2 \tag{6.30}$$

that emphasizes the dependency of f_x from the velocity field. Hence, equation 6.13 will be written as

$$\mu \frac{\partial^2 u}{\partial y^2} - \sigma_e u B^2 = \frac{\partial p}{\partial x} \tag{6.31}$$

where the minus sign in front of the second term in the LHS has been introduced as a consequence of the opposite direction of the Lorentz force with respect to the positive x axis direction. Equation 6.31 is a second-order, non-homogeneous, with constant coefficients (consequently our assumptions) and un-damped partial different equation. It can be written again as follows

$$\frac{\partial^2 u}{\partial y^2} + \left(-\frac{\sigma_e B^2}{\mu}\right) u = \frac{1}{\mu} \frac{\partial p}{\partial x} \tag{6.32}$$

which typical solution is

$$u\left(y\right) = c_1 \exp\left\{-B\sqrt{\frac{\sigma_e}{\mu}}y\right\} + c_2 \exp\left\{B\sqrt{\frac{\sigma_e}{\mu}}y\right\} + u_p\left(y\right) \tag{6.33}$$

where $u_p\left(y\right)$ is the particular solution obtained through the imposition of the non-homogeneous condition. Introducing the definition of Hartmann number (firstly proposed by Julius Hartmann), that is the ratio between the magnitude of Lorentz force and viscous forces

$$\mathrm{Ha} = Bh\sqrt{\frac{\sigma_e}{\mu}} \tag{6.34}$$

the general solution can be written as follows

$$u\left(y\right) = c_1 \exp\left\{-\text{Ha}\frac{y}{h}\right\} + c_2 \exp\left\{\text{Ha}\frac{y}{h}\right\} + u_p\left(y\right) \tag{6.35}$$

thus, with the definitions of hyperbolic functions

$$\cosh\left(\theta\right) = \frac{e^\theta + e^{-\theta}}{2}, \qquad \sinh\left(\theta\right) = \frac{e^\theta - e^{-\theta}}{2} \tag{6.36}$$

we can write the solution as follows (according to [39])

$$u\left(y\right) = a\cosh\left(\text{Ha}\frac{y}{h}\right) + b\sinh\left(\text{Ha}\frac{y}{h}\right) + u_p\left(y\right) \tag{6.37}$$

hence, we need to impose the boundary conditions, i.e. the no-slip conditions at the two walls (bottom and top). Thus we have

$$u\left(y = -h\right) = 0 = u\left(y = +h\right) \tag{6.38}$$

which gives us the possibility to analitically solve the problem. Indeed, we have

$$\begin{cases} 0 = a\cosh\left(-\text{Ha}\right) + b\sinh\left(-\text{Ha}\right) + u_p\left(y\right) \\ 0 = a\cosh\left(\text{Ha}\right) + b\sinh\left(\text{Ha}\right) + u_p\left(y\right) \end{cases} \tag{6.39}$$

now, remembering that the hyperbolic cosine is an even function, while the hyperbolic sine is an odd function, we have

$$\cosh\left(\text{Ha}\right) = \cosh\left(-\text{Ha}\right)$$
$$\sinh\left(\text{Ha}\right) = -\sinh\left(-\text{Ha}\right) \tag{6.40}$$

namely we can write system 6.39 as follows

$$\begin{cases} 0 = a\cosh\left(\text{Ha}\right) - b\sinh\left(\text{Ha}\right) + u_p\left(y\right) \\ 0 = a\cosh\left(\text{Ha}\right) + b\sinh\left(\text{Ha}\right) + u_p\left(y\right) \end{cases} \tag{6.41}$$

hence, we can simply find a and b. We have

$$\begin{cases} a = -\dfrac{u_p\left(y\right)}{\cosh\left(\text{Ha}\right)} \\ b = 0 \end{cases} \tag{6.42}$$

namely, the velocity profile is expressed by

$$u\left(y\right) = u_p\left(y\right)\left[1 - \frac{\cosh\left(\text{Ha}\frac{y}{h}\right)}{\cosh\left(\text{Ha}\right)}\right] \tag{6.43}$$

again, as in the previous cases, the maximum of the velocity is in the middle, hence $u_{max} = u\left(y = 0\right)$, i.e.

$$u_{max} = u_p\left(y\right)\frac{\cosh\left(\text{Ha}\right) - 1}{\cosh\left(\text{Ha}\right)} \tag{6.44}$$

hence, the dimensionless velocity profile reads

$$\frac{u\left(y\right)}{u_{max}} = \frac{\cosh\left(\text{Ha}\right) - \cosh\left(\text{Ha}\frac{y}{h}\right)}{\cosh\left(\text{Ha}\right) - 1} \tag{6.45}$$

hence, with the same concepts applied before for the Poiseuille flow, we can evauate the normalization vorticity as follows

$$\frac{\omega_z\left(y\right)}{\omega_{z,max}} = \frac{\sinh\left(\text{Ha}\frac{y}{h}\right)}{\sinh\left(\text{Ha}\right)} \tag{6.46}$$

Figure 6.23 shows the velocity and vorticity for the Hartmann flow.

(a) *Velocity.*
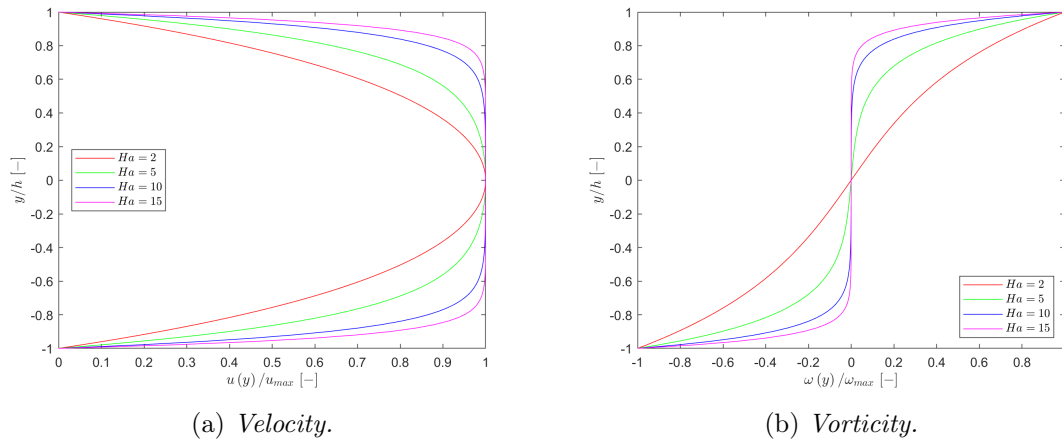
(b) *Vorticity.*

Figure 6.23: Hartmann flow: normalization of the velocity and vorticity profiles.

6.2.4 Considerations and discussion

Finally, we have obtained two different solutions. Now we are going to analyze them from a physical point of view. We can approximate the hyperbolic functions with their Maclaurin expansion. Indeed, for $\theta \to 0$, and for $n = 0, 1, 2, ..., k$, we have

$$\cosh(\theta) = \sum_{n=0}^{k} \frac{\theta^{2n}}{(2n)!} + \mathcal{O}\left(\theta^{2k+1}\right), \qquad \sinh(\theta) = \sum_{n=0}^{k} \frac{\theta^{2n+1}}{(2n+1)!} + \mathcal{O}\left(\theta^{2k+2}\right) \quad (6.47)$$

thus, for $n = 0$, we have

$$\cosh(\theta) \sim 1 + \frac{\theta^2}{2}, \qquad \sinh(\theta) \sim \theta \quad (6.48)$$

hence, when the Hartmann number is very low, we can approximate the solution 6.45 with its Maclaurin expansion. In this sense, for Ha $\to 0$, we will have

$$\frac{u(y)}{u_{max}} \sim 1 - \left(\frac{y}{h}\right)^2 \quad (6.49)$$

which represents exactly the Poiseuille velocity profile. This is extremely correct. Indeed, from a physical point of view, the Hartmann number expresses, as mentioned before, the ratio between the electromagnetic forces on the viscous forces. Hence, it has a relationship with the typical dimensionless Magneto-Fluid Dynamic parameters. In fact, we have

$$\text{Ha} = \sqrt{\text{S Re}_m \text{ Re}} \quad (6.50)$$

where S is the Magnetic force number, Re_m is the Magnetic Reynolds number and Re si the classical Reynolds number. As a consequence, this means we can divide the solution of the Magneto-Fluid Dynamic problem in two subspaces based, for instance, on the Hartmann number

- **Small Hartmann number**: in this case, there are not huge differences in the fluid dynamic behavior with or without the application of external magnetic fields. In this situation, the inducted magnetic field, to a first approximation, can be neglected. Hence, we are considering only the imposed magnetic field. This is exactly the situation in which the development of the models discussed in this Master's Thesis work is based. Consequently, we do not expect huge variations from the typical parabolic profile. The presence of the Lorentz force requires only an acceleration or

deceleration of the fluid inside the channel test case. Hence, in this situation, the velocity profile is approximately described by

$$\frac{u\left(y\right)}{u_{max}} \sim 1 - \left(\frac{y}{h}\right)^2 \tag{6.51}$$

- **High Hartmann number**: instead, in this situation, the effects of the magnetic field cannot be neglected. The velocity profile is not parabolic. Increasing the Hartmann number, the velocity profile flattens in the middle region. This is due to the fact that, while the Hartmann number is increasing the effect of Lorentz force is going to overtake the effects of viscous forces. In this sense, if we are considering Lorentz force along the negative direction of x axis, the velocity profile is decelerating. On the other hand, in the region near the wall, in the typical fluid dynamic boundary layer, the effects of the magnetic field are bigger than in the other regions. Hence, a new layer is present, which is called the Hartmann layer. However, although this is not the topic of this Master's Thesis, it could be a starting point for future implementations. More generally, we can say that in this subspace the velocity profile is described by

$$\frac{u\left(y\right)}{u_{max}} = \frac{\cosh\left(\mathrm{Ha}\right) - \cosh\left(\mathrm{Ha}\frac{y}{h}\right)}{\cosh\left(\mathrm{Ha}\right) - 1} \tag{6.52}$$

The global process could be explained in this way. If there is not a magnetic field, the fluid constrain is only based on the walls. With the introduction of an external magnetic field, some modifications in the flow field appear. The interaction between the imposed electric and magnetic fields and the motion of the charged particles creates the conduction current. The conduction current is made up of convective and conductive terms. The cross-product between the conduction current and the external applied magnetic field generates the Lorentz force. On the other hand, the scalar product between the conduction current and the imposed external electric field originates the Joule heating that is present in the energy equation. The Lorentz force produces modifications in the velocity profile. Its magnitude is related to the magnitude of the viscous forces through the Hartmann number. At this point, the problem has to be split into two different approaches that depend on the magnitude of the Magnetic Reynolds number, which expresses the ratio between the induction and the convection of the magnetic field

$$\mathrm{Re}_m = \frac{uL}{\nu_m} = uL\mu_0\sigma_e \tag{6.53}$$

where ν_m is the magnetic diffusivity (in S.I. it reads $\left[m^2/s\right]$), μ_0 is the vacuum permeability (in S.I. it reads $[H/m]$) and σ_e is the electrical conductivity (in S.I. it reads $[S/m]$).

- **Small Magnetic Reynolds number**: in this case, the induction magnetic field is overlooked by the convection quantities. In other words, the applied magnetic field is undisturbed by the flow and its value remains constant. The presence of the induction magnetic field can be neglected, thus no additional equations must be added in the system to solve. This is the typical situation on which this Master's Thesis work is focused. Hence, no Ampère equation is called by the solver and no additional magnetic field is present. The total magnetic field is only made up of the initial applied one, and it is responsible for the Lorentz force. Thus, the modification of velocity profile is present, but their normalization with respect to the maximum velocity is the same as Poiseuille flow.

- **High Magnetic Reynolds number**: in this second case, the induction magnetic field is not negligible. In this sense, we need to add another vectorial equation in the

full system that describes the flow field. This is called magnetic induction equation and it reads

$$\frac{\partial \mathbf{B}}{\partial t} + \nabla \cdot (\mathbf{u} \otimes \mathbf{B} - \mathbf{B} \otimes \mathbf{u}) = -\varepsilon_0 c^2 \nabla \times \left(\underline{\boldsymbol{\sigma}}_e^{-1} \nabla \times \mathbf{B} \right) \qquad (6.54)$$

In this situation, the magnetic field is strongly coupled with the fluid motion, not only with the Ampère's law but also in the momentum equation where the Maxwell tensor is present and modification of pressure appears. This is the typical situation studied by Hartmann and that characterizes the Hartmann flow. In fact, in this situation, the strongly coupled between the magnetic field and flow field introduces the variations of the magnetic field along the x direction. Hence, the Lorentz force is not uniform, but it changes along the perpendicular direction to the velocity one. In particular, the induced magnetic field is null in the middle of the channel and at the wall. The function that describes its behavior is odd. In this sense, the modification of the velocity profile is mainly caused by the induced magnetic field.

(a) *Velocity.*

(b) *Vorticity.*
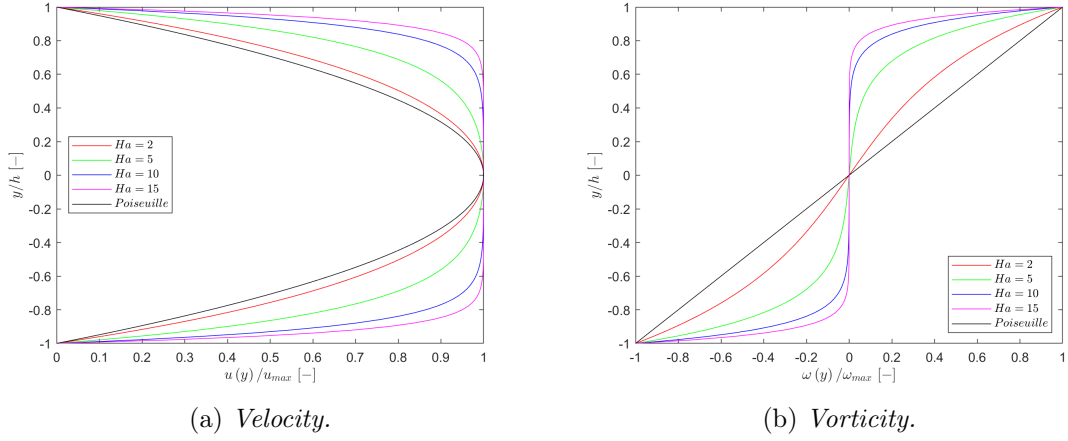
Figure 6.24: Poiseuille and Hartmann flows: effect of the Hartmann number.

Now, we are going to analyze the numerical results obtained. To make it possible, we firstly need to analyze the situation in which we are. In other words, we have divided the physical solution domain in two different ways, based on two different dimensionless parameters: Hartmann number and Magnetic Reynolds number. What is the situation we are considering? Answering this question is important to notice that the ratio between the Hartmann number and the Magnetic Reynolds number is greater than one

$$\mathrm{Re}_m \ll \mathrm{Ha} = \sqrt{\mathrm{S}\, \mathrm{Re}_m\, \mathrm{Re}} \qquad (6.55)$$

where S is the Magnetic force number which represent the ratio between the magnetic and the inertial forces, it is defined as follows

$$\mathrm{S} = \frac{\mathrm{N}}{\mathrm{Re}_m} \qquad (6.56)$$

where N is the Stuart number, which describes the ratio between the electromagnetic and the inertial forces. It is defined as $\mathrm{N} = B^2 L \sigma_e / (\rho u) = \mathrm{Ha}^2 / \mathrm{Re}$. In addition, we remember that in our application, as described in the previous Chapters, we are considering a physical model based on the assumption of the small Magnetic Reynolds number, thus no induction magnetic field is present in our model. In this situation, the physical model implemented in the High-Order Unifying Framework is valid for

$$\mathrm{Re}_m \ll 1 \qquad (6.57)$$
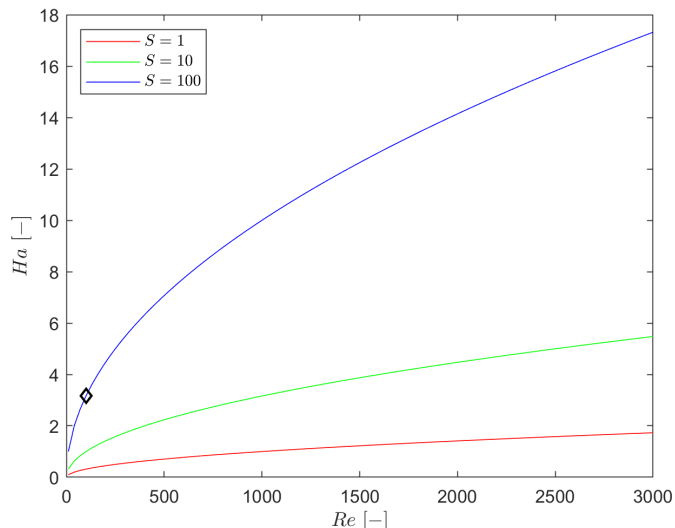
Figure 6.25: Hartamann number from equation 6.50 as function of the Magnetic Reynolds number and the Magnetic force number. Diamond is the case of our simulations for Navier-Stokes model.

Subsequently, our solution is valid when we neglect the additional induction magnetic field that arises from the interaction between the flow field and the external applied magnetic field. Namely, we expect that the velocity profile of our numerical simulations is not affected by the induced magnetic field but, in other words, they will be a modification of the Poiseuille velocity profile, i.e. the Hartmann velocity profile when the Hartmann number is low. Indeed, from its definition 6.55, we are expecting it will be small. Actually, if we consider that in our test simulations we have set the Magnetic Reynolds number equal to $Re_m = 0.001$ (very small to satisfay the assumption of the model implemented), the Reynolds number $Re = 100$ (laminar case) and the Magnetic force number $S = 100$, we will have $Ha \sim 3$, exactly what we expected. Even if we decide to increase the Hartmann number, no effects will be visibly present because of the absence, in the full system, of the induction magnetic field equation. Hence, the growth of the Hartmann number is only associated with the effect of the electromagnetic source term or with the typical behavior of viscous flow based on the Reynolds number. Thus, if we fix the Reynolds number, the ratio between the inertial and viscous forces is established. Subsequently, variations of the Hartmann number are only associated with variations of the Magnetic force number which expresses the ratio between the Lorentz forces and the inertial ones. Therefore, the effects of Lorentz forces depend on the magnitude of the Magnetic force number. However, we cannot modify the dimensionless parameter as we want. Indeed, in the latter case, we could obtain no physical solution and the computation will go bankrupt. To verify the full Navier-Stokes implementation with presence of external applied electromagnetic fields, two diffent steps have been done. In the first one we are considering a fix value of the electrical conductivity. This value has been chosen compatible with the temperature of the mixture. In the second case, the electrical conductivity is computed for each element by the solver and the Mutation++ library. The last one is the real case, where, as a consequence of the variations of the temperature along the channel, the value of the electrical conductivity cannot be though as constant.

6.2.5 Navier-Stokes testing: fixed σ_e

In this section we are going to test a simplified version of the model implemented in the High-Order Unifying Framework. In this first stage, we have fixed the value of the electrical conductivity as a constant. This is not a real physical application. Indeed, in the previous Chapters, we have shown that the electrical conductivity can be assumed as scalar only in simplified version. In addition, it increases rapidly with the temperatures when they are high. However, this is the first step to understand if the model has been implemented correctly. We run several incompressible simulations with the following parameters: Mach number Ma = 0.2, Reynolds number Re = 100, Magnetic force number S = 100, ratio of the specific heats $\gamma = 1.4$, reference length $L = 1$, pressure of reference 1 atm. The initial mesh has $n_e = 136$ triangular elements. The functions for each elements have been chosen to be parabola, i.e $p = 2$. The adaptation of the mesh is based on 15 iterations with the value of the step equal to 1.2. The computation for each iteration has been automatically stopped when the residuals will reach the threshold equal to 10^{-8}. The final mesh is shown in figure 6.26. Due to the small computational resources we were not able to perform more accurate simulations, however, they are satisfactory to understanding the correct implementation of the model. We use a channel with width 10.5, height 2. We prescribed far-field inflow boundary conditions at $x = -0.5$ to avoid the possibility of reverse flows, after the symmetry plane is present. Then, finally the wall from $x = 0$ to $x = 10.5$. After, outflow boundary conditions is present. This situation is obviously replicated in the upper part of the channel. We did not impose any pressure and/or temperature gradient, hence they are computed automatically by the boundary conditions. We imposed the external magnetic field in the positive direction of the y axis, i.e. $\mathbf{B} = (0, B_y, 0)^T$, with $B_y = 2$. The external applied electric field is reported in table 6.5. We fixed the electrical conductivity equal to $\sigma_e = 0.1$, typical value of the temperature of the mixture $T = 3250\ K$. In figure 6.28 is shown the Paraview post-processing for different cases. According to [57] that, for laminar flow between parallel plates, found the hydrodynamics entry length to be approximated as follows $L_e = 2.11 + 0.0168$ Re, to be sure and more conservative, we have conducted the post-processing from $L \geq 80$. Anyway, we can take a look at the mesh in figure 6.26 to understand when the flow can be considered fully developed and we can start the post-processing. In this sense, we are sure that the flow is completely developed under the condition imposed by us. In figure 6.28 shows the post-processing of the dimensionless velocity for two models: the Navier-Stokes high-enthalpy and the simplified Navier-Stokes for low Magnetic Reynolds number by imposing null the electric and the magnetic fields. As we expected, we can notice the perfect deal between the two solutions. The only differences are related with the computational time, although these are still small (figure 6.39). For the points near the exit of the channel, the outflow boundary condition can disturb the flow. This is shown in figures 6.30 and 6.31. Anyway, in figure 6.31 good deals are provided between the numerical solutions for different cases and the analytical Hartmann solution computed with the Hartmann number of the problem. In the same figure also the differences with the Poiseuille flow are provided, exactly what we expected from figure 6.24.

Table 6.5: Channel Navier-Stokes test cases.

	Case A	Case B	Case C	Case D	Case E
E_z	-4	-2	0	2	4
$\mathbf{j} \times \mathbf{B}_{appl.}\vert_x$	< 0	< 0	< 0	> 0	> 0
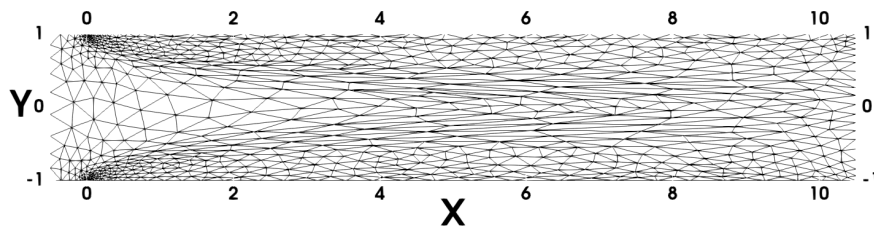
Figure 6.26: Adapted mesh for the channel test case with the Navier-Stokes model. After 15 iterations, starting from a very coarse mesh mades up of $n_e = 136$, we obtain this mesh with $n_e = 1482$. In each element the surfaces are parabolic functions, i.e. $p = 2$.

Firstly, we have tested the model without the presence of externally applied magnetic and electric fields. In this sense, the Paraview post-procesing of the dimensionless velocity is shown in figure 6.28. The latter is also plotted in figure 6.29, where the effects of the Lorentz force are shown. In fact, when the Lorentz force is in the positive direction of the x axis the flow is accelerating, hence the velocity profiles are on the right side of the classical Navier-Stokes high-enthalpy solution. In the opposite case, when the Lorentz force is the negative direction of the x axis, the contrary happened. No variations are present in the two simulation, exactly what we expected. Hence, we can affirm that the model works well. Obviously, in the Navier-Stokes model with the presence of external electromagnetic sources, the computational cost will be higher than in the case where the code is linked to Mutation++ library only to compute the classical transport properties, i.e. dynamic viscosity and thermal conductivity. Obviously, in the Magneto-Fluid Dynamic model implemented in this work the effects of the high temperature are taken into account. Indeed, otherwise the model would have no physical sense because for the low temperatures the electrical conductivity is null.
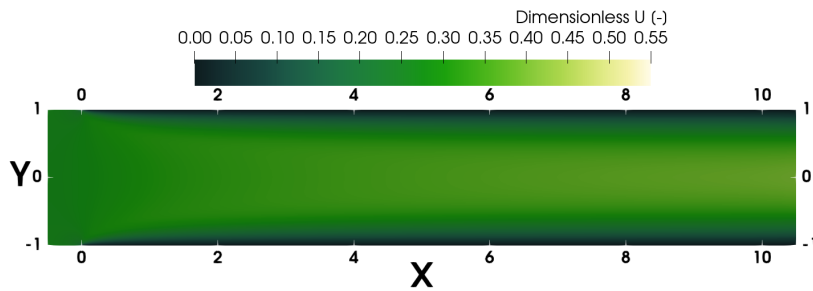
(a) *Navier-Stokes high-enthalpy.*
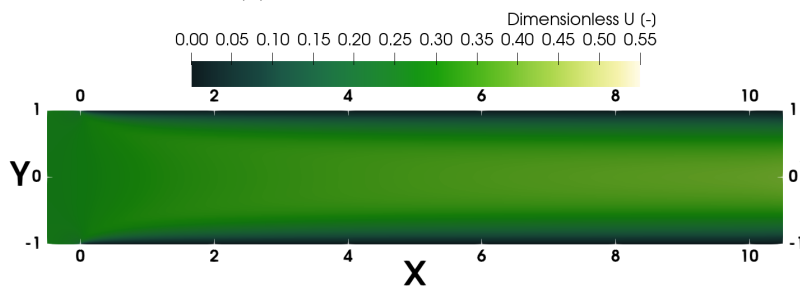
(b) *Navier-Stokes electromagnetic.*

Figure 6.27: Channel Navier-Stokes test case: post-processing, fixed electrical conductivity.
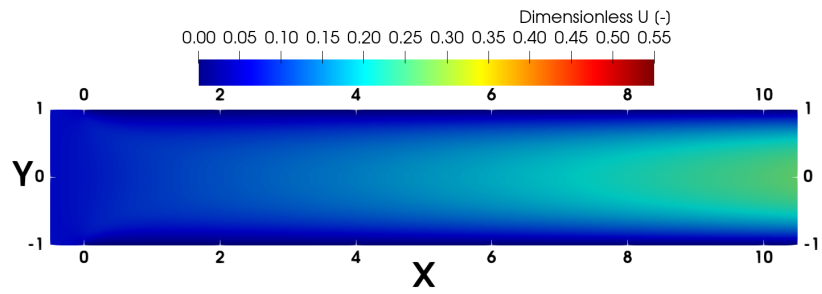
(a) *Case A.*
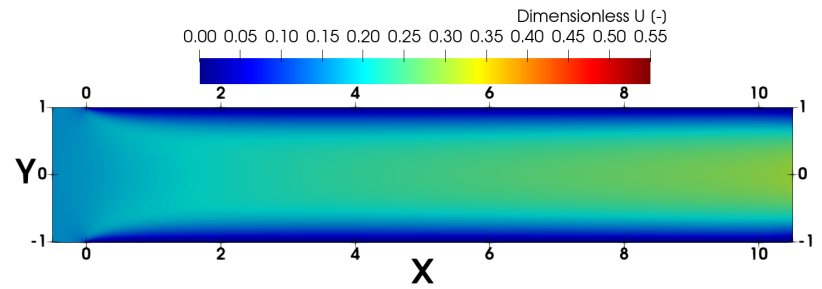
(b) *Case B.*
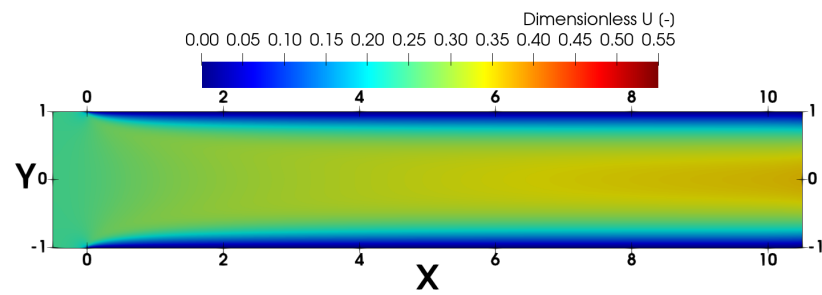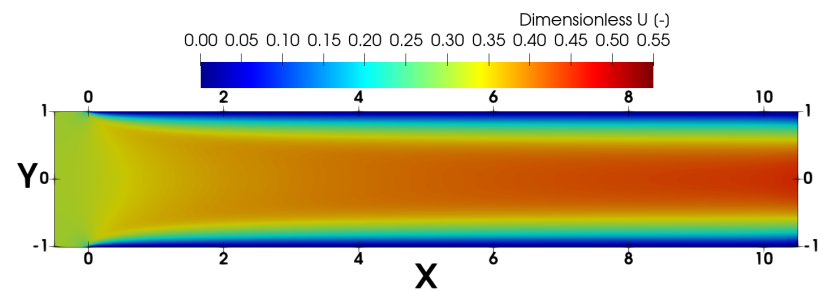
(c) *Case C.*

(d) *Case D.*
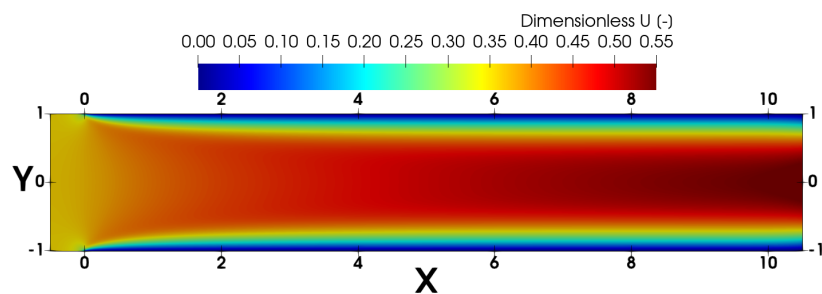
(e) *Case E.*

Figure 6.28: Channel Navier-Stokes test case: fixed value of electrical conductivity.

(a) $x = 80$.

(b) $x = 85$.

(c) $x = 90$.

(d) $x = 95$.

(e) $x = 100$.

(f) $x = 105$.
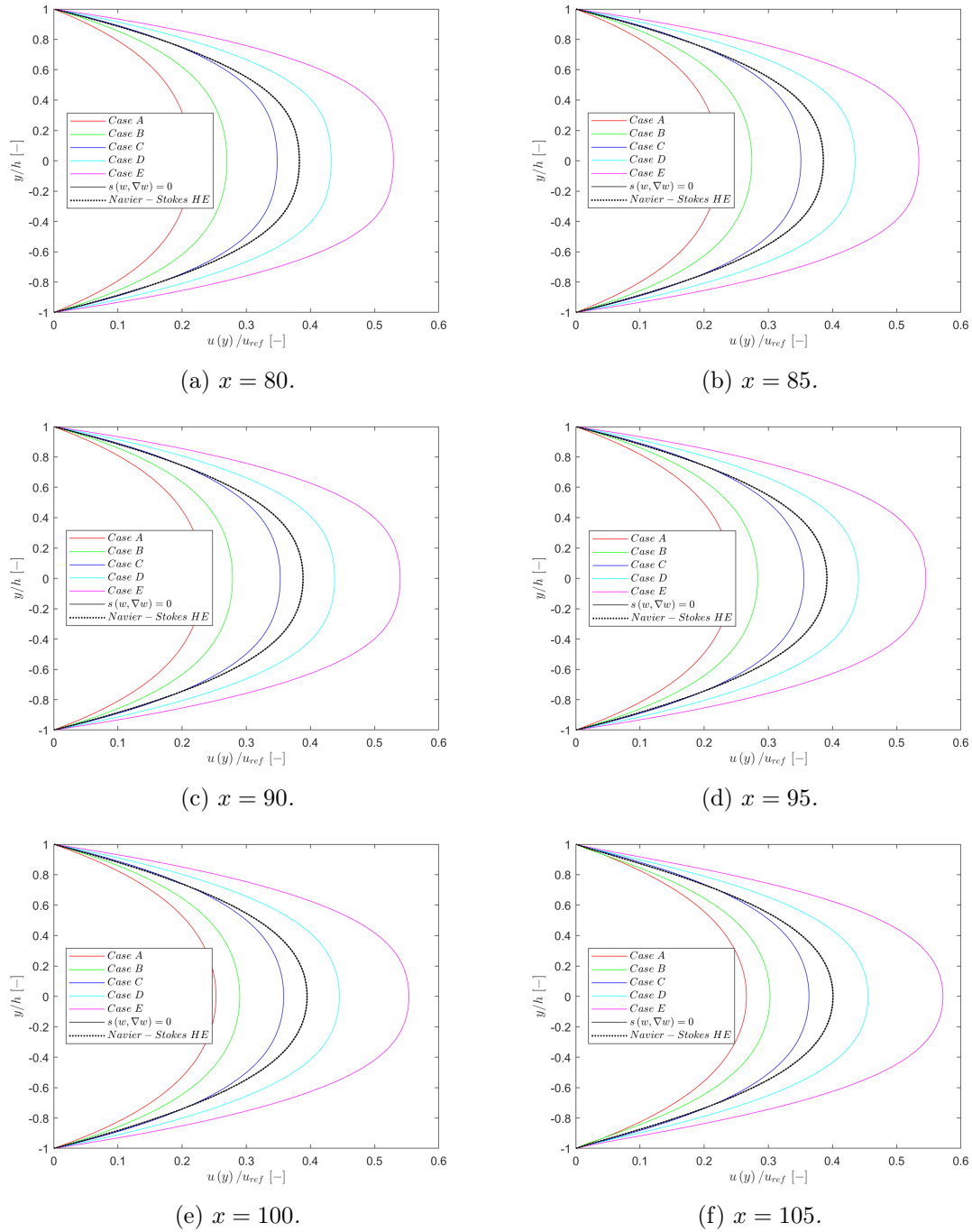
Figure 6.29: Channel Navier-Stokes test case: comparison of the velocity profiles, fixed electrical conductivity.

(a) $x = 80$.

(b) $x = 85$.

(c) $x = 90$.

(d) $x = 95$.

(e) $x = 100$.

(f) $x = 105$.
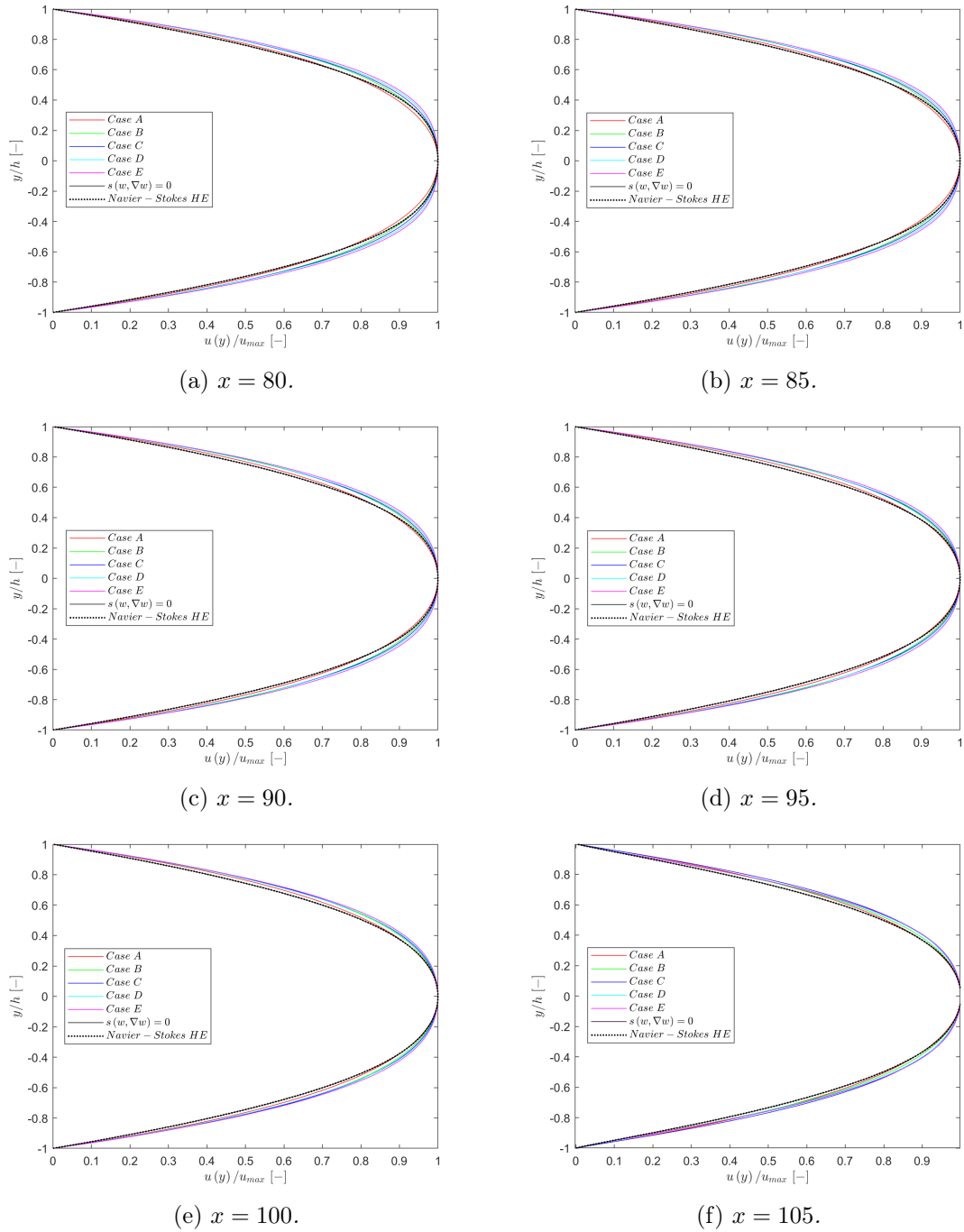
Figure 6.30: Channel Navier-Stokes test case: comparison of the dimensionless velocity profiles, fixed electrical conductivity.

6.2.6   Navier-Stokes testing: computation σ_e

In this section, a more accurate and real solution of what has been reported in the previous section is presented. We are going to consider in the code the development presented in the previous Chapter, where, based on the Devesse's idea [20], we link the transport properties between the High-Order Unifying Framework and the Mutation++ library. Hence, the computational cost will be, obviously, higher than the previous simulations. The same mixture is considered, i.e. air with 11 species with the same thermodynamic database. The temperature of the mixture is fixed, again, at $T = 3250\ K$. In additon, the Mach value is Ma = 0.2. The reference length is $L = 1$, while the initial ratio of specific heat is fixed to $\gamma = 1.4$. We use the same initial mesh of the previous case, i.e. $n_e = 136$. On the same concept, we prescibed the same boundary conditions. The number of the iterations is always fixed at 15, with the same step 1.2. The computation for each iteration has been automatically stopped when the residuals will reach the threshold equal to 10^{-8}. The Magnetic Reynolds number is Re$_m$ = 0.001, while the Magnetic force number is S = 100, like the Reynolds number Re = 100. We imposed an external magnetic field $\mathbf{B} = (0, B_y, 0)^T$, with $B_y = 2$. The electric field is assumed on the z direction, i.e. $\mathbf{E} = (0, 0, E_z)^T$ and different values of the external electric fields are present in table 6.5. Figures 6.32, 6.33, 6.34 and 6.35 show the Paraview post-processing for the velocity, the electrical conductivity , the temperature and the pressure, respectively. We can notice how the electrical conductivity does not remain constant along the channel, but it is decreasing. In the mean time, exactly the same happens for the pressure, while the behaviour of the temperature is opposite. Anyway, the value of the electrical conductivity is diminishing along the channel. Hence, the effects of the variations of the pressure are stronger than the temperature ones. In other words, the influence of the pressure is greater. In fact, the temperature is going to increase along the channel, as a consequence, we are expecting that the value of the electrical conductivity will increase. But, actually, we have just mentioned that it is decreasing as a consequence of the reduction of the pressure. In figures 6.36, 6.37 and 6.38 we can find the post-processing of the dimensionless velocity profiles for different stations along the channel. This is exactly what shown in the Paraview post-processing in figure 6.32. As already mentioned in the previous section, we understand that when the Lorentz forces are in the positive direction of the x axis the flow is accelerating, hence the velocity profiles are bigger than in the opposite case, i.e. when the flow is decelerating. The same concepts of the previous section must be applied to analyze these results. In addition, we can affirm that a more accurate relationship is present in the normalized velocity profiles. This is due to the fact that the electrical conductivity is computed, thus the solutions are physically significant. In the previous section this did not happen.

(a) $x = 80$.

(b) $x = 85$.

(c) $x = 90$.

(d) $x = 95$.

(e) $x = 100$.

(f) $x = 105$.
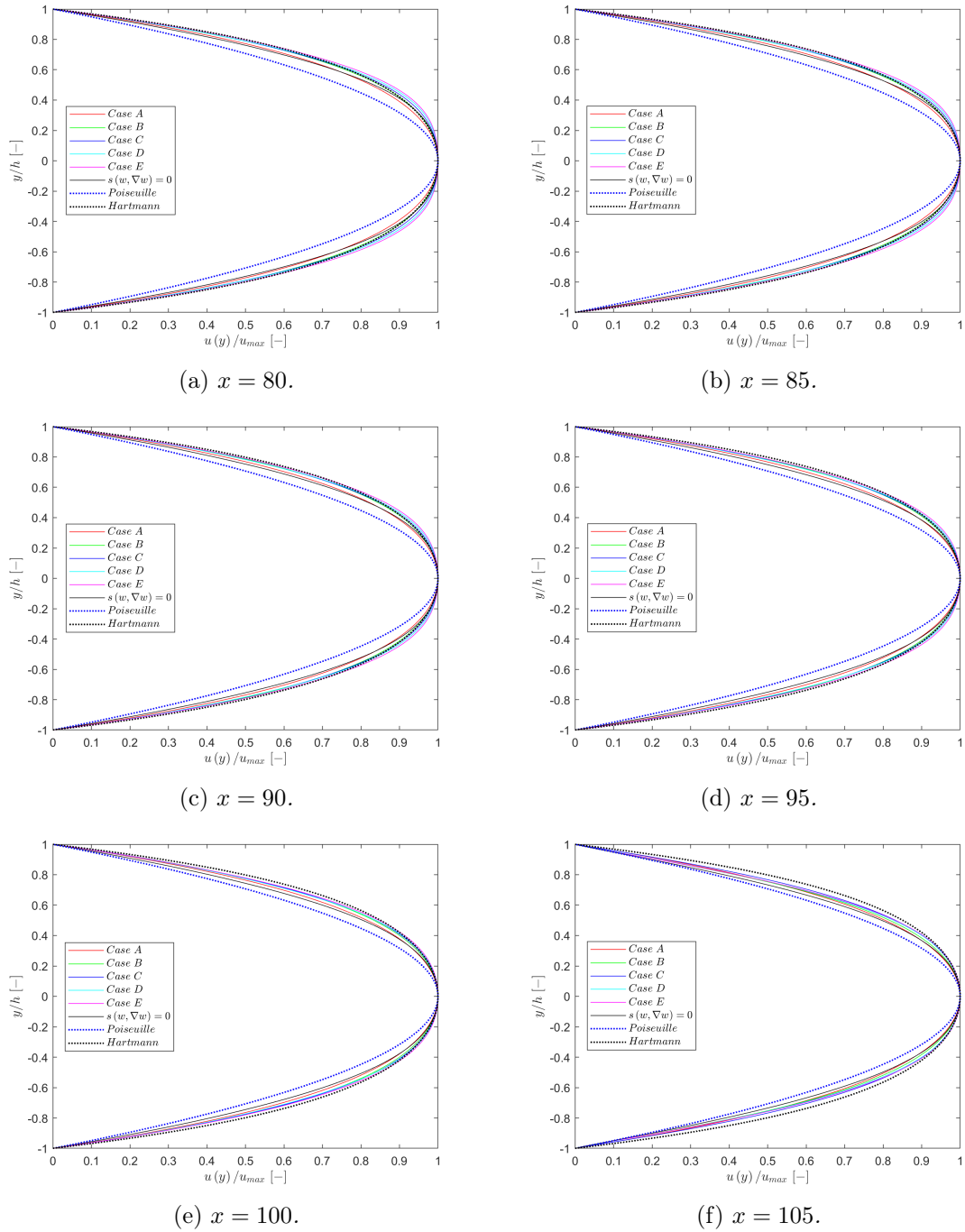
Figure 6.31: Channel Navier-Stokes test case: comparison of the dimensionless velocity profiles with Poiseuille and Hartmann solutions, fixed electrical conductivity.
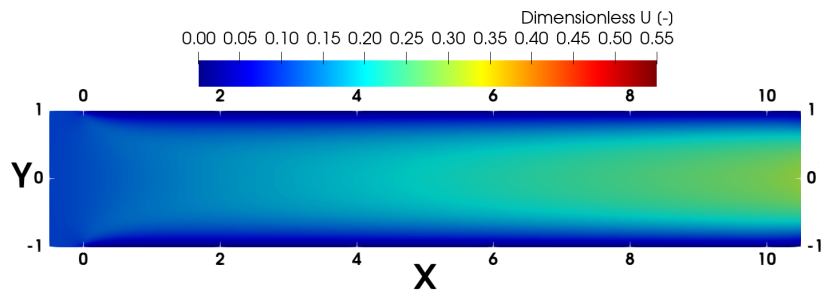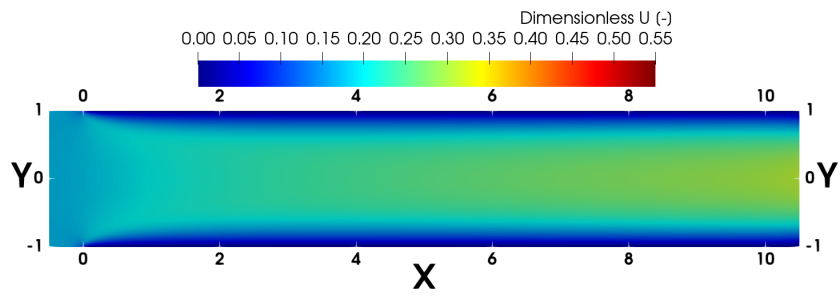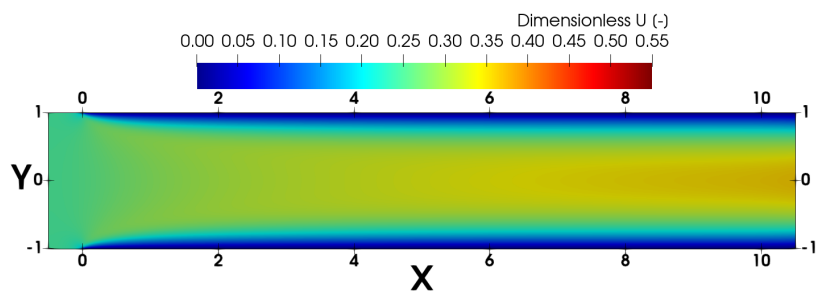
(a) *Case A.*
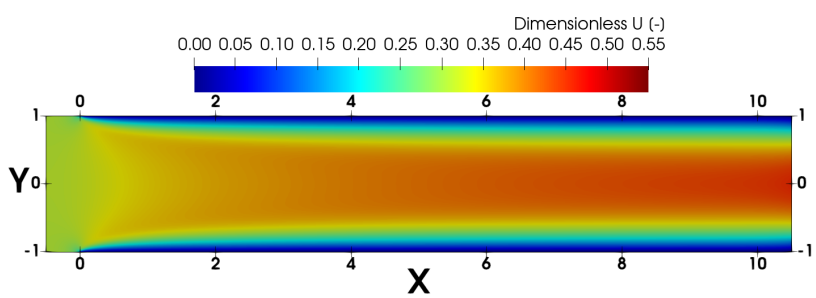
(b) *Case B.*
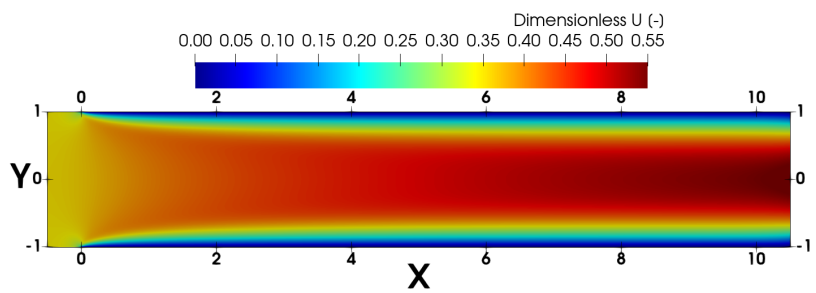
(c) *Case C.*

(d) *Case D.*

(e) *Case E.*

Figure 6.32: Channel Navier-Stokes test case: velocity, electrical conductivity computed.
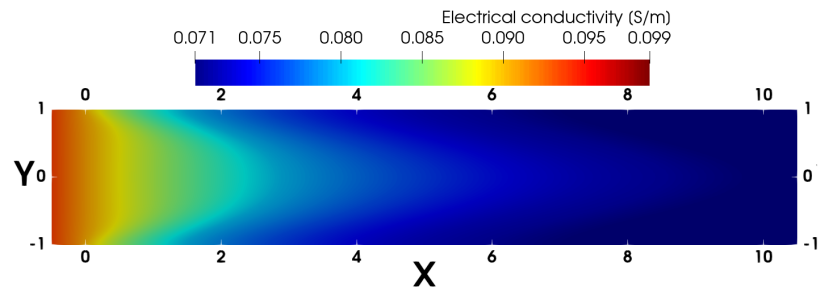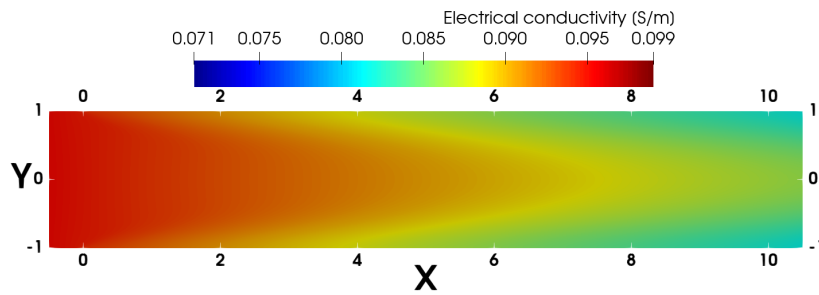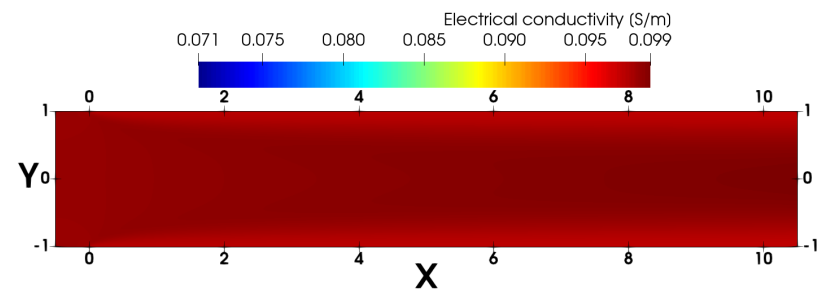
(a) *Case A.*
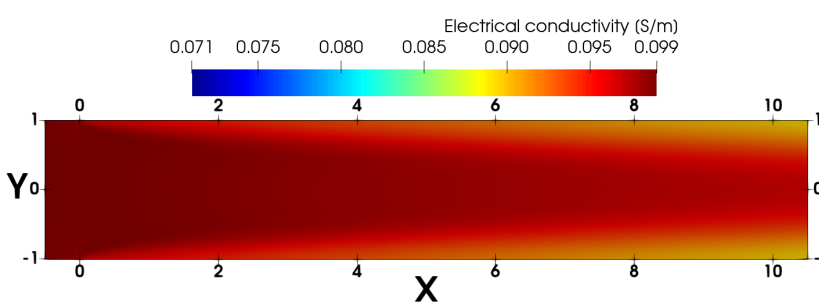
(b) *Case B.*
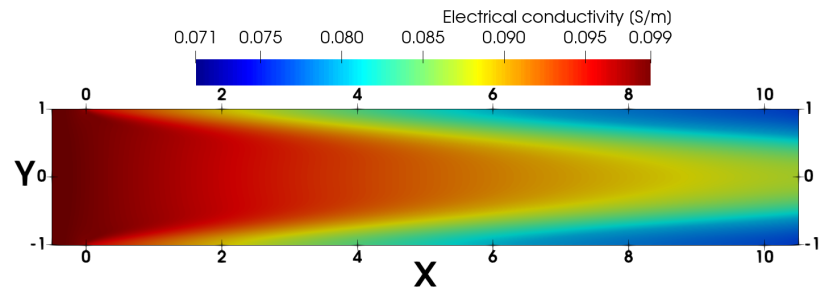
(c) *Case C.*

(d) *Case D.*

(e) *Case E.*

Figure 6.33: Channel Navier-Stokes test case: electrical conductivity computed.
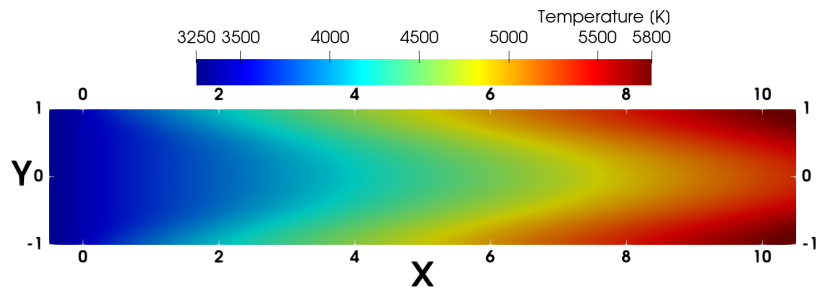
(a) *Case A.*
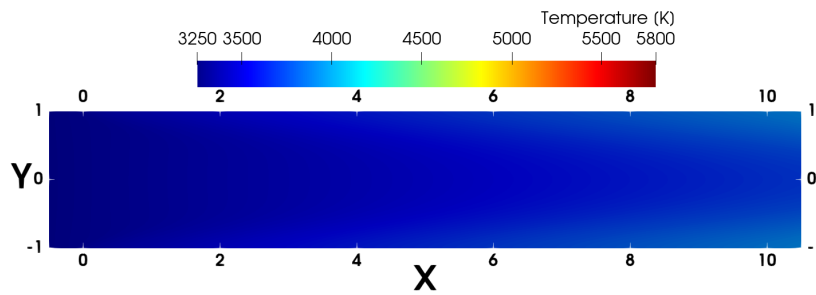
(b) *Case B.*
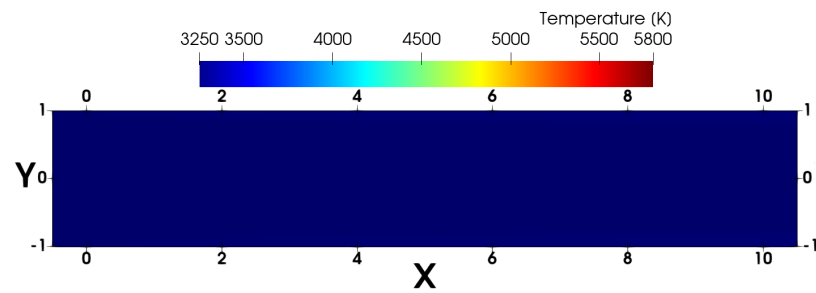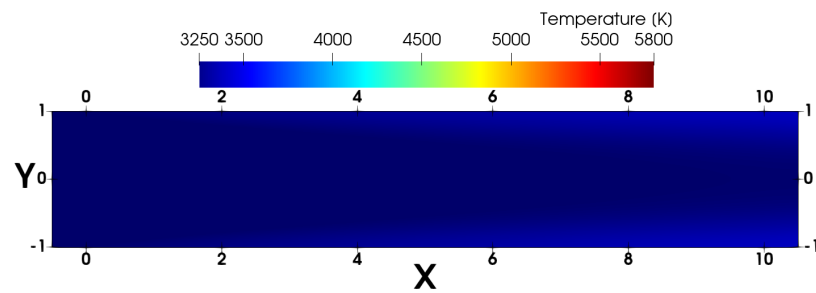
(c) *Case C.*

(d) *Case D.*
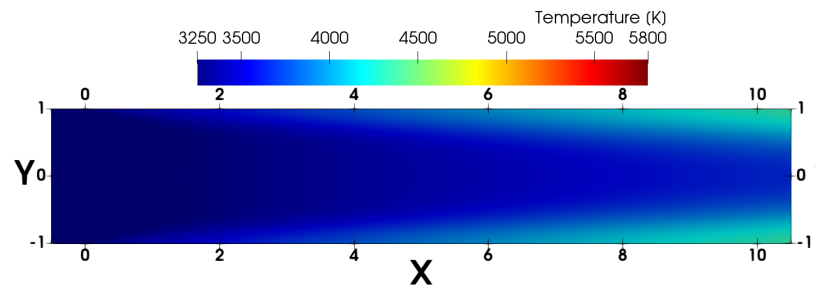
(e) *Case E.*

Figure 6.34: Channel Navier-Stokes test case: temperature, electrical conductivity computed.

(a) *Case A.*

(b) *Case B.*

(c) *Case C.*

(d) *Case D.*

(e) *Case E.*
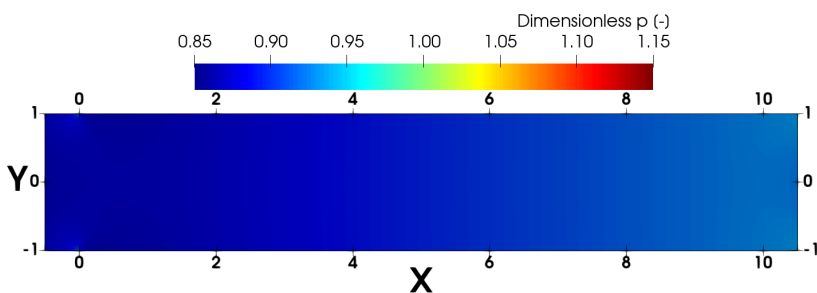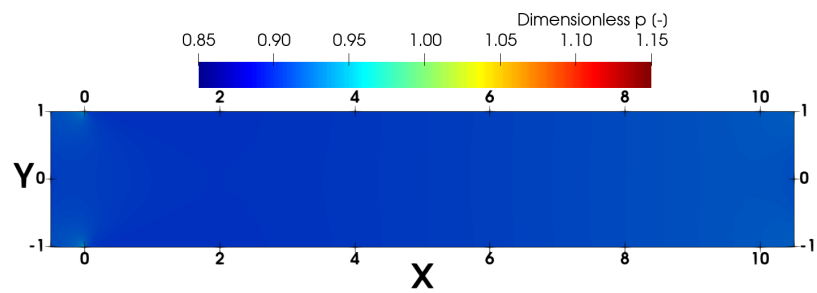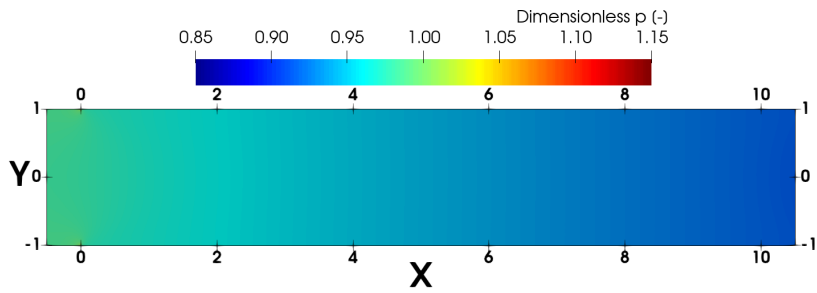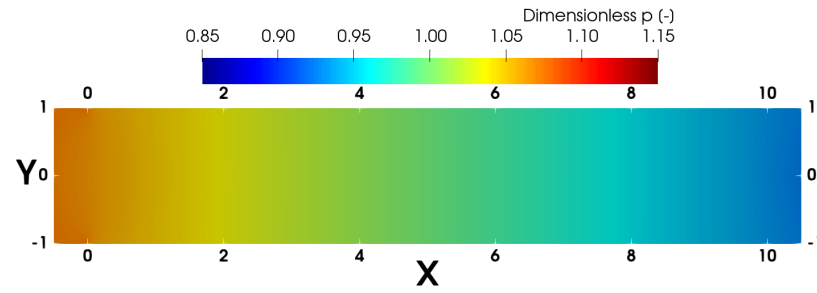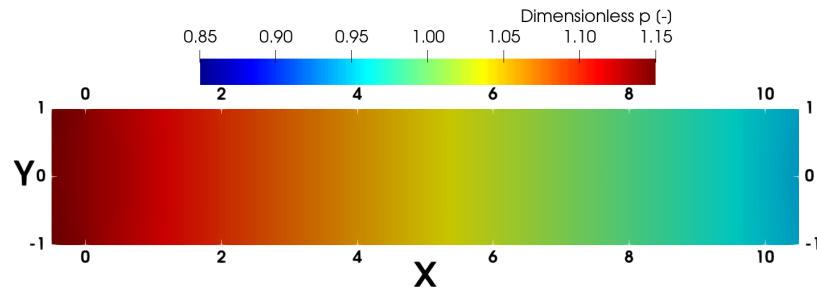
Figure 6.35: Channel Navier-Stokes test case: pressure, electrical conductivity computed.

(a) $x = 80$.

(b) $x = 85$.

(c) $x = 90$.

(d) $x = 95$.

(e) $x = 100$.

(f) $x = 105$.
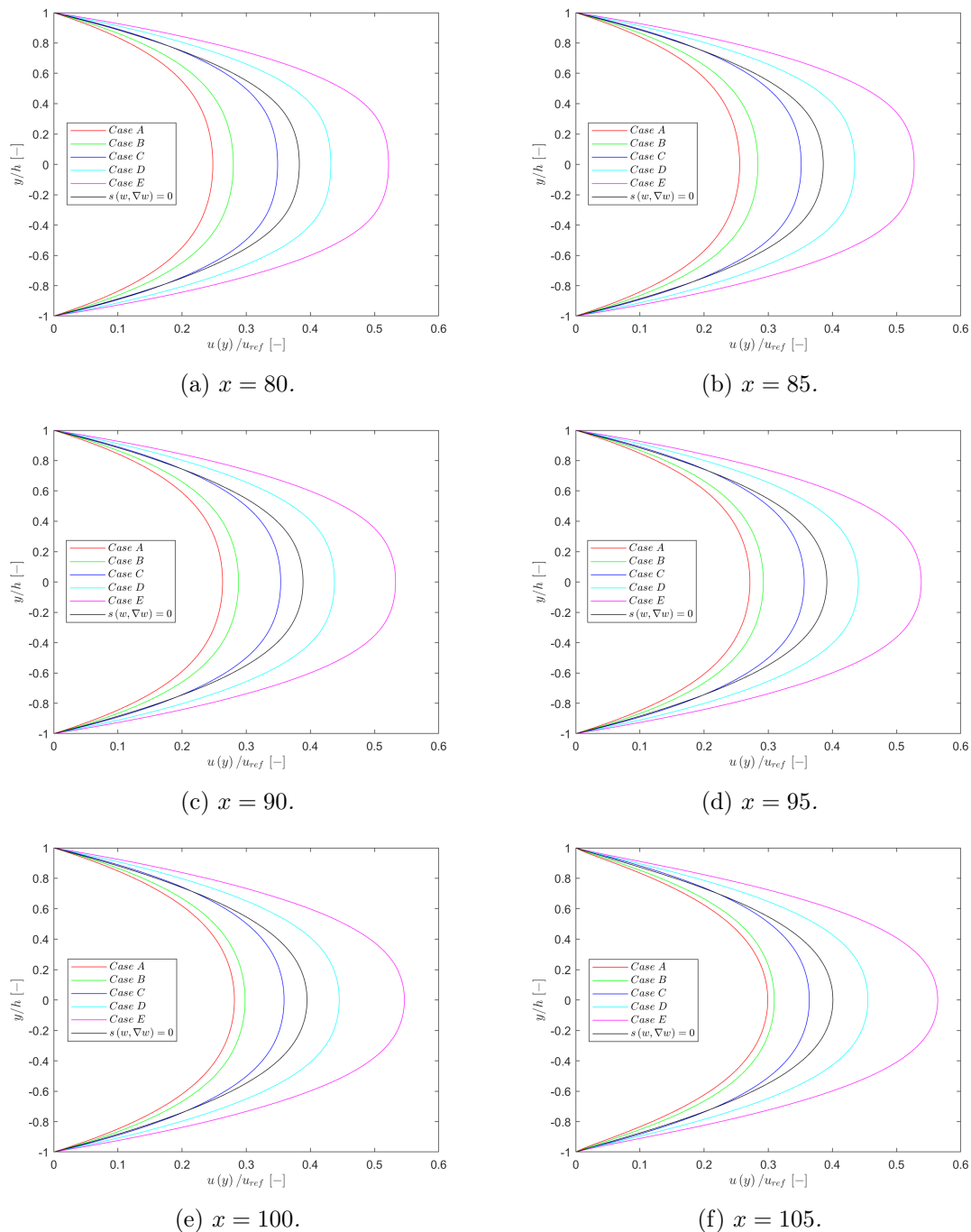
Figure 6.36: Channel Navier-Stokes test case: comparison of the velocity profiles, electrical conductivity computed.

(a) $x = 80$.

(b) $x = 85$.

(c) $x = 90$.
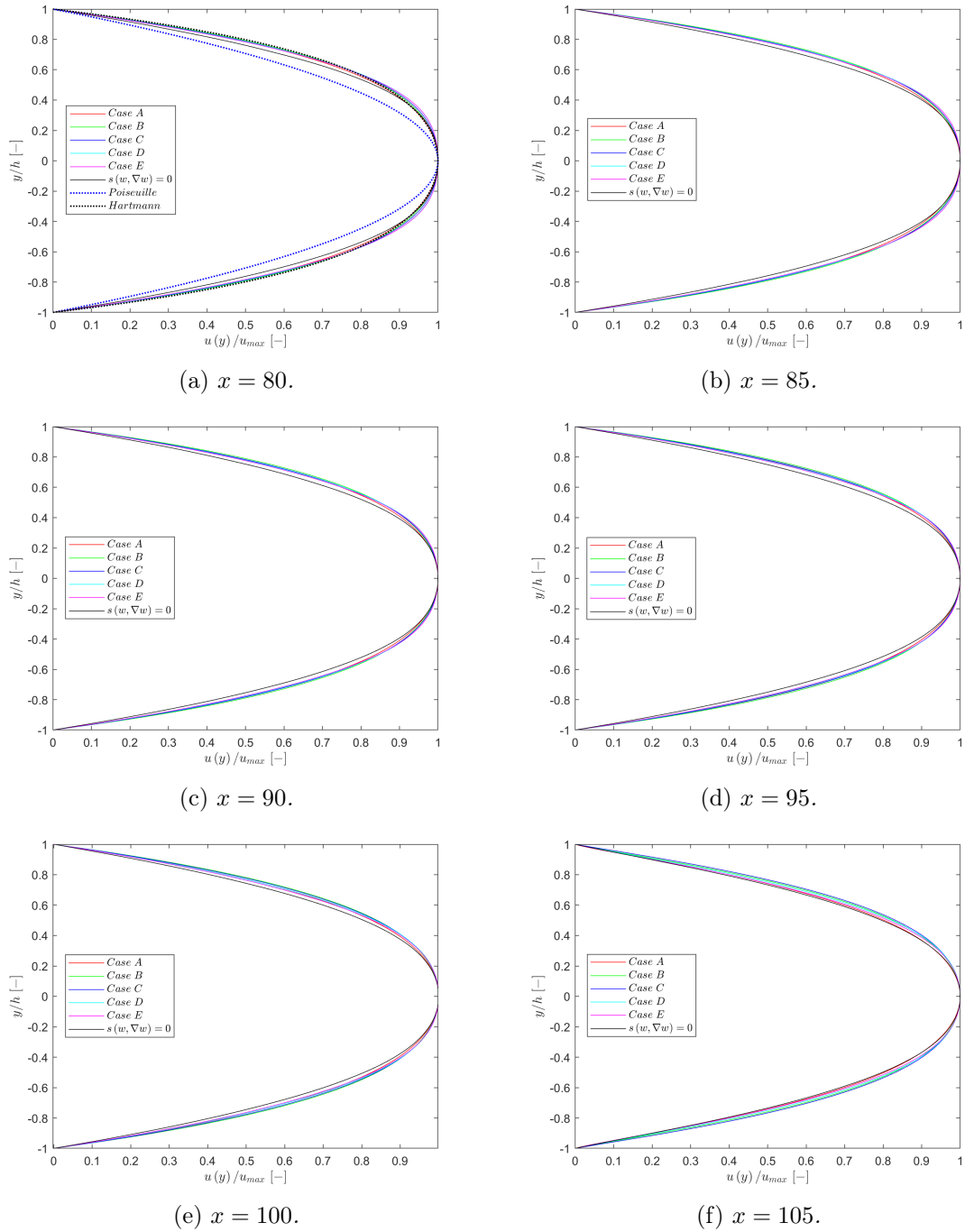
(d) $x = 95$.

(e) $x = 100$.

(f) $x = 105$.

Figure 6.37: Channel Navier-Stokes test case: comparison of the dimensionless velocity profiles, electrical conductivity computed.
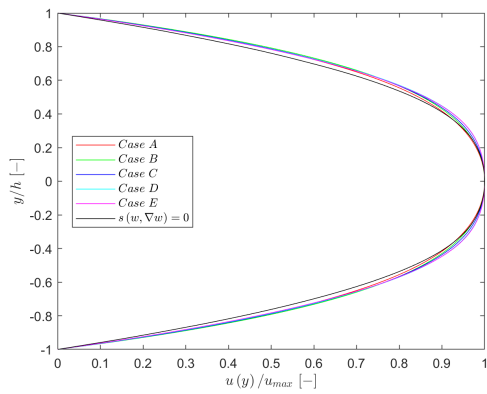
(a) $x = 80$.
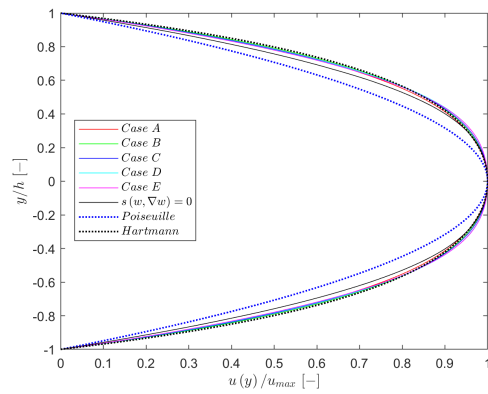
(b) $x = 85$.
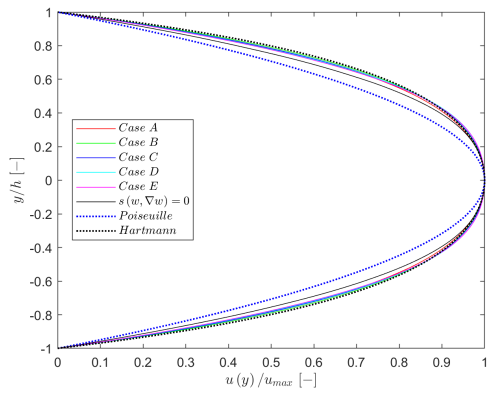
(c) $x = 90$.
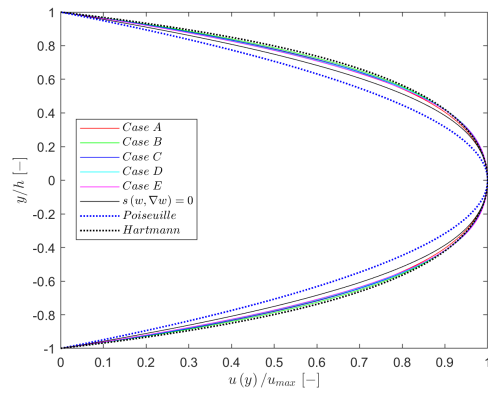
(d) $x = 95$.
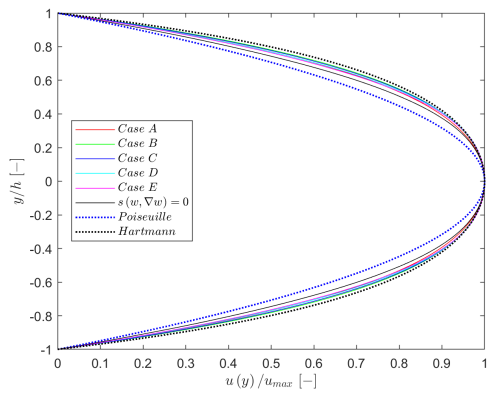
(e) $x = 100$.
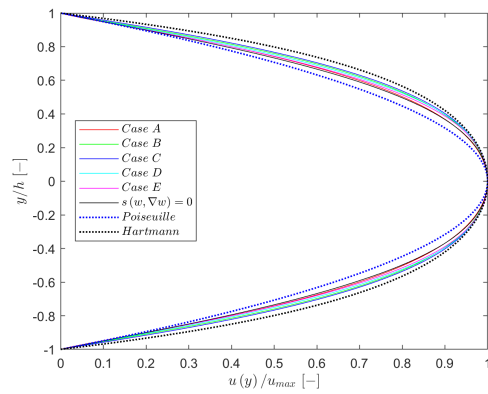
(f) $x = 105$.

Figure 6.38: Channel Navier-Stokes test case: comparison of the dimensionless velocity profiles with Poiseuille and Hartmann solutions, electrical conductivity computed. Hartmann number has been fixed to 3, the exact value of the simulations. Note the perfect deal between numerical and analytical data for $x \leq 95^+$, thus when the effects of the outfow are not present.

6.3 Summary

In this Chapter the validation procedure has been shown. Starting from the Euler implementation, three different supersonic test cases have been conducted: channel, shock, and expansion. Then, we have switched to testing the Navier-Stokes implementation. In this context, two different laminar and subsonic test cases were studied. In the first one, we have fixed the typical value of the electrical conductivity for the corresponding temperature of the mixture, in the second one, following the ideas presented in the previous Chapter, the electrical conductivity has been computed by the code for each triangular element of the mesh. Hence, different values of the electrical conductivity for distinct positions along the channel are reported in the post-processing. This is correlated to the evolution of the pressure and the temperature along the channel. Finally, for the Navier-Stokes cases, the normalized velocity profiles were compared to the analytical solution provided by Hartmann. Perfect deal is present when no effect of the outflow boundary condition is present. Thus, the model can be considered valid. It is also important to notice that, exactly as in the classical Navier-Stokes simulations, no variations of the pressure along the perpendicular direction to the wall is present. However, it is important to notice form figures 6.39 and 6.40 that the global time for the two types of Navier-Stokes simulations is lower when the code computes also the electrical conductivity. This is due to the fact that the solution is more physical. Anyway, when the flow is subsonic, no huge variations in the total time for the classical Navier-Stokes high-enthalpy are present with respect to the model that we have implemented by imposing null electric and magnetic fields. The opposite happens in the supersonic regime, where, as shown in figures 6.4, 6.10 and 6.17 the time for the computation of the solution with null electric and magnetic fields is the biggest. All the other times are between the two extreme conditions (Navier-Stokes high-enthalpy and Navier-Stokes with null electric and magnetic fields).
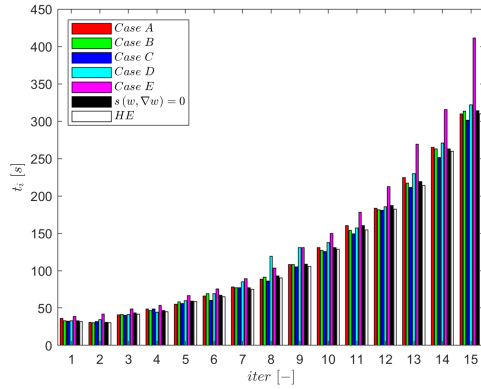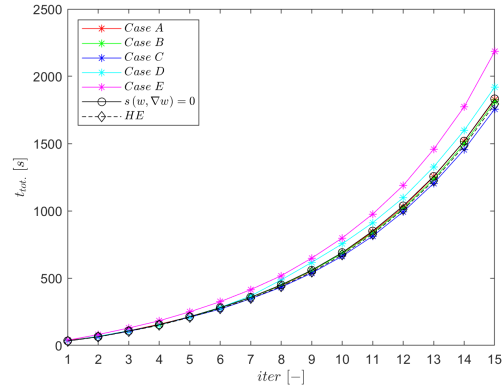
(a) *Time of each iteration.*   (b) *Total time.*

Figure 6.39: Channel Navier-Stokes test case: time of the simulations, electrical conductivity fixed.
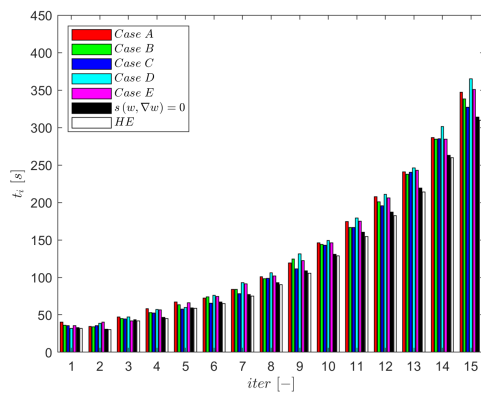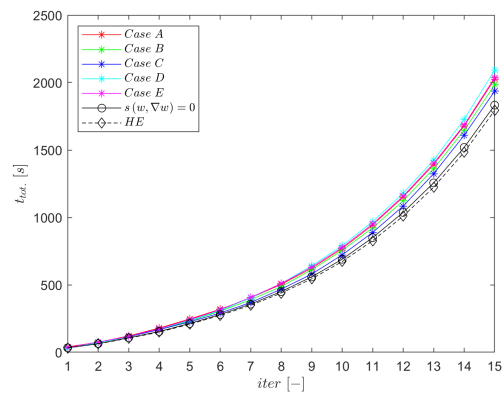
(a) *Time of each iteration.*   (b) *Total time.*

Figure 6.40: Channel Navier-Stokes test case: time of the simulations, electrical conductivity computed.

Chapter 7

Conclusions

In this Master's Thesis work we implemented a new Magneto-Fluid Dynamics model for low Magnetic Reynolds number regime in the High-Order Unifying Framework [59]. In this Chapter, we are going to summarize the main steps and results.

7.1 General review

The project has been conducted following the classical approach to develop and study a problem from a numerical point of view. The flow chart has been shown in Chapter 1.

In the first phase of the project, we studied the modeling part of electrically conducting flows and ionized gas mixtures. We perturbed the BTE equation and we found the different contributions of electrons and heavy particles to the transport properties. No contribution of electrons is present in the balance law of the momentum. They appear in the momentum equation only with the term related to the Lorentz force. The Chapman-Eskong methods gave us the possibility to obtain the Euler and the Navier-Stokes equations. Then, the classical conservation law has been obtained. In Chapter 3, a wide-ranging discussion about the governing equations of the Magneto-Fluid Dynamics has been presented. We analyzed the Navier-Stokes and the Maxwell equations separately, then, we brought them all together to obtain the full MFD system. At this point, as a consequence of the stiffness due to the high disparity between the propagation velocities of the signals of the two systems, the *MHD approximation* has been introduced. Hence, the simplified version of the MFD system has been shown. Then, two limiting cases were presented, both based on the Magnetic Reynolds number. The dimensional analysis of the induced magnetic field equation has shown that, for a low Magnetic Reynolds number regime, the magnetic field can be considered as rigid, i.e. externally applied and no presence of inducted contribution. In this context, with the assumption of chemically non-reacting flows under the low Damkoler number regime (frozen flow), the equations of the models have been presented. Subsequently, we have introduced the high-order methods and the HDG solver [59]. At the end of Chapter 5, the implementation of the model has been presented. To take into account the effects of the third component of the cross product present in the Lorentz force, a new routine in the `EvalSource` function has been created such that it does not consider the dimension of the problem, but it computes all the terms of the cross product, and only at the end, it checks the real dimension of the problem to take into account the needs components of the vector. The same has been implemented for the Joule heating.

Finally, the validation is presented. We started from the Euler model to evaluate the correct implementation of the source terms. We used three different test cases: channel, shock, and expansion. All supersonic. For the last two also the adaptation procedure has been presented. Then, we switched to the Navier-Stokes implementation. We tested it with a laminar, incompressible high-temperature flow inside a channel. Comparison with the an-

alytical solution provided by Hartmann is presented [39]. We have made two different tests on the same geometry. The first one when we imposed the typical value of the electrical conductivity for that temperature of the ionized gas mixture. Then, we have computed also the solution for the real case, when, due to the effects of variations in temperature and pressure along the channel, the electrical conductivity's value changes for each triangular element of the mesh. The velocity profiles computed have been compared with the analytical solution provided by Hartmann and computed with the same Hartmann number of the simulation. We can notice that, when the outflow boundary conditions does not affect the solution, the normalized velocity profiles are exactly computed by the code, even though we used small computational resources. This also shows the high-order capabilities of the HDG solver used in this project. To obtain more accurate results also in the region near the outflow, new boundary conditions should be applied, e.g. periodic boundary conditions or the imposition of the outlet pressure. In this sense, no effects regarding the numerical computational of variables on the edges of the computational domain will be present. However, this needs to be checked, but it is the most probable explanation for this type of problem. Anyway, the implemented model provides good and physical results. Possible experimental validations could be checked again for the correct implementation. Figure 7.1 shows the main results. The model should provide good results in the VKI Plasmatron 7.2 in the region near the object tested. In this region, under the condition of cartesian flow, the presence of the induced magnetic field could be though negligible, hence the magnetic field can be considered rigid and the low Magnetic Reynolds number model could be work fine. However, this needs yet to be tested and could be considered as further work. Anyway, under the ambipolar assumption, the usage of this model is not useful. Indeed, for the ambipolar assumption, the density current is negligible, hence no Lorentz force and Joule heating will be taken into account. The model with the only high-enthalpy effects will provide us good numerical results with lower global time for the simulation than the Magneto-Fluid Dyanmics version with null electric and magentic fields.

(a) $x = 85$.   (b) $x = 90$.
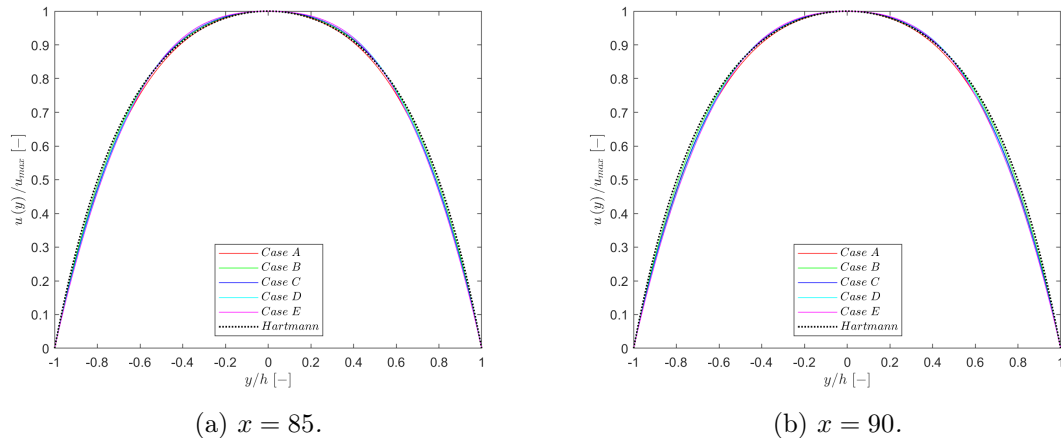
Figure 7.1: Final results for the normalized velocity profiles, and comparison with the analytical Hartmann solution for Ha ~ 3.16.

7.2   Future implementantions

Starting from this point, many works could be done in the future. For instance, the first one can be the implementation of appropriate boundary conditions for the electromagnetic source term. Indeed, in this version of the code, the externally applied electric and magnetic fields are considered all over the computational domain. We can think about

considering them applied only in a specific point. In this sense, the variations of the solutions will be local. To implement them, the suggestion is to start from the cartesian version of the code. In these terms, in parallel, future works could be also related to the implementation of the axisymmetric version of the code. This could provide more accurate results for the Plasmatron 7.2. Again, like in this project, the suggestion is to start from the axisymmetric version with the only imposition of externally applied electric and magnetic fields. Then, the possibility to extend the previously mentioned future work for the cartesian version of the code to the axisymmetric version can be also applied. In addition, the code needs improvements in the parallelized concept. Possible works could be regarding the possibility to extend the Mach number range of the simulation. In this sense, with very high-temperature effects, other further implementations are linked with the possibility to evaluate the transport property from an anisotropic point of view. The same idea, when external electromagnetic fields will be applied, can be extended to the electrical conductivity. This physical model concerning the possibility to insert external electric and magnetic fields can be also applied to the other already existing models: multi-species, turbulence, etc... Regarding the last, a new study can be done analyzing the effects of externally applied magnetic and/or electric fields in turbulence regimes. The previous studies with the backward-facing step show that its effects are to reduce the recirculation zone behind the step with the increase of the Hartmann number.

Finally, of course, the implementation of the model for high Magnetic Reynolds number is also a possible future work. In this context, the adding of a vectorial equation will modify all the eigenvalues and eigenvectors of the Jacobians, hence also the boundary conditions need to be computed again in the proper way.

The numerical work illustrated in this Paper provides many topics for further research to be explored by the future studies.
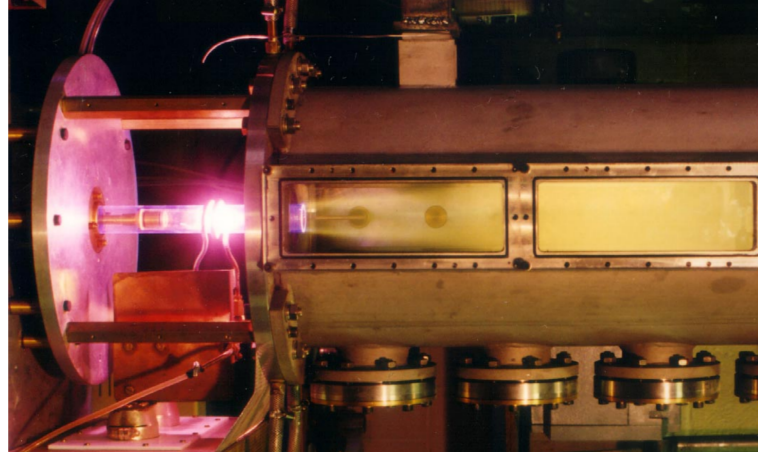
Figure 7.2: VKI Plasmatron. The picture was taken from [54].

Appendix A

MFD template

The simplified Magneto-Fluid Dynamic template implemented in the High-Order Unifying Framework [59] is here shown. All the functions that the model needs are written, the implementation is not shown. In the next Appendix, only the code for the source terms is exhibited.

We remind that the model for low Magnetic Reynolds number is composed, in the dimensionless form, as follows

$$\tilde{\nabla} \cdot (\tilde{\rho}\tilde{\mathbf{u}}) = 0$$

$$\tilde{\nabla} \cdot (\tilde{\rho}\tilde{\mathbf{u}} \otimes \tilde{\mathbf{u}} + \tilde{p}\underline{\mathbf{I}}) - \frac{\sqrt{\gamma}\,\mathrm{Ma}}{\mathrm{Re}}\tilde{\nabla} \cdot \underline{\tilde{\boldsymbol{\tau}}} = \sqrt{\gamma}\,\mathrm{Ma}\,\mathrm{S}\,\mathrm{Re}_m\,\left(\tilde{\rho}_c\tilde{\mathbf{E}}_{appl.} + \tilde{\mathbf{j}} \times \tilde{\mathbf{B}}_{appl.}\right)$$

$$\tilde{\nabla} \cdot \left(\tilde{\rho}\tilde{H}\tilde{\mathbf{u}}\right) - \frac{\sqrt{\gamma}\,\mathrm{Ma}}{\mathrm{Re}}\tilde{\nabla} \cdot \left(\underline{\tilde{\boldsymbol{\tau}}}\tilde{\mathbf{u}} - \frac{\gamma}{(\gamma-1)\,\mathrm{Pr}}\tilde{\mathbf{q}}\right) = \sqrt{\gamma}\,\mathrm{Ma}\,\mathrm{S}\,\mathrm{Re}_m\,\left(\tilde{\mathbf{j}} \cdot \tilde{\mathbf{E}}_{appl.}\right)$$

$$(\mathrm{A.1})$$

```cpp
#ifndef NAVIERSTOKESHEEB_H
#define NAVIERSTOKESHEEB_H

#include "../dummymodel.h"
#include "../ThermodynamicsEB/MutationAir11EB_NS.h"

template <int D, int COMP=D+2, class THERM = MutationAir11EB_NS<D,COMP>>
class CompressibleNavierStokesHEEB : virtual public DummyModel<D, COMP> {

public:

  // CHARACTERIZATION OF THE MODEL
  static const int  Components = COMP;
  static const bool Convection = true;
  static const bool Diffusion  = true;
  static const bool Source     = true;

  static const InitType inittype = IT_Constant;

  static const int NumDerVar        = x;
  static const int NumBdryCoeffs     = x;
  static const int NumBdryFluxWeight = 1;
  static const int NumVolFunctionals = 0;

  // USER-DEFINED PARAMETERS
  static double mach;
  static Vec<D-1> angle;
  static double chord;
  static double reynolds;
  static double reynolds_m;
  static double S_force_m;
  static double stab_visc;

  // GAS PARAMETERS (values from THERM)
  static double gamma_infty;
  static double p_infty;
  static double rho_infty;

  // DEPENDENT VARIABLES
  static Vec<D> v_infty;
  static double E_infty;
  static double c_infty;
  static double C_infty;
  static double H_infty;
  static double cvTtot;
  static double ptot;
  static Vec<COMP> w_infty;
  static double amu;
  static double amusource;
```

```cpp
// DECLARATION OF FUNCTION THAT THE MODEL NEEDS

// Setting the output string
static void GetFilename(stringstream & oss);

static void GetDerVarName(int dervar, string & name);




// Computing the initial conditions
template <typename SCAL>
static void EvalInitial(SpatialParams<D> & sparam,
                        Vec<COMP, SCAL> & res);




// Computing the primitive variables
template <typename SCAL>
static void EvalPrim(Vec<COMP, SCAL> & state,
                     Vec<D, SCAL> & U,
                     SCAL & p,
                     SCAL & T);

template <typename SCAL>
static int GetConstrConsVar(int i);

template <typename SCAL>
static SCAL EvalConstrPrimVar(int i, Vec<COMP, SCAL> & state,
                              SpatialParams<D> & sparam);




// Computing of the derived variables
template <typename SCAL>
static void EvalDerVar(Vec<COMP, SCAL> & state,
                       SpatialParams<D> & sparam,
                       Vec<NumDerVar, SCAL> & dervar);




// Computing convective fluxes
template <typename SCAL>
static void EvalConvFlux(Vec<COMP, SCAL> & state,
                         SpatialParams<D> & sparam,
                         Mat<COMP, D, SCAL> & res);

template <typename SCAL>
static void EvalMaxEigenvalue(Vec<COMP, SCAL> & state,
                              SpatialParams<D> & sparam,
                              SCAL & res);
```

```cpp
template <typename SCAL>
static void EvalConvEigenSystem(Vec<COMP, SCAL> & state,
                                SpatialParams<D> & sparam,
                                double fix,
                                Vec<COMP, SCAL> & eig,
                                Mat<COMP, COMP, SCAL> & eigvr,
                                Mat<COMP, COMP, SCAL> & eigvl);



// Computing diffusive fluxes
template <typename SCAL>
static void EvalDiffVars(Vec<COMP, SCAL> & state,
                         Mat<COMP, D, SCAL> & grad,
                         Vec<D, SCAL> & U,
                         SCAL & p,
                         SCAL & T,
                         Mat<D, D, SCAL> & gradU,
                         Vec<D, SCAL> & gradp,
                         Vec<D, SCAL> & gradT,
                         SCAL & visc,
                         SCAL & cond);

template <typename SCAL>
static void EvalDiffFlux(Vec<COMP, SCAL> & state,
                         Mat<COMP, D, SCAL> & grad,
                         SpatialParams<D> & sparam,
                         Mat<COMP, D, SCAL> & res);

template <typename SCAL>
static void ApplyK(Vec<COMP, SCAL> & state,
                   Mat<COMP, D, SCAL> & grad,
                   Mat<COMP, D, SCAL> & rhs,
                   SpatialParams<D> & sparam,
                   Mat<COMP, D, SCAL> & res);

template <typename SCAL>
static Mat<D, D, SCAL> EvalStrainRate(Mat<D, D, SCAL> & gradU);



// Computing source terms
template <typename SCAL>
static void EvalSource(Vec<COMP, SCAL> & state,
                       Mat<COMP, D, SCAL> & grad,
                       SpatialParams<D> & sparam,
                       Vec<COMP, SCAL> & res);



// Computing boundary conditions and boundary state
```

```cpp
template <typename SCAL>
static void EvalFarfield(Vec<COMP, SCAL> & state,
                         SpatialParams<D> & sparam,
                         Vec<COMP, SCAL> & bcstate);


template <typename SCAL>
static void EvalSlipwall(Vec<COMP, SCAL> & state,
                         SpatialParams<D> & sparam,
                         Vec<COMP, SCAL> & bcstate);


template <typename SCAL>
static void EvalInflow(Vec<COMP, SCAL> & state,
                       SpatialParams<D> & sparam,
                       Vec<COMP, SCAL> & bcstate);


template <typename SCAL>
static void EvalOutflow(Vec<COMP, SCAL> & state,
                        SpatialParams<D> & sparam,
                        Vec<COMP, SCAL> & bcstate);


template <typename SCAL>
static void EvalNoslipwallAdiabatic(Vec<COMP, SCAL> & state,
                                    SpatialParams<D> & sparam,
                                    Vec<COMP, SCAL> & bcstate);


template <typename SCAL>
static void EvalNoslipwallIsothermal(Vec<COMP, SCAL> & state,
                                     SpatialParams<D> & sparam,
                                     Vec<COMP, SCAL> & bcstate);


template <typename SCAL>
static void EvalBdryState(int bcnr,
                          Vec<COMP, SCAL> & state,
                          SpatialParams<D> & sparam,
                          Vec<COMP, SCAL> & bcstate);


template <typename SCAL>
static void EvalBdryGradient(int bcnr,
                             Vec<COMP, SCAL> & state,
                             Mat<COMP, D, SCAL> & grad,
                             SpatialParams<D> & sparam,
                             Mat<COMP, D, SCAL> & bcgrad);


template <typename SCAL>
static void EvalBdryConvFlux(int bcnr,
                             Vec<COMP, SCAL> & state,
                             SpatialParams<D> & sparam,
                             Vec<COMP, SCAL> & res);


template <typename SCAL>
static void EvalBdryDiffFlux(int bcnr,
```

```
                            Vec<COMP, SCAL> & state,
                            Mat<COMP, D, SCAL> & grad,
                            SpatialParams<D> & sparam,
                            Vec<COMP, SCAL> & res);


  template <typename SCAL>
  static void EvalBdryCoefficients(int bcnr,
                              Vec<COMP, SCAL> & fcn,
                              Vec<COMP, SCAL> & fvn,
                              SpatialParams<D> & sparam,
                              Vec<NumBdryCoeffs, SCAL> & res);




  // Others
  static void EvalBdryFluxWeight(int bcnr,
                              SpatialParams<D> & sparam,
                              Mat<NumBdryFluxWeight, COMP> & res);


  template <typename SCAL>
  static void EvalVolFunctionals(Vec<COMP, SCAL> & state,
                              SpatialParams<D> & sparam,
                              Vec<NumVolFunctionals, SCAL> & res);


  static void LoadParameters(shared_ptr<PDE> apde);

};


// DEFAULT VALUES
...


// INCLUDE EXTERNAL FILE.h
#include "x.h"
```

Appendix B

Electromagnetic source terms

We remind that the source terms are made up as follows

$$\underline{\mathbf{s}}\left(\mathbf{w}, \nabla \mathbf{w}\right) = \begin{pmatrix} 0 \\ \rho_c \mathbf{E}_{appl.} + \mathbf{j} \times \mathbf{B}_{appl.} \\ \mathbf{j} \cdot \mathbf{E}_{appl.} \end{pmatrix} \qquad (B.1)$$

In addition, In Chapter 5 the flow chart has been already shown. Here the code based on that flow chart.

```cpp
template <int D, int COMP, class THERM>
template <typename SCAL>
void CompressibleNavierStokesHEEB<D, COMP, THERM>
::EvalSource(xxx) {

    SCAL rho      = state(0);
    Vec<D,SCAL> m = state.Rows(1,D+1);

    Vec<D,SCAL> U = 1. / rho * m;

    Vec<3,SCAL> J;
    Vec<D,SCAL> LorF;
    SCAL JHeat;

    THERM::EvalJ(state, U, J);
    THERM::EvalLorentzForce(state, J, LorF);
    THERM::EvalJouleHeating(state, J, JHeat);

    res = 0.;
    res.Rows(1,D+1) = LorF;
    res(D+1) = JHeat;

    for (int dd = 0; dd < COMP; ++dd){
        res(dd) *= amusource;
    }

  }
```

```
template <typename SCAL>
static void EvalJ(xxx) {

    SetMixtureState(state);
    SCAL RHOC;
    GetRHOC(state,RHOC);
    SCAL EC;
    GetEC(state, EC);

  if (D == 2){
  J(0) = (RHOC * U(0)) + (EC * (electric_field[0] + (U(1) * magnetic_field[2])));
  J(1) = (RHOC * U(1)) + (EC * (electric_field[1] - (U(0) * magnetic_field[2])));
  J(2) = (RHOC * U(2)) + (EC * (electric_field[2] + ((U(0) * magnetic_field[1]) - (U(1) * magnetic_field[0]))));
  } else if (D == 3){
  J(0) = (RHOC * U(0)) + (EC * (electric_field[0] + ((U(1) * magnetic_field[2]) - (U(2) * magnetic_field[1]))));
  J(1) = (RHOC * U(1)) + (EC * (electric_field[1] + ((U(2) * magnetic_field[0]) - (U(0) * magnetic_field[2]))));
  J(2) = (RHOC * U(2)) + (EC * (electric_field[2] + ((U(0) * magnetic_field[1]) - (U(1) * magnetic_field[0]))));
  }

  }
```

```
template <typename SCAL>
static void EvalLorentzForce(xxx) {

    SetMixtureState(state);
    SCAL RHOC;
    GetRHOC(state,RHOC);

  if (D == 2){
  LorF(0) = (RHOC * electric_field[0]) + ((J(1) * magnetic_field[2]) - (J(2) * magnetic_field[1]));
  LorF(1) = (RHOC * electric_field[0]) + ((J(2) * magnetic_field[0]) - (J(0) * magnetic_field[2]));
  } else if (D == 3){
  LorF(0) = (RHOC * electric_field[0]) + ((J(1) * magnetic_field[2]) - (J(2) * magnetic_field[1]));
  LorF(1) = (RHOC * electric_field[0]) + ((J(2) * magnetic_field[0]) - (J(0) * magnetic_field[2]));
  LorF(2) = (RHOC * electric_field[0]) + ((J(0) * magnetic_field[1]) - (J(1) * magnetic_field[0]));
  }

}


template <typename SCAL>
static void EvalJouleHeating(xxx) {

  JHeat = 0.0;
  for (int dd=0; dd<3; ++dd)
  JHeat += J(dd) * electric_field[dd];

}
```

Bibliography

[1] John D Anderson. *Modern compressible flow*. Tata McGraw-Hill Education, 2003.

[2] John D Anderson Jr. *Hypersonic and high-temperature gas dynamics*. American Institute of Aeronautics and Astronautics, 2006.

[3] Chay WC Atkins and Ralf Deiterding. Simulations of flow in thermochemical nonequilibrium using adaptive mesh refinement. 2019.

[4] Aravind Balan, Michael Woopen, and Georg May. Adjoint-based hp-adaptation for a class of high-order hybridized finite element schemes for compressible flows. In *21st AIAA Computational Fluid Dynamics Conference*, page 2938, 2013.

[5] Satish Balay, Shrirang Abhyankar, Mark F Adams, Jed Brown, Peter Brune, Kris Buschelman, Lisandro Dalcin, Alp Dener, Victor Eijkhout, W Gropp, et al. Petsc users manual revision 3.13. 2020.

[6] Francesco Battista. Magneto-fluid-dynamic methods for hypersonic aerothermodynamic and space propulsion applications. 2009.

[7] Francesco Battista, Tommaso Misuri, and Mariano Andrenucci. A magneto-fluid-dynamic model and computational solving methodologies for aerospace applications. *Fluid Dynamics, Computational Modeling and Applications*, page 121, 2012.

[8] Graham Candler, Dimitri Mavriplis, and Loretta Trevino. Current status and future prospects for the numerical simulation of hypersonic flows. In *47th AIAA Aerospace Sciences Meeting Including the New Horizons Forum and Aerospace Exposition*, page 153, 2009.

[9] Eric Ching, Yu Lv, and Matthias Ihme. Discontinuous galerkin method for predicting heat transfer in hypersonic environments. *Bulletin of the American Physical Society*, 61, 2016.

[10] Eric Ching, Yu Lv, and Matthias Ihme. Lagrangian particle tracking in a discontinuous galerkin method for hypersonic reentry flows in dusty environments. In *APS Division of Fluid Dynamics Meeting Abstracts*, pages A32–008, 2017.

[11] Eric J Ching and Matthias Ihme. Development of a particle collision algorithm for discontinuous galerkin simulations of compressible multiphase flows. *Journal of Computational Physics*, 436:110319, 2021.

[12] Eric J Ching, Yu Lv, Peter Gnoffo, Michael Barnhardt, and Matthias Ihme. Shock capturing for discontinuous galerkin methods with application to predicting heat transfer in hypersonic flows. *Journal of Computational Physics*, 376:54–75, 2019.

[13] C Ciucă, Pablo Fernandez, ALEXANDRA Christophe, Ngoc Cuong Nguyen, and Jaime Peraire. Implicit hybridized discontinuous galerkin methods for compressible magnetohydrodynamics. *Journal of Computational Physics: X*, 5:100042, 2020.

[14] Bernardo Cockburn, George E Karniadakis, and Chi-Wang Shu. The development of discontinuous galerkin methods. In *Discontinuous Galerkin Methods*, pages 3–50. Springer, 2000.

[15] Domenic D'Ambrosio. Coupling between electro-magnetics and fluid-dynamics: Physical and numerical aspects. *VKI Lecture Series 2004-01*.

[16] Domenic D'Ambrosio and Domenico Giordano. A numerical method for two-dimensional hypersonic fully coupled electromagnetic fluid dynamics. In *36th AIAA Plasmadynamics and Lasers Conference*, page 5374, 2005.

[17] Domenic D'Ambrosio and Domenico Giordano. Electromagnetic fluid dynamics for aerospace applications. *Journal of thermophysics and heat transfer*, 21(2):284–302, 2007.

[18] Domenic D'Ambrosio and Domenico Giordano. Two-dimensional numerical methods in electromagnetic hypersonics including fully coupled maxwell equations. In *39th Plasmadynamics and Lasers Conference*, page 4013, 2008.

[19] Domenic D'Ambrosio, Domenico Giordano, and Domenico Bruno. Fully coupled maxwell/navier-stokes simulation of electromagnetic hypersonics including accurate transport models. In *40th AIAA Plasmadynamics and Lasers Conference*, page 3910, 2009.

[20] Koen Devesse. Implementing a multi-species flow model in a hybridized discontinuos galerking framework. Master's thesis, The von Karman Institute for Fluid Dynamics, 2020.

[21] Catarina Garbacz, Marco Fossati, Walter Maier, Juan J Alonso, James Scoggins, Thierry Magin, and Thomas D Economon. Numerical study of shock interference patterns for gas flows with thermal nonequilibrium and finite-rate chemistry. In *AIAA Scitech 2020 Forum*, page 1805, 2020.

[22] Domenico Giordano. Hypersonic-flow governing equations with electrmagnetic fields. *VKI Lecture Series 2004-01*.

[23] Benjamin Graille, Thierry E Magin, and Marc Massot. Kinetic theory of plasmas: translational energy. *Mathematical Models and Methods in Applied Sciences*, 19(04):527–599, 2009.

[24] Ralf Hartmann and Paul Houston. Adaptive discontinuous galerkin finite element methods for the compressible euler equations. *Journal of Computational Physics*, 183(2):508–532, 2002.

[25] Frédéric Hecht. Bamg: bidimensional anisotropic mesh generator. *User Guide. INRIA, Rocquencourt*, 17, 1998.

[26] Frédéric Hecht, Olivier Pironneau, A Le Hyaric, and K Ohtsuka. Freefem++ manual, 2005.

[27] Scoggins J. *Development of numerical methods and study of coupled flow, radiation, and ablation phenomena for atmospheric entry*. Phd thesis, Université Paris-Saclay, 2017.

[28] Antony Jamenson. *Advanced Computational Fluid Dynamics*. Stanford University, CA, 2016.

[29] AF Kolesnikov. Technical report 1556. *Institute of Mechanics, Moscow State University, Moscow*, 1974.

[30] Yu Lv and Matthias Ihme. Discontinuous galerkin method for multicomponent chemically reacting flows and combustion. *Journal of Computational Physics*, 270:105–137, 2014.

[31] R MacCormack. Three dimensional magneto-fluid dynamics algorithm development. In *40th AIAA Aerospace Sciences Meeting & Exhibit*, page 197, 2002.

[32] Robert MacCormack. A computational method for magnetofluid dynamics. In *32nd AIAA Plasmadynamics and Lasers Conference*, page 2735, 2001.

[33] Robert MacCormack. Conservation form method for magnetofluid dynamics. In *39th Aerospace Sciences Meeting and Exhibit*, page 195, 2001.

[34] Robert W MacCormack. Numerical computation in magnetofluid dynamics. In *Computational Fluid Dynamics for the 21st Century*, pages 369–384. Springer, 2001.

[35] Thierry E Magin and Gérard Degrez. Transport algorithms for partially ionized and unmagnetized plasmas. *Journal of computational Physics*, 198(2):424–449, 2004.

[36] Thierry E Magin and Gérard Degrez. Transport properties of partially ionized and unmagnetized plasmas. *Physical review E*, 70(4):046412, 2004.

[37] Georg May. Hybridized discontinuos galerkin methods: formulation and discrete adjoint. 2015.

[38] Georg May. *Numerical methods for PDE*. 2018.

[39] M Mitchner and C H Kruger, Jr. Partially ionized gases.

[40] Ngoc Nguyen, Per-Olof Persson, and Jaime Peraire. Rans solutions using high order discontinuous galerkin methods. In *45th AIAA Aerospace Sciences Meeting and Exhibit*, page 914, 2007.

[41] Ngoc Cuong Nguyen, Jaume Peraire, and Bernardo Cockburn. An implicit high-order hybridizable discontinuous galerkin method for linear convection–diffusion equations. *Journal of Computational Physics*, 228(9):3232–3254, 2009.

[42] Ngoc Cuong Nguyen, Jaume Peraire, and Bernardo Cockburn. An implicit high-order hybridizable discontinuous galerkin method for nonlinear convection–diffusion equations. *Journal of Computational Physics*, 228(23):8841–8855, 2009.

[43] Ngoc Cuong Nguyen, Jaume Peraire, and Bernardo Cockburn. Hybridizable discontinuous galerkin methods. In *Spectral and High Order Methods for Partial Differential Equations*, pages 63–84. Springer, 2011.

[44] Ngoc Cuong Nguyen, Jaume Peraire, and Bernardo Cockburn. An implicit high-order hybridizable discontinuous galerkin method for the incompressible navier–stokes equations. *Journal of Computational Physics*, 230(4):1147–1170, 2011.

[45] Chul Park, Richard L Jaffe, and Harry Partridge. Chemical-kinetic parameters of hyperbolic earth entry. *Journal of Thermophysics and Heat transfer*, 15(1):76–90, 2001.

[46] Jaime Peraire, Ngoc Nguyen, and Bernardo Cockburn. A hybridizable discontinuous galerkin method for the compressible euler and navier-stokes equations. In *48th AIAA Aerospace Sciences meeting including the New Horizons forum and aerospace exposition*, page 363, 2010.

[47] Per-Olof Persson and Jaime Peraire. Sub-cell shock capturing for discontinuous galerkin methods. In *44th AIAA Aerospace Sciences Meeting and Exhibit*, page 112, 2006.

[48] Matteo Pini, S Vitale, Piero Colonna, Giulio Gori, A Guardone, T Economon, JJ Alonso, and F Palacios. Su2: the open-source software for non-ideal compressible flows. In *Journal of Physics: Conference Series*, volume 821, page 012013. IOP Publishing, 2017.

[49] Pierre Schrooyen, Koen Hillewaert, Thierry E Magin, and Philippe Chatelain. Fully implicit discontinuous galerkin solver to study surface and volume ablation competition in atmospheric entry flows. *International Journal of Heat and Mass Transfer*, 103:108–124, 2016.

[50] James B Scoggins, Carleton P Knisely, and Thierry E Magin. Crossed contributions to electron and heavy-particle transport fluxes for magnetized plasmas in the continuum regime. In *AIP Conference Proceedings*, volume 1786, page 130002. AIP Publishing LLC, 2016.

[51] James B Scoggins, Vincent Leroy, Georgios Bellas-Chatzigeorgis, Bruno Dias, and Thierry E Magin. Mutation++: Multicomponent thermodynamic and transport properties for ionized gases in c++. *SoftwareX*, 12:100575, 2020.

[52] James B Scoggins and Thierry E Magin. Development of mutation++: Multicomponent thermodynamic and transport properties for ionized plasmas written in c++. In *11th AIAA/ASME joint thermophysics and heat transfer conference*, page 2966, 2014.

[53] Chi-Wang Shu. High-order finite difference and finite volume weno schemes and discontinuous galerkin methods for cfd. *International Journal of Computational Fluid Dynamics*, 17(2):107–118, 2003.

[54] Magin T.E. *A Model for Inductive Plasma Wind Tunnels*. Phd thesis, Université Libre de Bruxelles, 2004.

[55] Jordi Vila-Pérez, Matteo Giacomini, Ruben Sevilla, and Antonio Huerta. Hybridisable discontinuous galerkin formulation of compressible flows. *Archives of Computational Methods in Engineering*, 28(2):753–784, 2021.

[56] Quentin Wargnier, A Alvarez Laguna, JB Scoggins, NN Mansour, Marc Massot, and TE Magin. Consistent transport properties in multicomponent two-temperature magnetized plasmas-application to the sun atmosphere. *Astronomy & Astrophysics*, 635:A87, 2020.

[57] Janusz Wojtkowiak and Czeslaw O Popiel. Inherently linear annular-duct-type laminar flowmeter. 2006.

[58] Michael Woopen, Aravind Balan, and Georg May. A hybridized discontinuous galerkin method for three-dimensional compressible flow problems. In *52nd Aerospace Sciences Meeting*, page 0938, 2014.

[59] Michael Woopen, Aravind Balan, and Georg May. A unifying computational framework for adaptive high-order finite element methods. In *22nd AIAA Computational Fluid Dynamics Conference*, page 2601, 2015.

[60] Michael Woopen, Aravind Balan, Georg May, and Jochen Schütz. A comparison of hybridized and standard dg methods for target-based hp-adaptive simulation of compressible flow. *Computers & Fluids*, 98:3–16, 2014.

[61] Michael Woopen, Thomas Ludescher, and Georg May. A hybridized discontinuous galerkin method for turbulent compressible flow. In *44th AIAA Fluid Dynamics Conference*, page 2783, 2014.

[62] Michael Woopen, Georg May, and Jochen Schütz. Adjoint-based error estimation and mesh adaptation for hybridized discontinuous galerkin methods. *International journal for numerical methods in fluids*, 76(11):811–834, 2014.